THE STUDY OF REACTOR WALL FOULING IN GAS-SOLID FLUIDIZED BEDS CAUSED BY ELECTROSTATIC CHARGE GENERATION

by
ANDREW SOWINSKI

B.A.Sc., University of Ottawa, 2007



uOttawa

Thesis submitted to the Faculty of Graduate and Postdoctoral Studies in partial fulfillment of the requirements for

DOCTOR OF PHILOSOPHY IN CHEMICAL ENGINEERING

Department of Chemical and Biological Engineering
Faculty of Engineering
University of Ottawa

© Andrew Sowinski, Ottawa, Canada, 2012

ABSTRACT

Electrostatic charge generation is unavoidable in gas-solid fluidized beds due to the repeated particle-particle and particle reactor wall contacts and separations. In industrial operations such as in polyethylene production this phenomenon results in the significant problem of reactor wall fouling, known as "sheeting". To better understand the underlying charging mechanisms involved in gas-solid fluidized beds in an attempt to eliminate and/or reduce the effect a novel on-line electrostatic charge measurement technique was developed, which concurrently provided information on both the degree of fluidized bed electrification and reactor wall fouling. A Faraday cup replaced the windbox of the fluidized bed while another cup was placed at the top of the column. The distributor plate was uniquely designed for the systematic removal of bed particles and those adhered to the column wall for their charge measurement with the bottom Faraday cup, and the charge of the entrained particles was measured by the top Faraday cup. This is the first study which allowed the charge measurement of particles in the bulk of the bed, particles adhered to the column wall, and those entrained, simultaneously. In addition, this method uniquely permitted the evaluations of the degree of reactor wall fouling under different operating conditions.

An experimental program was designed to investigate the influence of bed hydrodynamics (fluidizing gas velocity and particle size), fluidization column wall material, and the addition of different solid additives. Fluidizing particles were polyethylene resin from an industrial reactor. Bi-polar charging was observed where the elutriated particles were oppositely charged compared to those in the bulk of the bed and those adhered to the column wall. Particles within the wall coating were also found to be bi-polarly charged. With the resin tested as received, a certain sized particles (350-575 μm) adhered to the column wall. The specific charge of the particles near the column wall was found not to be a definite indication of the amount of wall fouling. Increasing the gas velocity promoted wall fouling and elevated the charge density of the particles within both bubbling and slugging flow regimes. The effect of solid additive injection was examined with two static drivers known to reduce wall fouling in industrial operations, a deactivated catalyst, and the catalyst support. It was found that the catalyst promoted, while one of the static drivers reduced wall fouling.

RÉSUMÉ

La génération de charge électrostatique dans un lit fluidisé gaz-solide est inévitable dû au contact et à la séparation répétitives entre les particules elles-mêmes et entre celles-ci et les parois du réacteur. Lors d'opération industrielle, telle que la production de polyéthylène, ce phénomène cause des problèmes sévères d'encrassement des parois du réacteur, connus sous le nom de « sheeting ». Une nouvelle technique de mesure en ligne de charge électrostatique a été développée, et cette technique fournit simultanément l'information sur le degré d'électrification d'un lit fluidisé et de l'encrassement sur la paroi d'un réacteur. Un collecteur de Faraday a remplacé la boîte à vent du lit fluidisé, tandis qu'un autre collecteur a été placé au sommet de la colonne. La plaque de distribution a été uniquement conçue pour l'enlèvement systématique des particules du lit ainsi que celles qui ont adhéré à la paroi de la colonne afin de mesurer leur charge avec le collecteur de Faraday inférieur et la charge des particules entraînées a été mesurée par le collecteur de Faraday supérieur. Cette étude est la première qui permet la mesure simultanée de la charge des particules dans le lit, des particules adhérées à la paroi de la colonne et de celles entraînées. De plus, cette méthode unique a permis l'évaluation du degré d'encrassement de la paroi du réacteur sous diverses conditions d'opération.

Un programme expérimental a été conçu pour étudier l'influence de l'hydrodynamique du lit (vitesse du gaz de fluidisation et la taille des particules), des matériaux du mur de la colonne de fluidisation et de l'ajout de différents additifs solides. Les particules fluidisées étaient de la résine de polyéthylène venant d'un réacteur industriel. Une charge bipolaire a été observée où les particules entraînées étaient chargées de façon opposée par rapport à celles chargées dans la masse du lit et celles adhérées à la paroi de la colonne. Les particules retrouvées dans l'encrassement ont également montré une charge bi-polaire. Avec la résine testée telle que reçue, les particules d'un certaine taille (350-575 μm) ont collé à la paroi de la colonne. La charge spécifique des particules à la proximité de la paroi de la colonne n'était pas une indication précise du montant d'encrassement sur le mur. L'augmentation de la vitesse du gaz a favorisé l'encrassement et la densité de charge des particules dans les régimes de bullage et de pistonnage. L'injection de deux promoteurs statiques connus pour réduire l'encrassement dans les

opérations industrielles, d’un catalyseur désactivé ou du support à catalyseur a été examinée. Le catalyseur a favorisé l’encrassement, tandis que l'un des pilotes statiques l’a réduit.

TABLE OF CONTENTS

Abstract ..... **i**
Résumé ..... **ii**
Table of Contents ..... **iv**
List of Tables ..... **ix**
List of Figures ..... **x**
Nomenclature ..... **xix**
Acknowledgements ..... **xxi**

CHAPTER 1. INTRODUCTION **1**
1.1. Gas-Solid Fluidization ***2***
1.1.1. Particle Force Balance 4
1.1.2. Example of Industrial Process 10
1.2. Electrostatic Charge Generation ***11***
1.2.1. Electrostatic Charging Mechanisms 12
1.2.1.1. Contact Charging 15
1.2.1.2. Frictional Charging 18
1.2.1.3. Induction Charging 19
1.2.2. Electrostatic Charge Generation Between Similar Insulators 20
1.2.3. Factors Influencing Electrostatic Charging 21
1.3. Electrostatics in Gas-Solid Fluidized Beds ***22***
1.3.1. Attractive/Repulsive Forces 25
1.3.1.1. Electrostatic Force 26
1.3.1.2. Image Force 27
1.3.1.3. The van der Waals Force 28
1.3.1.4. Summary 29
1.4. Quantification of Electrostatic Charge in Gas-Solid Fluidized Beds ***32***
1.4.1. Electrostatic Probes 32
1.4.1.1. Vertical Probes 33
1.4.1.2. Horizontal Probes 34
1.4.1.3. Industrial Measurement Techniques 34

1.4.1.4. Problems with Electrostatic Probes 35
1.4.2. Faraday Cups 37
1.4.2.1. Problems with the Faraday Cup Technique 39
1.4.3. Other Techniques 40
1.4.4. Summary 42
1.5. Parameters Affecting Electrostatic Phenomena in Gas-Solid Fluidized Beds 42
1.5.1. Fluidizing Gas Velocity 43
1.5.2. Particle Size and Material 44
1.5.3. Fluidization Column Material 46
1.5.4. Summary 46
1.6. Methods for Controlling Electrostatic Charge Generation 47
1.6.1. Treating the Column Inner Wall 48
1.6.2. Additive Injection 48
1.6.2.1. Gas Injection 48
1.6.2.2. Solid Injection 49
1.6.2.3. Liquid Injection 50
1.6.3. Summary 52
1.7. Thesis Objectives 53
1.8. Thesis Outline 54

CHAPTER 2. ON-LINE CHARGE MEASUREMENT TECHNIQUE 56
2.1. Design Considerations 56
2.2. Measurement Considerations 60
2.3. Preliminary Testing 63
2.3.1. Effect of Knife Gate Valve Opening 63
2.3.2. Electrometer Measurement Drifts 64
2.4. Summary 68

CHAPTER 3. MATERIALS, EXPERIMENTAL APPARATUS AND PROCEDURES 69
3.1. Materials 69
3.1.1. Fluidizing Gas 69

3.1.2. Fluidizing Particles 69
3.1.2.1. SEM and EDX Analysis 74
3.1.2.2. Particle Size Distribution 74
3.1.2.2.1. Sensitivity Analysis on PSD Measurements 75
3.1.2.3. Particle Mass Distribution 77
3.1.2.4. Particle Charge Distribution 79
3.1.3. Solid Additives 82
3.1.3.1. SEM and EDX Analysis 84
3.1.3.2. Additive Particle Size 84
3.2. Experimental Apparatus 85
3.2.1. Fluidization Column 85
3.2.2. Distributor Plate 88
3.2.3. Bottom Faraday Cup 88
3.2.4. Top Faraday Cup 89
3.2.5. Bench Scale Faraday Cup 90
3.2.6. Instrumentation 91
3.3. Experimental Procedures 93
3.3.1. Minimum Fluidization Velocity 93
3.3.2. Fluidization Experiment 94
3.3.2.1. Fluidization with Additive Injection 96
3.3.2.2. Repeatability of Experiments 96
3.4. Summary 102

CHAPTER 4. BENCH-SCALE CHARGING EXPERIMENTS 103

CHAPTER 5. EFFECT OF FLUIDIZING GAS VELOCITY 110
5.1. Experimental Conditions 114
5.2. Results and Discussion 114
5.2.1. Mass 114
5.2.2. Particle Size Distribution 116
5.2.3. Particles Absolute and Specific Charge 120

5.2.4. Specific Charge-to-Specific Surface Area Ratio 124
5.2.5. Wall Layer Coating 124
5.2.6. Electrostatic Probe Measurements 128
5.3. Summary 131

CHAPTER 6. EFFECT OF PARTICLE SIZE 133
6.1. Experimental Conditions 135
6.2. Results and Discussion 135
6.2.1. Initial Particles Charge Distribution 136
6.2.2. Mass 136
6.2.3. Particle Size Distribution 140
6.2.4. Particles Absolute and Specific Charge 141
6.2.5. Specific Charge-to-Specific Surface Area Ratio 144
6.2.6. Wall Layer Coating 147
6.2.7. Electrostatic Probe 150
6.3. Summary 153

CHAPTER 7. EFFECT OF COLUMN WALL MATERIAL 154
7.1. Experimental Conditions 156
7.2. Results and Discussion 157
7.2.1. Charge of the PE Film 157
7.2.2. Mass 159
7.2.3. Particle Size Distribution 160
7.2.4. Particles Specific and Absolute Charge 162
7.2.5. Specific Charge-to-Specific Surface Area Ratio 165
7.2.6. Wall Layer Coating 166
7.2.7. Charged Particle Separator 168
7.3. Summary 171

CHAPTER 8. EFFECT OF SOLID ADDITIVE INJECTION 172
8.1. Experimental Conditions and Methodology 176

8.2. Results and Discussion ***177***
8.2.1. Additive Charging 178
8.2.1.1. Pseudo-Triboelectric Series 187
8.2.1.2. Proposed Charge Generation Mechanism 188
8.2.1.3. Proposed Charge Dissipation Mechanisms 190
8.2.1.4. Proposed Additive Coating and Mechanism 192
8.2.2. Fluidization Experiments with PE_A and PE_C Resin 195
8.2.2.1. Mass 195
8.2.2.2. SEM Pictures 198
8.2.2.3. Particle Size Distribution 209
8.2.2.4. Particles Absolute and Specific Charge 212
8.2.2.5. Specific Charge-to-Specific Surface Area Ratio 216
8.2.2.6. Wall Layer Coating 219
8.2.2.7. Charged Particle Separator 222
8.2.2.8. Electrostatic Probe 224
8.2.3. Additional Experiments with Additive B 230
8.2.3.1. Mass 231
8.2.3.2. PSD 236
8.2.3.3. Particles Absolute Charge and Specific Charge 239
8.2.3.4. Specific Charge-to-Specific Surface Area Ratio 248
8.2.3.5. Wall Layer Coating 251
8.2.3.6. Electrostatic Probes 253
8.3. Conclusions ***260***

CHAPTER 9. CONCLUSIONS AND RECOMMENDATIONS 262
9.1. Conclusions ***262***
9.2. Recommendations for Future Work ***270***
References 272
APPENDIX A Apparatuses From Other Works Found in Literature 279
APPENDIX B SEM Pictures of Polyethylene Particles and Additives 287
APPENDIX C Preliminary Testing 297
APPENDIX D Additive Experiments with PE_A at 4 u_{mf} 303

LIST OF TABLES

Table 1.1: Geldart Particles Classification (adapted from Gupta and Sathiyamoorthy, 1999; Geldart, 1973). 10
Table 1.2: Work functions of various materials (adapted from Tanue and Masuda, 2006). 17
Table 1.3: A triboelectic series (adapted from Montgomery, 1959 and Cross, 1987). 18
Table 1.4: Parameters that could affect electrostatic charge generation in a gas-solid fluidized bed. 53
Table 3.1: Polyethylene A Particles Physical, Chemical and Electrical Properties. 71
Table 3.2: Polyethylene B Particles Physical, Chemical and Electrical Properties. 72
Table 3.3: Polyethylene C Particles Physical, Chemical and Electrical Properties. 73
Table 3.4: Additives A, B, C, and F Physical, Chemical and Electrical Properties. 83
Table 3.5: Comparison of u_{mf} determined by different methods. 93
Table 3.6: Average values for the tests and the sources of deviation. 102
Table 5.1: Summary of previous studies performed on the effect of fluidizing gas velocity on electrostatic charge generation in gas-solid fluidized beds. 112
Table 5.2: Experimental conditions used for testing the effect of fluidizing gas velocity. 114
Table 6.1: Summary of previous studies on the effect of particle size on electrostatic charge generation in gas-solid fluidized beds. 134
Table 6.2: The experimental conditions used for the experiments on the effect of particle size. 135
Table 7.1: Summary of previous studies on the effect of the column material on electrostatic charge generation in gas-solid fluidized beds. 155
Table 7.2: The experimental conditions used for the experiments on the effect of the column material. 156
Table 8.1: Summary of previous studies performed on the effect of addition of solid additives on electrostatic charge generation in gas-solid fluidized beds. 174
Table 8.2: The experimental conditions used for the experiments on the effect of solid additive injection. 176
Table 8.3: The charging behavior of all additives found through experiments with carbon steel plate, stainless steel injector and empty fluidization column. 179
Table 8.4: The d_P50_N of samples taken from the CPS Faraday cups. 184
Table 8.5: Pseudo-triboelectric series for all materials in the fluidized bed. 188
Table 8.6: Predicted surface polarity due to triboelectrification between different surfaces coming into contact inside the fluidized bed. The left value corresponds to the column on the left and the right value corresponds to the row on the top. 188
Table 8.7: The particles specific surface area (A), and total available surface area within each region of the fluidization system. 195

LIST OF FIGURES

Figure 1.1: Schematic of a typical gas-solid fluidized bed. 4
Figure 1.2: Force balance on an electrically neutral particle within a fluidized bed. 5
Figure 1.3: The ratio of drag and buoyant forces over the gravitational force on a neutral particle for varying particle size and fluidizing gas velocity. 7
Figure 1.4: Different fluidization flow regimes formed with increasing fluidizing gas velocity (adapted from Kunii and Levenspiel, 1991). 8
Figure 1.5: The graphical representation of the Geldart classification of particles (adapted from Kunii and Levenspiel, 1991). 9
Figure 1.6: An industrial example of a gas-solid fluidized bed reactor for the catalytic polymerization of polyethylene (adapted from Goode et al., 1989). 11
Figure 1.7: The work function, φ, of two different metals 1 and 2, where e is the elementary charge and V_c is the contact potential (copied from Matsusaka and Masuda, 2003). 13
Figure 1.8: The relationship between the specific charge and total ion concentration for different polymer blends (copied from Fenzel-Alexander et al., 1994). 14
Figure 1.9: a) An example of surface electric potential using kelvin probe force microscopy (KFM), and b) Surface potential of polydimethylsiloxane (PDMS) before and after contact charging (copied from Baytekin et al., 2011). 15
Figure 1.10: The mechanism for contact charging. 16
Figure 1.11: The mechanism of frictional charging. 18
Figure 1.12: a) The effect of rubbing velocity between two polymer films on the voltage output (adapted from Ohara 1979), and b) the change in polarity of polyethylene terephthalate disc rubbed against a metal brush caused by frictional charging (adapted from Cross, 1987 from Zimmer, 1970). 19
Figure 1.13: The mechanism of induction charging. 20
Figure 1.14: Industrial polyethylene gas-solid fluidized bed reactor showing the locations of sheeting formation (adapted from Hendrickson, 2006). 25
Figure 1.15: The force balance on a single particle (with an either positive or negative charge of q) inside a gas-solid fluidized bed with a conductive wall where $q1, i$ is the image charge on the conductive surface. 26
Figure 1.16: The Bond number as a function of particle size for the electrostatic force, image force, and van der Waals forces. 31
Figure 1.17: The decrease in measurement accuracy due to particle adhesion on the electrostatic probe and a relative humidity (ψ) of 20% and expanded bed height (H_e) of 0.11m (adapted from Fujino et al., 1985). 36
Figure 1.18: Schematics showing a) the components of a Faraday cup, and b) how the Faraday cup measures the charge of an object. 38

Figure 2.1: Overall schematic of a) a simple fluidization column, and b) a modified column with two online Faraday cups. 59
Figure 2.2: Pictures of the modified knife-gate valve replacing the distributor plate. 60
Figure 2.3: Various measurement regions within the fluidized bed. 62
Figure 2.4: The change in charge of the particles due to opening the knife gate valve. 64
Figure 2.5: The electrometer background signal measurement from the top Faraday cup for a period of one hour. No particles were present and no gas was sent through the fluidized bed. 66
Figure 2.6: Charge measurement by the electrometer attached to the top Faraday cup. No particles were present, while the gas velocity increased at 10 SLPM every five minutes. 67
Figure 2.7: The electrometer measurement drift of the bench-scale Faraday cup without any particles present for one hour. 68
Figure 3.1: The difference in particle size (d_P10, d_P50, d_P90) against a reference particle size (d_{PR}) for different multiples of the refractive index of the particles. 76
Figure 3.2: The difference in particle size (d_P10, d_P50, d_P90) against a reference particle size (d_{PR}) for different refractive indices of the dispersant. Pure water has a refractive index of 1.33 and pure ethanol has a refractive index of 1.36. 77
Figure 3.3: Polyethylene resins (PE_A, PE_B and PE_C) average volume distribution from PSD analysis, and the mass distribution from sieved tests. 78
Figure 3.4: Picture and schematic of the Charged Particle Separator. 80
Figure 3.5: The initial polyethylene resins m%, q/m, and d_P50 measured using Charged Particle Separator (PP stands for positive plate). 81
Figure 3.6: PSD of the additives A, B, C and F. 85
Figure 3.7: Overall schematic of the experimental setup. 86
Figure 3.8: Picture of the fluidized bed. 87
Figure 3.9: Schematic and picture of the bottom Faraday cup. 89
Figure 3.10: Schematic and picture of the top Faraday cup. 90
Figure 3.11: Picture of the bench-scale Faraday cup. 91
Figure 3.12: Schematic of the electrostatic probe. 92
Figure 3.13: The q/m of the Initial, Fines, Dropped, and Loosely Bound particles for the repeated experiments at 1.5 u_{mf} and 60 min of fluidization. 99
Figure 3.14: The m% of the Fines, Dropped, Loosely Bound, and Tightly Bound particles for the repeated experiments at 1.5 u_{mf} and 60 min of fluidization. 100
Figure 3.15: The d_P50_N of the Initial, Fines, Dropped, and Loosely Bound particles for the repeated experiments at 1.5 u_{mf} and 60 min of fluidization. 101
Figure 4.1: A picture of the bench-scale Faraday cup with an angled carbon steel plate placed above it. 104

Figure 4.2: Repetitions of carbon steel plate test with PE_B and PE_C polyethylene particles, when the particles were dropped directly into a Faraday cup versus particles were dropped onto an angled carbon steel plate before falling into a Faraday cup. 105
Figure 4.3: Carbon steel plate charging of sieved PE_A particles. 107
Figure 4.4: Proposed charging mechanisms found inside the fluidized bed between the small and large polyethylene particles (PE), and with the carbon steel column wall. 109
Figure 5.1: The m% of the PE_A particles collected from the Fines, Dropped, Loosely Bound, Tightly Bound, and Wall regions of the fluidized bed at different fluidization gas velocities. 116
Figure 5.2: Examples of PSD in different regions of the fluidized bed at 1.5 and 4 u_{mf}. 117
Figure 5.3: The d_P50_N of the PE_A particles from the Initial, Fines, Dropped, Loosely Bound, and Tightly Bound regions of the fluidized bed at different fluidization gas velocities. ..118
Figure 5.4: The theoretical largest diameter of particles estimated to be elutriated from the fluidization column, and the measured d_P50_N particle size of the Fines at different gas velocities. 119
Figure 5.5: Examples of cumulative charge of the Fines measured during the 60 min of fluidization for different fluidizing gas velocities. 121
Figure 5.6: The q/m of the PE_A particles from the Initial, Fines, Dropped, and Loosely Bound regions of the fluidized bed at different fluidizing gas velocities. 122
Figure 5.7: The q/A of the PE_A particles from the Initial, Fines, Dropped, and Loosely Bound regions of the fluidized bed at different fluidizing gas velocities. 124
Figure 5.8: Examples of wall layer pictures for PE_A particles after 60 min of fluidization at 1.5 u_{mf} and 4 u_{mf}. 126
Figure 5.9: The diagram of the proposed wall particle layering mechanism. 128
Figure 5.10: Examples of current measured by electrostatic probe for fluidization gas velocities of 1.5 and 4.0 u_{mf} over the period of 60 min of fluidization. 130
Figure 6.1: The initial net q/m of particles for different size ranges using the Charged Particle Separator in different Faraday cups (FC). 136
Figure 6.2: The m% of the Dropped, Loosely Bound, and Wall particles for different particle size ranges at 1.5 u_{mf}. 138
Figure 6.3: The m% of the Dropped, Loosely Bound, and Wall particles for different particle size ranges at 4 u_{mf}. 139
Figure 6.4: The d_P50_N of the Initial, Dropped, Loosely Bound, and Tightly Bound particles with different particle size ranges at 1.5 and 4 u_{mf}. 140
Figure 6.5: The particles net q/m in the Initial, Dropped, and Loosely Bound regions for different particle size ranges at 1.5 and 4 u_{mf}. 142
Figure 6.6: Examples of the Dropped particle measurement where Loosely Bound particles also fell with the Dropped particles. Results are presented for particles size range of 600-710 μm at 4 u_{mf}. 144

Figure 6.7: Particles q/A in the Initial, Dropped, and Loosely Bound regions for different particle size ranges at 1.5 and 4 u_{mf}. 146
Figure 6.8: Images of the wall layer coating with different particle size ranges before and after tapping the column wall at 1.5 u_{mf}. 148
Figure 6.9: Images of the wall layer coating with different particle size ranges before and after wall tapping at 4 u_{mf}. 149
Figure 6.10: Images of the wall fouling of four out of seven repeated experiments with 600–710 µm particles at 4 u_{mf}. 150
Figure 6.11: The current measurement from different sieved particle size ranges for 60 min of fluidization at 1.5 u_{mf}. 151
Figure 6.12: The current measurement from different sieved particle size ranges for 60 min of fluidization at 4 u_{mf}. 152
Figure 7.1: A picture of the polyethylene film added to the interior of the fluidization column. 157
Figure 7.2: Example of the PE film charging PE_B particles. 159
Figure 7.3: The m% of the PE_B particles in the Fines, Dropped, Loosely Bound, Tightly Bound, and Wall regions of the fluidized bed with different column materials. 160
Figure 7.4: Examples of the normalized PE_B particles size distribution found in different regions of the fluidized bed with the carbon steel column and PE film sleeve. 161
Figure 7.5: The d_P50_N of the PE_B particles in the Initial, Fines, Dropped, and Loosely Bound regions of the fluidized bed with different fluidization column wall material. 162
Figure 7.6: Cumulative charge of Fines measured for repeated trials for 60 min of fluidization with different column materials. 163
Figure 7.7: The net q/m of the particles in the Initial, Fines, Dropped, and Loosely Bound regions of the fluidized bed with different column wall materials. 164
Figure 7.8: The q/A of the particles in the Initial, Fines, Dropped, and Loosely Bound regions of the fluidized bed with different column wall materials. 166
Figure 7.9: Examples of images from wall coating with carbon steel and PE film wall materials. 167
Figure 7.10: Example of particles coating on the PE film removed from column after the Wall particles were removed. 167
Figure 7.11: The m%, q/m, and d_P50_N results for the Loosely Bound particles using the CPS with the carbon steel and PE Film materials. 170
Figure 8.1: The Faraday cup set up used to measure the charge of additives passing through the injector unit. 179
Figure 8.2: Charging behaviour of Additives A, B, C and F in contact with a carbon steel plate, passing through a stainless steel injector, and injected into an empty fluidization column. 180
Figure 8.3: The d_P50_N of additives A, B, C and F found in the Top Faraday cup and on the distributor plate for the Empty Column experiment at 0.67 u_{mf}. 182

Figure 8.4: Typical charge distribution of Additives A, B, C, and F determined by the Particle Charge Separator at different applied voltage (V). 184
Figure 8.5: Empty column experiments performed with Additive A, B, C, and F at different gas velocities. 186
Figure 8.6: The d_P50_N of additives A, B, C and F found in the Top Faraday cup and on the distributor plate for the Empty Column experiments at different fluidizing gas velocities. 187
Figure 8.7: Proposed charging mechanisms found inside the fluidized bed between the polyethylene particles (PE), all additive particles (X), and the column wall. 189
Figure 8.8: Images of additive coating in different areas of the gas-solid fluidized bed upon the completion of the Empty Column experiments. 193
Figure 8.9: The m% of the Fines, Dropped, Loosely Bound, Tightly Bound, and Wall particles for experiments performed with and without additives with both PE_A and PE_C resin. 197
Figure 8.10: SEM Pictures of the Fines, Dropped, Loosely Bound, and Tightly Bound particles when Additive A was present with the PE_A resin. 200
Figure 8.11: SEM Pictures of the Fines, Dropped, Loosely Bound, and Tightly Bound particles when Additive B present with the PE_A resin. 201
Figure 8.12: SEM Pictures of the Fines, Dropped, Loosely Bound, and Tightly Bound particles when Additive C present with the PE_A resin. 202
Figure 8.13: SEM Pictures of the Fines, Dropped, Loosely Bound, and Tightly Bound particles when Additive F present with the PE_A resin. 203
Figure 8.14: SEM pictures of PE_C particles from the Fines and Dropped regions, and FC1 and FC3 with Additive A for 60 minute fluidization. 205
Figure 8.15: SEM pictures of PE_C particles from the Fines and Dropped regions, and FC1 and FC3 with Additive B for 60 minute fluidization. 206
Figure 8.16: SEM pictures of PE_C particles from the Fines and Dropped regions and FC1 and FC3 with Additive C for 60 minute fluidization. 207
Figure 8.17: SEM pictures of PE_C particles from the Fines and Dropped, regions, and FC1 and FC3 with Additive F for 60 minute fluidization. 208
Figure 8.18: The d_P50_N of the Initial, Fines, Dropped, Loosely Bound, and Tightly Bound particles for experiments performed with and without additives with PE_A and PE_C resins 211
Figure 8.19: Examples of the cumulative charge of the Fines measured during 60 min of fluidization with and without the additives with both PE_A and PE_C resin. 213
Figure 8.20: The net q/m of the Initial, Fines, Dropped, and Loosely Bound particles for experiments performed with and without additives with both PE_A and PE_C resin. 214
Figure 8.21: The qA of the Initial, Fines, Dropped, and Loosely Bound particles for experiments performed with and without additives with both PE_A and PE_C resin. 218

Figure 8.22: Pictures of the wall particle layer with and without additives with both PE_A and PEC resin. 221
Figure 8.23: The CPS results for the Loosely Bound PE_C particles with and without any additive after 60 min of fluidization. 223
Figure 8.24: The current and charge measurements for trials with no additive for 60 min of fluidization with PE_A and PE_C resin present. 225
Figure 8.25: The current and charge measurements for trials with Additive A for 60 min of fluidization with PE_C. 226
Figure 8.26: The current measurements for trials with Additive B for 60 min of fluidization with PE_A and PE_C resin. 227
Figure 8.27: The current measurements for trials with Additive C for 60 min of fluidization with PE_C resin. 228
Figure 8.28: The current measurements for trials with Additive F for 60 min of fluidization with PE_A and PE_C resin. 229
Figure 8.29: The m% particles in the Fines, Dropped, Loosely Bound, Tightly Bound, and Wall regions of the fluidized bed after 60 min of fluidization with different Additive B experiments. 233
Figure 8.30: The particles m% found in the Fines, Dropped, Loosely Bound, Tightly Bound, and Wall regions of the fluidized bed after 15 and 60 min of fluidization with different Additive B experiments. 235
Figure 8.31: The d_P50_N of particles collected from the Initial, Fines, Dropped, Loosely Bound, and Tightly Bound regions of the fluidized bed after 60 min of fluidization with different Additive B experiments. 237
Figure 8.32: The d_P50 of particles from the Initial, Fines, Dropped and Loosely Bound regions of the fluidized bed after 15 and 60 min of fluidization with different Additive B experiments. 238
Figure 8.33: Examples of the cumulative charge of Fines under different Additive B experiments for 60 min of fluidization. 240
Figure 8.34: Examples of the cumulative charge of Fines with Additive B injected every 15 minutes into the fluidized bed over 60 minutes of fluidization and Additive B injected prior to fluidization (PE-B). 241
Figure 8.35: The net q/m of the particles found in the Fines, Dropped, Loosely Bound, and Wall regions of the fluidized bed after 60 min of fluidization with different Additive B experiments. 243
Figure 8.36: Examples of the cumulative charge of the Fines under different Additive B experiments during 15 min of fluidization. 245
Figure 8.37: The particles net q/m in Initial, Fines, Dropped, and Loosely Bound regions of the fluidized bed after 15 and 60 min of fluidization with different Additive B experiments. 247

Figure 8.38: The net q/A of particles in Fines, Dropped, and Loosely Bound regions of the fluidized bed after 60 min of fluidization with different Additive B experiments.....249
Figure 8.39: The net q/A of different Additive B experiments in the Fines, Dropped, Loosely Bound and Wall regions of the fluidized bed after 15 min of fluidization.....250
Figure 8.40: Typical pictures of the wall particle layer before removing the Loosely Bound particles with different Additive B conditions after 60 min of fluidization. 252
Figure 8.41: Typical pictures of the wall particle layer before removing the Loosely Bound particles with different Additive B conditions for different fluidization periods.....253
Figure 8.42: The electrostatic probe measurements (in both current and charge modes) for PE resin fluidization experiments performed with Additive B injected into the bed and Additive B pre-coating the column wall. 255
Figure 8.43: The electrostatic probe measurements (current mode) for experiments performed with Additive B injected into the bed multiple times during fluidization and the cumulative charge simultaneously measured by the Top Faraday cup. 257
Figure 8.44: The electrostatic probe measurements (in current and charge mode) for experiments performed with and without Additive B during 15 min of fluidization.....259

Figure A.1: Vertical probe apparatus (adapted from Ciborowski and Wlodarski, 1962).....280
Figure A.2: Vertical probe apparatus (adapted from Kisel'nikov et al., 1967). 280
Figure A.3: Vertical probe apparatus (adapted from Bafrnec and Bena, 1972). 280
Figure A.4: Vertical probe apparatus used (adapted from Rojo et al., 1985). 280
Figure A.5: Vertical probe apparatus (adapted from Fujino et al., 1985).....281
Figure A.6: Vertical probe apparatus (adapted from Guardiola et al., 1992). 281
Figure A.7: The horizontal probe and Faraday cup apparatus (adapted from Tardos and Pfeffer, 1980).....281
Figure A.8: The horizontal probe apparatus (adapted from Ham et al., 1992).....281
Figure A.9: The horizontal probe apparatus (adapted from Park et al., 2002). 282
Figure A.10: The horizontal probe apparatus (adapted from Moughrabiah et al., 2009). 282
Figure A.11: The non-contacting horizontal probe apparatus (adapted from by Boland and Geldart, 1971/72).....282
Figure A.12: The horizontal probe apparatus (adapted from Fulks et al., 1985).....283
Figure A.13: The horizontal probe apparatus (adapted from Goode et al., 1989). 283
Figure A.14: The horizontal probe apparatus (adapted from Newton et al., 1999). 283
Figure A.15: The electrostatic probe apparatus (adapted from Hagerty et al., 2005). 283
Figure A.16: The sampling Faraday cup apparatus (adapted from Fasso et al., 1982). 284
Figure A.17: The sampling Faraday cup apparatus (adapted from Wolny and Opalinski, 1983).....284
Figure A.18: a) The Faraday cup grid, and b) schematic of the scooper used to sample particles (adapted from Ali et al., 1998).....284
Figure A.19: The 7 vertical Faraday cup method (adapted from Zhao et al., 2000). 285
Figure A.20: The Faraday cup fluidization column (adapted from Mehrani et al., 2005). 285

Figure A.21: Inner rings method (adapted from Gajewski, 1985).....286
Figure A.22: Capacitance probe method (adapted from Wolny and Kazmierczak, 1989).....286
Figure A.23: The induction elevator ring method (adapted from Murtomaa et al., 2003). 286
Figure B.1: The SEM pictures of the PE_A resin at three different sieved particle size ranges using the LVSTD (left) and BSE detectors (right) at 100x magnification.....289
Figure B.2: The SEM pictures of the PE_B resin at three different sieved particle size ranges using the LVSTD (left) and BSE detectors (right) at 100x magnification.....290
Figure B.3: The SEM pictures of the PE_C resin at three different sieved particle size ranges using the LVSTD (left) and BSE detectors (right) at 100x magnification.....291
Figure B.4: The SEM pictures of Additive A at different magnifications. At 100x the LVSTD and BSE detectors were used. At 750x and 7000x the SE detector was used.....293
Figure B.5: The SEM pictures of Additive B at different magnifications. At 100x the LVSTD and BSE detectors were used. At 750x and 7000x the SE detector was used.....294
Figure B.6: The SEM pictures of Additive C at different magnifications. At 100x the LVSTD and BSE detectors were used. At 750x and 7000x the SE detector was used.....295
Figure B.7: The SEM pictures of Additive F at different magnifications. At 100x the LVSTD and BSE detectors were used. At 750x and 7250x the SE detector was used.....296
Figure C.1: The electrometer background charge and current measurement of the electrostatic probe placed at the bottom of the fluidization column for a period of one hour. No particles were present and no gas was sent through the fluidized bed.....299
Figure C.2: The electrometer measurement of the electrostatic probe placed at the bottom of the fluidization column. Tests were performed on both current mode and charge mode. No particles were present with increasing gas volumetric flow rate.....300
Figure C.3: Example of determining the minimum fluidization gas velocity through experimentation using PE_A particles. 301
Figure D.1: The m% of the Fines, Dropped, Loosely Bound, Tightly Bound and Wall particles for experiments performed with and without additives with PE_A at 4 u_{mf}. 305
Figure D.2: SEM Pictures of the Fines, Dropped, Loosely Bound, and Tightly Bound particles when Additive A present at 4 u_{mf} with the PE_A resin. 306
Figure D.3: SEM Pictures of the Fines, Dropped, Loosely Bound, and Tightly Bound particles when Additive B present at 4 u_{mf} with the PE_A resin. 307
Figure D.4: SEM Pictures of the Fines, Dropped, Loosely Bound, and Tightly Bound particles when Additive C present at 4 u_{mf} with the PE_A resin. 308
Figure D.5: SEM Pictures of the Fines, Dropped, Loosely Bound, and Tightly Bound particles when Additive F present at 4 u_{mf} with the PE_A resin.....309
Figure D.6: The d_P50_N of the Initial, Fines, Dropped, Loosely Bound, and Tightly Bound particles for experiments performed with and without additives with PE_A resins at 4 u_{mf}. 310
Figure D.7: Examples of the cumulative charge of the Fines measured during 60 min of fluidization with and without the additives with PE_A at 4 u_{mf}.....311

Figure D.8: The net q/m of the Initial, Fines, Dropped, and Loosely Bound particles for experiments performed with and without additives with PE_A at 4 u_{mf}. 312
Figure D.9: The net q/A of the Initial, Fines, Dropped, and Loosely Bound particles for experiments performed with and without additives with PE_A at 4 u_{mf}. 313
Figure D.10: Pictures of the wall particle layer with and without additives using the PE_A resin at 4 u_{mf}. 314
Figure D.11: The current measurements for trials with no additive for 60 min of fluidization with PE_A resin at 4 u_{mf}. 315
Figure D.12: The current measurements for trials with Additive B for 60 min of fluidization with PE_A resin at 4 u_{mf}. 316
Figure D.13: The current measurements for trials with Additive F for 60 min of fluidization with PE_A resin at 4 u_{mf}. 317

NOMENCLATURE

Symbol	Description	Units
A	Area	m^2
A	Hamaker Constant	J
$\hat{A}$	Specific surface area	m^2/g
Ar	Archimedes number	-
C_d	Drag coefficient	-
d_a	Diameter of curvature at the surface asperities	m
d_C	Column diameter	m
d_P	Particle diameter	µm
$d_{P,N}$	Normalized particle diameter	-
d_P10	Particle diameter at the 10^{th} percentile	µm
d_P50	Particle diameter at the 50^{th} percentile (median)	µm
d_P90	Particle diameter at the 90^{th} percentile	µm
$\vec{F}_b$	Buoyant force	N
$\vec{F}_d$	Drag force	N
$\vec{F}_E$	Electrostatic force	N
$\vec{F}_g$	Gravitational force	N
$\vec{F}_i$	Image force	N
$\vec{F}_{vdW,P}$	van der Waals force between two particles	N
$\vec{F}_{vdW,w}$	van der Waals force between a particle a wall	N
g	Gravitational force constant	m/s^2
L/D	Static bed height to column diameter ratio	-
P	Perimeter	m
q	Charge	nC
$\hat{q}/\hat{A}$	Specific charge to specific surface area ratio	$\mu C/m^2$
q/m	Specific charge	µC/kg
Re_P	Reynolds number	-
r	Distance between two point charges	m
R_F	Force ratio	-
u	Superficial gas velocity	m/s
u_{mf}	Minimum fluidization gas velocity	m/s
V_P	Volume of a single particle	m^3
z_{PP}	Distance between two particles	m
z_{PW}	Distance between a particle and wall	m
α	Material specific parameter for Equation 1.12	-
β	Material specific parameter for Equation 1.12	-
$\mathbb{C}$	Circularity	-
ϕ	Sphericity	-

ε_f	Permittivity of the fluid	F/m
ε_w	Permittivity of the wall	F/m
ρ_f	Density of fluid	kg/m^3
ρ_P	Density of particle	kg/m^3
σ	Surge charge density	C/m^2

Acronym	**Description**
BSE	Backscatter Electron Detector
CPS	Charged Particle Separator
EDX	Energy-Dispersive X-ray spectroscopy
KFM	Kelvin Force Microscopy
LVSTD	Low Vacuum Seconday Tescan Dectector
MSDS	Material Safety Data Sheet
PC	Poly
PE	Polyethylene
PVC	Polyvinylchloride
SE	Secondary Electron Detector
SEM	Scanning Electron Microscopy
SLPM	Standard Litres Per Minute

ACKNOWLEDGEMENTS

I would like to express my appreciation to my supervisor Dr. Poupak Mehrani for her support, guidance and trust in me helping her in the building and growth of her first research project and group.

I would like to also thank my group members, in particular Amanda Giffin and Fawzi Salama, who helped me with my experiments and discussions and theories through the course of my research. I would also like to thank the undergraduate students that were under my supervision during the five years, namely, Leigh Miller, Mike Stewart, Antonio Mayne, Bassam Javed, Mahima Sharma, and Khaled Atieh. I hope they learned from me as much as I did from them.

This work could not have been completed without the help from the staff of the Department of Biological and Chemical Engineering at the University of Ottawa: Gérard Nina, Louis Tremblay, Francine Pétrin and Sylvie Saindon, and especially Franco Ziroldo who was assigned to the project from the very beginning and was always able to provide solutions to the mechanical problems encountered.

I would like to thank Dr. Michael Muhle and Dr. F. David Hussein from Univation Technologies, LLC, for their guidance, and support as well as supplying all the resins, polymer film and additives used in this work. The Natural Sciences and Engineering Research Council of Canada (NSERC) are also thanked for their financial contributions.

I also wish to thank my graduate student peers for providing entertaining and insightful memories over the last five years. I would also wish to thank my other friends for helping me maintain balance in my life. I especially would like to thank my parents, brother, grandmother, and the rest of my family for their continual support and enthusiasm even if they did not fully understand what a gas-solid fluidized bed is. Finally, I cannot thank enough, the continual support and enthusiasm of my wife-to-be, Kathleen Vissers, who put up with my early mornings, late nights, and constant need to organize every aspect of our life.

Chapter 1.
INTRODUCTION

In gas-solid fluidization, solid particles are subjected to an upward flow of gas, which transforms the particles into a fluid-like state (Kunii and Levenspiel, 1991). Gas–solid fluidization is a common process found in many chemical industries with applications in gas–solid catalytic reactions, drying, mixing, granulation and coating. One major problem observed in some gas-solid fluidized beds is the occurrence of electrostatic charge generation. Due to the significant number of particle–particle and particle-reactor wall contact and separation, the occurrence of electrostatic charge generation in these types of reactors is almost unavoidable resulting in problems such as particle agglomeration, particle-reactor wall adhesion, and electrostatic discharge.

One industrial example where the significant effects of electrostatic charge generation in gas-solid fluidized bed reactors have been observed for many years is in the production of polyolefin. Specifically in polyethylene gas-solid fluidized bed reactors, bed electrification has been reported to be the cause of particle agglomeration (i.e., formation of undesired polymer chunks) and reactor wall fouling (known as "sheeting"). Sheeting is known to be a significant drawback since particle sheets can break off the reactor wall and clog the distributor plate, causing considerable operational down time due to reactor shut down and clean up. There are currently well over 100 polyethylene reactors worldwide producing nearly 20 million tonnes of polyethylene per year. An example of such operation is that of Dow Chemical plant located in Prentiss (Alberta, Canada) that produces 750,000 tonnes of polyethylene each year. Depending on the severity, a sheeting incident generally results in 2 to 3 days of reactor downtime, but could create up to 30 days of total production loss in serious cases. Overall, these challenges result in large economic losses due to decreased production and higher maintenance costs. For example, assuming the marginal cost of polyethylene production ranging between 440-550 USD/tonne (considering only the cost of raw materials and product), the economic loss of a plant, the size of the Prentiss plant, related to reactor downtime could be in the range of 1.0 to 1.2 million USD/day. Therefore, there is great incentive to reduce or eliminate electrostatic effects in

polyethylene reactors. In recent years, polymerization industry has focused on determining ways to reduce the electrostatic phenomena within the polyethylene catalytic gas-solid fluidized bed reactors (Fulks et al., 1985; Goode et al., 1989; Chirillo et al., 1985; Song et al., 1995; Newton et al., 1999; Hagerty et al., 2005; Yu et al., 2007, Hagerty et al., 2011). Despite the patents published claiming to have developed a charge reduction method (e.g., injection of static drivers), the problem still persists. These methods have been derived mostly by trial and error and thus their exact mechanism often is unknown. The amount of electrostatic charging in industrial reactors can differ based on various parameters such as the type and grade of polymer (polyethylene, polypropylene) produced and the catalyst (Zeigler-Natta, metallocene) utilized. Therefore, some reduction techniques may not be suitable for all processes. For example, in cases where a new catalyst is developed and implemented, the existing reduction technique may become ineffective and, therefore, more rigorous testing would be required for each new type of catalyst. More importantly, the method used or its degree of application relies on electrostatic charge measurements to determine the degree of reactor sheeting; however, only after there is a sheeting incident and the reactor is shutdown, can the amount of wall sheeting truly be determined.

Although the electrostatic charging and build-up in gas-solid fluidized beds have been studied over the years, the prediction and control of bed electrification have not yet been effectively achieved due to the lack of understanding of the fundamental concepts behind solids charging in these systems. Even to this day, it is often very difficult, and at time even impossible, to predict the magnitude and/or the polarity (positive or negative) of the charge that a solid may possess after it has been in contact with other objects. The hydrodynamics of gas-solid fluidized beds are complex before even taking into account the electrostatic effects. Therefore, a comprehensive study of electrostatics in relation to gas-solid fluidization is necessary to reduce unpredictability, to increase fundamental knowledge, and to consequently aid in the reduction of this phenomenon in some systems.

1.1. Gas-Solid Fluidization

Since its first industrial application in 1942 with catalytic cracking (Kunii and Levenspiel, 1991), fluidization has become a large area of interest in both industry and academia due to its

characteristics such as excellent heat transfer capabilities, and/or excellent gas-solid surface contact for reaction. Fluidization has evolved considerably since 1942 and fluidized beds have been incorporated into various industries.

A typical gas-solid fluidized bed is shown in Figure 1.1 where the fluidizing gas enters the bottom of the column through the windbox region before being passed through the distributor plate and into the main section of the column where it fluidizes a bed of particles. The section above the particles bed, which provides room for the bed to expand, is referred to as the freeboard region. If the terminal velocity of the fluidizing particles is lower than the fluidizing gas velocity, particles will be entrained from the column. To prevent particle entrainment, an expanded section is generally added to quickly decrease the fluidizing gas velocity causing the particles to fall back into the bed.

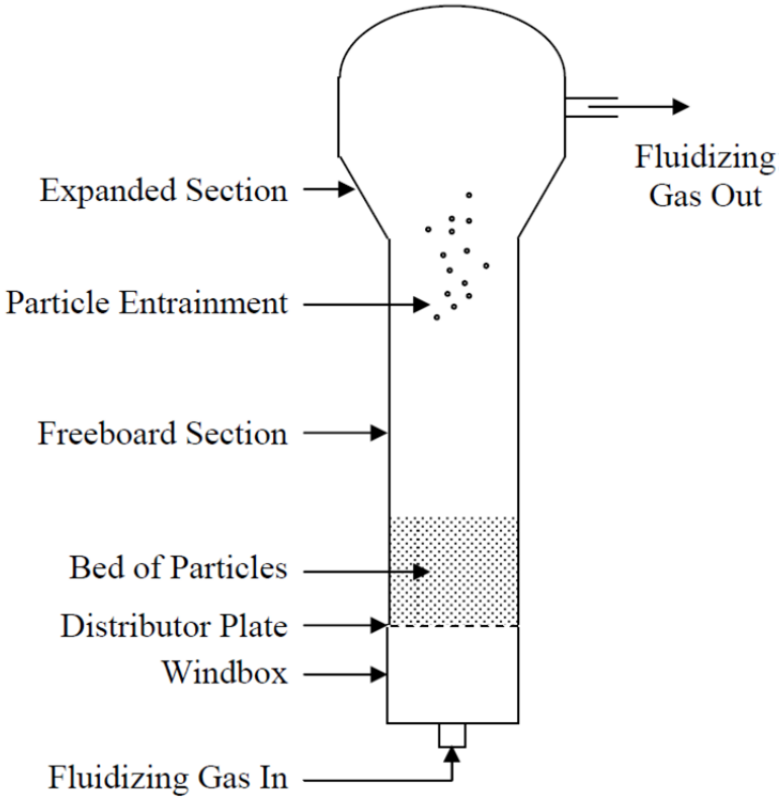


Figure 1.1: Schematic of a typical gas-solid fluidized bed.

1.1.1. Particle Force Balance

A general force balance on an electrostatically neutral particle within a fluidized bed, neglecting wall effects and the presence of other particles, is shown in Figure 1.2. When a gas is passed upwards through a bed of particles, at a high enough velocity, the drag force ($\vec{F}_d$) and buoyant force ($\vec{F}_b$) will be balanced with the gravitational force ($\vec{F}_g$) and, thus the particles will enter a fluidized state (Kunii and Levenspiel, 1991).

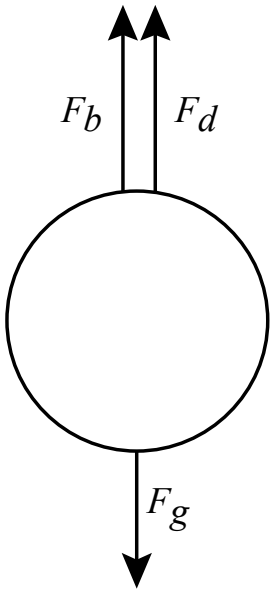


Figure 1.2: Force balance on an electrically neutral particle within a fluidized bed.

The drag force can be calculated from Equation 1.1.

$$\vec{F}_d = \frac{1}{2} C_d \rho_f u^2 A \qquad [1.1]$$

where ρ_f is the fluid density (kg/m^3), u is the superficial fluid velocity (m/s), A is the projected cross sectional area of the particle (m^2) and C_d is the unitless drag coefficient which is a function of the particle Reynolds number (Re_P). There are numerous correlations to determine the drag coefficient. Haider and Levenspiel (1989) provide an empirical correlation of the drag coefficient based on of Re_P as shown in Equation 1.2.

$$C_d = \frac{24}{Re_P}\left[1 + \left(8.1716e^{-4.0655\phi}\right)Re_P^{0.0964+0.5565\phi}\right] + \frac{73.69\left(e^{-5.0748\phi}\right)Re_P}{Re_P + 5.378e^{6.2122\phi}} \qquad [1.2]$$

where ϕ is the sphericity of the particle and Re_P is defined in Equation 1.3.

$$Re_P = \frac{\rho_f u d_P}{\mu} \quad [1.3]$$

where d_P is the diameter of the particle (m) and μ is the viscosity of the fluid (kg/m·s). The buoyant force exerted on the particle is calculated as per Equation 1.4.

$$\vec{F}_b = \rho_f V_P g \quad [1.4]$$

where V_P is the volume of a single particle (m^3) and g is the gravitational force constant (9.81 m/s^2). Similarly gravitational force on the particle is shown in Equation 1.5.

$$\vec{F}_g = \rho_P V_P g \quad [1.5]$$

Assuming a spherical particle, Equations 1.1, 1.3, and 1.4 respectively become:

$$\vec{F}_d = \frac{\pi}{8} C_d \rho_f u^2 d_P^2 \quad [1.6]$$

$$\vec{F}_b = \frac{\pi}{6} \rho_f g d_P^3 \quad [1.7]$$

$$\vec{F}_g = \frac{\pi}{6} \rho_P g d_P^3 \quad [1.8]$$

A balance with the above forces can now be performed. Combining Equations 1.6 to 1.8 into a ratio of the upward forces (drag and buoyant) over the downward forces (gravitational) yields R_F (Equation 1.9).

$$R_F = \frac{\vec{F}_d + \vec{F}_b}{\vec{F}_g} = \frac{\rho_f \left(\frac{3}{4} C_d u^2 + g d_P\right)}{\rho_P g d_P} \qquad [1.9]$$

Assuming spherical single particles and constant ρ_f and ρ_P, Equation 1.9 can be plotted for different particle size and gas velocities where $R_F = 1$ would be the point of minimum fluidization (Figure 1.3).

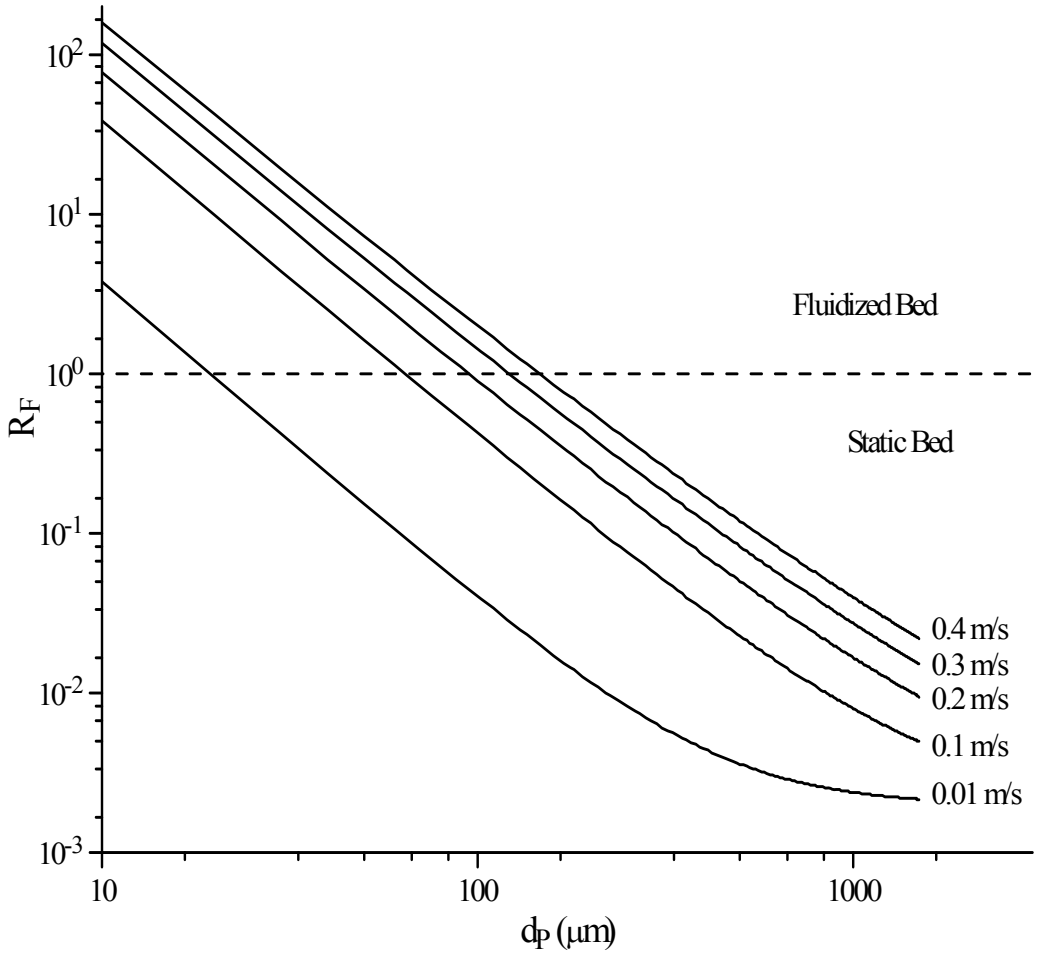


Figure 1.3: The ratio of drag and buoyant forces over the gravitational force on a neutral particle for varying particle size and fluidizing gas velocity.

Increasing the size of the particle increases the magnitude of gravitational force faster than the drag force requiring a larger gas velocity to fluidize the particles. This force balance was based on a single particle using the superficial gas velocity. In a gas-solid fluidized bed the velocity around a single particle will be larger due to the interstitial gas velocity which will be based on

the bed void fraction. This will subsequently reduce the superficial gas velocity required to fluidize a bed of particles. Once this minimum velocity is obtained, the particles show fluid-like properties and the gas velocity at this state is referred to as the minimum fluidization velocity (u_{mf}). Increasing the gas velocity beyond minimum fluidization changes the hydrodynamics of the bed leading to different fluidization flow regimes (Figure 1.4). Past minimum fluidization, the excess gas forms bubbles, which rise to the top of the bed and burst. If the gas velocity is further increased, the bubble sizes increase until the bubble diameters reach half of the column diameter (axial slugs) or become equal to the column diameter (flat slugs). Turbulent fluidization and pneumatic transport (lean phase fluidization) regimes are attained if the fluidizing gas velocity is further increased.

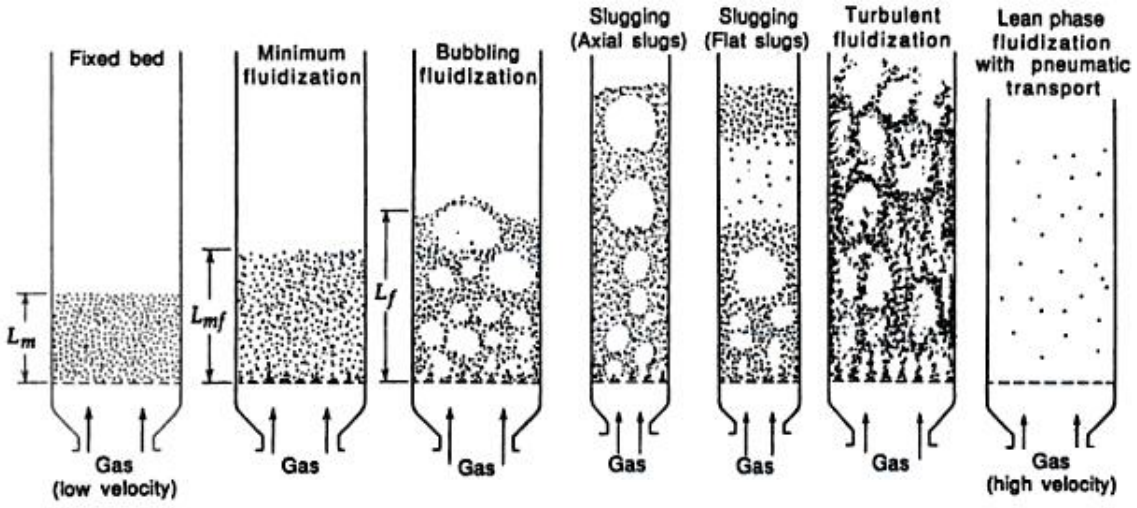


Figure 1.4: Different fluidization flow regimes formed with increasing fluidizing gas velocity (adapted from Kunii and Levenspiel, 1991).

As shown in the equations above, the minimum fluidization velocity is a function of the fluidizing gas properties, as well as the particle size and density.

Some particles are easily fluidizable while others are cohesive and have proven to be difficult to substantially fluidize. The most common classification for particles is found by Geldart (1973) as shown graphically in Figure 1.5, which separates particles into four distinct groups based on their diameter and density. Each group behaves differently in a gas-solid fluidized bed. Table 1.1 summarizes some of the key differences.

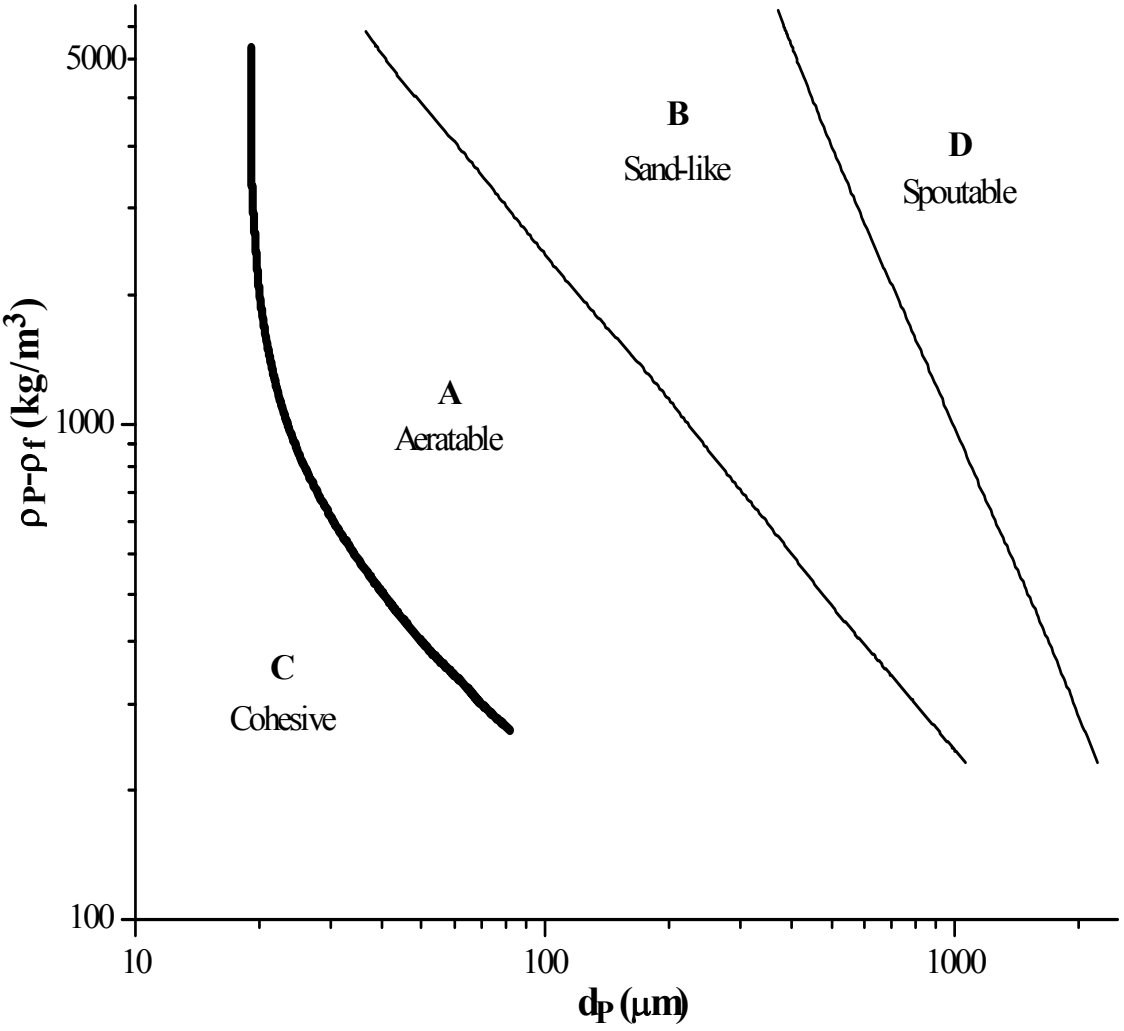


Figure 1.5: The graphical representation of the Geldart classification of particles (adapted from Kunii and Levenspiel, 1991).

Table 1.1: Geldart Particles Classification (adapted from Gupta and Sathiyamoorthy, 1999; Geldart, 1973).

	Geldart Group			
	A Aeratable	**B** Sandlike	**C** Cohesive	**D** Spoutable
Particle Size (μm)	300-100	40-500	< 60	> 500
Density (kg/m^3)	< 1400	1400-4000	< 1400	> 1400
Expansion	Large even before bubbling	Small	Difficult to fluidize	Particles are spoutable and therefore behave like a spouted bed
Mixing	Rapid even with few bubbles	Little in the absence of bubbles	Poorer than Groups A and B	Relatively very poor
Slugging	Slugs produced at high superficial gas velocity and break	Slugs have no evidence of breakdown	Difficult to produce slugs	Particles behave as a spoutable bed, therefore no slugging present

1.1.2. Example of Industrial Process

One of the industrial applications of gas-phase fluidization is in catalytic polymerization of polyethylene (Figure 1.6) which has been carried out as early as the 1980s (Fulks et al., 1985, Goode et al., 1989). In these reactors, the catalyst particles (usually Ziegler-Natta or metallocene catalysts) are injected into the fluidization column directly into the bed of fluidizing particles (polyethylene particles) with an inert gas such as nitrogen. These catalyst particles are then fluidized by dry ethylene gas, co-monomer and hydrogen with a balance of nitrogen, which undergoes a chain polymerization reaction to form polyethylene particles. The highly exothermic reaction occurs on the surface of the catalyst particle where the polymer chains continue to grow into a larger polyethylene granule, resulting in each polyethylene particle containing the catalyst at its core, with some other catalyst fragments throughout the growing polyethylene particle. The unreacted catalyst particles are entrained from the bed with the ethylene gas and recirculate through the system several times before being completely spent. The gas is then cooled through a heat exchanger (HE) prior to mixing with make-up feed gas and re-entering the fluidized bed.

The product is preferably withdrawn from the column close to the distributor plate (Fulks et al., 1985). Previously, such reactors were operated under steady-state conditions with operating temperatures and pressures ranging from 70 °C to 100 °C and 0.55 MPa to 0.76 MPa, respectively (Chirillo et al., 1989), but with newer technologies and types of catalysts, the operating pressures between 0.69 MPa to 3.4 MPa with temperatures ranging between 30 °C to 120 °C are applied (Hagerty et al., 2007).

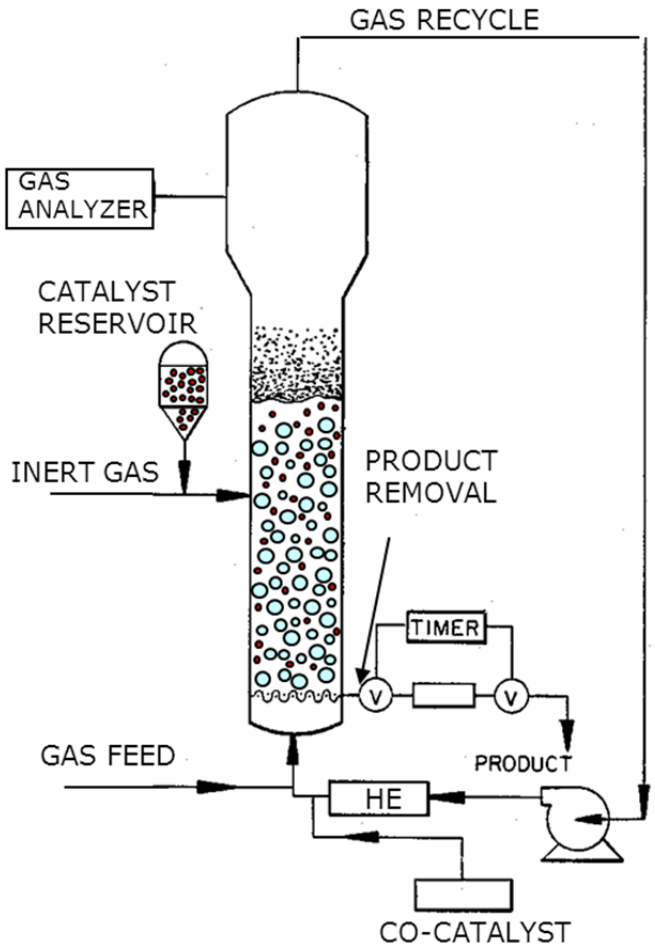


Figure 1.6: An industrial example of a gas-solid fluidized bed reactor for the catalytic polymerization of polyethylene (adapted from Goode et al., 1989).

1.2. Electrostatic Charge Generation

When objects come into contact with each other, electrons and/or ions could migrate from one solid to the other resulting in electrostatic charge generation. In gas-solid fluidization, the charging mechanisms are usually dominated by triboelectrification through contact, and

frictional charging. Induction charging can also be present in such systems when the fluidization column is made of a conductive material. It is important to mention that it has been found that there is a maximum limit to the surface charge that solid objects can obtain in air. If the surface charge of a material approaches $2.6x10^{-5}$ C/m^2, then the surrounding air will break down and ionize, thus neutralizing some of the charges on the surface of the material (Cross, 1987).

1.2.1. Electrostatic Charging Mechanisms

Even though some of the charge generation mechanisms are known, the actual species that are being transferred are not well understood. There are three main theories of charge transfer between solids: electron transfer, ion transfer, and material transfer.

The electron transfer is believed to be the mechanism involved with triboelectrification between two conductive surfaces (Lacks and Sankaran, 2011). It has been shown that the amount of charge transferred is proportional to the contact potential, which in turn is related to the difference in objects work functions as shown in Figure 1.7 (Harper, 1967; Lowell and Rose-Innes, 1980). The work function, φ, is defined as the minimum energy, measured in eV, necessary to give an electron to be able to release it from the surface of a solid, or in other words the energy required to move an electron from the Fermi energy level into vacuum (Cross, 1987). The Fermi level is the energy level that has a 50% chance of being occupied by an electron (Cross et al., 1987).

When the metals are in contact, the electrons are transferred from the surface with the lower work function to that with the higher work function. However, with insulators this effect is generally less predictable. There have been studies that determined the effective work function of insulators in attempts to correlate electron transfer to the work function of the material (Davies, 1969; Trigwell et al., 2001). However, the electron mobility in an insulator is low due to the large amount of energy required for an electron to enter the conductive energy level, and therefore the work function of insulators are more difficult to be quantified (Cross, 1987). Lowell and Truscott (1986) concluded that there are always defects in insulators that allow for some electrons to exist at high energy levels and can remain in this elevated state for extended periods of time. These high level energies would contribute to the charge transfer between two surfaces.

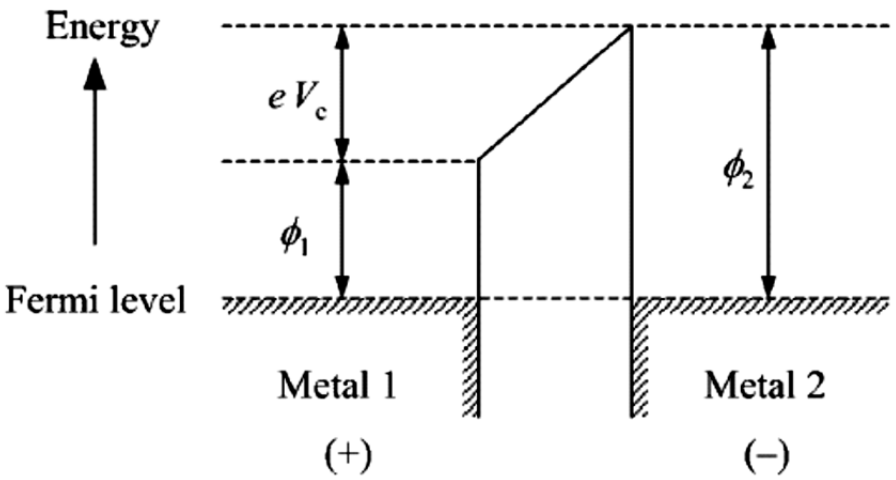


Figure 1.7: The work function, φ, of two different metals 1 and 2, where e is the elementary charge and V_c is the contact potential (copied from Matsusaka and Masuda, 2003).

In some cases with insulating materials, mobile ions are present which can transfer between surfaces. If the ions close to the surface of the material are loosely bound, then it is possible that oppositely charged ions on the other surface can attract and detach them from the material. Fenzel-Alexander et al. (1994) were able to control the amount of loosely bounded ions in a polymer-ionomer system and showed a direct correlation in the ion concentration to the polarity and charge of the polymer (Figure 1.8). McCarty et al., (2007) found similar and more predictable results using polystyrene microspheres.

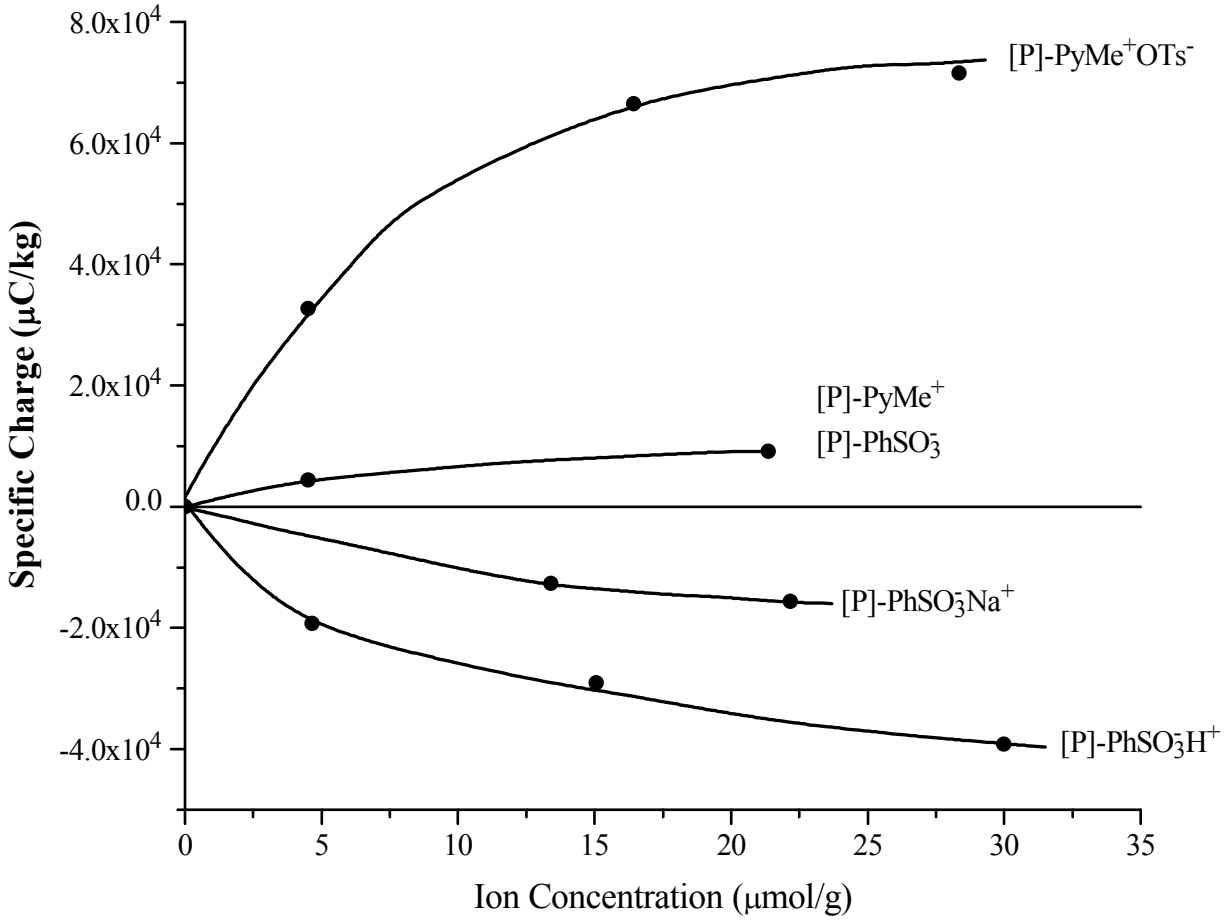


Figure 1.8: The relationship between the specific charge and total ion concentration for different polymer blends (copied from Fenzel-Alexander et al., 1994).

With the material transfer mechanism, when two materials come into contact, for example Material A and Material B, minute pieces of material from Material A transfers onto the surface of Material B, or vice versa. At first such mechanism was generally believed not to be likely (Lowell and Rose-Innes, 1980), but recent research has shown that this is likely possible in some cases (Baytekin et al., 2011; Williams, 2012). Baytekin et al. (2011) was able to show that when two small flat pieces of same polymeric material were contacted together, although one would predominantly charge positive and the other negative, there still existed positive and negative regions on each surface (Figure 1.9). Therefore the surface of polymers was bi-polar in nature. If the two surfaces come into contact with each other, there is a chance that a positively charged region comes into contact with a negatively charged region, which can lead to break-off and transfer of material.

Currently it is unclear as which of these mechanisms is the dominating force for electrostatic charge generation and whether it is possible that all three can occur simultaneously (Williams, 2012).

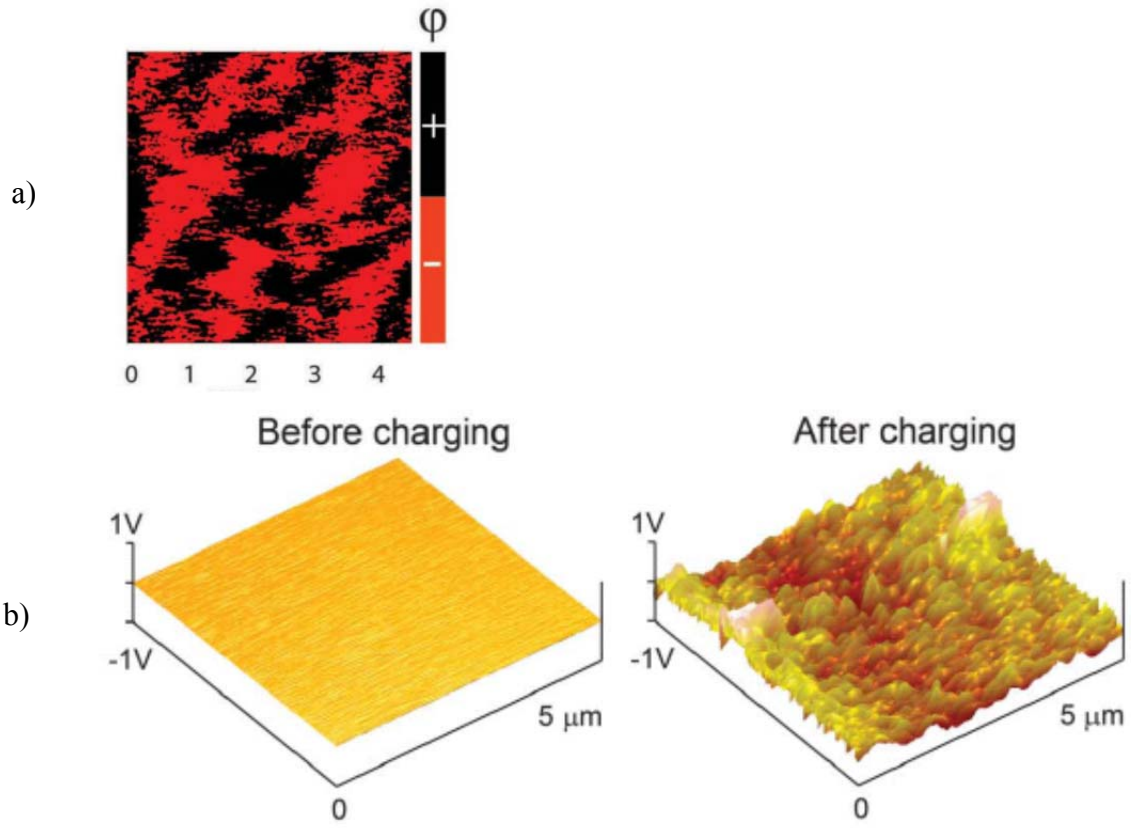


Figure 1.9: a) An example of surface electric potential using kelvin probe force microscopy (KFM), and b) Surface potential of polydimethylsiloxane (PDMS) before and after contact charging (copied from Baytekin et al., 2011).

1.2.1.1. Contact Charging

Contact charging or triboelectrification occurs when two solids come into contact with each other, electrons are transferred from one surface to another, forming a double electric layer (Figure 1.10). This is due to the difference in the initial Fermi energy levels of the materials at the point of contact. At this point, if the electrostatic and van der Waals forces are stronger than gravitational and/or drag forces, the solids will remain attached (Kisel'nikov et al., 1967), otherwise they will detach with each solid taking one of the layers of the charge (Ciborwoski and Wlodarski, 1962). After separation, the solid that has lost electrons becomes predominantly

positively charged and the one that has gained electrons becomes predominantly negatively charged.

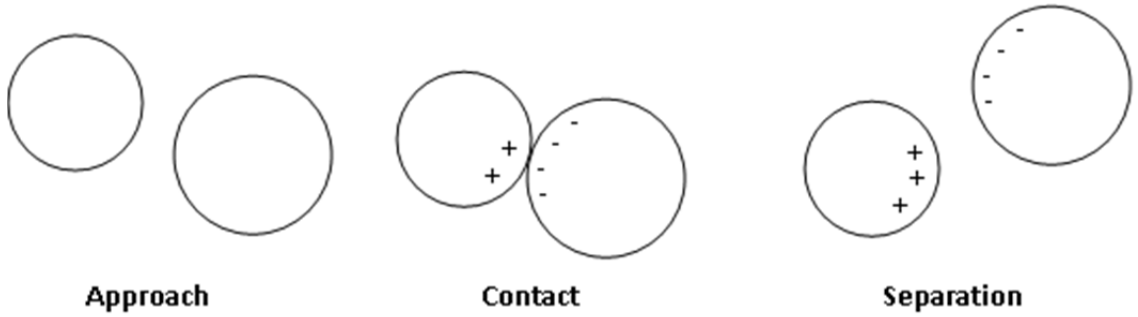


Figure 1.10: The mechanism for contact charging.

The amount of charge transferred between surfaces due to this mechanism depends on numerous factors including the number of electron/ion donor and acceptor sites that exist at or near the surface of both solids (Bailey, 1984). In addition, it is related to the work function of the solids in contact. A material with a higher work function has a higher probability of holding the electrons at its surface when compared to a material with a lower work function. Table 1.2 lists the work function of various materials found by Tanue and Masuda (2006). Since the work function is related to the energy levels on the surface of solids, it can be affected by parameters such as surface impurity or surrounding environment relative humidity and therefore it would be difficult to be accurately measured. Most of such measurements were normally done under vacuum, but inconsistent results on work functions of metals and polymers have still been reported (Cross, 1987).

The charge polarities obtained by different materials as they contact each other have been determined by many researchers and have been arranged in tables referred to as triboelectric series. Triboelectric series (analogous to the electrochemical series of metals) are used to qualitatively predict the charging polarity between two materials, with those located at the top of the table becoming positively charged against any material situated below (Table 1.3). Unfortunately, the order of the materials in atriboelectric series is ambiguous since a number of researchers have also published conflicting series (Cross, 1987). This is due to the fact that the charge polarity of a material can be influenced by different factors such as surface finish,

preconditioning, purity, moisture content, and shape (Cross, 1987; Jones, 1997). The unpredictable nature of solids work function and their surface polarity is one of the reasons why electrostatic charge generation due to contact charging is not very well understood in many systems.

Table 1.2: Work functions of various materials (adapted from Tanue and Masuda, 2006).

Material	Work Function (eV)	Material	Work Function (eV)	Material	Work Function (eV)
Zn	3.63	BaO	1.1	Polyethylene	5.24 ± 0.24
C	4	CaO	1.60 ± 0.2	Polyethylene	6.04 ± 0.47
Al	4.06 – 4.26	Y_2O_3	2	Polypropylene	5.43 ± 0.16
Cu	4.25	No_2O_3	2.3	Polypropylene	5.49 ± 0.34
Ti	4.33	ThO_2	2.54	Polystyrene	4.77 ± 0.20
Cr	4.5	Sm_2O_3	2.8	Polyvinyl chloride	4.86 ± 0.73
Ag	4.52 – 4.74	UO_2	3.15	Poly carbonate	3.85 ± 0.82
Si	4.60 – 4.91	FeO	3.85	PMMA	4.30 ± 0.29
Fe	4.67 – 4.81	SiO_2	5	Polytetrafluoroethylene	6.71 ± 0.26
Co	5	Al_2O_3	4.7	Polyimide	4.36 ± 0.06
Ni	5.05 – 5.35	MgO	4.7	Polyethylene Terephthalate	4.25 ± 0.10
Pt	5.12 – 5.93	ZrO_2	5.8	Nylon66	4.08 ± 0.06
Au	5.31 – 5.47	TiO_2	6.21	Pylex7740	4.84 ± 0.21

Table 1.3: A triboelectic series (adapted from Montgomery, 1959 and Cross, 1987).

	Material	Polymer Type
+	Wool	
	Nylon	
	Viscose	Cellulose
	Cotton	
	Silk	
	Acetate rayon	Cellulose acetate
	Lucite or Perspex	PMMA
	Polyvinyl alcohol	
	Dacron	Copolyester of ethylene glycol and terephthalic acid
	Orlon	Polyacrylonitrile
	PVC	
	Dynel	Copolymer acrylonitrile/vinyl chloride
	Velon	Copolymer vinylidene chloride/vinyl chloride
	Polyethylene	
-	Teflon	PTFE

1.2.1.2. Frictional Charging

Charging by friction is associated with the surfaces of solids being rubbed against each other (Figure 1.11). The frictional force generates thermal energy which results in temperature increase at the contact points between the materials leading to charge transfer (Cross, 1987). Upon the separation of the surfaces, one becomes predominantly positively charged and the other predominantly negatively charged.

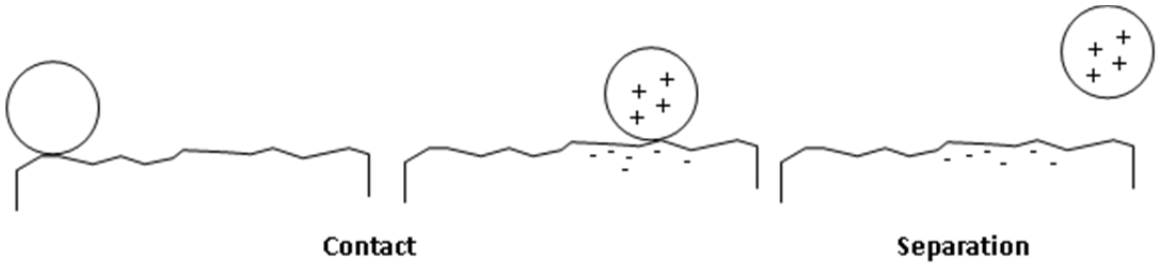


Figure 1.11: The mechanism of frictional charging.

For this mechanism, it has been found that the energy of rubbing (i.e. amount of frictional energy), which is a function of the rubbing pressure, temperature, and velocity, often affects the amount of charge transfer more than the nature of the two materials in contact (Cross, 1987). Montgomery (1959) concluded that charges increase as the rubbing velocity increases. Figure

1.12 presents the same effect clearly shown by Ohara (1979) where they measured the induced voltage from the surface charges of two polymer films rubbed against each other at different velocities, one being stationary and one in motion. It was also reported that the charge polarity of polymers rubbed against a metal can change as the rubbing velocity and temperature vary (Zimmer, 1970; Ohara, 1979; Cross, 1987). In addition, frictional energy to the contact area would ultimately affect the work functions of the materials involved. In many cases the distinction between contact and frictional charging has not been properly reported and has led to some confusing results in the literature (Cross, 1987).

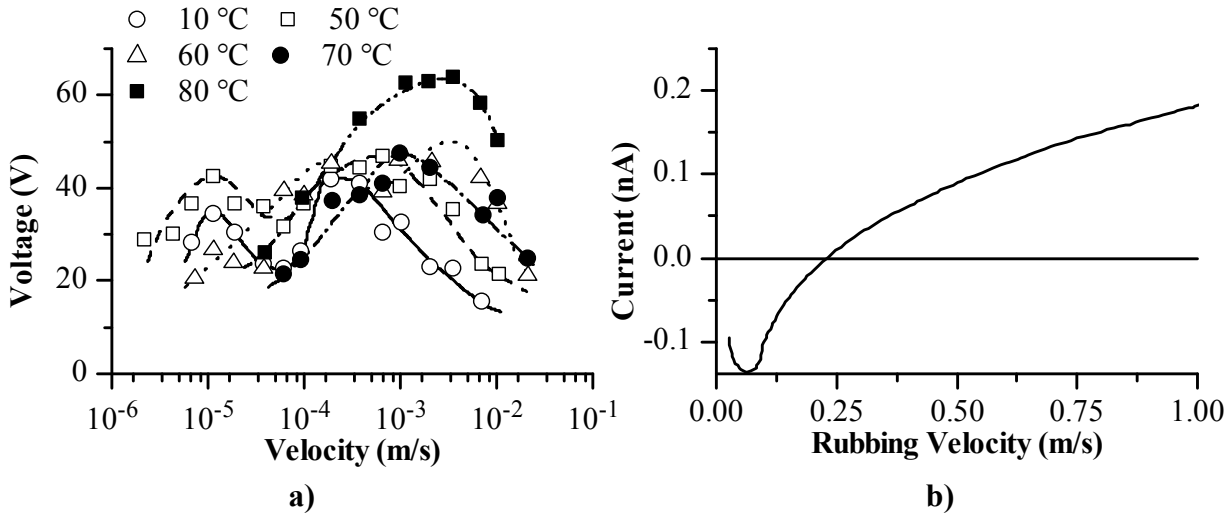


Figure 1.12: a) The effect of rubbing velocity between two polymer films on the voltage output (adapted from Ohara 1979), and b) the change in polarity of polyethylene terephthalate disc rubbed against a metal brush caused by frictional charging (adapted from Cross, 1987 from Zimmer, 1970).

1.2.1.3. Induction Charging

Induction charging occurs when an already charged object comes near a conductive object and its electric field causes the object to become polarized (Figure 1.13). If the charged object is then removed and the conductive object is grounded, the grounded object will be left with a net charge (Cross, 1987). Induction charging is thought to be only applicable to electrically conductive materials (Cross, 1987). Ali et al. (1999), used a metallic fluidized bed found that that some of the insulating fluidized particles charged from tribocharging as well as induction charging provided that the two materials were within proximity of each other for a large amount of time (72 h).

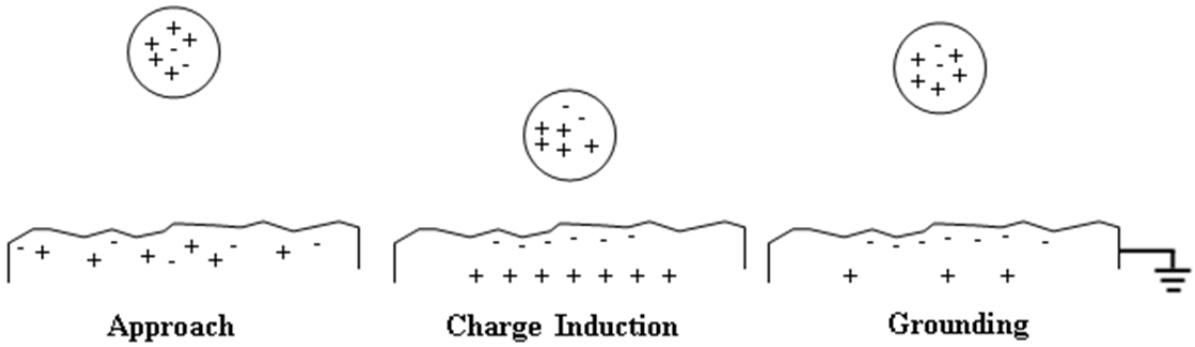


Figure 1.13: The mechanism of induction charging.

1.2.2. Electrostatic Charge Generation Between Similar Insulators

From the above discussion, it is possible to hypothesize that insulators composed of the same material should not generate any electrostatic charge when in contact since the intrinsic properties are the same. However, it has been proven experimentally that this is not the case. Komatsu et al. (2004) fabricated two identical disks of the same polymer and rubbed them together in counter directions and found opposite charging on each disk. This was tested with both polycarbonate (PC) and polyvinyl chloride (PVC). Forward et al. (2009a) used granular particles and constructed an apparatus that caused only particle-particle interactions and found charge segregation within the particles. Pham et al. (2011) used two identical insulator cylinders and rotated one cylinder onto the other stationary surface. This allowed for continuous triboelectrification in a single region on the stationary cylinder and a large charging region on the rotating region. This resulted in an increase in magnitude of the surface potential on the rotating cylinder with an increase in the number of rotations. When Teflon was used the rotations resulted in a positive increase in the surface potential and when Nylon was used, the surface potential had a negative increase with increasing rotations. This is mainly due to asymmetrical charging (where a small surface area is repeatedly contacted with a larger and continuously changing surface), and due to some statistical variations in the actual material surface properties (Lacks and Sankaran, 2011). The statistical variations in identical materials arise from a different number of electron donor states found on each surface. Therefore, as the two surfaces come into contact with each other, even though the materials are the same and would have on average the same amount of electron donor states and the local area of contact, but the balance between electron donor and acceptor states may be different, causing for a net charge transfer.

Such phenomenon has also been observed with particles of different size but of the same material contacting each other (Zhao et al., 2003). The particle size dependency is sometimes attributed to a difference in work functions (Zhao et al., 2003); however, other researchers believe that this is due to the differences in the number of electron donor sites (Lacks and Levandovsky, 2007; Lacks and Sankaran, 2011). Assuming that there is an abundance of electron acceptor sites for all particle sizes, there is a difference in the number of donor sites where the larger the particle would have more donor sites it would have due to an increase in surface area. As particles come into contact with each other, the particles will continue donating electrons to the other surface until there are no more donating sites, but will continuously accept electrons. Since the larger particles have more donor sites, it will on average donate more electrons and therefore become more positively charged, whereas the smaller particles would become more negatively charged (Duff and Lacks, 2008; Lacks and Levandovsky, 2007; Lacks et al., 2008). It should be noted that the opposite trend has also been observed specially with works conducted in gas-solid fluidized beds where entrained fines were found to be positively charged and larger bed particles to be negatively charged (Ali et al., 1999; Mehrani et al., 2005; Giffin and Merhani, 2010; Liu et al., 2010).

1.2.3. Factors Influencing Electrostatic Charging

Electrostatic charging has been known for many centuries, but its mechanisms, especially with contacts such as insulator-conductor and insulator-insulator, are not well understood (Boland and Geldart, 1971/72). One of the main challenges with understanding insulator charging is the unpredictable charging caused by the non-uniform distribution of charge on the surface of these materials (Fasso et al., 1982). Electrostatic charging is a surface phenomenon that only affects 8 in every million surface atoms (Cross, 1987), and even minor variations of the state of the solid surface can lead to large dissimilarities of the magnitude and polarity of their charge (Fujino et al., 1985). Consequently, this makes the prediction of the amount of charging extremely difficult.

Overall, the amount of charge transfer between surfaces in contact can depend on numerous factors including: state of the surface (chemical composition, moisture content, roughness and sphericity), size, the amount of surface charge before contact, environmental conditions (composition, pressure, temperature and relative humidity), presence of electromagnetic fields,

type of contact (touching, impacting, rubbing), orientation of objects during impact, duration of contact and relative velocity of objects (Rojo et al., 1985; Moughrabiah et al., 2009; Ducati et al., 2010; Baytekin et al., 2011). Li and Li (2005) found that surface roughness affects the amount of contact between two objects which can significantly alter the electrical properties of each object. Baytekin et al. (2011) found that the contact pressure and contact time had little effect on the charge transfer between two polymer surfaces.

1.3. Electrostatics in Gas-Solid Fluidized Beds

Due to the very nature of gas-solid fluidized beds (i.e. vigorous mixing of particles inside the bed), it is practically impossible to avoid the generation of electrostatic charges. As early as the 1940s, researchers have encountered electrostatic effects in fluidized beds by observing the adhesion of particles to vessel walls and its influence on the fluidization conditions (Jones, 1997).

Overall in a gas-solid fluidized bed, electrostatic charge generation may be largely caused by three distinct types of interactions:

1. *Particle-Gas Contact:* When the fluidizing gas passes over particles, there is a possibility of charge transfer between the two phases. However, Mehrani et al. (2005), showed that with larger particles (>500 μm), the particle-gas charging was negligible under ambient conditions, provided that the particle does not reach the maximum surface charge where the air breaks downs and ionizes. They also concluded that in all the cases reported to date, the breakdown of air did not occur. This may not hold true at higher pressures; however, no literature has been found reporting on this issue.

2. *Particle-Wall Contact:* Interactions between the particles and the fluidized bed column wall are typically only limited to the particles that are closest to the wall. Both charging mechanisms (contact and frictional charging) can occur in this case. However, frictional charging most likely dominates due to the movement of the particles inside the fluidized bed which results in a circular motion with particles

sliding down the reactor wall (Figure 1.14). Overall, particle-wall contact is more prevalent in lab-scale settings where the cross sectional area of the fluidized bed is small.

3. *Particle-Particle Contact:* Interactions between fluidizing particles can occur throughout the fluidization column and are generally dominated by contact charging, though some degree of frictional charging may also occur. In commercial-scale fluidized beds with large cross sectional areas, particle-particle interactions would dominate over those of the particle-wall (Hendrickson, 2006).

Problems associated with fluidized bed electrification can be summarized as: particle-wall adhesion, inter-particle cohesion and electrostatic discharge. Particle adhesion to the fluidization column wall can also effectively alter the bed hydrodynamics, as well as the electrostatic charge generation. Many researchers have reported the presence of particle-column wall adhesion in their work, which was generally performed in dry conditions with transparent non-conducting columns such as Plexiglas (Ciborowski and Wlodarski, 1962; Ham et al., 1992; Guardiola et al., 1992). Poor fluidization of FCC particles in a dry system was also shown to be a direct result of particle-column wall adhesion (Ham et al., 1992). Guardiola et al. (1992) reported that particularly in dry circumstances, the attractive force between particles and the column wall is strong enough to have particles stick to the wall. Fujino et al. (1985), Gajewski (1985), and Revel et al. (2003) concluded that the static electricity in a fluidized bed was largest at the column wall which could lead to particle-wall adhesion. Boland and Geldart, 1971/72 stated that the smallest particles and the particles with the greatest specific surface area were the most prone to becoming adhered to the column wall.

An industrial example where the negative effects of electrostatic phenomena are clearly reported is in polymerization fluidized bed reactors. In these types of reactors, when polymer and/or catalyst particles gain electrostatic charge, they can adhere to the reactor wall while the exothermic polymerization reaction continues, causing polymer particles to fuse together and form sheets. The major problem then occurs when these sheets become so large that the gravitational force breaks them off the reactor wall, making them fall to the bottom of the reactor. These sheets can then clog the distributor plate leading to frequent reactor shut down and

clean up. As well, when the sheets break off, it has been found that more electrostatic charges are generated which can subsequently trigger more sheeting (Goode et al., 1989). Sheeting has been categorized as hot and cold sheets. Hot sheets occur when a catalyst particle adheres to the reactor wall and continues with the exothermic polymerization process. At higher temperatures, polymer particles can melt onto the column wall leading to more particles (polymer and catalyst) forming reactor wall sheets (Fulks et al., 1985). Cold sheets occur when a polymer layer is formed on the column wall where the polymer would act as an insulator and lower the temperature near the reactor wall (Goode et al., 1989). Sheets are found to be typically formed at locations approximately half the diameter of the fluidization column above the distributor plate (Goode et al., 1989), where the drag forces along the column wall are at a minimum as shown in Figure 1.14 (Hendrickson, 2006). The sheets typically range from 0.00635 m to 0.0127 m in thickness, 0.0762 m to 0.457 m in width, and 0.305 m to 1.52 m in length (Goode et al., 1989). This corresponds to sheets that are a few square centimeters to a few square meters large (Hendrickson, 2006). Two types of sheeting are typically known based on their location, wall and dome sheeting (Figure 1.14). Dome sheeting is also called drooling and occurs when molten polymer adheres to the dome of the reactor. The drool can fall down into the reactor and onto the distributor plate causing some fouling problems (Hendrickson, 2006).

It has been reported that the first signs of sheeting can occur only after the production of 6 to 10 times the weight of the bed in the reactor (Hagerty et al., 2005) or in as little as half a day of production (Yamaguchi et al., 1995). Goode et al. (1989) reported that a pilot-scale reactor had to be shut down after only 59 hours of operation because of reactor wall sheeting. A common sign indicating the onset of sheeting in a polymerization reactor is when the skin temperature measured by thermocouples at the reactor wall deviates from the reactor bed temperature up to 20°C (Song et al., 2005). However, by this time it is usually too late to save the reactor. Some companies have measured the voltage in a gas-solid fluidized bed, but the voltage can be difficult to interpret because of sheeting since it can start very locally but can spread quickly throughout the reactor (Chirillo et al., 1989).

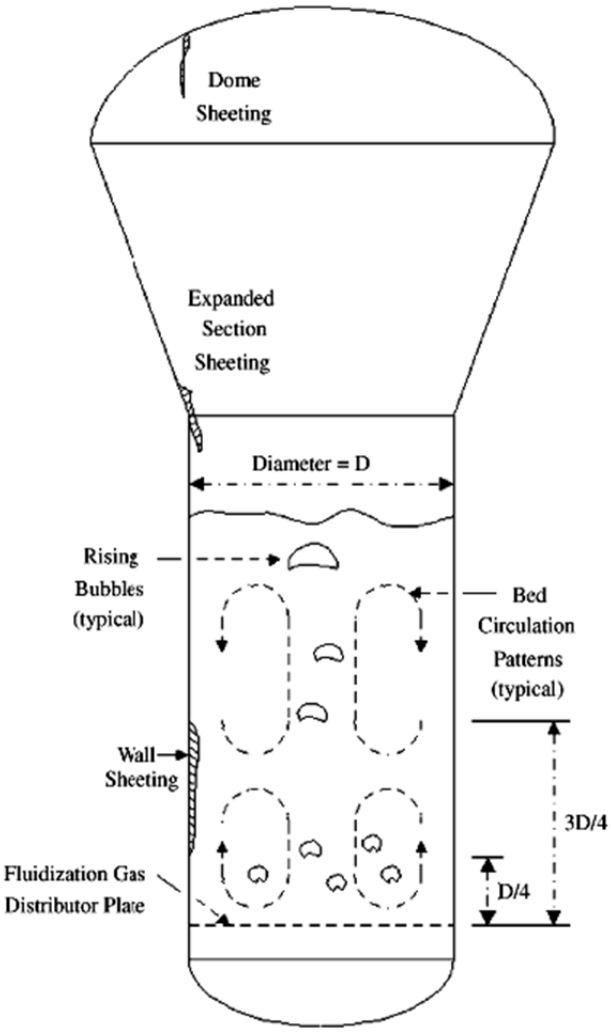


Figure 1.14: Industrial polyethylene gas-solid fluidized bed reactor showing the locations of sheeting formation (adapted from Hendrickson, 2006).

1.3.1. Attractive/Repulsive Forces

The adhesive and repulsive forces within a gas-solid fluidized bed are often neglected. The van der Waals, electrostatic and image forces all have an impact on particles motion inside a fluidized bed. A force balance including drag, buoyancy, and gravitational forces on a particle in a gas-solid fluidized bed is shown in Figure 1.15 and described in detail in the following sections. The particle is assumed to have either a negative or a positive charge.

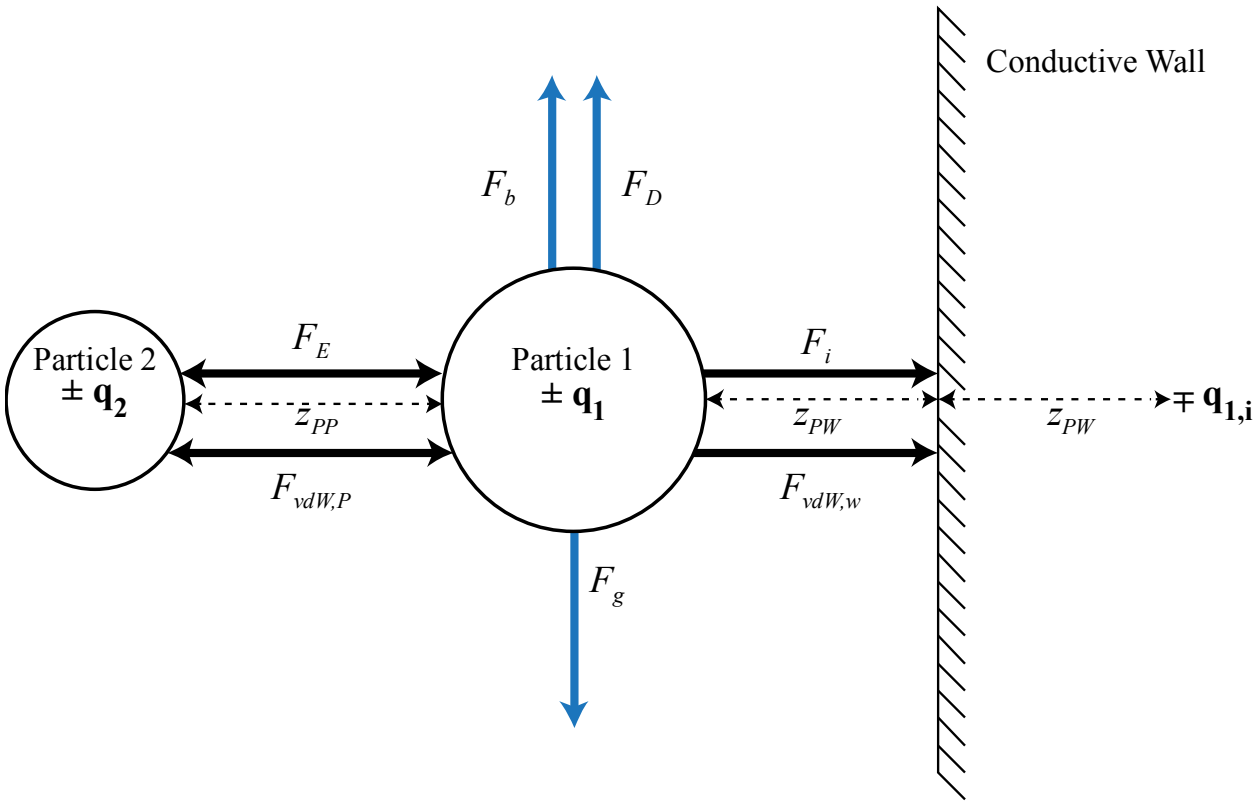


Figure 1.15: The force balance on a single particle (with an either positive or negative charge of q) inside a gas-solid fluidized bed with a conductive wall where $q_{1,i}$ is the image charge on the conductive surface.

1.3.1.1. Electrostatic Force

The electrostatic force ($\vec{F}_E$) between two point charges, r distance apart, can be expressed with Coulomb's Law as shown in Equation 1.10.

$$\vec{F}_E = \frac{q_1 q_2}{4\pi\varepsilon_f r^2} \qquad [\,1.10\,]$$

where q_1 and q_2 are the charges on the two particles (C), the particles, ε_f is the permittivity of the medium or fluid (F/m). Assuming that the size of the particles is similar and if the particles are in contact with each other with the gap between the particles being much smaller than their diameter, the electrostatic force can be shown by Equation 1.11 (Masuda et al., 2006).

$$\vec{F}_E = \frac{\pi\sigma_1\sigma_2}{\varepsilon_f} d_P^2 \qquad [\ 1.11\ ]$$

where σ_1 and σ_2 are the surface charge densities of the particles (C/m^2). For two equally sized particles of same material in contact with each other, the electrostatic force takes the form shown in Equation 1.12 (Feng, 2000).

$$\vec{F}_E = \frac{q_2^2}{4\pi\varepsilon_f d_P^2}\left\{\alpha\left[\left(\frac{q_1}{q_2}\right)^2 + 1\right] - \beta\frac{q_1}{q_2}\right\} \qquad [\ 1.12\ ]$$

where α and β are material specific parameters (Valverde et al., 2008). The parameters α and β are usually calculated using the Galerkin finite-element method based on the permittivity of the spheres (Feng, 2000). For example $\alpha \cong 0.25$ and $\beta \cong 1.3$ for amorphous silica assuming that the permittivity of the spheres was 3.36×10^{-11} F/m (Valverde et al., 2008).

1.3.1.2. Image Force

As a charged object approaches a conductive surface, the charge of the object projects an image onto the surface and acts as an attractive force to the surface that can be calculated by Equation 1.13 (Masuda et al., 2006).

$$\vec{F}_i = \frac{1}{4\pi\varepsilon_f}\,\frac{\varepsilon_w - \varepsilon_f}{\varepsilon_w + \varepsilon_f}\,\frac{q_1^2}{(2z_{PW})^2} \qquad [\ 1.13\ ]$$

where q_1 is the charge of the particle, z_{PW} is the distance between the particle and the wall (m), and ε_w is the permittivity of the wall material (F/m).

The image force is considered when the fluidization column wall is made of an electrically conductive material (e.g., carbon steel). For a conductive material where $\varepsilon_w = \infty$, taking the limit of ε_w approaches infinity yields.

$$\vec{F}_i = \frac{q_1^2}{4\pi\varepsilon_f(2z_{PW})^2} \quad [1.14]$$

1.3.1.3. The van der Waals Force

The van der Waals forces on particles are due to the interactions of fluctuating dipole fields (Gady et al., 1996; Valverde et al., 2008). The van der Waals force between different sized particles ($\vec{F}_{vdw,P}$) is shown in Equation 1.15.

$$\vec{F}_{vdw,P} = \frac{Ad_{P1}d_{P2}}{12(d_{P1}+d_{P2})z_{PP}^2} \quad [1.15]$$

where A is the Hamaker constant (J), and z_{PP} is minimum intermolecular distance between the two particle surfaces (m). For most solids the Hamaker constant is approximately 10^{-19} J and the minimum intermolecular distance is approximately 3×10^{-10} to 4×10^{-10} m (Valverde et al., 2008). Assuming that particles are of equal size, the above equation can be simplified to Equation 1.16.

$$\vec{F}_{vdW,P} = \frac{Ad_P}{24z_{PP}^2} \quad [1.16]$$

The van der Waals force between a single particle and the fluidization column wall ($\vec{F}_{vdW,w}$) is shown in Equation 1.17.

$$\vec{F}_{vdW,w} = \frac{Ad_P}{24z_{PW}^2} \quad [1.17]$$

Due to the short range of molecular interaction, the van der Waals must be determined by the local radius of curvature at the surface asperities at the contact point (Valverde et al., 2009). Therefore the d_P of the above equations must be replaced with the size of the surface

asperities, d_a. A typical value for d_a is approximately 0.2 μm for powders (Schaeffer et al., 1995) and is independent of particle size (Valverde et al., 2008).

1.3.1.4. Summary

Using Figure 1.15 as a reference and assuming that the charge of each particle can be expressed as a point charge and that Particles 1 and 2 are equally charged and sized, the above force equations become:

$$\vec{F}_E = \frac{q_1^2}{4\pi\varepsilon_f(d_P + z_{PP})^2} \quad [\ 1.18\ ]$$

$$\vec{F}_i = \frac{q_1^2}{4\pi\varepsilon_f(d_P + 2z_{PW})^2} \quad [\ 1.19\ ]$$

$$\vec{F}_{vdW,P} = \frac{Ad_P}{24(d_P + z_{PP})^2} \quad [\ 1.20\ ]$$

$$\vec{F}_{vdW,w} = \frac{Ad_P}{12\left(\frac{d_P}{2} + z_{PW}\right)^2} \quad [\ 1.21\ ]$$

The charge of the particles can be estimated by the specific charge of the particles found in this work using Equation 1.22.

$$q = \frac{\pi}{6}\left(\frac{q}{m}\right)\rho_P d_P^3 \quad [\ 1.22\ ]$$

With equal sized particles Equations 1.18 and 1.19 become

$$\vec{F}_E = \frac{\pi \rho_P^2 d_P^6 \left(\frac{q}{m}\right)_1^2}{144 \varepsilon_f (d_P + z_{PP})^2} \quad [\ 1.23\ ]$$

$$\vec{F}_i = \frac{\pi \rho_P^2 d_P^6 \left(\frac{q}{m}\right)_1^2}{144 \varepsilon_f (d_P + 2z_{PW})^2} \quad [\ 1.24\ ]$$

Normally the adhesive forces are divided by the weight of the particle (Equation 1.8) to obtain the granular Bond number (Bo) which is a measure of the particle cohesiveness (Valverde et al., 2008). With a Bond number ≥ 1, the particles have an affinity to aggregate together or adhere to surfaces (Nase et al., 2001). An example of the Bond number for the different forces as a function of particle size is plotted in Figure 1.16. It should be noted that the column wall can also become charged with the continuous contact of particles; however, the measure of charge density of the wall would be difficult to measure and therefore is not included in the adhesive force balance described above.

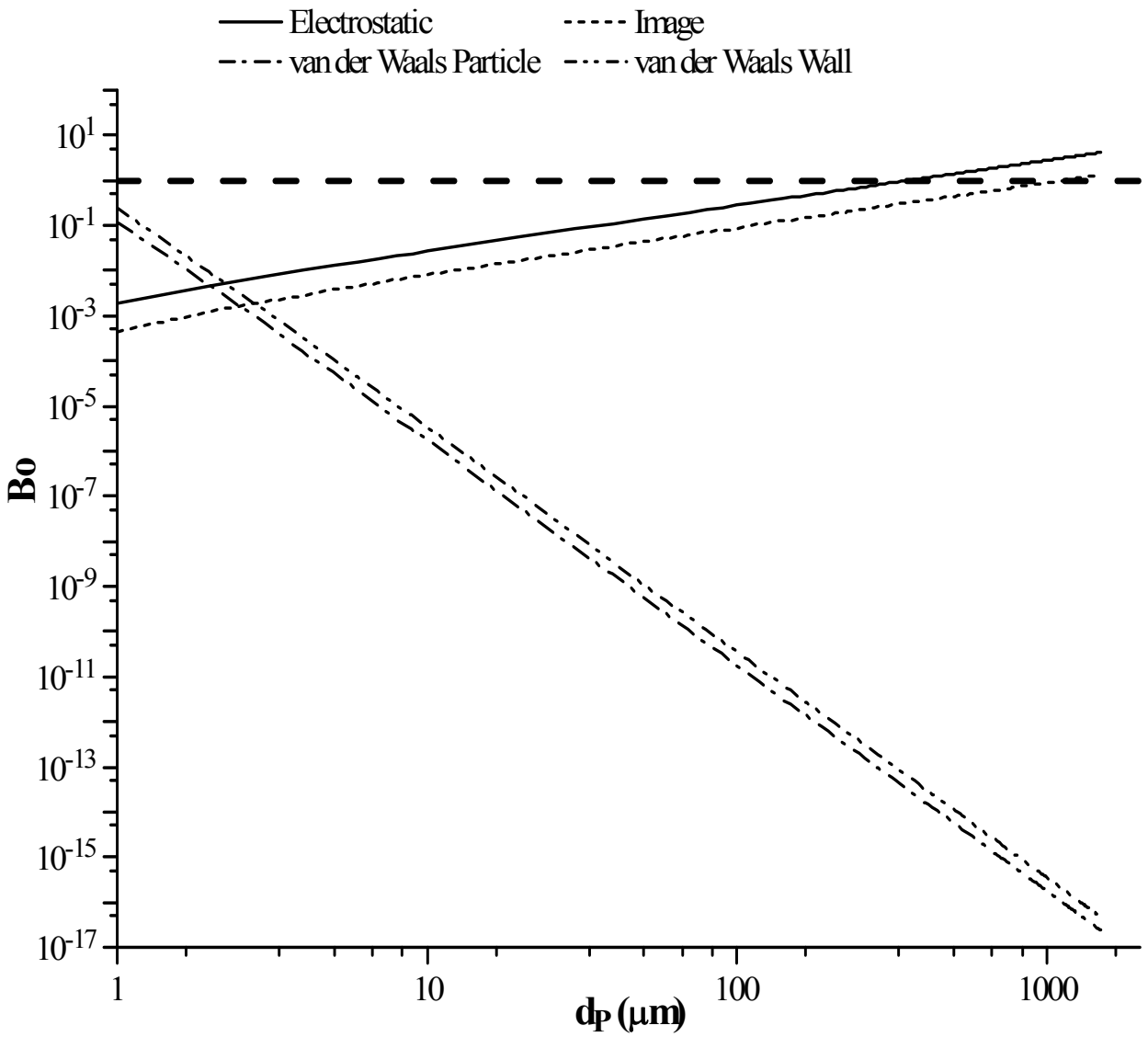


Figure 1.16: The Bond number as a function of particle size for the electrostatic force, image force, and van der Waals forces.

From Figure 1.16, it is clear that the electrostatic and image forces have large impacts on particles that are approximately greater than 250 μm. However, the van der Waals forces would not have a significant effect for particle sizes greater than 5 μm. Hendrickson (2006) stated that these forces can be relatively equal for a particle size up to approximately 150 μm but the van der Waals forces generally do not play an important role in gas-solid fluidized beds unless the particles are Geldart Group C particles.

Although these attractive and repulsive forces are present inside a gas-solid fluidized bed, their actual calculation on every single particle within the bed is nearly impossible due to the

following reasons. Firstly, the electrostatic force on every single particle will be affected by all other particles surrounding it, where each of these particles has their own charge and distance. Secondly, the distance between each particle and the column wall cannot be easily measured and therefore the image force cannot be computed. Regardless of their computation, these forces are ever present in a gas-solid fluidized bed and will directly influence particle motion, agglomeration, and particle-wall adhesion.

1.4. Quantification of Electrostatic Charge in Gas-Solid Fluidized Beds

Over the years, researchers have attempted to measure the degree of particle charging within gas-solid fluidized beds. Almost all of the measurement techniques employed can be grouped into two categories: electrostatic probes and Faraday cups.

1.4.1. Electrostatic Probes

Electrostatic probes have been used in fluidized beds to measure the cumulative potential inside the reactor, as well as on the reactor walls. The fundamental principle behind this measurement technique is that a real charge induces an image of itself onto a conducting surface such as carbon steel, stainless steel, titanium, platinum, nickel, Monel® alloy, copper, aluminum, etc. (Hagerty et al., 2005). Electrostatic probes are either placed vertically (parallel to the column axis) or horizontally (perpendicular to the column axis) within the fluidization column. These probes can be protruding into the column where the probe comes into contact with particles (contacting probes) or they can be placed on the column wall where they will be shielded by a layer of the wall (non-contacting probes). According to Newton et al. (1999), with contacting probes, the probe can pick up measurements from:

1. Neutral particles hitting the probe (triboelectric charge generation).
2. Charged particles hitting the probe.
3. Charged particles that only come close enough to the probe such that they induce their charge onto the probe.

A non-contacting probe would not be physically present within the bed and, therefore, it can only detect induced charges from particles that are in close proximity.

1.4.1.1. Vertical Probes

Vertical electrostatic probes were extensively used in the earliest works performed on quantifying the degree of electrification in gas-solid fluidized beds. Ciborowski and Wlodarski (1962) built an electrode out of platinum wire shaped as a sphere that was 0.5 mm in diameter and was located in the centre of the bed. It was designed to be moved vertically along the axis of the column (Figure A.1). The probe was connected to an electrometer measuring the voltage inside the bed. Kisel'nikov et al. (1967) measured the electric potential between a copper electrode placed vertically along the axis of the column and the distributor plate (Figure A.2). Bafrnec & Bena (1972) also measured the potential of the bed with a brass probe that was 6 mm in diameter and was placed vertically in the axis of the column at the top of the particles bed (Figure A.3).

Rojo et al. (1985) used a vertical electrostatic probe, but treated the fluidized bed as a capacitor where the copper probe was the positive plate of the capacitor and the distributor was the negative plate (Figure A.4). The authors concluded that the geometry of the set-up had an impact on the voltage reading based on a mathematical interpretation of the fluidized bed. It was shown that the higher the probe was in the bed, the higher was the voltage reading, but not necessarily the net charge of the bed. Fujino et al. (1985) set up a study similar to previous works with a vertical 6 mm diameter probe constructed of brass that was supported by a nylon thread and connected to an electrometer that measured the voltage within the bed and it could be positioned at different heights along the axis of the column (Figure A.5). Guardiola et al. (1992, 1996) used a similar approach to Rojo et al. (1985) by constructing a vertical probe out of copper bar 5 mm in diameter and also measured the potential difference between the probe and the stainless steel distributor plate (Figure A.6). Forward et al. (2009b) used a vertical probe that measured the charge of particles in a specialized fluidized bed. To only measure the effect of particle-particle interactions, a single holed distributor plate was used such that only the particles in the middle of the bed are fluidized. The probe measured the current and was a 3.18 mm stainless steel rod shielded with quarts glass.

1.4.1.2. Horizontal Probes

Tardos and Pfeffer (1980) placed a horizontal nickel probe directly into the centre of the bed and measured the current signal from the system (Figure A.7). Ham et al. (1992) inserted a stainless steel rod horizontally at the top of the bed of particles, but focused on measuring the potential within the bed instead of the current (Figure A.8). This method also was adapted by Park et al. (2002) and Chen et al. (2003) who used a 3.2 mm stainless steel ball probe to measure the voltage of the bed (Figure A.9). Moughrabiah et al. (2009) used eight horizontal 5.3 mm stainless steel ball probes that were placed in pairs at four different heights along the fluidization column (0.15, 0.31, 0.55, and 0.89 m above the distributor plate) and at two different radial positions and measured the cumulative charge (Figure A.10).

All of the horizontal electrostatic probes mentioned above protrude into the bed. Boland and Geldart (1971/1972) constructed a probe that was placed near the surface of the column wall, but did not protrude into the bed (Figure A.11). This non-contacting probe would detect the charge of the particle close to the wall of the column through induction by current measurement.

Recently, Yu et al. (2010) measured the voltage at different heights in a fluidized bed using a 1 mm diameter copper bar and hemisphere horizontal probe. The probe was covered with a Teflon and brass sleeve and inserted at different heights in the bed. Liu et al. (2010) used 7 horizontal probes (two different radius positions at three different heights and one probe above the bed height) in a pressurized gas-solid fluidized bed. The probes used in their system were the same probes as used by Moughrabiah et al. (2009).

The horizontal probes can measure the degree of electrification of a fluidized bed radially; however, they cannot be adjusted vertically unless multiple probes are used similar to those used by Moughrabiah et al. (2009).

1.4.1.3. Industrial Measurement Techniques

There have been numerous patents over the past few decades that have discussed electrostatic measurement techniques for industrial polymerization reactors mainly using electrostatic probes and quantifying the charge generation by the voltage or the current measurement. A group of

patents from Union Carbide Corporation (USA) focused on the voltage reading of a 12.7 mm spherical ball probe protruding horizontally from the reactor column by about 0.0254 m (Fulks et al., 1985; Goode et al., 1989; Chirillo et al., 1989; Song et al., 1995). The probe was located on the reactor wall at approximately half the column diameter (approximately 1.5 to 1.8 m) above the distributor plate (Figure A.12 and Figure A.13). This location was chosen as it had been known to be an area within the fluidized bed that was prone to sheeting (Chirillo et al., 1989).

Newton et al. (1999) proposed that measuring current rather than voltage is a better measure of the degree of bed electrification (Figure A.14). The authors argued that the current is more reproducible than voltage results. As well, electrostatic probes that measure voltage were very fragile because of a layer of ceramic that must be used to resist electrical breakdown. Added safety precautions such as grounding bars and spark/arc protectors must also be used when the voltage is measured. A probe that measures the current does not need any extra safety precautions and can be built for mechanical strength, which is much more suitable for industrial sized gas-solid fluidized beds. Hagerty et al. (2005, 2011) placed electrostatic probes in many locations within a pilot-scale system; in the recycle line, in the upper portion of the bed, in the lower (conventional) portion of the bed, and also on the distributor plate (Figure A.15). The electrostatic probes measured the current and were approximately 0.02 m in diameter for most cases and constructed of carbon steel.

1.4.1.4. Problems with Electrostatic Probes

Most of the research that has been done on quantifying electrostatics in gas solid fluidized beds has focused on the use of electrostatic probes. However, these probes have been known to lose their accuracy as particles can adhere to the tip of the probe as fluidization progresses. Fujino et al. (1985) showed that as more particles adhered to an electrostatic probe, the less accurate the measurement of the probe became (Figure 1.17). Similarly, Guardiola et al. (1996) reported that below a certain relative humidity the electrostatic probe used had particles adhered to it and the results could not be accurately reproduced.

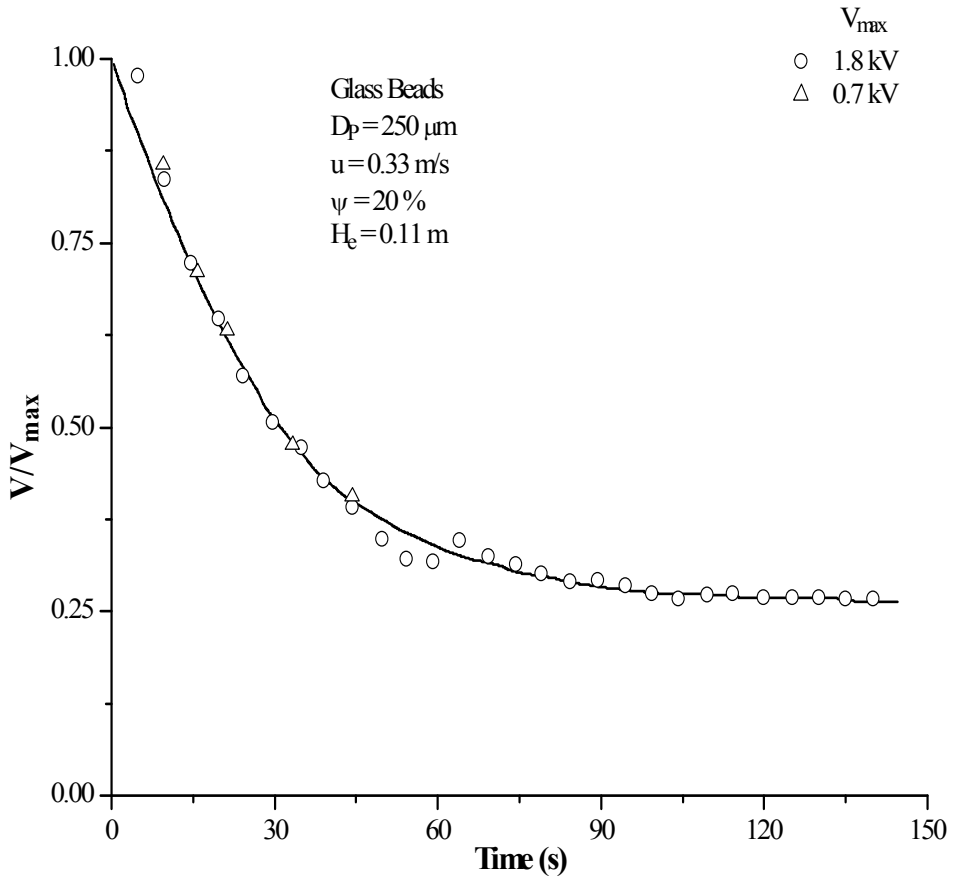


Figure 1.17: The decrease in measurement accuracy due to particle adhesion on the electrostatic probe and a relative humidity (ψ) of 20% and expanded bed height (H_e) of 0.11m (adapted from Fujino et al., 1985).

Many other researchers have also observed particle adhesion to electrostatic probes (Ciborowski and Wlodarski, 1962; Fasso et al., 1982; Fujino et al., 1985; Guariola et al., 1996). Fasso et al. (1982) attempted to construct a parallel plate type of probe to measure the electrostatic potential in the bed but abandoned the project because of high fluctuations in the current measurement caused by a large amount of particles adhered to the plates.

Since most electrostatic probes are placed inside the fluidized bed, they could disturb the bed hydrodynamics (Ham et al., 1992). They can also cause additional charging to particles that come into contact with the probe (Gajewski, 1985; Murtomaa et al., 2003). More importantly it is difficult to actually interpret what the probe is measuring (Gajewski et al., 1985) due to the two phase flow and the motion of the particles (Fujino et al., 1985). Tardos and Pfeffer (1980)

stated that the current recorded by the probe was not reflective of the charge on the surface of particles because the probe also measured the induced charges of particles passing by.

In addition, according to Rojo et al. (1985), the direct measurement of the voltage is not an appropriate way to quantify the electrostatics in the fluidized bed since a higher voltage does not always signify a higher electrostatic charge. An appropriate model is required to convert the voltage into current or charge, and many of the works did not apply the model correctly. Bartilucci et al. (2003) reported that in some cases probes were unable to detect the presence of excessive static electricity most likely because particles coated electrostatic probes during the fluidization process. Thus, they also measured the charge of particle samples with a Faraday cup and compared the results with the electrostatic probes and observed a significant difference in the charge. According to Tardos and Pfeffer (1980), the only real way to measure the charge of fluidizing particles is the direct method of using a Faraday cup.

1.4.2. Faraday Cups

As shown in Figure 1.18a, a Faraday cup is a double walled container where the outer cup is grounded to form an electrical shield from any external fields that could affect the measurement. The inner measurement cup is connected to an electrometer that measures charge by measuring the voltage of the cup across a known capacitor. Between the outer and inner cup an electrically insulating material is placed to resist the flow of charge from the inner cup to the grounded outer cup. When a charged object is placed inside the inner cup, an equal and opposite charge is induced onto the inner wall of this cup, which is transferred and stored on the capacitor inside the electrometer (Figure 1.18b). In other words, the electrometer measures the same polarity and charge as the object placed inside the inner cup (Cross, 1987).

A Faraday cup measures the net charge of the objects present in the cup. Therefore, if there are both positively and negatively charged objects present, the sum of the charges will be measured. As well, any charges that are produced within or by the Faraday cup are not measured because the presence of both positive and negative charges leads to a zero net charge.

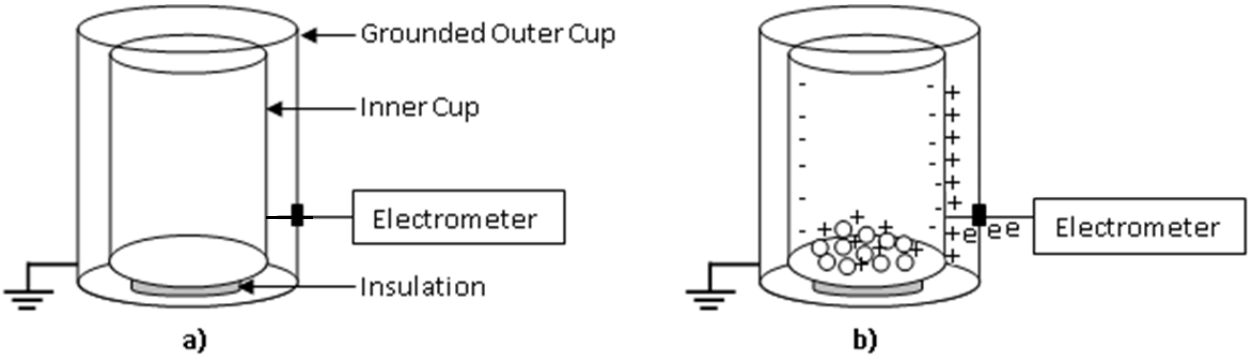


Figure 1.18: Schematics showing a) the components of a Faraday cup, and b) how the Faraday cup measures the charge of an object.

The Faraday cup method has been employed by several researchers to directly measure the net charge build-up inside gas-solid fluidized beds; however, they mainly differ based on their sampling techniques. Tardos and Pfeffer (1980) used a Faraday cup as well as a horizontal probe, which was discussed earlier (Figure A.7). The system involved having a Faraday cup placed below the fluidization column. A tube was placed in the axis of the column with a locking mechanism that was used to open and close the tube so that a sample of bed particles could be removed and fall into the Faraday cup.

Fasso et al. (1982) also used a tube type method to sample particles from the axis of the column in the freeboard area of the bed into the Faraday cup (Figure A.16), but the tube was connected to a vacuum pump to facilitate the removal and collection of the particles. Wolny and Opaliński (1983) employed a similar set-up to sample some particles from the bed, which was transported to an external Faraday cup (Figure A.17).

Ali et al. (1998) employed nine Faraday cups that were placed in a cross formation that crudely mimicked a circle (Figure A.18a). Samples were taken from a fluidized bed with a specially designed scooper and dropped above a grid of Faraday cups (Figure A.18b). The scooper itself was designed to remove a pellet sized group of particles from the bed that would be of similar volume. When the particles were dropped over the grid of Faraday cups, they were separated by the repulsive forces into one of the nine cups. The charge, mass, and size distribution of particles in each Faraday cup was then measured and compared. Ali et al. (1999) used a similar fluidized bed where they utilized the scooper to systematically remove particles from different heights and positions in the bed such as the centre and close to the wall of the column, and place them into an

external Faraday cup. Their method gave insight on the distribution of charge on a wide range of particle sizes within the gas-solid fluidized bed.

Zhao et al. (2000, 2002 and 2003) investigated the distribution of charge on a wide size range of particles. They constructed seven Faraday cups placed vertically, one top of the other, below the fluidization column (Figure A.19). In the centre of the column, a tube was placed that had an array of holes to allow particles to pass through and fall into the Faraday cups below. This system allowed the particles to separate in both vertical and radial directions by the gravitational force, and the repulsive forces caused by electrostatics. Smaller particles settled in the topmost Faraday cups, and larger particles settled in the bottommost Faraday cups. Zhao et al. (2003) used the same apparatus described above, but also included a tube under vacuum similar to Fasso et al. (1982) that would collect any entrained fine particles.

Mehrani et al. (2005 and 2007) took a unique approach and constructed a gas-solid fluidized bed that acted as the inner cup of a Faraday cup (Figure A.20). This system however, was only able to detect charges leaving the Faraday cup fluidization column, either by the fluidizing gas or any entrained particles.

Moughrabiah et al. (2009) constructed a high pressure fluidization column and primarily focused on using horizontal electrostatic probes. They did however, sample some particles from some ports along the column wall and measured their charge by using a Faraday cup. How the samples were taken was not explained in the literature and it is difficult to speculate since it was done at particularly high pressures.

1.4.2.1. Problems with the Faraday Cup Technique

The Faraday cup technique is useful for directly measuring the net charge of a sample of the bed particles, which provides an advantage over the electrostatic probes studied. However, similarly to the electrostatic probes, there are some drawbacks to this technique.

The largest problem that occurs when using Faraday cups, which is practically unavoidable, is the additional charge generation and/or dissipation that could happen during the sampling of the

particles (Rojo et al., 1985). Any contact between particles and other particles, or any device, could lead to unwanted charging and/or discharging; which should ultimately be avoided or at the very least reduced whenever possible (Ham et al., 1992). Some techniques employed a tube sampling system to remove particles from the fluidized bed; however, any internal sampling device would certainly disturb the fluidizing gas flow, fluidization pattern and ultimately the charge build up within the fluidized bed (Tardos and Pfeffer, 1980).

A Faraday cup is useful for measuring the net charge of a sample of the bed particles, however continuously removing samples from the bed decreases the amount of particles within the system over time (Rojo et al., 1985), therefore making it difficult to study the dynamics of the electrostatic charge generation within the fluidized bed (Gajewski, 1985). In addition, if only small samples are taken at certain locations inside the bed, results would provide only a local measurement, which may or may not be representative of the entire fluidized bed (Mehrani et al., 2005). Faraday cups are useful for determining the net charge of a cluster of particles, but if both positive and negative charges are present, then the Faraday cups are ineffective at determining the maximum charge obtained per particle (Hendrickson, 2006).

Faraday cups are in general much more representative of the actual charge of particles, but due to the disadvantages caused by the sampling method, they are normally not applied. As well, due to the probable difficulties with sampling at high pressure, it is typically not employed in an industrial setting.

1.4.3. Other Techniques

There have been a handful of other methods employed by some researchers that were based on the principles of electrostatic probes and Faraday cups. Gajewski (1985) lined a column with 0.015 m wide copper rings spaced 0.005 m apart (Figure A.21). Each ring was able to detect the current induced onto the ring by particles that were adhered to the ring and particles that were in close proximity. This idea was unique, but also had a few drawbacks such as the presence of the rings on the inside of the fluidization column, which would alter the particle-wall contact giving rise to particle-copper ring contact rather than the actual contact with the column wall. More importantly, the rings were only 0.005 m apart, and therefore each ring could have been affected

by the electric field induced by the charged particles above and below each ring, in turn affecting the measured electrostatic profile. This system would also be prone to measurement accuracy problems, similar to electrostatic probes in the case where the particles covered the rings. Finally, the system was only able to measure the current on or close to the wall of the column, which is not particularly useful for large diameter columns where the particle-particle interactions are more of the dominating charging mechanism.

Wolny and Kazmierczak (1989) attempted to measure the charge of only a few particles at a time by placing two vertical plates near the top of the bed (Figure A.22). A pneumatic gun was placed inside the fluidization vessel that could shoot out air and propel a small sample of particles between the plates. The plates acted as a capacitor and therefore the net charge of the particles could be calculated from the voltage measurement. This system was very limited in its application since it could only measure the charge of a few particles at the top of the fluidized bed. In addition, the introduction of a pneumatic gun would severely disrupt the flow and electrostatic charging of particles. This system would not be practical for a fluidization system with entrained particles because these particles would interfere with the measurements.

Murtomaa et al. (2003) created an elevator type ring sensor that remained on the outside of a miniaturized fluidized bed (Figure A.23). The elevator ring was designed to measure the voltage caused by particles close to the column wall by induction. This technique had the advantage of measuring the voltage of the bed at numerous heights without introducing any additional charging or disruption of gas or particle flow. However, since the measurement technique is based on induction, the technique can only measure the charge of the particles close to the column wall, and would not be useful for columns of large diameter, as well as columns constructed out of conductive material.

Valverde et al. (2008) also designed a method that subjected a gas-solid fluidized bed to an electric voltage of 30 kV. The electric field was used to cause the charged nanoparticles (12 nm) to travel to the column wall. They used a high speed camera to track the motion of particle agglomerates. With velocity of the agglomerates measured from the high speed camera, the charges of the agglomerates were estimated indirectly using Stoke's Law. This technique would not be very practical for larger scale fluidization columns with an opaque or conductive column.

As well, introducing an electrostatic voltage across the fluidization column would disrupt the bed hydrodynamics and alter the electrostatic charges generated in the fluidized bed.

1.4.4. Summary

Electrostatic charge generation in gas-solid fluidized beds is unpredictable at times due to the complicated mechanisms involved that is dependent on numerous factors including particle surface physical and chemical properties, column material, fluidizing gas properties, etc. Over the years, researchers have developed different measurement techniques to quantify the degree of bed electrification. However, the comparison of their results is extremely difficult because each system is uniquely different from the rest. Most groups have studied the electrostatic effects in glass columns which, though useful for visual observations, are rarely used in industrial processes. There have also been a wide range of particle materials and sizes that have been investigated with little to no overlapping data. Again, this makes a comparison and an overall understanding of the electrostatic charge generation difficult, leading to some conflicting results. This creates challenged in determining as whether a measurement technique is producing an accurate measurement of particle charging. To be able to fully understand the complete mechanism behind the unwanted charge generation in gas-solid fluidized beds, it is vital that a more thorough and systematic study of electrostatic phenomena is performed with an adequate online measurement technique.

1.5. Parameters Affecting Electrostatic Phenomena in Gas-Solid Fluidized Beds

Although the occurrence of electrostatic phenomena and its negative effects have been reported for many years, the actual mechanism behind the charge generation and dissipation, and the parameters affecting them are still not very well understood. In general, the focus of most academic research and industrial groups has been on two different areas: determining the effect of different parameters on electrostatic charge generation in gas-solid fluidized beds, and the study of different techniques to prevent or reduce this phenomenon.

It is known that charge generation and dissipation within a gas-solid fluidized bed can be affected by a variety of different operating parameters. The following sections summarize the

results reported in literature on the effects of fluidizing gas velocity, particle size and type, and fluidization column diameter and material, the parameters that have also partially been the focus of this thesis. A more detailed literature review of each parameter is provided within Chapter 4.

1.5.1. Fluidizing Gas Velocity

When the fluidizing gas velocity is increased, the particles within the fluidized bed are subjected to more drag force and thus more mixing. The increase in the amount of mixing in turn causes an increase in the particle-particle and particle-wall interactions within the system, leading to an increase in electrostatic charge generation (Ciborowski and Wlodarski, 1962; Kisel'nikov et al., 1967; Bafrnec and Bena, 1972; Fujino et al, 1985; Guardiola et al., 1992, Revel et al., 2003; Moughrabiah et al., 2009; Liu et al., 2010). Bafrnec and Bena (1972) have also mentioned that it is unclear whether the increase in fluidizing gas velocity increases the amount of charge generation, decreases the amount charge dissipation, or both.

The most charge generation of particles is reported to occur around a rising bubble in the fluidized bed since the bubbles cause particle mixing (Hendrickson, 2006). Tardos and Pfeffer (1980) reported that the positive and negative peaks in the measured current within a fluidized bed corresponded to the bubble passage by the electrostatic probe. Park et al. (2002) reported that the difference in the polarity of the current measured in the nose and the wake of a rising bubble signified the different charging mechanisms occurring in these two regions. However, they did not completely describe reasons behind the difference. Park et al. (2002) reported that the larger the bubbles, the higher the charge transfer and charge inducement were within the bed. Similarly, Ali et al. (1999) reported that the measured charge was also significant at the bottom of the bed near the distributor plate where bubbles were first formed. These findings are related to the effect of gas velocity since it affects the bubble size and in turn its rising velocity. Gajewski (1985) and Ham et al. (1992) have reported that the degree of bed electrification reaches a maximum and then starts to decline as the fluidizing gas velocity is increased. They concluded that the reason behind the drop in bed electrification was most likely caused by the onset of slugging. Rojo et al. (1985) and Guardiola (1996) also explained the occurrence of the same phenomenon where there exists a difference in particles motion between the bubbling and slugging fluidization regimes. They explained that in bubbling flow regime, the continuous

formation of gas bubbles and their rise to the surface of the bed creates an extensive amount of particle mixing. Within this regime, the bubble size and the rise velocity increase with increasing gas velocity, resulting in an increase in the amount of charge generation inside the bed. These findings suggest that, for the systems studied, particle-particle interactions generated more charge than particle-wall interactions due to the different behavior of bubbling and slugging flow regimes.

The comparison of bed electrification between bubbling and slugging flow regimes is limited to only four aforementioned papers. These studies, in addition to those focused on the effect of gas velocity in general have their charge measurement limited to only certain regions of the bed and to specific measurement techniques (i.e., mainly electrostatic probes), and to the knowledge of the authors none has provided any information of the magnitude of the reactor wall fouling. Therefore, further investigation in this area is necessary.

1.5.2. Particle Size and Material

Boland and Geldart (1971/72), Fasso et al. (1982) and Guardiola et al. (1996) all using electrostatic probes observed that as the mean fluidizing particle size increased, so too did the degree of bed electrification. Gajewski (1985) reported a similar trend up to a particle size of 2.5 mm, before the degree of electrification decreased. These findings were all for mono-sized particle systems; however, when a large range of particle sizes is present, which is common in polymerization fluidized bed reactors, the charging would be more complicated as it leads to what is known as bi-polar charging. Bi-polar charging occurs when particles of the same material can be either charge positively or negatively within the same bed of particles. Ali et al. (1998) showed that bi-polar charging is related to the particle size. This was later reproduced by Zhao et al. (2002) and Mehrani et al. (2005) in two different fluidization systems. Zhao et al. (2002) reported that an increase in particle size led to an increase from negatively to positively charged particles for a wide particle size distribution. Zhao et al. (2003) proposed that bi-polar charging may be occurring because of a difference in the work functions between larger and smaller particles, or surface impurities may be more prevalent in smaller particles. For instance, they mentioned that if there is a certain concentration of titanium oxide (TiO_2) within those particles, then, assuming that the concentration is constant throughout each particle, it is expected that the

smaller particles would have more TiO_2 at the surface than the larger particles. This could ultimately affect the charge transfer between particles. These researchers also performed some Scanning Electron Microscopy (SEM) analysis on some small and large industrial particles and noticed that the smaller particles had a rougher morphology as compared to the larger particles. Although there has been some lab-scale studies on the possible mechanism of bi-polar charging such as asymmetric charging and statistical variations of surface polarity (discussed in §1.2.1), still further research is required in this area to fully understand the entire mechanism of bi-polar charging within gas-solid fluidized beds and specifically its occurrence and effects in commercial-scale reactors.

The particle size distribution and density will dictate the quality of the fluidization and the forces that would play a dominant role within the bed. As discussed in §1.1.1, the dominating forces that are typically considered in gas-solid fluidization are drag and gravity. This can be seen through the correlations that estimate important fluidization parameters such as minimum fluidization velocity. However, depending on the system, electrostatic, van der Waals, and image forces could also play an important role. Depending on the particle size, the magnitude of electrostatic forces can be compared to the drag and van der Waals forces within the system (Hendrickson, 2006).

The effect of electrostatics on fine elutriated particles has also been investigated. Tardos and Pfeffer (1980) were the first to detect the charge of the entrained particles leaving the fluidization column. In 1982, Fasso et al. concluded that the amount of electrostatic forces will alter the amount of fine particles that are elutriated. Briens et al. (1992) demonstrated that the entrainment of fine particles out of the bed was directly related to the electrostatic forces. They claimed that if a large amount of electrostatic forces is present in the fluidized bed, then the fines may be trapped within the bed by larger particles and may not be elutriated.

The effect of the material of the particles has not been very well documented in literature mostly because each particle material was studied in a different fluidization system using a different measurement technique. In the rare cases where materials with different surface chemistry, conduction, or morphology were studied with the same fluidization system and measurement techniques, the particle sizes differed between the materials and therefore an accurate

comparison could not be made. The study of fluidizing particle material is of great importance in polymerization gas-solid fluidized beds where a mixture of two types of particles, polymer and catalyst, having completely different surface chemical and physical properties, exists inside the reactor.

1.5.3. Fluidization Column Material

The majority of academic research has focused on utilizing one fluidization column for the study of electrostatics and therefore not much literature could be found on the effect of the fluidization column material and diameter. Kisel'nikov et al. (1967) reported that the electric potential in a glass column was three times higher than the electric potential measured in a metal column. Boland and Geldart (1971/72) have concluded that non-conducting columns such as Perspex possess a lower surface conductivity than conductive materials and therefore the particle-wall interactions are stronger causing more electrostatic charges to be generated. Industrial reactors are usually constructed out of carbon steel (Fulks et al., 1985); however, such column material has hardly been utilized in academic research.

1.5.4. Summary

From different studies, it is evident that the electrostatic charging of particles will be affected by the fluidized bed hydrodynamics (such as fluidizing gas velocity and the particle size distribution). These parameters will influence the amount and the degree of bed mixing and, therefore, could alter the amount of particle-particle and particle-wall interactions, which will then affect the charge generation and dissipation of particles.

It is important to recognize that electrostatic charge generation and bed hydrodynamics are interrelated. The bed hydrodynamics could produce an abundance of charge within the bed and thus strong electrostatic forces which in turn could alter the bed hydrodynamics. Gajewski (1985) commented that electrostatics would potentially change the flow of the gas and subsequently the migration of the materials within the bed. In some cases, such as vinyl polyacetate particles, electrostatic forces within the bed caused channeling and large disturbances in bed hydrodynamics (Ciborowski and Wlodarski, 1962). When the electrostatic and van der Waals forces are stronger than the hydrodynamic forces, they can cause the formation of

agglomerates. These agglomerates will then alter the particle size distribution of the bed by increasing and decreasing the amount of larger and smaller particles, respectively. This would effectively change the bed hydrodynamics (Wolny & Kazmierczak, 1989) and if the fluidized bed is operating at or close to minimum fluidization, the bed could potentially defluidize. If agglomerates are large enough, they may not be able to be sustained by the fluidizing gas and therefore migrate to the bottom of the fluidized bed affecting the distributor plate.

Most of the research in the literature has focused on studying the effect of parameters that are easy to manipulate, such as the fluidizing gas velocity and relative humidity. Very few studies have focused on aspects such as particle size and material, and column material, all of which could play a vital role in electrostatic charge generation in gas-solid fluidized beds. In an industrial setting the particle material, size, and column material are usually set and therefore little work has gone into studying these parameters. However, to fully understand the mechanism behind particle charging in such systems, it is crucial to conduct the investigation in systems as similar as possible to these reactors, and with a single adequate online measurement technique.

1.6. Methods for Controlling Electrostatic Charge Generation

Hendrickson (2006) summarizes the main mechanisms for controlling electrostatic charge generation into three categories:

1. Decreasing the charge generation rate
2. Increasing the charge dissipation rate
3. Neutralizing the electrostatic charge by creating or injecting charges of opposite polarity

To achieve the above objectives, different methods have been investigated in the past including, treating the column wall, addition of static drivers, fluidizing gas humidification, using ionized gas, and grounding the column wall.

1.6.1. Treating the Column Inner Wall

There have been some reports that coating the inner fluidization column wall has led to a decrease in electrostatic charging with reactive systems. Fulks et al. (1985) reported that coating the reactor wall with a polymer film derived from a chromium-based compound, such as chromocene, before the beginning of polymerization, aided in the reduction of wall sheeting in industrial reactors. Similarly, Hagerty et al. (2005) reported that coating the reactor wall with polyethylene in a polymerization reactor reduced the amount of electrostatic charging. However, the mechanisms behind the charge reduction in the above literature are not known.

1.6.2. Additive Injection

The general concept for additive injection is to attempt to keep the net charge of the bed at a neutral level (approximately zero). For instance, if the electrostatic levels in the bed are predominantly positive, then a negative charging agent is injected into the fluidized bed (Goode et al., 1989). The additives injected into the bed can be gas, liquid, or solid, though majority of the research has been done with solid powders. It is important to remember that in industrial-scale operations, any additive that is injected into the fluidized bed reactor, whether gas, liquid, or solid, must not act as a catalyst poison, or significantly hinder the quality of the product.

1.6.2.1. Gas Injection

Goode et al. (1989) are one of the only known groups to have reported using gas injection to reduce the charges within an industrial reactor. The researchers injected both nitric oxide and oxygen along with nitrogen into a fluidized bed and noticed a drop in the bed electric potential. It is not clear why more research has not been conducted in this area. But it speculated that either the gas injection technique is not as effective as presented, or potentially the injected gases could act as a catalyst poison in some cases. In catalytic reactors, oxygen certainly would be prone to oxidize some of the metals present in the catalysts, possibly rendering the catalyst ineffective.

There have been a few studies that attempted to reduce the electrostatic charges within a fluidized bed by introducing an ionized gas into the system to neutralize the excess charge. However, Boland and Geldart (1971/72) claim that it is impractical to ionize the inlet air because

the ionized air would be prone to being attracted to conductive surfaces such as metal piping and would neutralize before even entering the fluidization column. Although other works have shown to have some mild success with neutralizing particles close to the ionizer (Revel et al., 2003), ionization has been shown not to be effective enough to penetrate the ions through larger fluidized beds and reduce sheeting (Fulks et al., 1985).

1.6.2.2. Solid Injection

Most of the reduction techniques and studies have focused on injecting solids into the fluidized beds as a method of charge reduction. Typical additive particle sizes range from 0.1 to 200 μm, but are generally around 10-100 μm and can behave as single particles or as agglomerates (Song et al., 1995). Solid additives have been shown to be quite effective and usually only 0.1 to 25 ppm are needed to significantly reduce electrostatic charge within an industrial reactor (Goode et al., 1989). There are a variety of additives that have been used including: aluminum stearate, aluminum oleate, ethoxylated amine, alkoxylated amines, carboxylic acids, polysulfones, polymeric polyamines, and sulfonic acids (Hagerty et al., 2005). Song et al. (1995) found that adding MgO, ZnO, Al_2O_3, CuO, or a mixture of them to the fluidized bed would cause an increase of positive electrostatic charges, whereas adding V_2O_5, SiO_2, TiO_2, and Fe_2O_3 would cause an increase in negative charges.

Wolny and Opalinski (1983) added active coal, titanium dioxide and pigment-A extract to a bed of highly charged polystyrene particles (1020-1200 μm) and noticed a significant decrease in the charge measured. All of the additives led to the breaking of agglomerates, as well as the removal of particles that were adhered to the column wall. Song et al. (1995) showed that carbon black was effective at reducing negative charges in a polymerization gas-solid fluidized bed; however, carbon black is typically not used because with low levels of this additive, the particles that are produced are black and therefore cannot be used to make colorable materials. This again signifies the issue that the additive must not hinder product quality. The effect of injecting a solid additive has also been compared to systems with high relative humidity. It was reported that aluminum powder injected to a dry air gas-solid fluidized bed of polystyrene particles (474 μm) had the same effect as increasing the relative humidity to 70 % (Wolny and Kazmierczak, 1989). The same trend was also reported by Guardiola et al. (1992) when steel particles were injected

into a different gas-solid fluidized bed composed of glass beads. Wang et al. (2009) studied the effect of five different solid additives (Al_2O_3, ZnO, Fe_2O_3, TiO_2, and MgO) on the bed electrification of linear low density polyethylene (LLDPE) particles using horizontal probes at six different bed heights. Tests were performed between 0.25 wt% to 1 wt% of additive. Of all the additives tested, Al_2O_3 seemed to be the most effective at reducing the electrostatic potential throughout the entire bed.

It is not very clear as to how the addition of solid additives alters the charging in fluidized beds. It may however be possible that the additives act as spacers between particles. Mehrani et al. (2007) took SEM pictures of polyethylene particles that were mixed with antistatic agent, Larostat 519, and showed that the additive was adhering to the larger polyethylene particles, which may have helped reduce the charge generation. Overall it can be concluded that the solid additives could either decrease the amount of particle charge generation, increase the amount of charge dissipation, or a combination of both. However, the exact nature of the effect is still not well understood.

1.6.2.3. Liquid Injection

Many researchers in academia have studied the effect of the fluidizing gas humidification and have generally found that moisture within the system aid in increasing the dissipation of charges and therefore when the relative humidity is increased, the net charge is decreased. This agrees well with the majority of the research for a variety of different particles (Ciborowski and Wlodarski, 1962; Boland and Geldart, 1971/72; Tardos and Pfeffer, 1980; Wolny and Kazmierczak, 1989; Guardiola et al., 1992; Ham et al., 1992; Park et al., 2002) all of whom used some form of electrostatic probe with the exception of Tardos and Pfeffer (1980) who also employed a Faraday cup. In some cases an increase in the relative humidity increased the degree of bed electrification to a maximum value before decreasing to zero (Ciborowski and Wlodarski, 1962; Ham et al., 1992). However, this trend may be particle specific as Fujino et al. (1985) reported that the electric potential within a gas-solid fluidized bed decreased with an increase of relative humidity when glass beads were used, however the electric potential increased with polymethyl methacrylate (PMMA) particles.

Similar to gas humidification, water has also been directly added to the fluidized bed for charge reduction. However, such research is primarily focused in an academic setting as the increasing amount of water in the system has been known to aid in the formation of particle agglomerates (Katz, 1957; Boland and Geldart, 1971/72), as well as act as a catalyst poison in catalytic reactors such as those in the polyethylene industry (Fulks et al., 1985; Goode et al., 1989). There have been some reports that water vapour has improved some of the results of the fluidization systems (Ciborowski and Wlodarski, 1962). Chirillo et al. (1989) added about 0.2 ppm by volume of water to a fluidization reactor and noticed that the water was able to reduce the static charging, as well as the presence of sheeting. Goode et al. (2000) also claimed that water was effective against positive static voltage in a reacting fluidized bed using a metallocene catalyst. However, the authors reported that the amount of water required was not reproducible and the electrostatic voltage did not always respond to the water injection.

Other liquid additives that have also been used to reduce the charges in the reactor are methanol, ethanol, isopropanol, methyl isobutyl ketone (MIBK), or acetone (Goode et al. 1989). Newton et al. (1999) reported that methanol is a poison for some catalysts and therefore probably not widely used. There were no other known reports on these liquids making it difficult to conclude their degree of effectiveness. Wang et al. (2009) studied the effect of ethanol in a fluidized bed of LLDPE using electrostatic probes. The researcher also studied triethylealuminum (TEA) diluted in n-hexane. TEA is sometimes used as a co-catalyst in olefin polymerization process. Adding ethanol at a flow rate of 0.1 mL/s (approximately 1060 mL for the total experiment) somewhat reduced the amount of electrostatic potential in the bed. With TEA there was a flip in the charge polarity where the positive electric potentials in the bed became negative and vice versa.

Grounding the reactor column wall in order to allow the electrostatic charges to dissipate from materials inside the column has been referred to as another possible charge reduction technique. However, this method would only be plausible with walls made of conductive materials since insulating materials such as glass would have very little electron movement and therefore this method would be ineffective (Boland and Geldart, 1971/72). Even conductive particles have been shown to have a general high electrical resistance for suspended particles (Pulsifer and Wheelock, 1978), and charged particles in contact with a grounded metal wall was shown not to

dissipate any charges to the wall (Servais and Bernot, 2000) and would really only be effective for a limited amount of particles inside the bed, namely those that are in close proximity of the wall (Park et al., 2002).

1.6.3. Summary

It is important to note that if a solid additive is used to maintain the electrostatic levels in a fluidized bed as neutral as possible, the additive must be continuously added to remain effective. Song et al. (1995) reported that adding MgO to a bed of charged polymer particles greatly reduced the electrostatic potential in the bed for about 10 to 15 minutes before the levels started to rise again. Bafrnec and Bena (1972) added 0.14 wt% of graphite to a fluidized bed and the voltage of the bed quickly approached zero; however after 10 hours all of the graphite in the system had rubbed off and the voltage in the bed subsequently increased. A successful ten day operation of a pilot scale polyethylene fluidized bed reactor was reported by Hagerty et al. (2005) when an additive (labeled AS-990) was continuously added to the system. However, it is not uncommon for one additive to work well for one system but not well for another, or to find some solid additives that appear to be effective for the first day or two of the operation but not later (Goode et al., 2000). In addition, it is notable that although the injection of an additive into a fluidized bed may result in a zero net charge, it may not mean that it has removed any wall sheeting or particle agglomeration already present in the bed.

There has been an ongoing study of different techniques that can be used to reduce the electrostatic charging in gas-solid fluidized beds in both academia and industry. However, the actual mechanism of how the additive aids in reducing the electrostatic charging is not well understood, which has led to most studies being performed by trial and error. Most importantly none of research mentioned above have determined the magnitude of reactor wall fouling and its change due to any of the reduction techniques applied. This is due to the measurement technique used that has mainly been electrostatic probes which are only able to provide the degree of bed electrification by current or voltage measurement. More research is undoubtedly required to fully understand the mechanisms that make an additive potent at reducing electrostatic charging in gas-solid fluidized beds and their effects on the amount of particle-reactor wall adhesion.

1.7. Thesis Objectives

An essential step to overcome the challenges due to gas-solid fluidized bed electrification is to understand the underlying charging mechanisms of the fluidizing particles within the bed. In order to fully understand the dynamics of electrostatics within such reactors, a suitable measurement technique is essential, one that is able to characterize the electrostatic effects for the entire fluidized bed, in addition to providing direct quantification of magnitude of reactor wall fouling. Moreover, it is important to determine parameters that influence bed electrification and investigate their effects, which will lead to a better understanding of this phenomenon. As can be seen in Table 1.4, these parameters can be classified into three categories based on their relationship to: the solid particles, the fluidizing gas, and the fluidization vessel.

Once the principle parameters have been identified, and an insight on the possible charging mechanisms within a fluidized bed has been determined, a suitable model can be proposed that could help predict electrostatic charge generation in gas-solid fluidized beds and hopefully aid in finding means of charge reduction or elimination. Given that a fluidized bed is a complex and dynamic system, it is very unlikely that a simple model would be able to be derived.

Table 1.4: Parameters that could affect electrostatic charge generation in a gas-solid fluidized bed.

Parameters	Fluidizing Particles	Fluidizing Gas	Fluidization Vessel
Diameter	x	-	x
Material	x	x	x
Size Distribution	x	-	-
Sphericity	x	-	-
Surface Roughness	x	-	x
Conductivity/Resistivity	x	-	x
Velocity	-	x	-
Temperature	-	x	-
Pressure	-	x	-

The overall goal of this thesis was to establish a comprehensive study of electrostatic phenomena in gas-solid fluidized bed reactors. The specific objectives were:

1. To develop an adequate on-line electrostatic charge measurement technique that would be able to quantify charge distribution in various regions of the fluidized bed, with the focus on reactor wall fouling region.
2. With the assistance of the measurement technique developed in the first objective, to investigate the influence of key operating parameters expected to impact charge generation and dissipation, and their significance. These parameters included:
    a. *Fluidized bed hydrodynamics*: fluidization gas velocity and particle size
    b. *Fluidization column:* column wall material
3. Using the measurement technique developed in part (1), to examine the direct effects of addition of solid additives such as catalysts and/or static drivers on reactor wall fouling. This research also enables the investigation of particle type (i.e., particles of different surface chemical and physical properties including chemical composition, roughness, sphericity, and electrical conductivity) on the extent of bed electrification and wall fouling.
4. Finally, from results obtained throughout the research to study the relationship between the magnitude of particles charge density within the bed and the level of reactor wall fouling.

Although above objectives are related to any gas-solid fluidized bed process that is suffering from electrostatic phenomenon, the experimental work was mainly focused on the polyolefin industry in which is affected the most.

1.8. Thesis Outline

The second chapter of this thesis focuses on the design and development of a novel measurement technique that enables the measurement of the electrostatic charge distribution in different regions of gas-solid fluidized beds, as well as the degree of reactor wall fouling. The chapter details the design principles behind the method, and its design and application to an atmospheric pilot-scale gas-solid fluidized bed. In addition, it describes the type of measurements that can be

performed with the help of this method. Results of this work were published in the Journal of Electrostatics (*Sowinski, A., Salama, F., Mehrani, P., 2009. New technique for electrostatic charge measurement in gas-solid fluidized beds. Journal of Electrostatics, 67 (4), 568-573*).

The third chapter focuses on the experimental equipment and methodology for the measurements. It details the materials, experimental apparatus, and instrumentations used, in addition to the procedures followed for various types of experiments performed.

Chapters four, five, six, seven and eight present and discuss results obtained from various experiments conducted. Chapter four focuses on bench-scale experiments undertaken in an effort to determine the charging mechanisms involved as polyethylene particles come into contact with the fluidization column wall.

Chapter five focuses on the effects of fluidization gas velocity. Part of this study was published in journal of Chemical Engineering Science (*Sowinski, A., Miller, L., Mehrani, P., 2010. Investigation of electrostatic charge distribution in gas-solid fluidized beds, Chemical Engineering Science, 65 (9), 2771-2781*).

Chapter six summarizes the results of investigation of effects of fluidizing particle size. The results from this chapter were also published in the journal of Chemical Engineering Science (*Sowinski, A., Mayne, A., Mehrani, P., 2012. Effect of fluidizing particle size on electrostatic charge generation and reactor wall fouling in gas-solid fluidized beds, Chemical Engineering Science, 71, 552-563*).

Chapter seven describes the results of testing done with different fluidization column wall materials. The eighth chapter focuses on the injection of solid additives and their effects on electrostatic charge generation inside the fluidized bed and the level of column wall fouling.

The final chapter, Chapter nine, summarizes the overall conclusions and recommendations for further research. Additional information such apparatuses from previous researchers, preliminary testing results, images of the particles used, minimum fluidization gas velocity results, and additional experimental results are found in the appendices.

Chapter 2.
ON-LINE CHARGE MEASUREMENT TECHNIQUE

To gain a better understanding of the dominating charging mechanisms and particle migration in gas-solid fluidized beds, as well as the parameters affecting them, it is essential to have an adequate electrostatic charge measurement technique to accurately quantify the amount of charges generated in various regions of the bed, with the focus on studying reactor wall fouling.

2.1. Design Considerations

After an extensive critique on previous measurement techniques applied in academia and industry, a new on-line measurement technique was designed to minimize the weaknesses of all the previous methods, and to be able to focus on the charge distribution and particle migration within the entire fluidization column. The new measurement technique was therefore developed to meet the following criteria:

1. To measure the total net charge of the bed particles rather than only providing local measurements.
2. To reduce the effect of particle adhesion on the measurement device.
3. To reduce the amount of particle handling involved.
4. To minimize altering the bed hydrodynamics due to the presence of the measurement device.
5. To be able to quantify the amount of reactor wall fouling.
6. To provide information on charge distribution within the entire fluidized bed by measuring both the charge of the bed particles, including particles fouling the reactor wall, and those of the entraining fine particles.
7. To be flexible enough such that it would allow tests to be performed on a variety of parameters such as fluidizing gas velocity, particle type and size, column material and diameter, etc.

The Faraday cup method was chosen as the main technique over electrostatic probes in order to directly measure the net charge of the bulk of the bed particles (Criteria 1), and to prevent a reduction in the accuracy of measurements due to particle adhesion (Criteria 2). The Faraday cup method was applied in a unique way where the windbox section of the fluidization column was replaced with a Faraday cup directly below the distributor plate (Figure 2.1a). This arrangement allowed the bed particles to fall directly into the Faraday cup (if the distributor plate was removed) for their charge measurement, reducing any amount of particle handling (Criteria 3). Also since the Faraday cup was not inside the fluidization section of the bed, the bed hydrodynamics were not affected (Criteria 4).

In order to be able to drop the bed particles into the Faraday cup, the distributor plate was required to be designed in such a way that it could be quickly removed and easily replaced back into the column for subsequent fluidization experiments. Therefore to ensure consistency and efficient operation of opening and closing the distributor plate, an automatic mechanical method was preferred. This was achieved by replacing the distributor plate with a pneumatically controlled knife gate valve (Figure 2.2). The valve blade was modified to act as a perforated distributor plate for fluidization.

The Faraday cup assembly consisted of the body of the windbox section acting as the outer cup of the Faraday cup, which was grounded to electrically shield the inner cup. The inner cup was directly connected to an electrometer for charge measurement. The two cups were electrically isolated from each other by Teflon studs. The spacing between the two cups allowed the fluidizing gas to reach the distributor plate. Both cups were fabricated out of copper, a highly electrically conductive material. This Faraday cup could easily be removed so that the collected particles mass to be measured and samples be taken for particle size distribution analysis. This also allowed the inner wall of the fluidization column to be examined, allowing the qualitative assessment of the degree of wall fouling (Criteria 5). When reactor fouling was present, the Faraday cup could be replaced, followed by the tapping the column to dislodge any loosely bound particles from the column wall into the Faraday cup for the measurement of the particles charge.

To investigate the charge distribution within the fluidized bed as a whole, the measurement of the charge of the entrained fine particles was also necessary (Criteria 6). Therefore, another Faraday cup was placed directly at the top of the fluidization column enclosing a filter bag to immediately capture all the particles as entrained during the fluidization and to measure their charge (Figure 2.1b). Placing the cup at this location, rather than further downstream, eliminated any additional charging, or change in the charge of the particles due to contact with parts of the apparatus other than the main fluidization column. The filter bag placed inside the inner cup trapped the entrained fines while allowing the fluidizing gas to pass through. The inner cup had an open end at the top to allow the fluidizing gas to leave the system. Both the inner and the outer cups were made out of copper and were electrically isolated from each other by Nylon bolts. The inner cup was directly attached to a digital electrometer that measured the cumulative charge. This Faraday cup was designed to be detached from the column so that the filter bag inside its inner cup could be removed for the measurement of the mass and size distribution of the collected particles.

Both Faraday cups were designed to be situated above and below the fluidization column so that they would not interfere with the particles fluidization within the bed. Furthermore, they could easily be adapted to any other systems allowing for an extensive study of various operating parameters (Criteria 7).

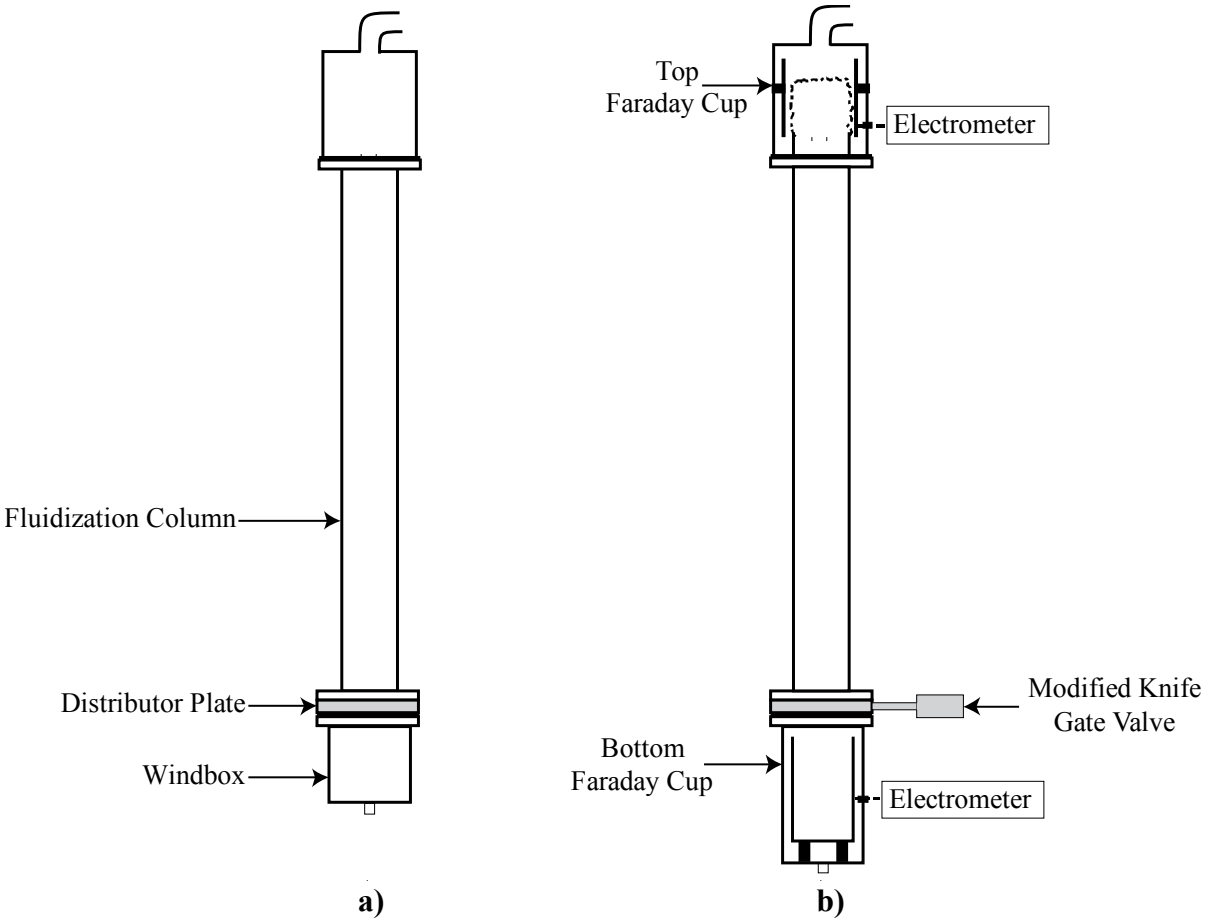


Figure 2.1: Overall schematic of a) a simple fluidization column, and b) a modified column with two online Faraday cups.

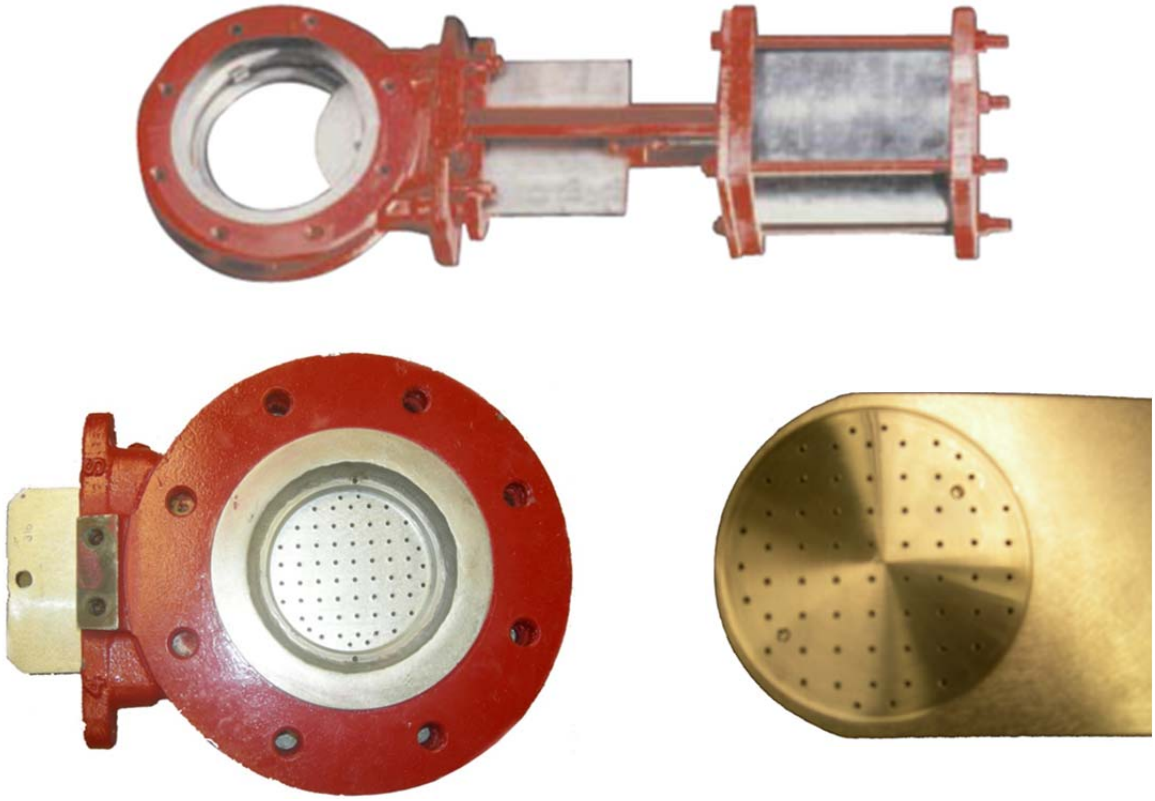


Figure 2.2: Pictures of the modified knife-gate valve replacing the distributor plate.

2.2. Measurement Considerations

To fully investigate the electrostatic charge distribution and particle migration within the fluidized bed, the system would be divided into four different sections as shown in Figure 2.3. For each region, the particles mass (m), charge (q), and size distribution (PSD) would be measured and recorded. The regions included:

Initial: Particles before being placed inside the fluidization column

Fines: Particles entrained from the column that were collected in the top Faraday cup during the fluidization period

Dropped: Bulk of particles that were dropped into the bottom Faraday cup upon the completion of the fluidization period

Wall: Particles that were adhered to the column wall and also dropped collected in the bottom Faraday cup after the removal of the Dropped particles

For all experiments, after tapping the column wall during the removal of Wall particles, as shown in Figure 2.3, some of the particles easily fell into the Faraday cup (**Loosely Bound**), while the rest of the particle would remain adhered to the column wall (**Tightly Bound**). The charge of the Tightly Bound particles was not measured since these particles needed to be physically removed from the system, effectively altering their charge. The sum of the Tightly and Loosely Bound particles would be referred to as Wall.

Using the mass of particles collected and their charge, the particles specific charge, q/m, can be calculated for each region of the fluidized bed. If the particles specific surface area, $\hat{A}$, is known, it can be divided by the particles specific charge to give the specific charge-to-specific surface area ratio, $\hat{q}/\hat{A}$, which provides an estimation of the charge on the surface of each particle.

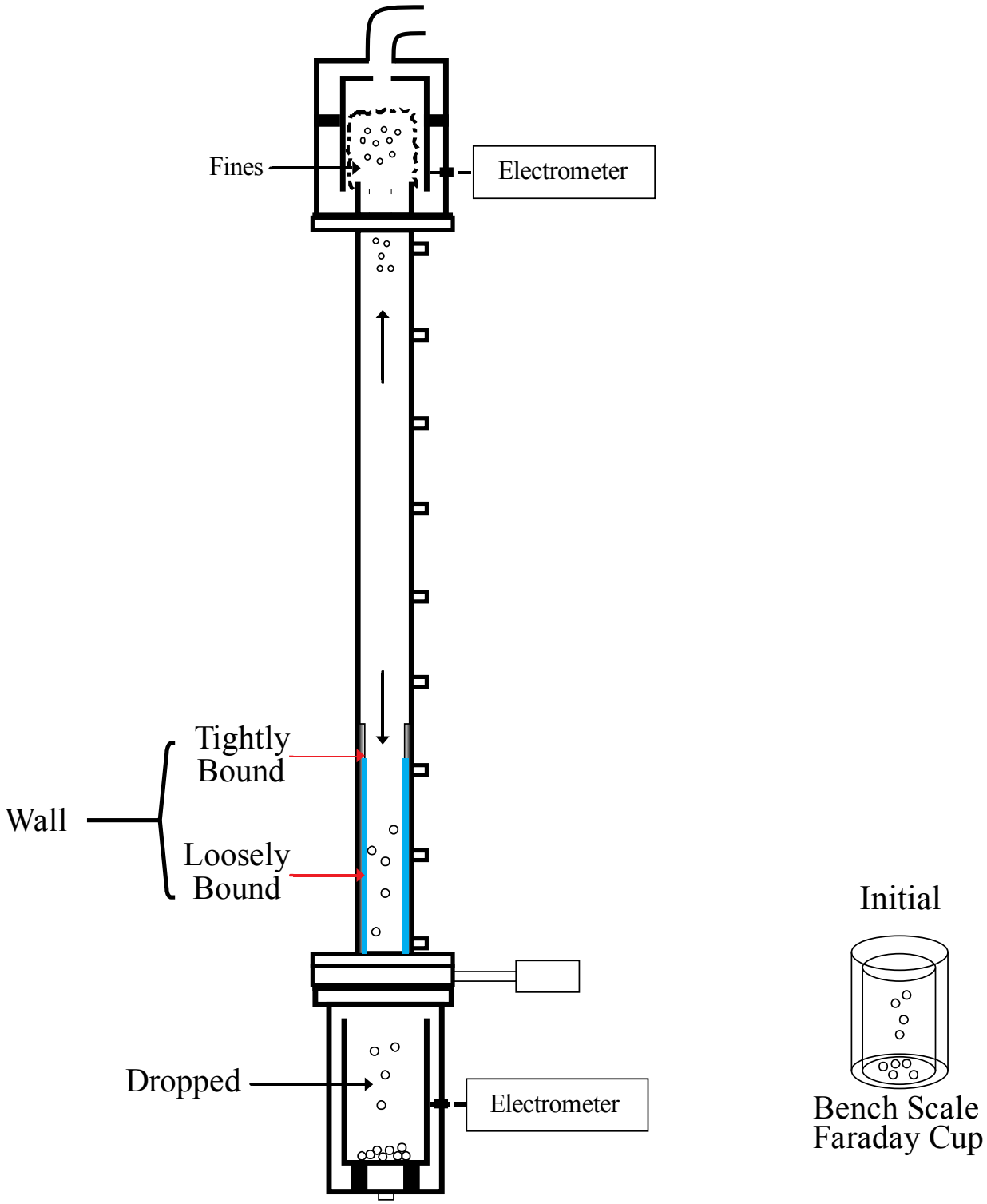


Figure 2.3: Various measurement regions within the fluidized bed.

2.3. Preliminary Testing

The measurement technique developed was applied to a pilot-scale fluidization column (with details discussed in Chapter 3). To ensure that the technique was sensitive enough to measure the electrostatic charges present with the fluidization column, some preliminary testing was then performed. First, the effect of opening the knife gate valve was tested to ensure that the quick movement of the valve blade (i.e., distributor plate did not alter the net charge of the Dropped particles). Second, since the fluidization experiments were planned to be performed for up to one hour at a time, the top Faraday cup was tested for any electrometer measurement drifts caused by any charge leakage from the fluidization system or from the capacitor found within the electrometer itself.

2.3.1. Effect of Knife Gate Valve Opening

To determine whether opening the knife gate valve introduced any significant charging to the Dropped particles, some preliminary tests were performed. First a known mass of polyethylene particles (same particles as those used in fluidization experiments with properties discussed in Chapter 3) were poured directly into the bench-scale Faraday cup shown in Figure 2.3 where their total net charge was measured and recorded. Then the inner cup of the bench-scale Faraday cup was used as a pouring device, minimizing the amount of additional charging, and the particles were poured directly into the fluidized bed from the top of the column. At this point two different scenarios were tested:

1. The knife gate valve was kept open while the particles were poured inside the fluidized bed such that the particles fell directly into the bottom Faraday cup of the fluidization column and their total net charge was measured.
2. The knife gate valve was closed before the particles were poured into the fluidized bed such that as the particles fell into the column they rested directly on the knife gate valve but did not undergo any more particle movement. After all of the particles were placed inside the column, the knife gate valve was opened and the particles dropped into the bottom Faraday cup where their net charge was measured.

These two tests allowed for the determination of the amount of charging from the opening of the knife gate valve. The two types of tests were performed six times each in random order, and the knife gate valve and the fluidization column were grounded between each experiment to eliminate any additional charging. The results are shown in Figure 2.4. The initial and the final charge of the particles were similar for both types of experiments. The particles final net q/m was measured to be -0.42 ± 0.17 μC/kg and -0.30 ± 0.10 μC/kg for experiments performed with the valve open and closed, respectively. Statistically, the difference between these results was insignificant.

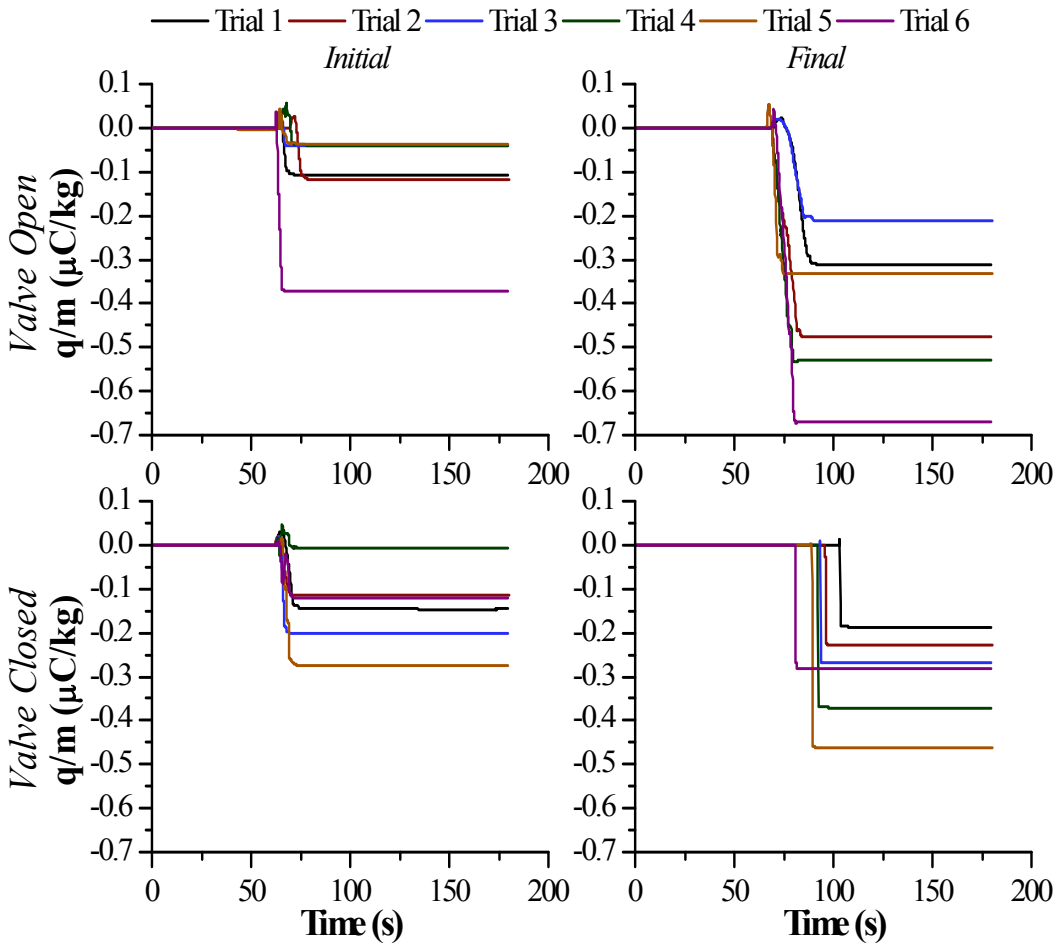


Figure 2.4: The change in charge of the particles due to opening the knife gate valve.

2.3.2. Electrometer Measurement Drifts

The electrometer measurement drift from the top Faraday cup was tested. Tests were performed for at least one hour and repeated four times. The fluidization system was set up exactly as a

standard experiment with the top Faraday cup and filter bag placed in the system but with no fluidizing particles present. The top Faraday cup was connected to a digital electrometer (Model 6415). Two types of experiments were conducted:

1. Recording the background measurement from the Faraday cup for one hour with no gas flowing through the fluidized bed.
2. Recording the background measurement from the Faraday cup while dried compressed building air (0% relative humidity) was sent through the fluidized bed continuously, and the gas volumetric flow rate increased at 10 SLPM every 5 minutes for a period of 100 minutes.

These two tests determined whether there was any electrometer signal drift, and if the fluidizing gas alone had any effect on the electrometer measurement. Figure 2.5 shows the results from the background signal measurement of the top Faraday cup for a period of one hour with no gas passing through the system. The maximum drift to occur was approximately 15 nC after one hour. It should be noted that these experiments where performed consecutively one after the other and as can be seen from Figure 2.5 the signal drift decreased after each repetition. It is plausible to assume that in order to minimize the measurement signal drift, the set up should be attached and left to stabilize for extended periods of time. However, a drift of 15 nC/h was deemed to be negligible in comparison to the charge measured for the entrained particles with fluidization experiments.

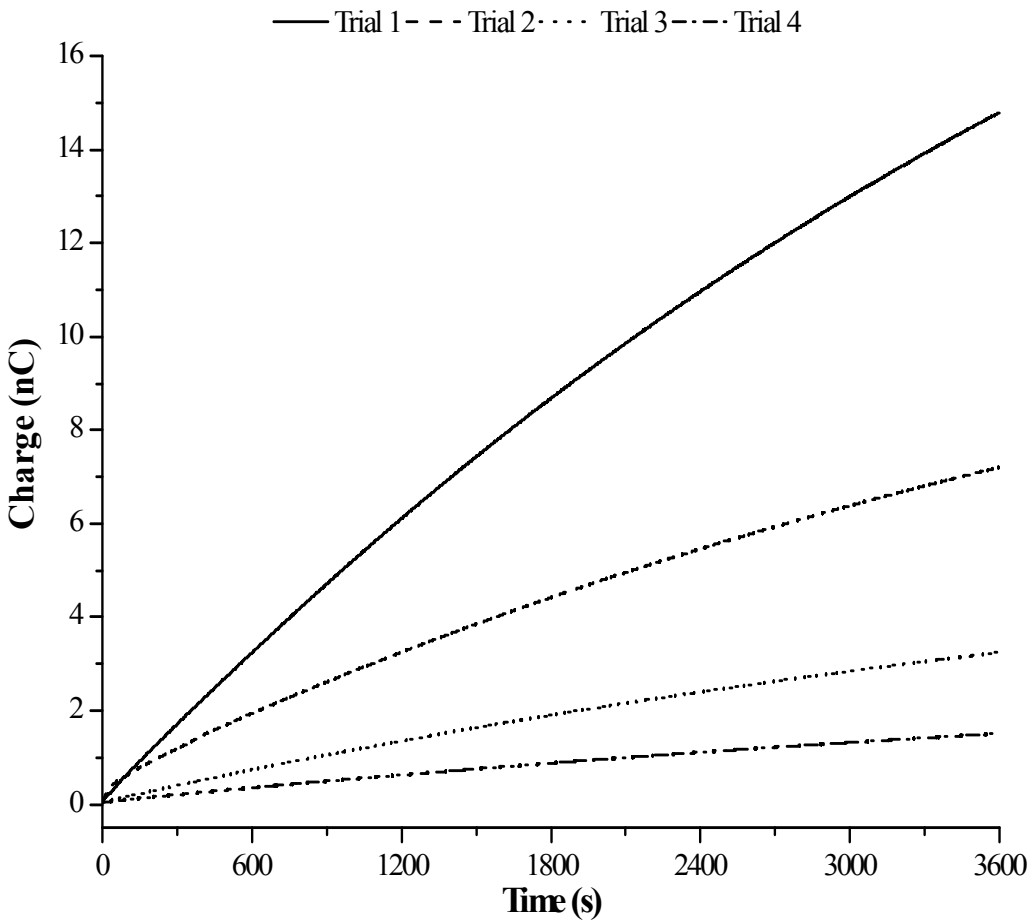


Figure 2.5: The electrometer background signal measurement from the top Faraday cup for a period of one hour. No particles were present and no gas was sent through the fluidized bed.

Figure 2.6 presents the cumulative charge measured by the top Faraday cup when the fluidizing gas flow rate was increased by 10 SLPM every five minutes. The cumulative charge did not alter from its drift. It should be noted that these experiments were also performed consecutively and in two cases the signal drift was positive while in the other two cases it was negative. This means that the electrometer signal drift from the top Faraday cup was not consistently predictable even when comparing to the experiments in Figure 2.5. However, in Figure 2.6, the maximum magnitude of the drift was only 2.5 nC, which was still lower than the 15 nC previously described. All these preliminary experiments showed that the measurements from the top Faraday cup were not affected by the fluidizing gas velocity.

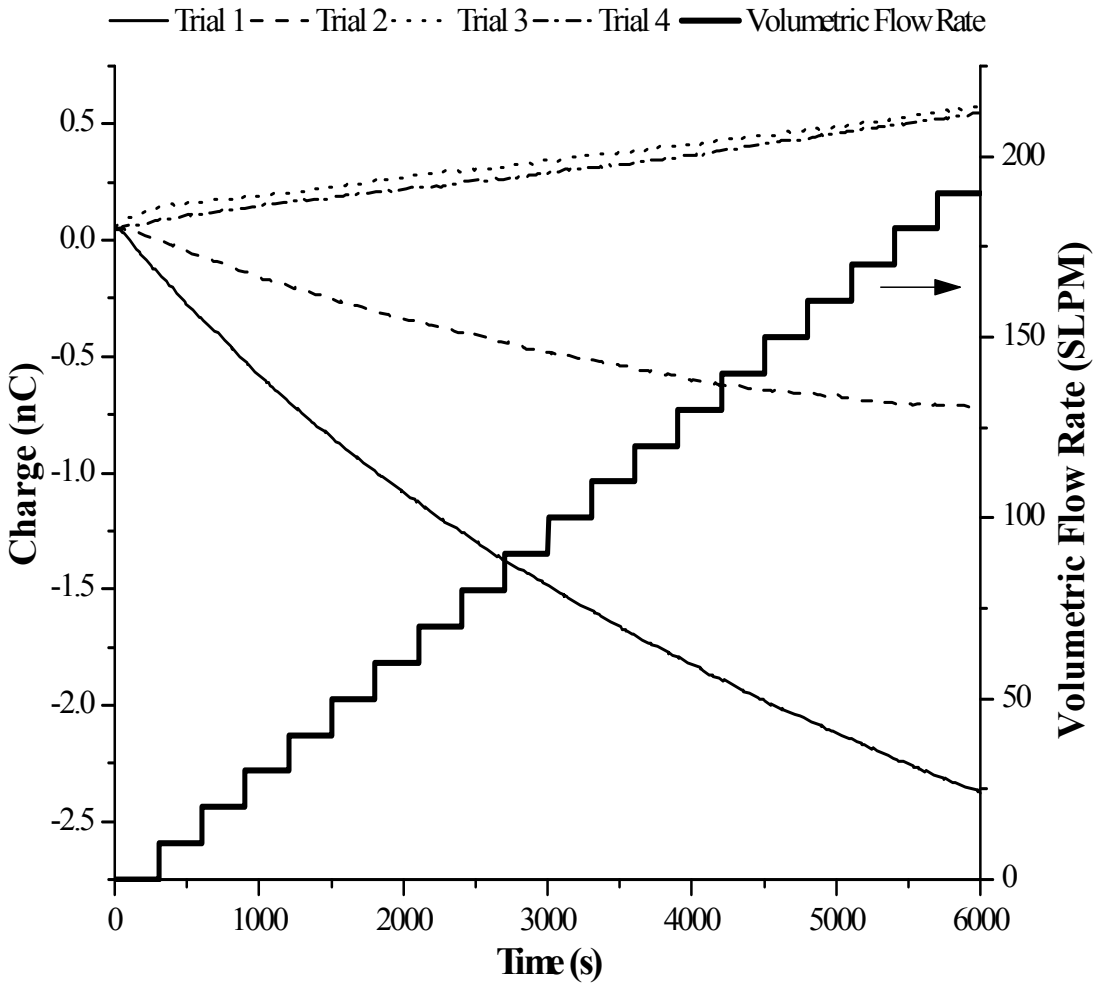


Figure 2.6: Charge measurement by the electrometer attached to the top Faraday cup. No particles were present, while the gas velocity increased at 10 SLPM every five minutes.

The electrometer measurement drift while attached to the bench-scale Faraday cup was also tested since the connections for this cup was through a triaxial cable with alligator clip connections. The electrometer was connected to the bench-scale Faraday cup and left under ambient conditions for one hour. The results for three repetitions are shown in Figure 2.7. The maximum signal drift was approximately -0.7 nC and deemed not to be significant.

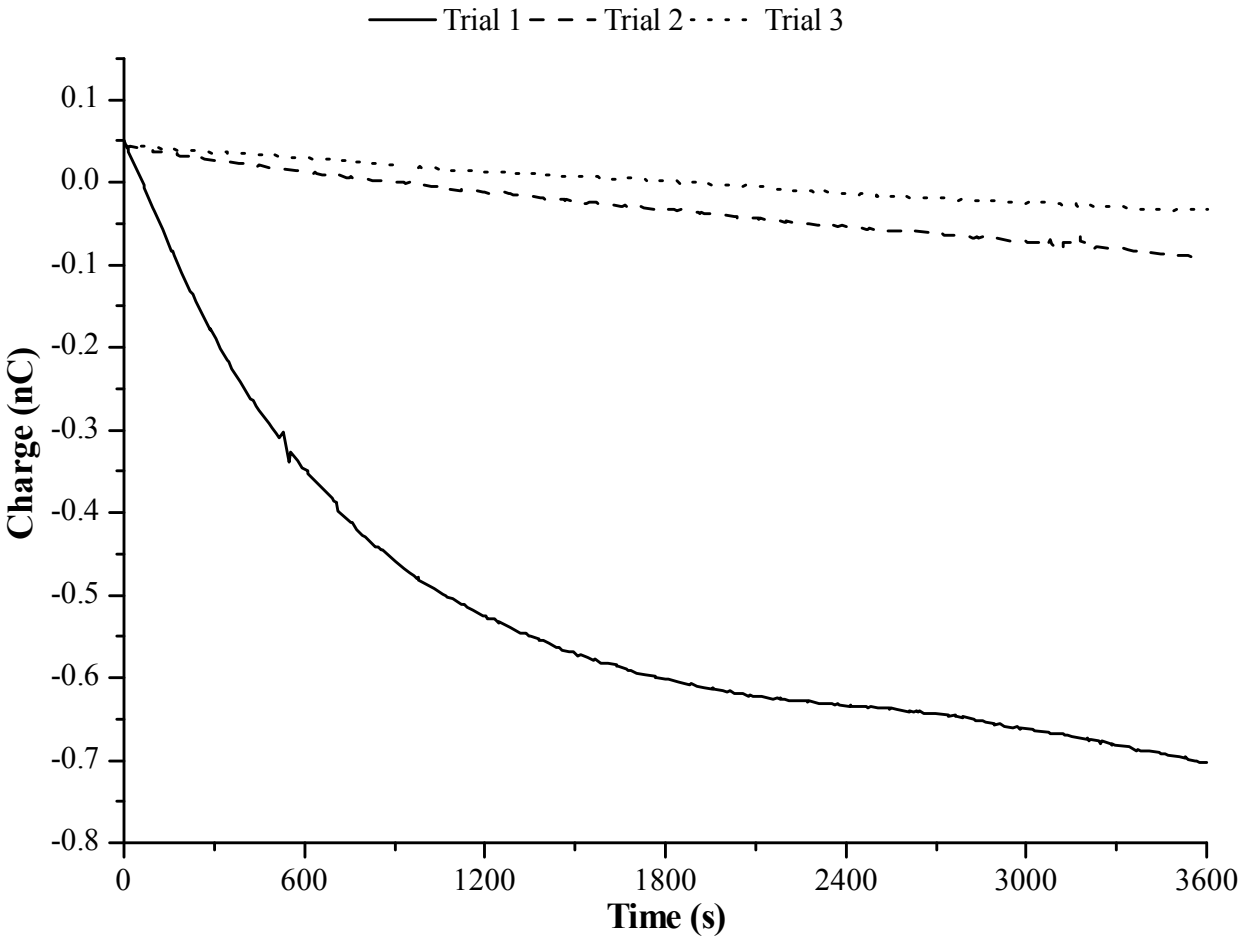


Figure 2.7: The electrometer measurement drift of the bench-scale Faraday cup without any particles present for one hour.

2.4. Summary

Improving from the drawbacks of previous measurement techniques, a novel online measurement technique was developed that is able to measure the particle, charge, size, and mass distributions in different regions of the fluidized bed. To ensure the integrity of the measurement system, preliminary testing was also performed on the effect of opening and closing the knife gate valve and any long term electrometer drifts on the measured charge. No significant change in the measured charge was found with these tests.

Chapter 3.
MATERIALS, EXPERIMENTAL APPARATUS AND PROCEDURES

This chapter focuses on characterization of materials used in this research including the solid particles and the fluidizing gas, as well as the experimental apparatus used and standard operating procedures followed throughout the course of various experiments performed.

3.1. Materials

The following section characterizes the fluidizing gas, fluidizing particles and the solid additives used during experiments.

3.1.1. Fluidizing Gas

Fluidizing gas used in all experiments performed in this research was compressed building air having a temperature of 23 ± 0.5 °C and relative humidity (RH) of 3.6 ± 0.36%. The air was dried to 0% RH with a dryer (Atlas Copco Model CD12) prior to entering the fluidization column.

3.1.2. Fluidizing Particles

Although the overall focus of this research was on investigation of electrostatic phenomenon in gas-solid fluidized beds in general, the experimental work was mainly focused on one application related to the polyethylene industry which has suffered the most from this phenomenon. Fluidizing particles utilized in all experiments were metallocene based linear low density polyethylene (LLDPE) resin, PE_A, PE_B, and PE_C directly received from commercial reactors of ExxonMobil and Dow Chemical Company (USA). The particle sizes and particle distributions in this work have been normalized to the average of the median particle diameter of PE_A from numerous experiments, due to confidentiality reasons.

Since electrostatic charging is a surface phenomenon, it is important to fully characterize the particles within the fluidized bed for their physical and chemical properties including their size, surface chemistry and morphology, etc. This will allow better understanding of the factors that may have the largest effect on electrostatic charge generation in gas-solid fluidized beds. The physical and chemical properties of all three types of polyethylene particles used are shown in Table 3.1 to Table 3.3. These tables present information on an initial sample of each resin as well as information on three different sieved particle size ranges for comparison purposes.

The particle densities were provided by Univation Technologies LLC (USA). Polyethylene is composed of only carbon and hydrogen atoms linked in a chain formation with some C_4H_9 branches and is known to be hydrophobic provided that no stabilizers or static drivers have been added (van Krevelen and te Nijenhuis, 2009). The resin provided may have contained a low level of static drivers; however, this was assumed not to affect the hydrophobicity of the polyethylene particles.

The electrical properties of the polyethylene resins were taken from literature. They included the work function (Masuda et al., 2006), conductivity (Hindermann-Bischoff and Ehrburger-Dolle, 2001), and permittivity (Pryer and Gale, 2003). The permittivity is a measure of the speed of an electric signal through a material whereas the conductivity (the inverse resistivity) is a measure of the ability for a material to conduct an electric current.

Table 3.1: Polyethylene A Particles Physical, Chemical and Electrical Properties.

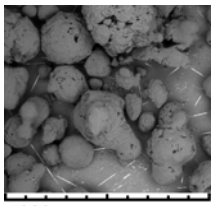
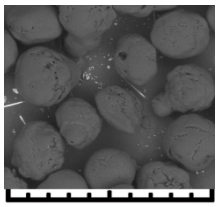
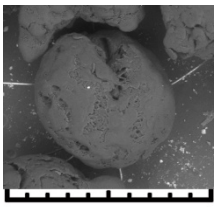
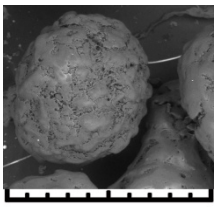
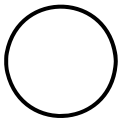
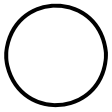
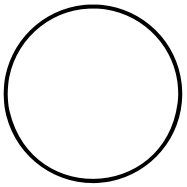
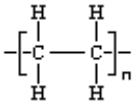
		PE_A Initial	**PE_A** 212 – 300 μm	**PE_A** 500 – 600 μm	**PE_A** 710 – 1000 μm
Surface Properties					
SEM		 5000 μm	 1000 μm	 1000 μm	 1000 μm
Sphericity		0.749	0.797	0.811	0.797
Morphology		Coarse	Coarse	Coarse	Coarse
Physical Properties					
Density	kg/m^3	920	920	920	920
d_P10_N		0.50 ± 0.08	0.32 ± 0.00	0.68 ± 0.01	1.12 ± 0.08
d_P50_N		1.00 ± 0.13	0.44 ± 0.00	0.91 ± 0.01	1.59 ±0.05
d_P90_N		1.91 ± 0.22	0.60 ±0.01	1.23 ±0.03	2.24 ±0.03
$\hat{A}$	m^2/g	0.0124 ± 0.0016	0.0214 ± 0.0030	0.0103 ± 0.0001	0.0063 ± 0.0001
Geldart Group		B	B	B	B
Mean Particle Size Comparison					
Chemical Properties					
Chemical Formula		$(C_2H_4)_n$			
Chemical Structure					
Metal Elements		-			
Polar Molecule		No			
Water adsorption		Hydrophobic			
Electrical Properties					
Permittivity	F/m	2.3			
Conductivity	S/m	$1.1x10^{-13}$			
Work Function	eV	5.3			

Table 3.2: Polyethylene B Particles Physical, Chemical and Electrical Properties.

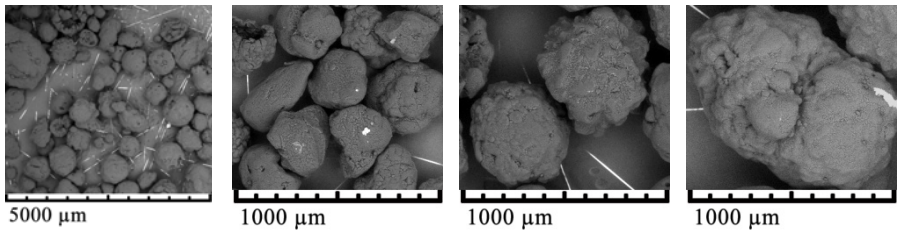
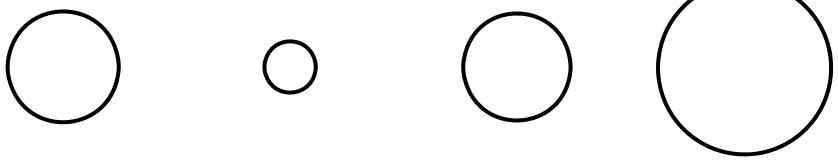
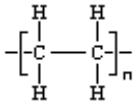
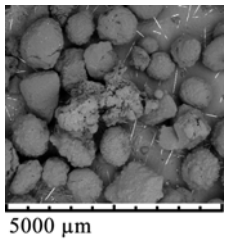
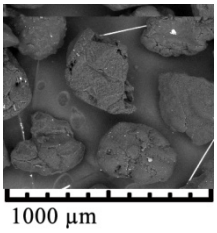
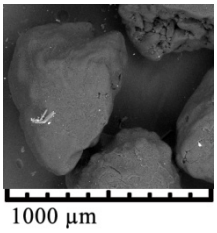
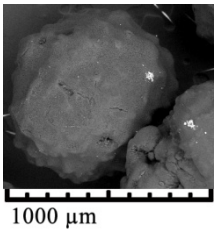
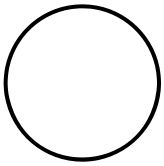
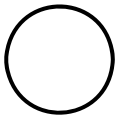
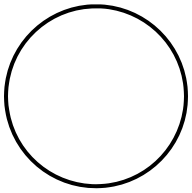
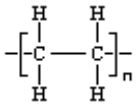
		PE_B Initial	**PE_B** 212 – 300 μm	**PE_B** 500 – 600 μm	**PE_B** 710 – 1000 μm
Surface Properties					
SEM					
Sphericity		0.797	0.799	0.598	0.723
Morphology		Coarse	Coarse	Coarse	Coarse
Physical Properties					
Density	kg/m^3	935	935	935	935
d_P10_N		0.52 ± 0.05	0.34 ± 0.00	0.72 ± 0.00	1.13 ±0.02
d_P50_N		1.01 ± 0.09	0.47 ± 0.00	0.98 ±0.01	1.58 ±0.02
d_P90_N		1.92 ± 0.18	0.64 ±0.00	1.36 ±0.02	2.20 ± 0.03
$\hat{A}$	m^2/g	0.0110 ± 0.0009	0.0219 ± 0.0001	0.0105 ± 0.0001	0.066 ± 0.00007
Geldart Group		B	B	B	B
Mean Particle Size Comparison					
Chemical Properties					
Chemical Formula		$(C_2H_4)_n$			
Chemical Structure					
Metal Elements		-			
Polar Molecule		No			
Water adsorption		Hydrophobic			
Electrical Properties					
Permittivity	F/m	2.3			
Conductivity	S/m	$1.1x10^{-13}$			
Work Function	eV	5.3			

Table 3.3: Polyethylene C Particles Physical, Chemical and Electrical Properties.

		PE_C Initial	**PE_C** 212 – 300 μm	**PE_C** 500 – 600 μm	**PE_C** 710 – 1000 μm
Surface Properties					
SEM					
Sphericity		0.647	0.626	0.549	0.765
Morphology		Coarse	Coarse	Coarse	Coarse
Physical Properties					
Density	kg/m^3	918	918	918	918
d_P10_N		0.81 ± 0.08	0.34 ± 0.05	0.71 ± 0.02	1.14 ± 0.04
d_P50_N		1.40 ± 0.11	0.46 ± 0.07	0.97 ± 0.04	1.64 ± 0.05
d_P90_N		2.31 ±0.09	0.62 ± 0.09	1.35 ± 0.10	2.30 ± 0.07
$\hat{A}$	m^2/g	0.0076 ± 0.0006	0.0227 ± 0.0026	0.0107 ± 0.0005	0.00640 ± 0.0002
Geldart Group		B	B	B	B
Mean Particle Size Comparison					
Chemical Properties					
Chemical Formula		$(C_2H_4)_n$			
Chemical Structure					
Metal Elements		-			
Polar Molecule		No			
Water adsorption		Hydrophobic			
Electrical Properties					
Permittivity	F/m	2.3			
Conductivity	S/m	$1.1x10^{-13}$			
Work Function	eV	5.3			

3.1.2.1. SEM and EDX Analysis

Scanning Electron Microscopy (SEM) and Energy-Dispersive X-ray spectroscopy (EDX) analyses were performed using the Tescan Vega-II XMU VPSEM machine located at Carleton University (Ottawa, ON). This machine allowed for the elemental analysis of the surface of particles, a qualitative measure of the surface roughness, as well as the calculation of the sphericity of particles.

The sphericity (ϕ) of the particles was calculated by taking the average of the circularity of numerous particles from the SEM pictures using Adobe Photoshop (Version CS5, Adobe Inc., USA). The circularity can be estimated by Equation 3.1.

$$\phi \approx \mathbb{C} = 4\pi\left(\frac{A}{P^2}\right) \qquad [3.1]$$

where $\mathbb{C}$ is the circularity, A is the projected area of the particle, and P is the perimeter of the particle. Due to the wide size distribution of the resin and quite irregularly shaped particles (from SEM pictures some particles appeared to be almost rectangular while others were more spherical) the sphericity calculations from SEM pictures only provided a rough estimation.

A qualitative measurement of the surface morphology was also performed using the SEM pictures where the surface roughness between size ranges and polyethylene samples was determined. Overall, all three resins had a similar surface morphology where the particles had rough surfaces. All particles were non-spherical but PE_A was the most spherical with a sphericity of approximately 0.8. There was no significant difference in the surface morphology or sphericity with different particle size ranges, with any of the resins.

3.1.2.2. Particle Size Distribution

The particle size distribution was performed using a Malvern Mastersizer 2000 with a Hydro 2000S particle dispersion unit. The Malvern Mastersizer 2000 uses laser diffraction to measure the volume particle size distribution of a sample of particles. The data from the sensors inside the

machine are analyzed through Mie theory based on particle light scattering (Barber and Hill, 1990). Only three parameters are required in order to develop an adequate model for Mie scattering: the refractive index of the particle, the absorption coefficient of the particle and the refractive index of the dispersant. These parameters were estimated from literary sources. A sensitivity analysis on some of the parameters is described in more detail in §3.1.2.2.1. The Hydro 2000S is a wet dispersion unit and since polyethylene particles are less dense than water, a 60 vol% of ethanol-water mixture was used to properly disperse the polyethylene particles in the sampler.

3.1.2.2.1. Sensitivity Analysis on PSD Measurements

Since the parameters that were used to determine particle size distribution were not measured but rather estimated from literary sources, a sensitivity analysis was performed on these parameters. The program that is designed to control the Malvern Mastersizer only stores the raw data from the sensors. Then using the input parameters, a transformation model on the raw data converts the data into a particle size distribution. Therefore a new transformation can occur with different parameters on the same raw data, and an appropriate sensitivity analysis can take place. The adsorption index is an indication of the amount of light that will be absorbed by the particles. For this system there were only 5 values (0, 10^{-1}, 10^{-2}, 10^{-3}, 10^{-4}) that could be used as the absorption index. Within the Malvern program there was a method of determining whether the selection was adequate. Therefore absorption index was already optimized and therefore was not included in this sensitivity study. The first parameter studied was the refractive index of the particles. Starting at a value of 1.52, the refractive index of the particle was adjusted from 1 (approximately 0.65 times the initial value) up to 3.04 (approximately twice the initial value). The d_P10, d_P50, and d_P90 of the Initial, Dropped, Loosely Bound, and Fines were selected to give a good representation of the effect of each parameter with particles of different size range. The difference between the particle diameter (at the 10^{th}, 50^{th}, and 90^{th} percentile) and the corresponding reference particle diameter (d_{PR}) at the base conditions was graphed (Figure 3.1). From this figure it is clear that the transformation model is not a linear and does depend on the size of the particles being measured. However, the difference in the particle size with reference to the base conditions was not significant where the maximum particle diameter deviation from the reference particle size was 0.6 μm, 16 μm. 1 μm, and 3 μm for the Initial, Dropped, Loosely

Bound, and Fines particles, respectively. These sizes are within any of the deviations that occur during normal sampling and therefore the refractive index of 1.52 was deemed to be a good estimate for the refractive index of the polyethylene particles for the size range studied.

The effect of the refractive index of the dispersant was also studied while keeping the refractive index of the particles at 1.52. The dispersant was composed of 60 vol% of ethanol and 40 vol% of water with a refractive index assumed to be 1.36, which is the refractive index of pure ethanol. The refractive index of pure water is close to that of ethanol at 1.33 and therefore a range of refractive indices were studied between these two extremes. As with the refractive index of the particles, the d_P10, d_P50, and d_P90 of the Initial, Dropped, Loosely Bound, and Fines were selected to investigate with, while looking at the difference between the particle diameter and the corresponding reference particle diameter (d_{PR}). The results are shown in Figure 3.2, with similar results as the refractive index of the particles. The data did not display any sort of linearity and with a maximum deviation in the reference particle diameter being 0.6 µm in any region.

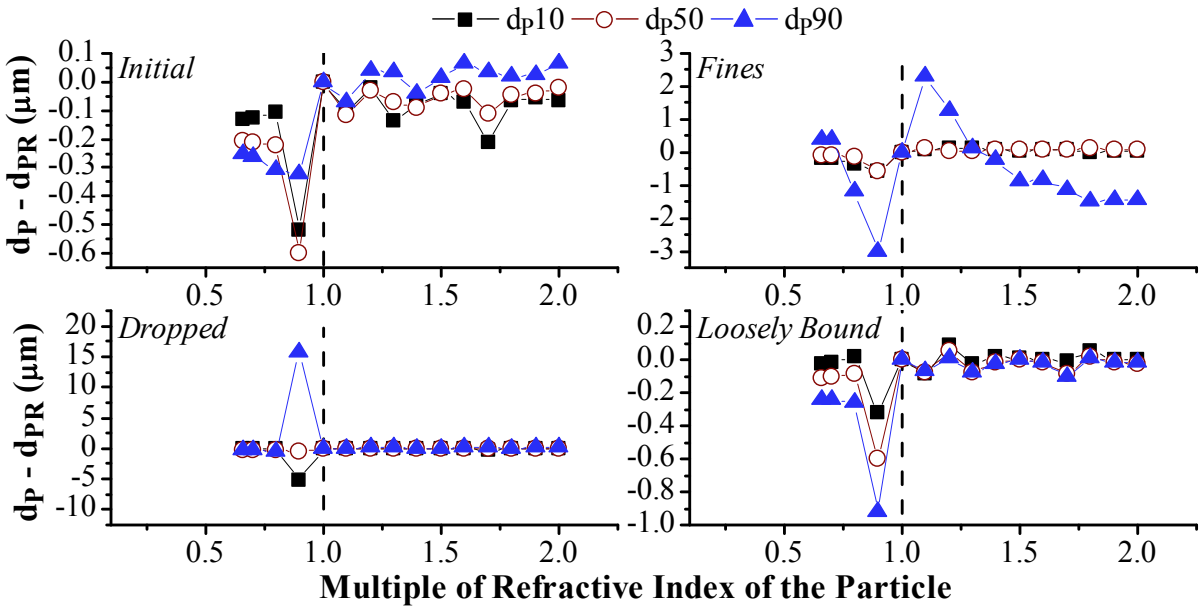


Figure 3.1: The difference in particle size (d_P10, d_P50, d_P90) against a reference particle size (d_{PR}) for different multiples of the refractive index of the particles.

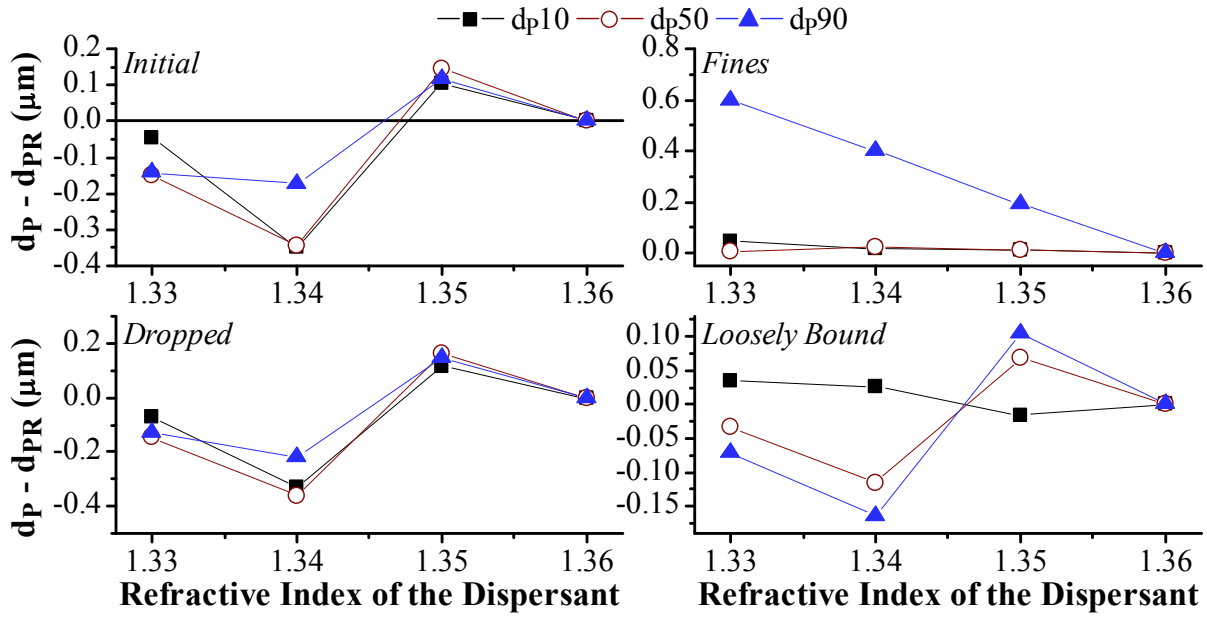


Figure 3.2: The difference in particle size (d_P10, d_P50, d_P90) against a reference particle size (d_{PR}) for different refractive indices of the dispersant. Pure water has a refractive index of 1.33 and pure ethanol has a refractive index of 1.36.

3.1.2.3. Particle Mass Distribution

The mass distribution analysis was performed by sieving small samples of the polyethylene particles with a sieve shaker (W.S. Tyler Ro-Tap Model RX-29) into eight different sizes using seven different sieves. The particles were sieved for 15 min before the mass was measured and a PSD analysis was performed for each sieve tray. This test was repeated at least five times per particle type, where the mass per tray was normalized to the amount of initial mass and were averaged to give the overall mass distribution. Both the mass and volume distribution are shown in Figure 3.3. From the distributions in the figure, PE_A contained the largest amount of smaller particles. PE_B was similar to PE_A but contained less of the fines but with a larger fraction of the bigger particles. PE_C was definitely the largest of the three resins, having the largest size distribution.

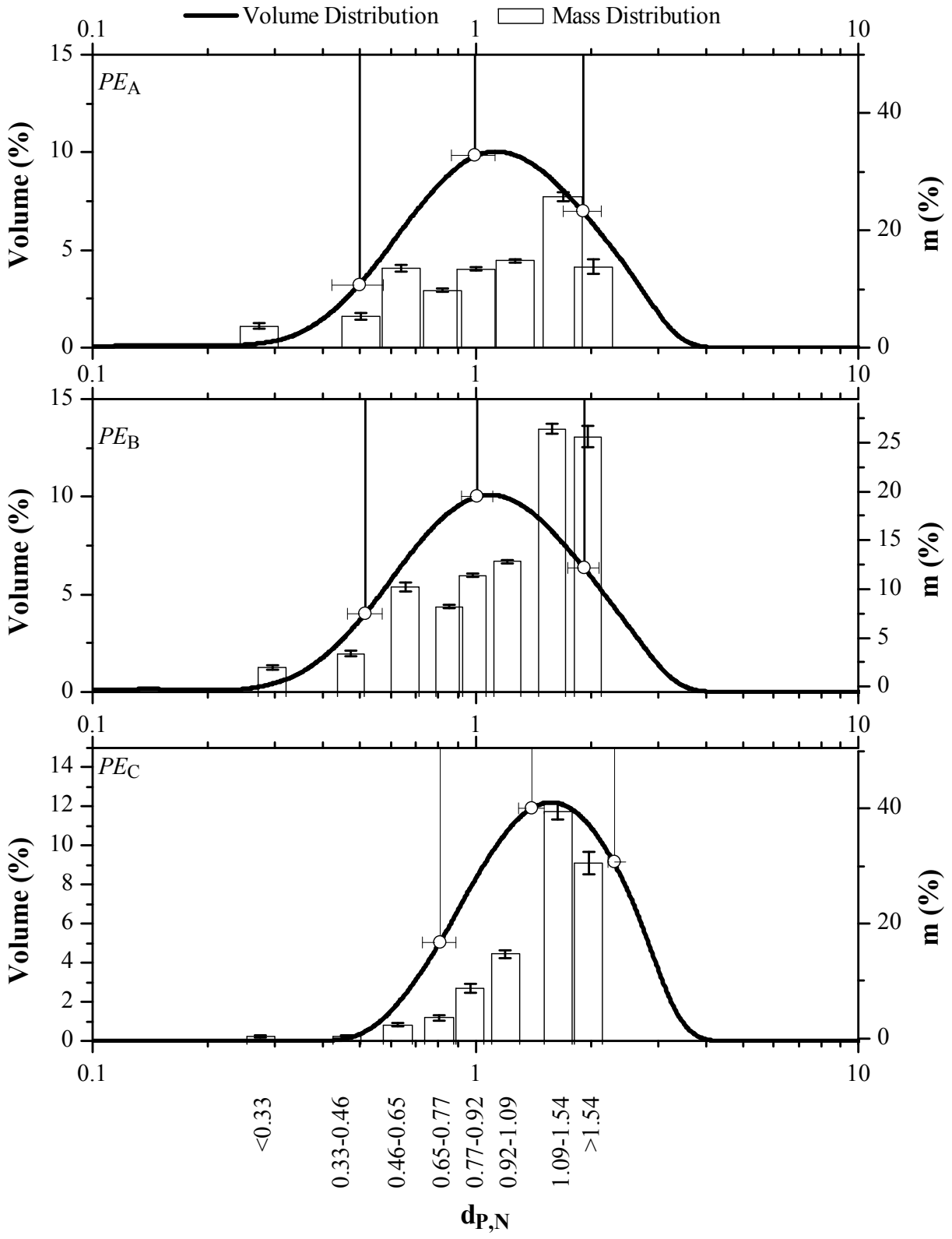


Figure 3.3: Polyethylene resins (PE_A, PE_B and PE_C) average volume distribution from PSD analysis, and the mass distribution from sieved tests.

3.1.2.4. Particle Charge Distribution

Faraday cup method quantifies electrostatic charge by measuring the net charge of the objects. Therefore in the case of fluidizing particles, the presence of bi-polarly charged particles would not be detected, except possibly for very small sample sizes. In order to determine whether a sample contains both positively and negatively charged particles and investigate the sample charge distribution, a Charged Particle Separator (CPS) apparatus was designed and built in-house.

As can be seen in Figure 3.4, the apparatus consisted of two copper plates situated in an angle above four Faraday cups. A high voltage power supply (Ultravolt HV Rack Model 1-250-00265) was used to positively charge one of the plates up to 40 kV, whereas the other plate was grounded to act as a negatively charged plate. Four digital electrometers (Keithley 6514) were attached to the four Faraday cups. All electrometers were also connected to a computer for data collection with LabView software. Small copper strips were placed on top of the Faraday cups, right at their edges, to prevent the electrical field generated by the positively charged copper plate and the particles as they travel down into the cups from affecting the measurements done by each cup. The entire system was enclosed in an isolative box for safety purposes (i.e., high voltage field). The box was made of Plexiglas at the front and top, and polyethylene sheet at the back and the bottom. The front side was designed to be easily removed at the end of each test so that particles collected in each cup to be removed for their mass and size distribution measurement.

Tests were repeated five times to ensure reproducibility. From Figure 3.5, it is clear that all resins initially started out bi-polarly charged where PE_A and PE_C particles collected in FC1 had a larger q/m than those of PE_B. Overall, it can be seen that particle size increased from positive plate to FC4 indicating that smaller particles were negatively charged and larger particles were positively charged.

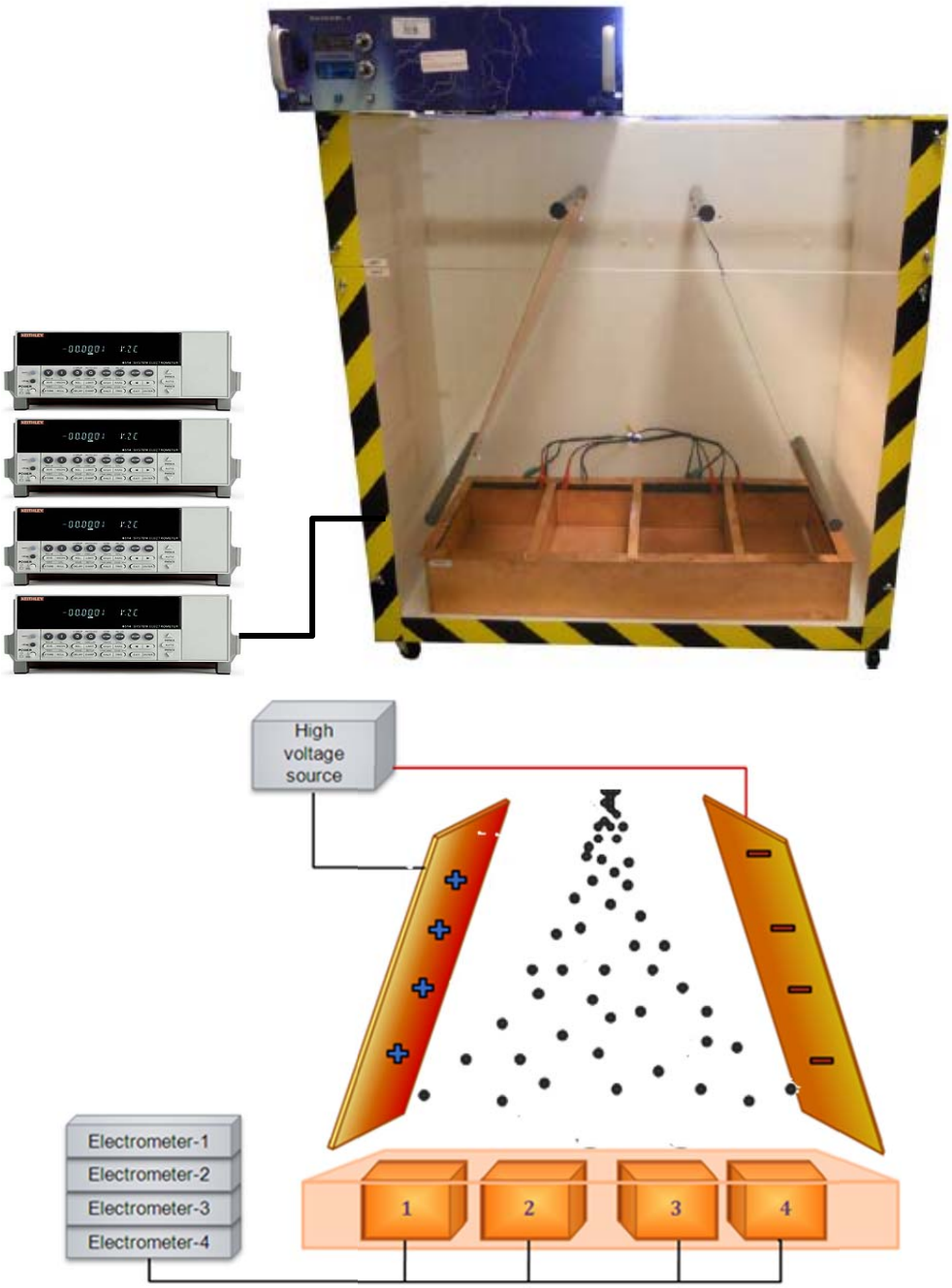


Figure 3.4: Picture and schematic of the Charged Particle Separator.

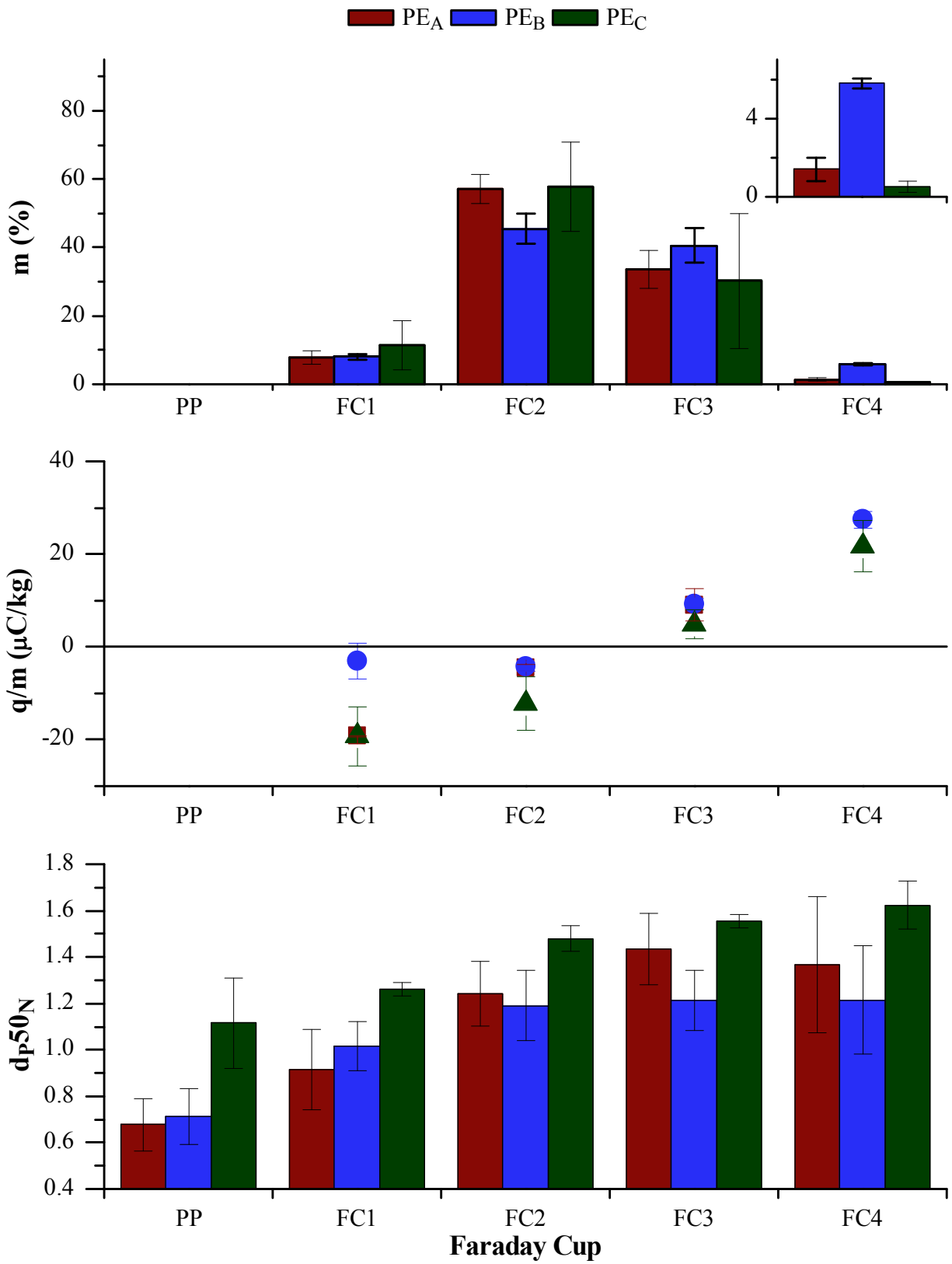
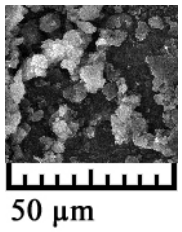
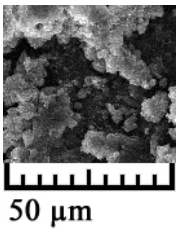
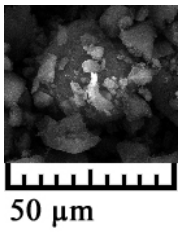
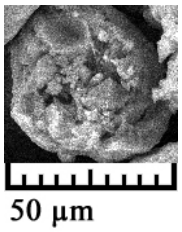


Figure 3.5: The initial polyethylene resins m%, q/m, and d_P50 measured using Charged Particle Separator (PP stands for positive plate).

3.1.3. Solid Additives

One objective of this research was to investigate the effect of solid additive injection on the reactor wall fouling and fluidizing particles charging. Four types of solid additives (A, B, C and F) were examined in this research with Additives A and B known to be static drivers that are used in industrial operations to reduce the amount of reactor wall fouling, whereas additive F was a deactivated metallocene catalyst and Additive C was the base of the same catalyst. Similarly to the polyethylene particles, the additives were characterized based on their physical and chemical properties with a summary presented in Table 3.4. Due to confidentiality reasons, the chemical formula and structure of the additives are not provided in this thesis.

Table 3.4: Additives A, B, C, and F Physical, Chemical and Electrical Properties.

		Additive A	Additive B	Additive C	Additive F
Surface Properties					
SEM		 50 µm	 50 µm	 50 µm	 50 µm
Sphericity		0.6514	0.7092	0.7003	0.8378
Morphology		Jagged	Bumpy	Jagged and sharp	Relatively smooth
Physical Properties					
Density	kg/m^3	878.2	1001.6	460	2100
d_P10_N		0.01	0.01	0.04	0.06
d_P50_N		0.12	0.03	0.08	0.10
d_P90_N		0.40	0.09	0.15	0.16
$\hat{A}$	m^2/g	0.379	0.363	0.439	0.0873
Flowability		Clumping	Clumping	Easy	Easy
Mean Particle Size Comparison		o	•	o	o
Chemical Properties					
Elements		-	Al	Si	Si, Zr, Al
Polar Molecule		Yes: Tertiary Amine with two OH groups	Yes: OH, COOH	-	-
Water adsorption		Hydrophilic	Hydrophilic	Hydrophilic	Hydrophilic
Electrical Properties					
Permittivity	F/m	-	-	-	-
Conductivity	S/m	-	-	-	-
Work Function	eV	-	-	5	-

As seen in Table 3.4, these additives varied in functional groups, size, surface morphology, and composition. The density of additives was taken from the material safety data sheets (MSDS), and through a literature search.

Most of the electrical properties for the additives were not known because these substances were very specific and sometimes proprietary materials and therefore no published literature values were known. Also some of the additives were a composite of a few different molecules, further increasing the difficulty of predicting their electrical properties. The work function for Additive C was taken from Tanue and Masuda (2006).

3.1.3.1. SEM and EDX Analysis

The SEM and EDX analysis was performed using the same facility as mentioned previously. The sphericity of the particles was calculated by taking the average of the circularity of numerous particles from the SEM pictures presented in Table 3.4.

3.1.3.2. Additive Particle Size

A PSD analysis was performed on all additives by the Malvern Mastersizer using ethanol as the dispersant (Figure 3.6). It can be seen that Additive A and B were the smallest particles followed by Additive C, and Additive F. It is important to note that Additive A appeared to be slightly bi-modal in nature, or this could be attributed to particle agglomeration during the measurement. During the measurements, sonication was used to attempt to break-up any agglomerates however this did not have any significant effect. Another type of experiment also confirmed the bi-modal size distribution of this additive. The test was performed where Additive A was injected into an empty fluidization column while compressed dry building air was passing through the column. Additive A showed particle separation where some of the particles were entrained and some left behind on the distributor plate. Samples taken from the top and the bottom of the column showed two distinct particle sizes validating the bimodal in nature this additive.

The average particle size and specific surface area ($\hat{q}/\hat{A}$) were taken from PSD tests conducted with Malvern Mastersizer. It should be noted that the specific surface area calculated by the Malvern Mastersizer was depended highly on the material density and absorption index, both of which found from different sources as mentioned above.

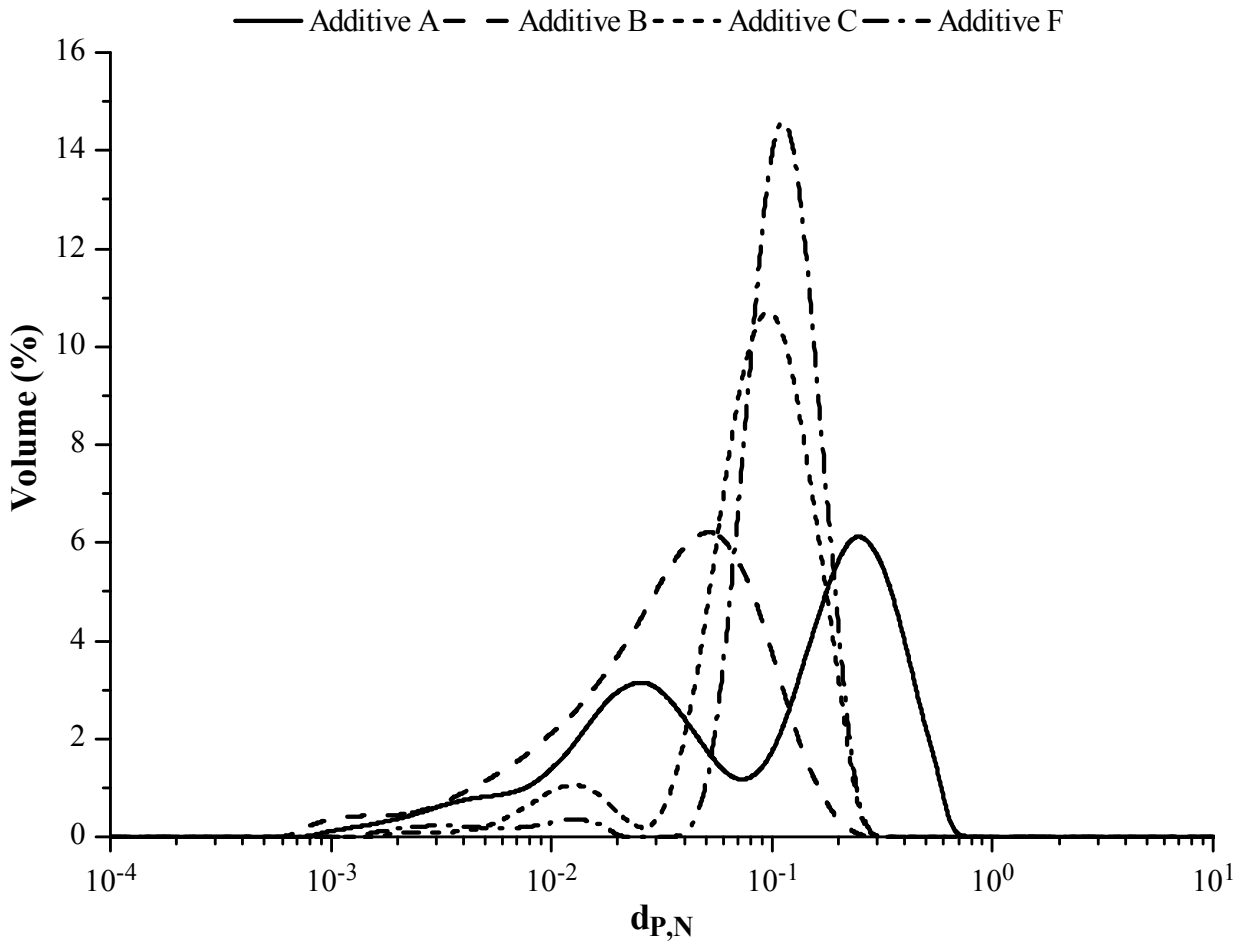


Figure 3.6: PSD of the additives A, B, C and F.

3.2. Experimental Apparatus

This section describes the implementation of the developed electrostatic charge measurement technique in a pilot-scale fluidization system (Figure 3.7).

3.2.1. Fluidization Column

The fluidization column was a three-dimensional metallic column (Figure 3.8). The downside to a metallic column is not being able to view inside of the fluidized bed. However, because particle-wall interactions play an important role in particles charging and reactor wall fouling, it was important to use typical industry conditions. The column was made out of carbon steel, 0.10 m in diameter and 1.27 m in height. Numerous ports were placed alongside of the column at different heights for mounting different instrumentations such as pressure transducers.

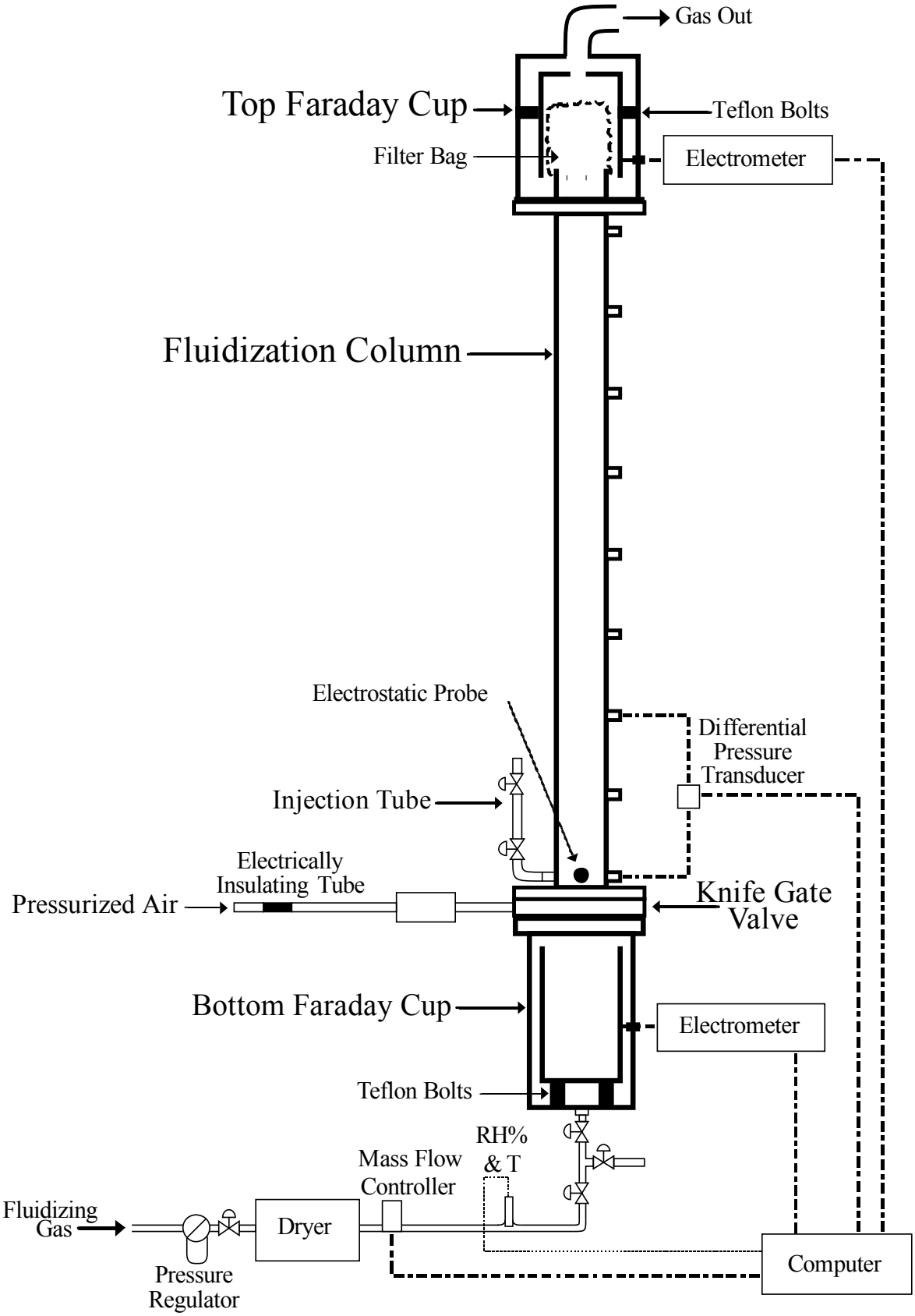


Figure 3.7: Overall schematic of the experimental setup.

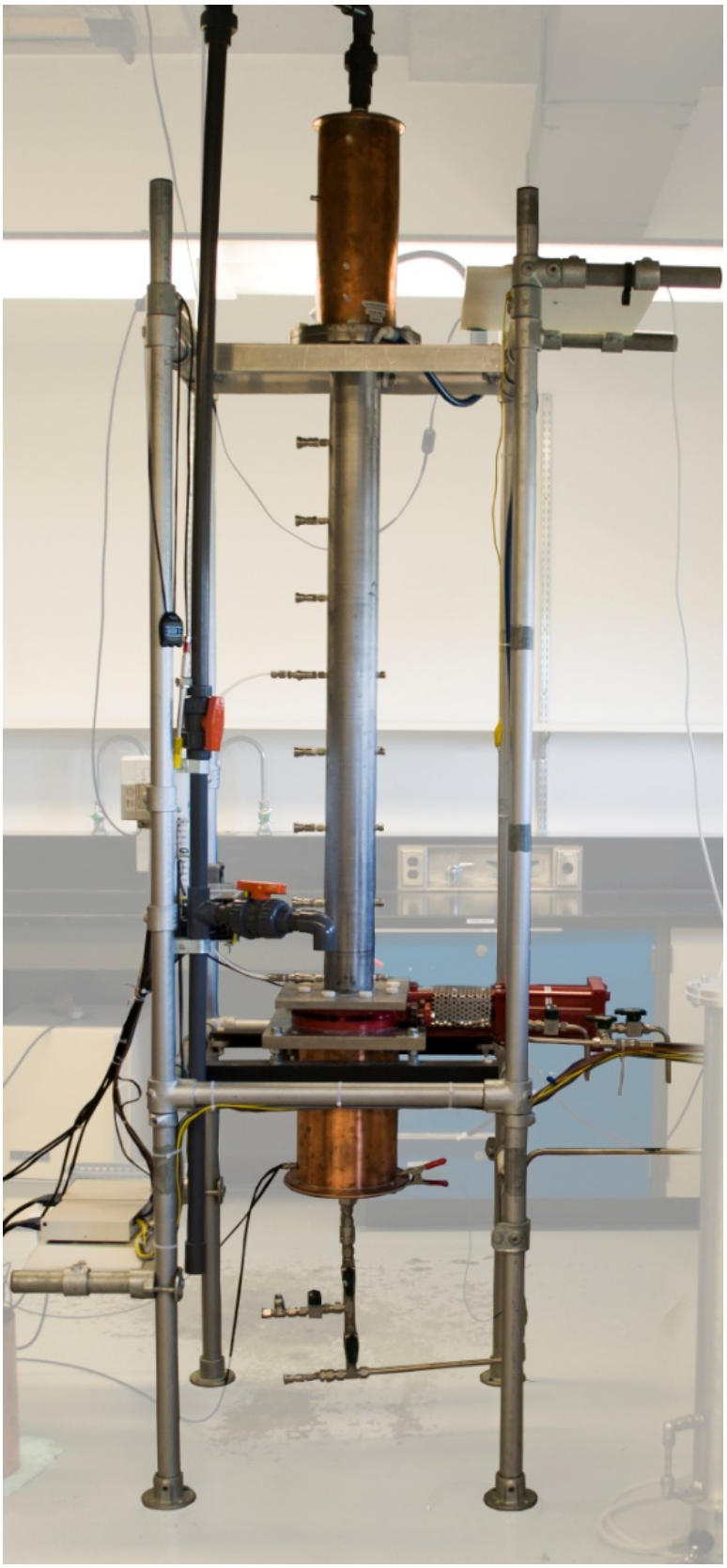


Figure 3.8: Picture of the fluidized bed.

3.2.2. Distributor Plate

In order to discharge the bed particles into the Faraday cup below the distributor plate, a special design was considered where the distributor plate was replaced by a knife gate valve. Figure 2.2 shows the picture of a 0.01 m (4 inch) Series G pneumatic knife gate valve utilized in this system supplied by the Red Valve Company Inc. (Carnegie, PA, USA). The valve was pneumatically controlled to freely open and close. Tests showed that the valve could open or close in approximately 0.4 seconds. The blade of the valve was fabricated from stainless steel and it was modified to act as a perforated distributor plate for fluidization. This was achieved by drilling 0.002 m diameter holes through the valve blade (Figure 2.2b). The bottom of the blade was recessed in order to place a 32 micron stainless steel screen that was sandwiched between the porous valve blade and an attached stainless steel plate with 0.004 m holes on its underside. The purpose of the screen was to prevent any fine particles to go through the distributor plate.

3.2.3. Bottom Faraday Cup

The bottom Faraday cup was constructed of two cylindrical copper columns separated by Teflon bolts to allow for complete electrical isolation of the inner vessel (Figure 3.9). The inner vessel was 0.1524 m in diameter and 0.2540 m in height, and was directly connected to a digital electrometer (Keithley Model 6514). The outer vessel was 0.2032 m in diameter and 0.3302 m in height, and was grounded. The bottom of the outer cup was flanged, which allowed to be opened so that the inner cup to be removed while the outer cup remained bolted to the fluidization column.

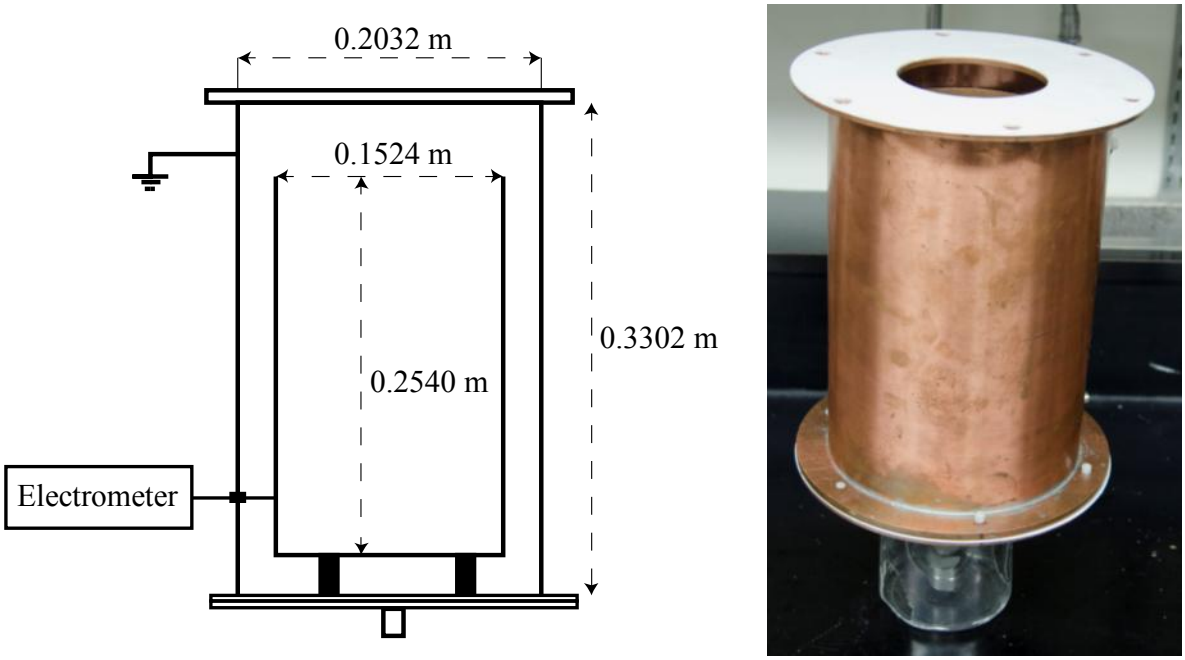


Figure 3.9: Schematic and picture of the bottom Faraday cup.

3.2.4. Top Faraday Cup

The top Faraday cup was designed in such a way that the entrained particles were trapped within the inner cup to measure their charge, as well as mass (Figure 3.10). The inner cup was 0.13 m in diameter and 0.20 m in height, while the grounded outer cup was 0.15 m in diameter and 0.26 m in height. Both cups were constructed out of copper. The inner cup was suspended inside the grounded outer cup with four Nylon bolts to ensure that the inner and outer cups were electrically isolated from each other with the inner cup being directly attached to a digital electrometer (Keithley Model 6514). The filter bag was attached to an extension of the fluidization column, which was in turn electronically isolated from the main fluidization column by a Teflon gasket and Nylon bolts. The filter bag was cleaned and reused for every experiment. In order to ensure that the entrained particles stayed within the filter bag when the fluidizing gas was stopped, as well as when the bag was removed for its weight measurement, the bag was filled with a dust lock filter (BC Air Filter with 26-30% dust capture efficiency of 1 μm particulates) which also contained some adhesive material.

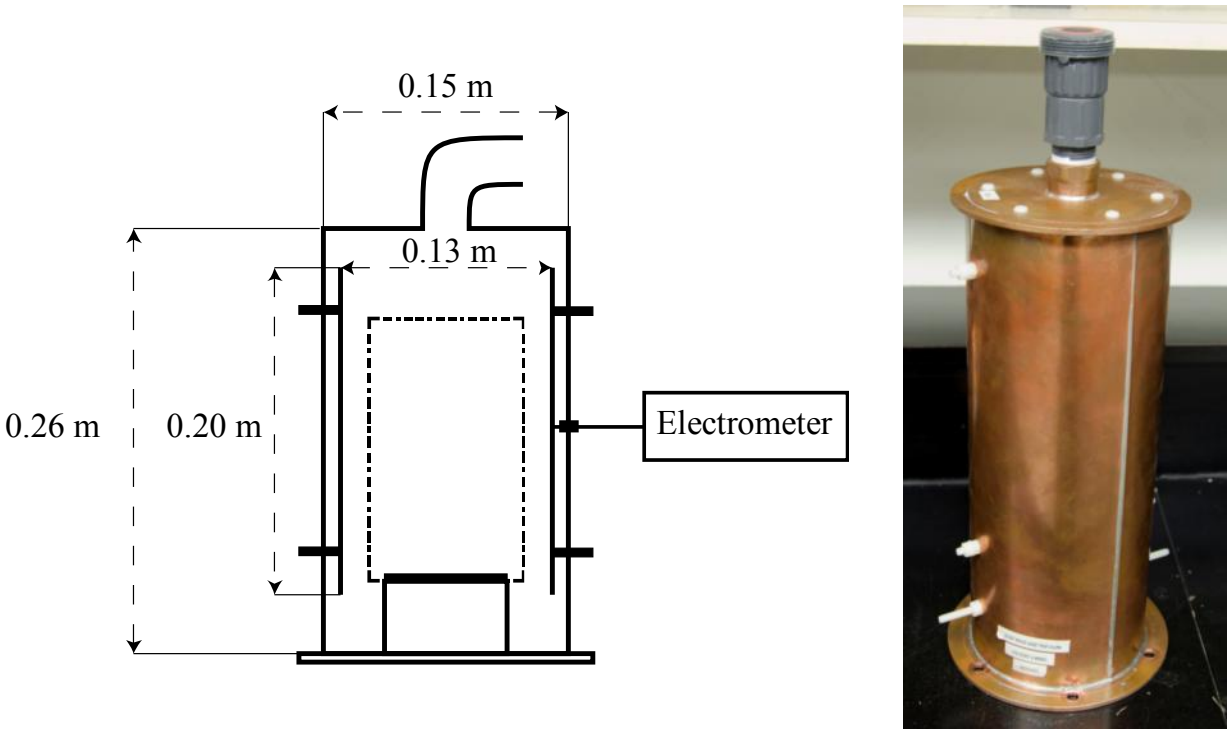


Figure 3.10: Schematic and picture of the top Faraday cup.

3.2.5. Bench Scale Faraday Cup

A bench-scale Faraday cup (Figure 3.11) was used to measure the initial charge of the fluidizing particles prior to their placement inside the fluidization column, and also to measure the total net particles charge in other preliminary and bench-scale tests. This Faraday cup was constructed out of two concentric cylindrical copper cups with a Teflon sheet placed between them to electrically isolate the two cups from each other. The inner cup was directly connected to a digital electrometer (Keithley Model 6514) and the outer cup was grounded to act as an electrical shield.

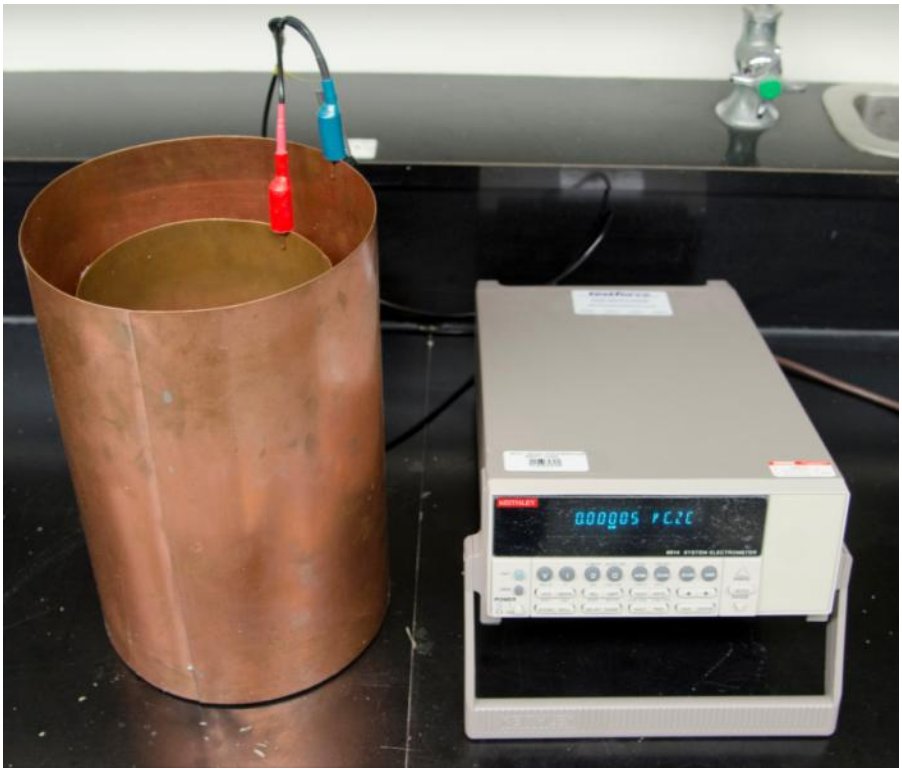


Figure 3.11: Picture of the bench-scale Faraday cup.

3.2.6. Instrumentation

A differential pressure transducer (Omega model PX-654) was used to measure pressure drops along the fluidized bed. A mass flow controller (MKS Model 1559A) with a range of 0-200 SLPM with an accuracy of ± 2 SLPM was attached to the gas feed line to adjust the gas flow rate to the fluidization column A Vaisala temperature and humidity transmitter (HMT338) with an accuracy of ± 1% between 0-90% relative humidity, and ± 1.7% between 90-100% was used to measure the humidity of the inlet gas. The temperature was measured with an accuracy of ± 0.2 °C.

Throughout all experimental runs, the mass of the particles was measured using a variety of mass balances from Denver Instrument. An analytical mass balance (SI-114, 0-110 g ± 0.0001g) was used for the measurement of the high precision measurements, namely for the entrained particles collected in the filter bag and the initial mass of the additive being injected. For all other measurements a large capacity mass balance (SI-6002) with a maximum capacity of 6 kg ± 0.1 g, was used.

Electrostatic charge measurements were conducted by a Keithley digital electrometer (Model 6514). Four different charge measurement ranges were available with this unit: 20 nC, 200 nC, 2 μC, 20 μC. For most charge measurements, a range of 2 μC was used; however, when large quantities of mass were collected inside the bottom Faraday cup the higher range of 20 μC was applied. Both the 2 and 20 μC ranges had an accuracy of ± 1 + 50 (%rdg + counts), where error was a combination of gain error (1) and offset error (50) which was defined as counts of the least significant digit.

Although the purpose of this research was to apply Faraday cup method for the electrostatic charge measurement, an electrostatic probe which is generally used in industrial applications (supplied by industrial collaborators, Univation Technologies LLC, Texas, USA) were also mounted within the system for comparison purposes. The probe was a contact ball probe where a cylindrical steel probe was wrapped in a Teflon tube before being covered in another metallic tube (Figure 3.12). The ball probes had an approximately 0.127 m diameter. The outer metallic tube was grounded and acted as an electrical shield. The ball probe were placed along the fluidization column; one at a distance of 0.025 m above the distributor plate (Figure 3.7), and both probes were connected to Keithley 6514 electrometers where either the charge or current were measured at approximately 10 Hz during the entire fluidization period. There are 10 different current measurement ranges on the unit ranging between 20 pA to 20 mA. A range of ± 2 μA with an accuracy of ± 0.1 + 10 (%rdg + counts) was used. Again the error was a combination of the gain error (0.1) and offset error (10) which is defined as count of the least significant digit. The probes were tested for any charge leakage during measurement with a similar procedure to that explained in §C.1. It was found that the background measurements from the electrostatic probe were also negligible.

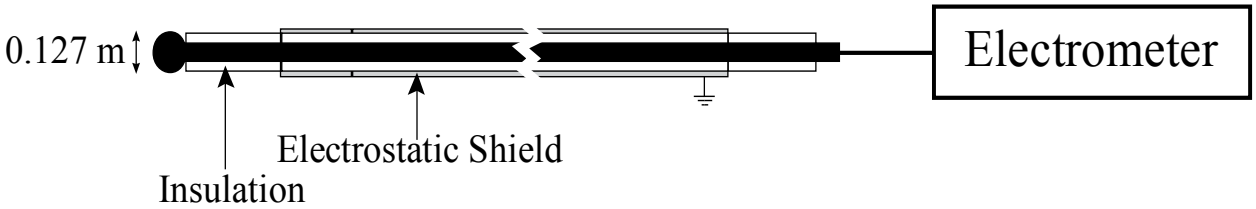


Figure 3.12: Schematic of the electrostatic probe.

3.3. Experimental Procedures

The following sections describe the procedures followed for various experiments performed in this work.

3.3.1. Minimum Fluidization Velocity

Since majority of the fluidization experiments were performed with the polyethylene resin as received (i.e., having a very wide size distribution) and the theoretical calculations of minimum fluidization velocity (u_{mf}) rely on a single particle diameter, this velocity was measured experimentally. For the experimental method, particles were poured into the fluidized bed and the gas volumetric flow rate was increased step wise at five minute intervals. At each flow rate, the differential pressure fluctuations between the top and bottom of the static bed where measured at 100 Hz and recorded by LabView software. These fluctuations were averaged to give the average pressure drop at a given gas velocity. The pressure drop increased linearly with increasing gas velocity until one point where the pressure drop remained relatively constant. The intersection between the sloped line of increasing pressure drop and the line through constant pressure drop was considered to be at the u_{mf} of the particles. The experiment was then repeated by decreasing the gas velocity stepwise in five minute intervals and an average of both of these values were used to determine the u_{mf} of the particles. An example of the experimental u_{mf} calculations can be seen in Figure C.3 (Appendix C). The experimental value was also compared to two theoretical correlations for calculating the u_{umf} as proposed by Grace (1982) and Kunii and Levenspiel (1991). A comparison of these values can be found in Table 3.5 with the detail calculations presented in §C.2.1.

Table 3.5: Comparison of u_{mf} determined by different methods.

Method	u_{mf} (m/s)
Experimental	0.131
Grace (1982)	0.136
Kunii and Levenspiel (1991)	0.130

During the minimum fluidization experiments, visual observations of the bed height were made by looking down into the column. These heights were then correlated to the fluidizing gas velocity. Concurrently, the qualitative measurements of the bed hydrodynamics were made for

when the bed approached minimum fluidization velocity and the transition from bubbling to slugging flow regime.

3.3.2. Fluidization Experiment

A standard operating procedure was followed for all experiments conducted in this research. Before each run, the interior of the fluidization column and the top surface of the knife gate was thoroughly cleaned, and then grounded to remove any remaining charge. In more recent experiments dry compressed air was sent through the system for at least one hour to ensure that the system was completely dry.

Fresh batches of particles were used for each experiment while maintaining a static height to column diameter ratio (L/D) of 4. The mass of particles was measured followed by their initial charge with a bench-scale Faraday cup before pouring the particles into the fluidization column. A sample of the Initial particles was taken for a PSD analysis. The mass of the filter bag, containing four layers of new dust lock filters, was measured. The filter bag was then attached to the top of the column with a Teflon connector, and the Faraday cup was attached to the top of the column with Teflon bolts. The top Faraday cup and the top electrostatic probe were then connected to two separate electrometers using low noise Bayonet Neill-Concelman (BNC) cables to measure the cumulative charge of elutriated fines during fluidization.

In order for the maximum charge generation within the system to be evaluated during fluidization, the fluidization column and the distributor plate were electrically isolated. This prevented any electrostatic dissipation to the ground from the fluidization column and the distributor plate.

The Faraday cup electrometer was set on the charge mode and that of the electrostatic probe on charge or current mode and a background measurement of 60 seconds was performed prior to fluidizing the particles to ensure that not a significant signal drift existed. The fluidization gas was then introduced into the column, slowly increasing in flow (at approximately 2 SLPM every second) until the desired flow rate was reached and was controlled by a mass flow controller. Particles were then fluidized at this flow rate for a period of time, typically 60 minutes.

During fluidization, the cumulative charge of the entrained fines found by the top Faraday cup, the electrostatic probe measurements (either current or charge), the bed differential pressure fluctuations, the fluidizing gas volumetric flow rate, and the fluidizing gas and the room temperature and relative humidity were monitored and recorded by LabView software.

Upon the completion of the fluidization period, another background signal measurement was done on the electrometers by continuing the electrometers measurements while the gas flow rate was slowly decreased to 0 SLPM (at approximately 2 SLPM every second). The background measurement was conducted for a period of 5 minutes.

The top Faraday cup was then removed to access the elutriated fines trapped within the filter bag. The filter bag was then removed to determine the mass of entrained fines and a sample of the Fines was taken for a PSD measurement.

The bottom Faraday cup was then connected to an electrometer with a low noise BNC cable and a background reading was measured as previously described. After one minute, the knife gate valve was opened so that the bulk particles would be dropped into the bottom Faraday cup for their charge to be measured. The bottom Faraday cup was then removed in order to measure the mass of the particles collected and a sample was taken for a PSD measurement.

Before putting the bottom Faraday cup back on the column, the qualitative measurement of the amount of wall fouling was conducted by taking a picture of the interior column wall from the bottom of the column. The bottom Faraday cup was then cleaned and placed back on the column. The charge of the Loosely Bound particles was measured after a background charge measurement of the empty Faraday cup was recorded for 60 seconds. In order to dislodge the Loosely Bound particles, the top of the column was lightly tapped with a mallet so that the particles attached to the column wall would dislodge from the wall and fall into the bottom Faraday cup. After there was no change in charge measured by the electrometer the tapping was stopped. The remaining particles were then attempted to be dislodged by using a stream of compressed building air through a small tube sent down the column from the top. The charge measurement was continued until again there was no change in the measured charge. After this point, the remaining particles on the wall were the Tightly Bound particles that could not be

removed without any additional particle handling. The bottom Faraday cup was then removed in order to measure the mass of the Loosely Bound particles. A picture of the remaining Tightly Bound particles was taken from the bottom of the column for a qualitative measurement of the amount of remaining wall fouling. Samples were taken from both the Loosely Bound and Tightly Bound particles for PSD analysis.

All data was logged and saved to a computer using LabView software (Version 8.5, National Instruments Inc., USA) at approximately 8 Hz.

3.3.2.1. Fluidization with Additive Injection

The experiments performed with the solid additives followed the same procedure as above with some exceptions. Prior to pouring the PE particles into the fluidization column, the additive injector apparatus, constructed out of stainless 316 with a 6.35 mm outer diameter at the narrowest point. (Figure 3.7), was placed into the column such that the injection tube extended the entire diameter of the column. This was done to reduce the chances of any PE particles clogging the injector when they were poured into the fluidization column. After the PE particles were poured into the column, a fraction of the additive was loaded into the injector and the unit was attached to an extra dry air line pressurized at 5.4 atm. Extra dry air was supplied from a gas cylinder. The injector was then partially withdrawn from the column, and the additive was injected into the bed of particles. More additive was then loaded into the injector and the unit was further withdrawn from the column and another injection was conducted. This procedure was repeated until no additive remained and the tip of the injector tubing was flush with the column wall.

Upon the completion of the additive injection, the fluidization experiments were performed following the procedure described in previous section.

3.3.2.2. Repeatability of Experiments

Due to the sporadic nature of gas-solid fluidization and the unpredictable nature of the electrostatic charge generation, the repeatability of electrostatic charging related experiments in

gas-solid fluidized beds is often disputed. In order to possibly determine the source of the variance (and ultimately the standard deviation), a hierarchical design approach was taken. Typically the hierarchical design allows for the estimation of the variance in the process, in batch samples, and in analytical tests on one output variable. The variance of the analytical tests can be measured by testing the same sample repeatedly, whereas the variance of the batch sample can be measured by taking the numerous samples from one batch (or experiment), and the process variance can be measured by repeating an experiment numerous times. For the system in this research, there were many output variables and therefore only a few of the variables were selected, namely the mass, d_P50_N, and q/m of the Initial, Fines, Dropped, Loosely Bound and Tightly Bound particles. The experiments were performed at least 10 times to limit the amount of process variation. The experiments were performed with PE_C resin as received and therefore for each trial the Initial particle size and charge distribution was not controlled.

For the q/m, the total net charge of the particles must be measured and since removing and replacing the particles changes their net charge, testing the repeatability of the Faraday cups measurement could not be found. Therefore, only the variance in the experiment could be determined. With the mass of the particles, the mass can be measured repeatedly on the same balance. Therefore, the variance of the analytical test can be measured as well as the experiment variance. In order to have a good measure of the variance in the analytical test (mass balance), the mass of the particles (Initial, Fines, Dropped, and Loosely Bound) were weighed five times consecutively. With the d_P50_N, the variances for the analytical test (PSD from the Malvern Mastersizer), the sample, and the process can be measured. Since less than 1 g of particles is required to perform a PSD, this hierarchal design also helps determine if there are any issues with sub sampling. For example, when the PSD is completed with the Dropped particles less than 1 g is used for a sample of over 900 g. It is questionable whether or not taking 1 g as opposed to a higher mass would have any significant difference in the measured PSD. Therefore in order to test this all samples that were taken were measured five times by the Malvern Mastersizer. For the Initial, Dropped, and Loosely Bound particles five samples were taken but for the Fines and Tightly Bound particles two samples were taken due to the limited amount of particles present in each region. This was done for at least 10 experiments.

The experiments were performed with the resin as received (i.e., having a wide size distribution) at 1.5 u_{mf} fluidizing gas velocity for a 60 min of fluidization period. The experiments were all done by one operator and all repeated in a row within one week. The results for the q/m for different repetitions are shown in Figure 3.13. The Initial particles q/m was relatively constant with some degree of variability. The Fines were always predominantly positive; however, the q/m had a large range between approximately 25 to 150 μC/kg. The Dropped particles were the most unpredictable where 3 out of the 11 experiments were positively charged while the rest were negatively charged. The Loosely Bound particles showed the most stable and consistent results with a q/m ranging 10 times out of 11 between approximately -60 to -80 μC/kg. Therefore from Figure 3.13, only the q/m of the Fines and the Dropped particles showed a large amount of variability.

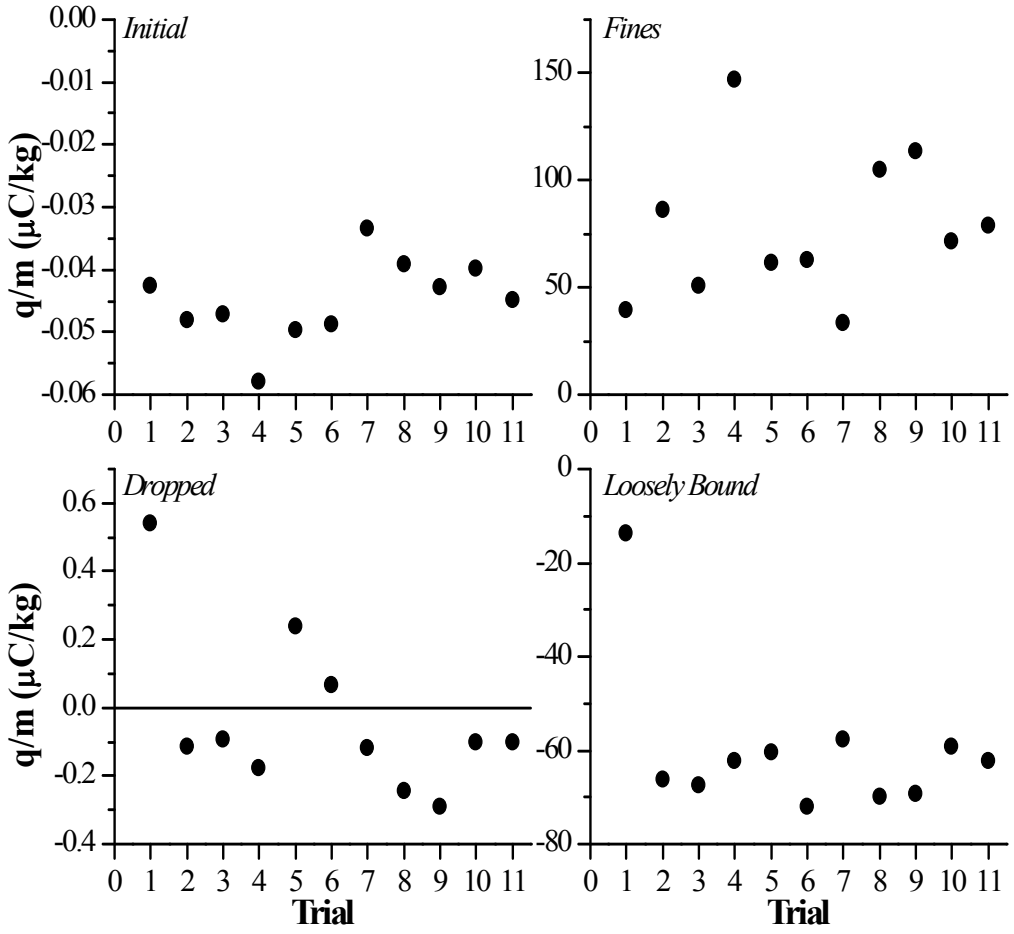


Figure 3.13: The q/m of the Initial, Fines, Dropped, and Loosely Bound particles for the repeated experiments at 1.5 u_{mf} and 60 min of fluidization.

Figure 3.14 shows the variability in the particles mass collected (m%). The m% is measured by dividing the mass found in a region by the particles initial mass; therefore the initial mass is not presented. The error bars on the graph represent one standard deviation of the repeated mass balance measurements. It is clear that majority of the deviations came with the Fines measurement, which was expected since the amount of particles collected was small in comparison to the other regions. The actual mass of the Fines collected was relatively consistent, as was the m% of the Loosely Bound particles. There was however some deviation in both the Dropped and the Tightly Bound particle for no known reason besides for experimental variation.

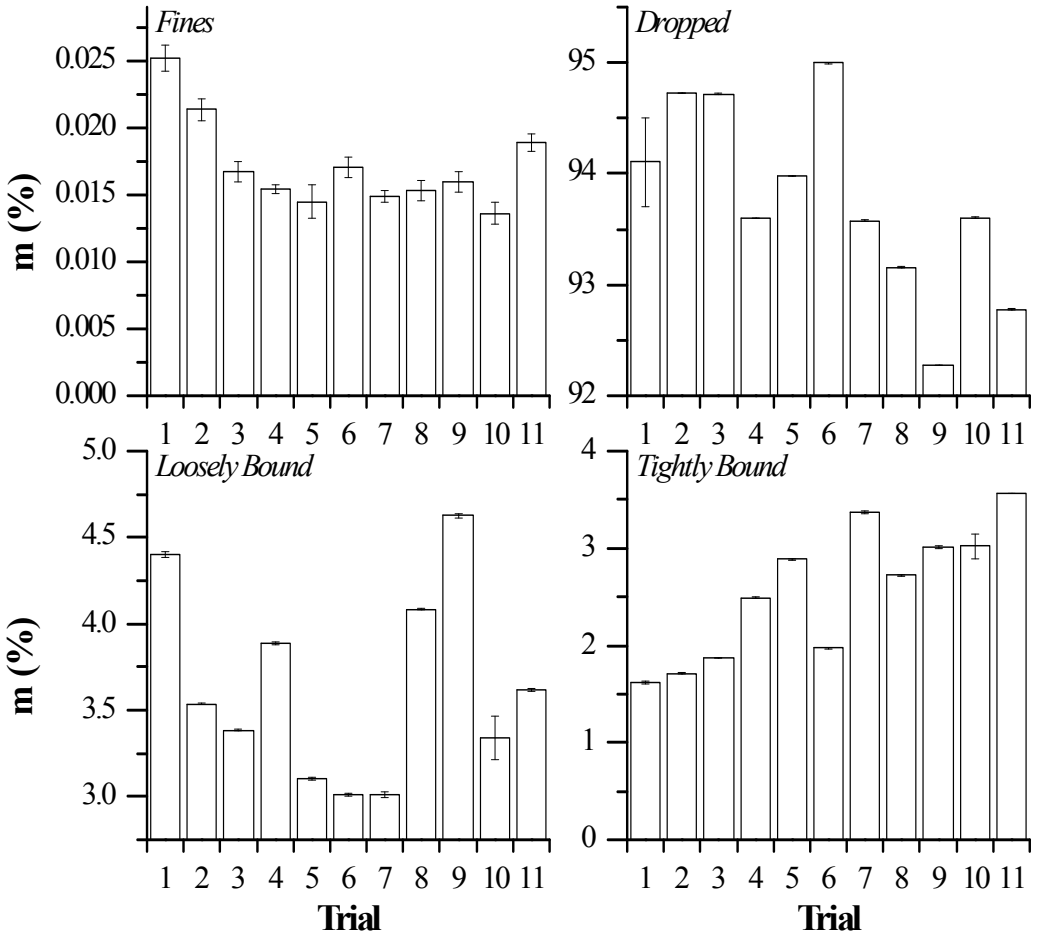


Figure 3.14: The m% of the Fines, Dropped, Loosely Bound, and Tightly Bound particles for the repeated experiments at 1.5 u_{mf} and 60 min of fluidization.

The d_P50_N of the particles in all regions is shown in Figure 3.15. The error bars represent the standard deviation of all the tests for all the samples of each particle region. The large error bars with the Initial, Dropped, and Loosely Bound particles mean that there was some degree of differences in the subsampling of the particle, suggesting some non-homogeneity in the samples. The Fines and Tightly Bound particles may not have shown such deviation due to only sampling twice in each region or by a more homogenous sample.

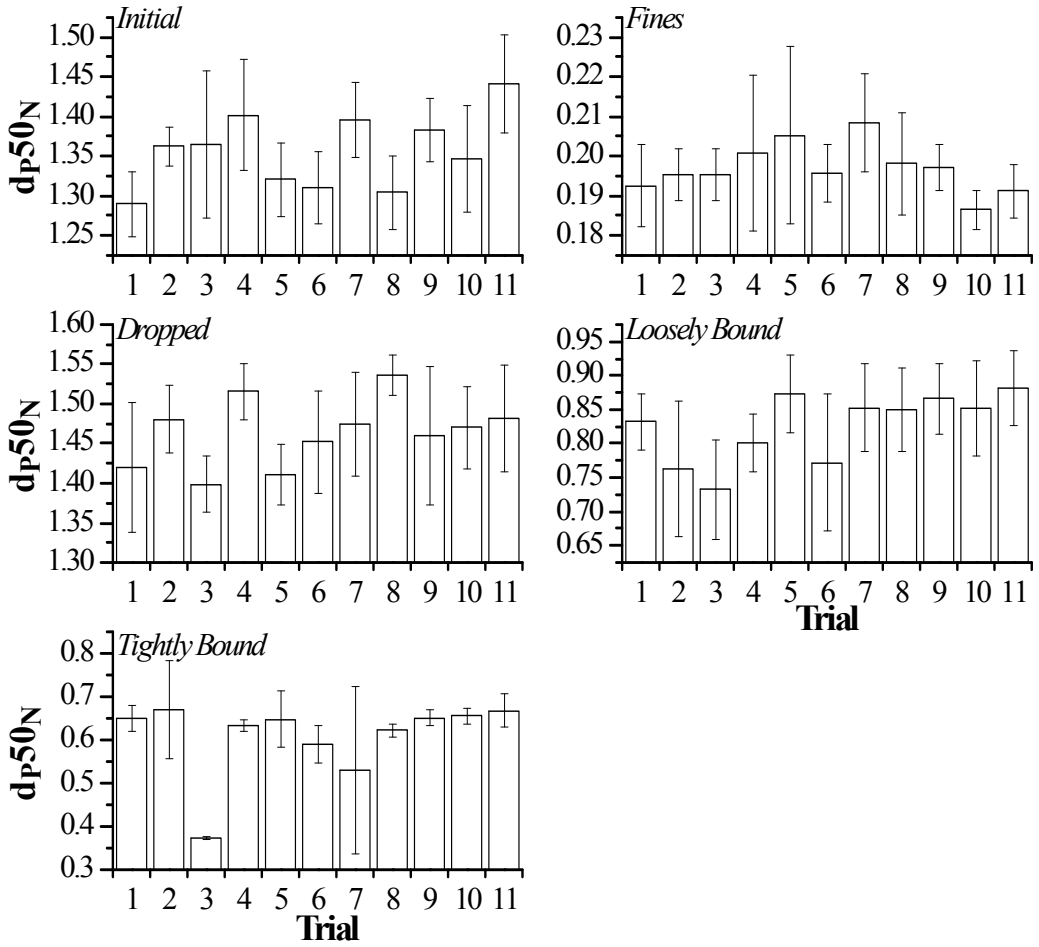


Figure 3.15: The d_P50_N of the Initial, Fines, Dropped, and Loosely Bound particles for the repeated experiments at 1.5 u_{mf} and 60 min of fluidization.

The results for the hierarchal design are summarized in Table 3.6. The standard deviation caused by the analytical tests, the samples, and the repetition was divided by the average value and is shown for each output variable (σ/μ). From results it is clear that a lot of the variability comes from the actual process with some issues with subsampling for measurement of the d_P50 of the particles. Overall, the variability of the system is caused by the uncontrolled particle size and charge distribution of the resin as received, the sporadic nature of fluidization, in addition to the presence of electrostatic charge generation. Since one of the goals of this research was to understand the charging effects of industrial resin, none of these sources of variability could be reduced.

Table 3.6: Average values for the tests and the sources of deviation.

Region	Measurement		Average	σ/μ		
				Repetition	Sample	Test
Initial	m	g	1063.57	2.30×10^{-4}	-	1.77×10^{-5}
	d_P50_N	-	1.36	0.030	0.040	0.020
	q/m	μC/kg	-0.04	0.15	-	-
Fines	m	%	0.017	0.20	-	0.046
	d_P50_N	-	0.20	-	0.060	0.045
	q/m	μC/kg	77.29	0.47	-	-
Dropped	m	%	93.76	0.0090	-	4.70×10^{-5}
	d_P50_N	-	1.46	0.024	0.035	0.023
	q/m	μC/kg	-0.037	8.33	-	-
Loosely Bound	m	%	3.64	0.15	-	0.011
	d_P50_N	-	0.83	0.050	0.086	0.010
	q/m	μC/kg	-60.02	0.28	-	-
Tightly Bound	m	%	2.57	0.26	-	0.015
	d_P50_N	-	0.61	0.121	0.023	0.191

3.4. Summary

The physical and chemical properties of all of the materials present in the fluidized system were thoroughly discussed. Dimensions and a detailed description of the experiment apparatus as well as the standard operating procedures were also presented. Finally, a statistical hierarchical approach was taken with 11 repeated experiments in order to estimate the sources of variance in the system. Overall, it was found that there is a large amount of variance between experimental trials due to the uncontrolled initial resin size distribution and the unpredictable nature of electrostatic charging.

Chapter 4.
BENCH-SCALE CHARGING EXPERIMENTS

In industrial gas-solid fluidized beds, particularly in polyethylene reactors, particles with various surface chemical and physical properties exist (i.e., polyethylene resin, catalyst, and additive particles). Consequently, the contacts between these particles themselves and with the reactor wall will play a large role in the magnitude of electrostatic charge generation within the fluidized bed and the extent of the reactor wall fouling. Therefore, it is critical to determine the fluidizing particle charging behaviour and a pseudo-triboelectric series for all the materials involved within the bed. This chapter summarizes the results obtained from bench-scale experiments undertaken in an attempt to better understand the underlying charging mechanisms involved from contacts between various materials used in the experiments performed in this thesis. The discussion presented here will then be referred to in the following chapters to aid in understanding the experimental results.

To test the charging behaviour of polyethylene resin in contact with the carbon steel fluidization column wall, a simple bench-scale test was performed. The testing involved contacting the polyethylene particles with a small carbon steel (CS) plate. The tests were performed with only PE_B and PE_C resins as received since not sufficient amount of PE_A resin had remained at the time that these experiments were conducted. Approximately 1.5 g of PE particles was first dropped directly into a bench-scale Faraday cup to measure the sample initial net q/m. Then, a similar sample was dropped onto an angled carbon steel plate situated above the bench-scale Faraday cup (Figure 4.1). The carbon steel plate was angled at approximately 42° from the horizontal and held in place by electrically insulated clamps. Between each test, the plate was cleaned and grounded to remove any excess charge, while it remained electrically isolated during the experiment. It was observed that as the particles were dropped onto the plate, some would bounce off and go directly into the Faraday cup and producing contact charging, whereas other particles would roll down the plate and introduce frictional charging.

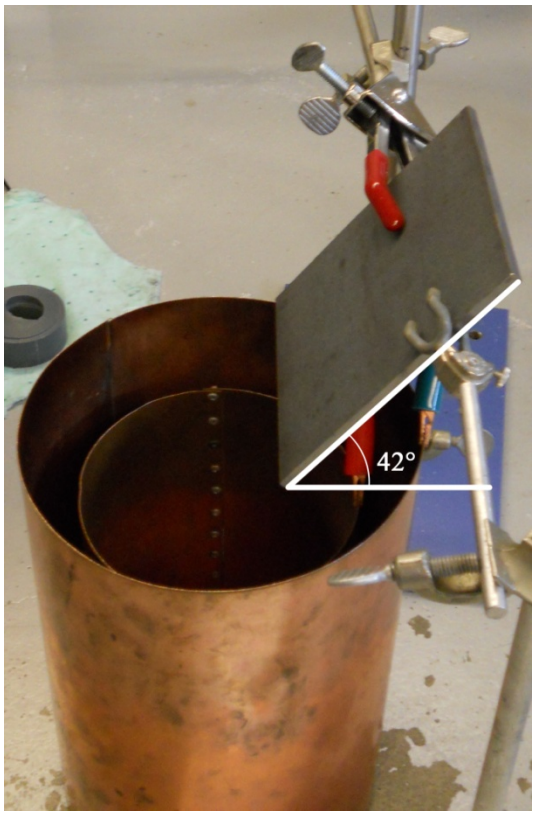


Figure 4.1: A picture of the bench-scale Faraday cup with an angled carbon steel plate placed above it.

As can be seen in Figure 4.2, the average net q/m of the particles for trials using the PE_B resin with and without contacting the carbon steel plate were on average $-5.86\times10^{-5} \pm 0.05$ μC/kg and $-2.40\times10^{-3} \pm 0.06$ μC/kg respectively, due to both positively and negatively charged samples. With the PE_C resin the net q/m without contacting the plate was -0.98 ± 0.65 μC/kg and -0.93 ± 0.34 μC/kg when contacting the plate. Results showed bi-polar charging within the samples of both resins PE_C resin having a larger negative net q/m, but with the final net q/m showed no significant difference. This was likely caused by small contact time between the particles and carbon steel plate. The majority of the particles that contacted the plate were large and would usually bounce off the plate once and into the Faraday cup. Therefore any change in charge due the particle contact with the plate would likely go undetected. The bench-scale experiment may have not allowed enough time for sufficient particle charging. However, in a gas-solid fluidized bed the number of polyethylene particle-reactor wall contacts would be much greater as the particles would be continually bombarded against the column wall which would generate more charge.

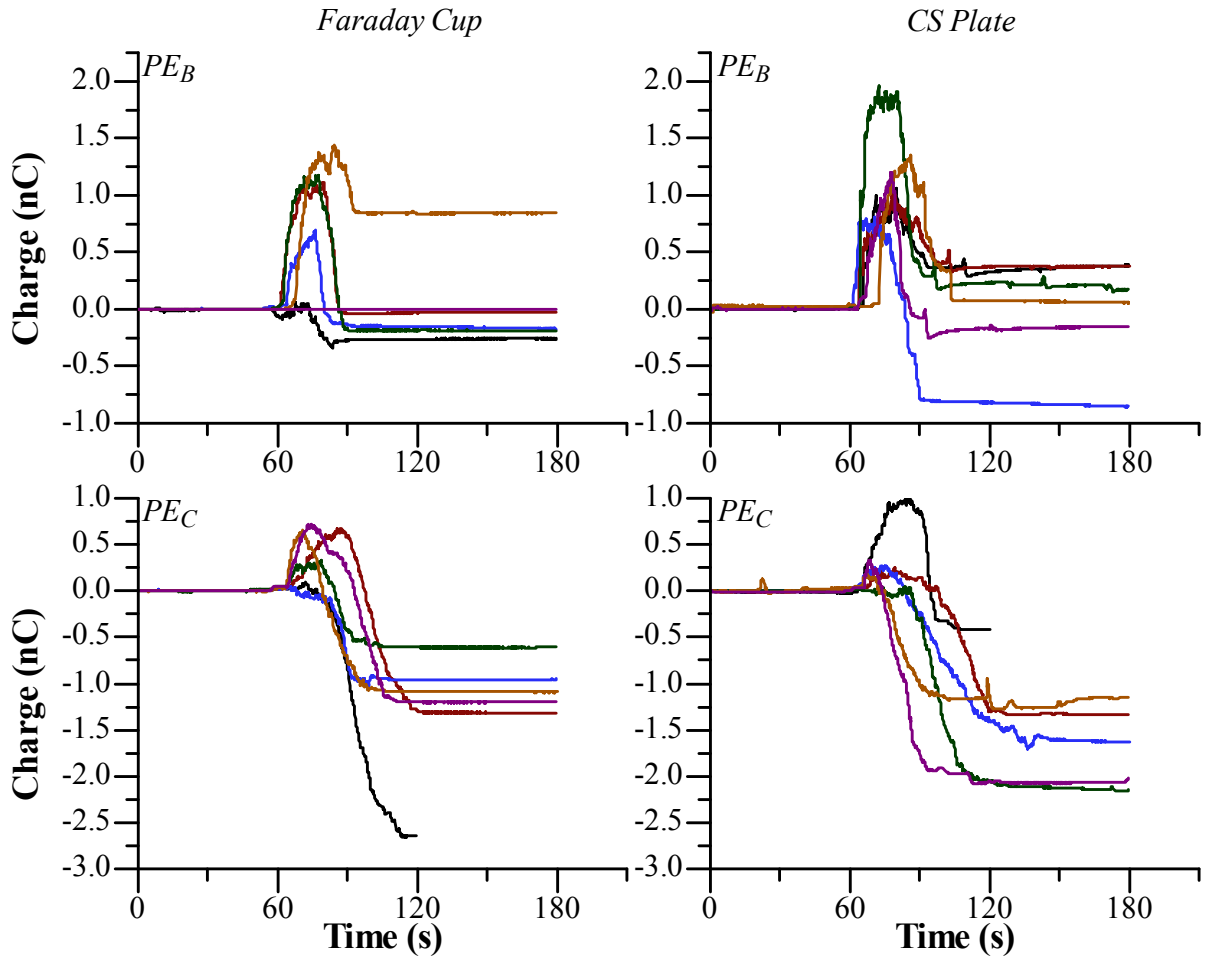


Figure 4.2: Repetitions of carbon steel plate test with PE_B and PE_C polyethylene particles, when the particles were dropped directly into a Faraday cup versus particles were dropped onto an angled carbon steel plate before falling into a Faraday cup.

The same test was also carried out with PE_A resin but sieved to narrow particle size ranges. The bi-polar effect on narrow particle sizes was more evident (Figure 4.3). For all particle size ranges there were trials that were either predominantly positively or negatively charged. However the smaller sized particles were on average positively charged and the larger particles were on average negatively charged. The particles in the middle of the particle size range (425 to 600 μm) did not have a tendency to be on average positively or negatively charged, meaning that these particles had a fifty percent chance of either positively or negatively charged.

When the sieved particles were contacted with the carbon steel plate overall there was not a large difference in their charge in comparison to pouring the particles directly into the Faraday cup. There were therefore likely not enough particle contacts that could generate enough electrostatic

charge to be detected by the electrometer. However, there was a clear difference in the charge of the smallest particles (212-300 μm) which on average were predominantly positively charged when poured directly into the Faraday cup and always predominantly negatively charged after contacting the carbon steel plate. Since the circumference of a smaller particle is smaller than a larger particle, the smaller particle would undergo more revolutions than the larger particle for a given distance. Therefore, it is likely that the surface of the smaller particles contacted the carbon steel plate more often than the larger particles, which contributed to more particles charging negatively. Also since the larger particles had a larger gravitational force, these particles were more prone of bouncing off of the plate, causing for only one point of contact with the CS plate and limiting the amount of possible charge transfer.

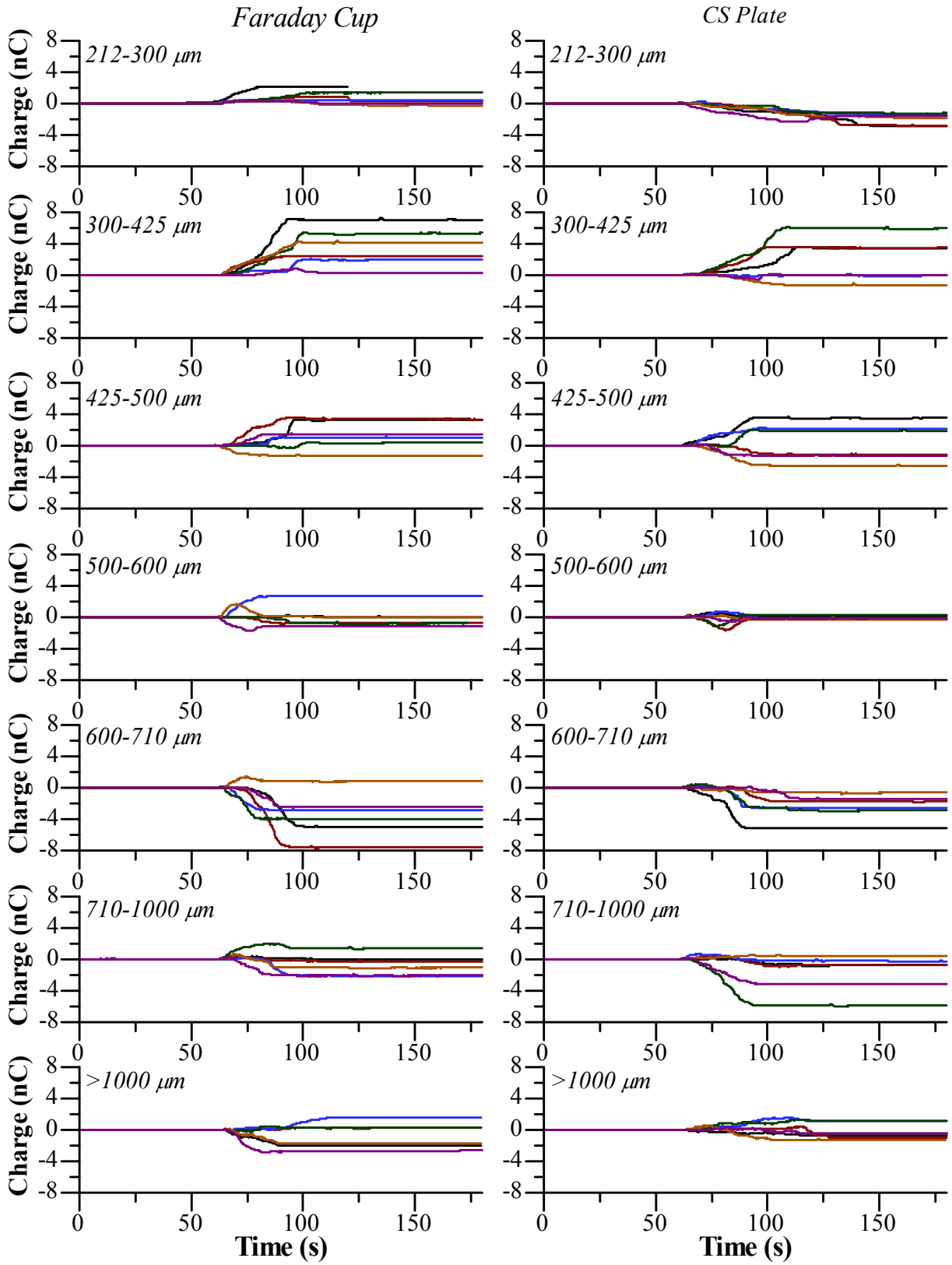


Figure 4.3: Carbon steel plate charging of sieved PE_A particles.

Smallest particles becoming more negatively charged in contact with the carbon steel plate indicated that polyethylene is the electron acceptor and the carbon steel plate is the electron donor object. This agrees well with the difference in the work function of the two materials, where it was found to be approximately 4.5 eV for steel and 5.3 eV for polyethylene (Masuda et al., 2006). As discussed in Chapter 1, since the work function of the carbon steel is smaller than that of PE particles, the carbon steel would be more prone to donate electrons.

The difference in the work function of particles of different sizes but identical material has been discussed in Chapter 1. There has been some work that suggest that smaller particles become more negatively charged when in contact with larger particles of the same material which would charge positively (Duff and Lacks, 2008; Lacks and Levandovsky, 2007; Lacks et al., 2008). It was concluded from bench-scale tests that the smaller PE particles were definitely becoming negatively charged with contact with the carbon steel plate, indicating that the smaller particles would become negatively charged with contact with the column wall in the fluidization experiments, if no particle-particle contacts are considered. However, looking at the fluidization experiments found in §3.3.2.2 for 11 identical trials, the Fines were always predominantly positively charged. Therefore, it is believed that within the fluidized bed the contact between smaller and larger PE particles results in the smaller PE donating electrons to the larger PE and becoming positively charged. A schematic of the contacting charging between the column wall and the polyethylene particles within the gas-solid fluidized bed is shown in Figure 4.4.

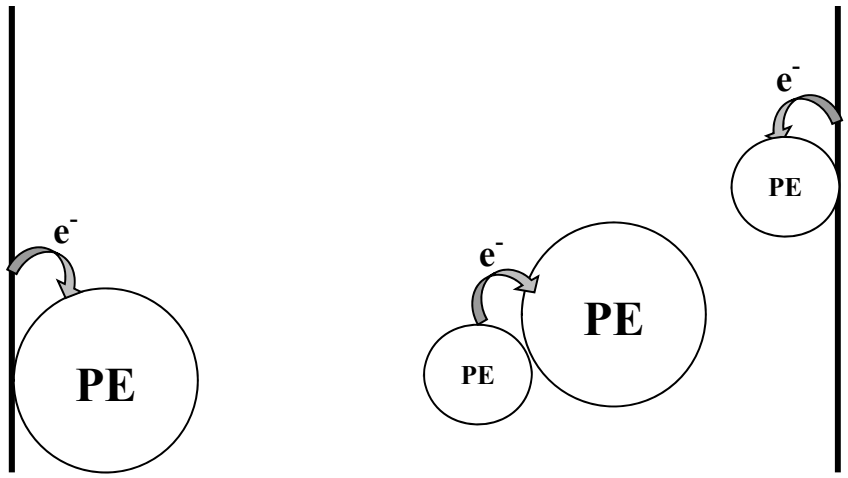


Figure 4.4: Proposed charging mechanisms found inside the fluidized bed between the small and large polyethylene particles (PE), and with the carbon steel column wall.

It should be noted that these charge generation mechanisms represent the average charge transfer expected between the different materials in a gas-solid fluidized bed. Due to the likely difference in work function, particle contact time and area, and the bi-polar nature of the fluidizing PE particles, it is likely that particles may charge differently in some instances than proposed by the above mechanisms. However, overall the above mechanism should hold true.

Chapter 5.
EFFECT OF FLUIDIZING GAS VELOCITY

The second objective of this thesis was to investigate the influence of fluidized bed hydrodynamics on the extent of bed particles charging and reactor wall fouling. Fluidizing gas velocity is one of parameters having an impact on the bed hydrodynamics. Increasing the gas velocity will cause the bed of particles to enter various flow regimes, such as bubbling and slugging. The particle-particle and particle-wall interactions differ between the two flow regimes and will inherently have a different impact on the electrostatic charge generation. Within the bubbling flow regime, the continuous formation of gas bubbles and their rise to the surface of the bed creates an extensive amount of particle mixing. Increasing the gas velocity within this flow regime not only results in the particles within the fluidized bed to be subjected to more drag force and thus more mixing, but also the higher amount of excess gas entering the fluidized bed creates larger bubbles which have higher rise velocity, which in turn can increase the number particle–particle and particle-reactor wall interactions leading to an increase in electrostatic charge generation. Within the slugging flow regime, the movements of sections of the bed along the column increases with elevating the gas velocity resulting in mainly in more particle-wall contacts. Table 5.1 summarizes previous works that investigated the effect of fluidizing gas velocity on bed electrification. Overall it was observed that the magnitude of bed charging increases due to the increase in the number of particle-particle interactions at higher gas velocities. The majority of works were limited to bubbling flow regime, with only four studies found to have conducted their testing at the onset of or within the slugging flow regime. As seen from Table 5.1, most works utilized electrostatic probes and none had focused on the impact of gas velocity on particle reactor wall fouling.

To better understand the charging mechanisms underlying bed electrification and reactor wall fouling, a comprehensive study on the effect of fluidizing gas velocity was conducted in two flow regimes of bubbling and slugging. The fluidization system developed in this work with its on-line charge measurement method enabled the evaluations of charge distribution within the fluidized bed and the degree of wall fouling for both fluidization regimes. Although slugging is

not a typical flow regime applied in industrial operations such as those in polyethylene production, it was studied due to generating different type of particle motion in comparison to that of the bubbling flow. When a fluidized bed is in slugging state, sections of the bed will move through the column as a single block with limited particle motion within it. Therefore, as the batch of particles is moved up and down the column, the particles motion will be mainly limited to the region close to the column wall and will be subjected and dominated by particle-wall interactions. This is different compared to that in the bubbling flow regime where there is vigorous mixing of particles resulting in the particle-particle interactions to be dominant. Therefore, the investigation bed electrification and reactor wall fouling within these two flow regimes will aide in distinguishing any differences between the effects of particle-particle and particle-wall interactions on charge generation within fluidized beds and on reactor wall fouling.

Table 5.1: Summary of previous studies performed on the effect of fluidizing gas velocity on electrostatic charge generation in gas-solid fluidized beds.

Authors	Year	Measurement Technique	Column Material	Particle Type	Particle Size μm	Effect of Increasing Gas Velocity
Ciborowski and Wlodarski	1962	Electrostatic Probe	Glass	Sand Polystyrol Vinyl Polyacetate	300-400 400-490 400-475	Increased the electrode potential.
Kisel'nikov et al.	1967	Electrostatic Probe	Metal	Polymeric Resins Polyacrylonitrile Ammonium Sulfate	-	Increased the bed electrification for all particles.
Bafrnec and Bena	1972	Electrostatic Probe	Metal	Glass Ballotini	170-200	Probe potential increased then reached a plateau.
Tardos and Pfeffer	1980	Electrostatic Probe and Faraday Cup	Plastic	Porcelain	2000	Surface charge increased and then started to decrease.
Fujino et al.	1985	Electrostatic Probe	Acrylic	Glass Beads	250	Increased electrostatic potential
Gajewski	1985	Copper Rings	Organic Glass	Polypropylene	2000	Increased electrostatic potential above the static bed height. Reached a peak and then started to decease.
Ham et al.	1985	Electrostatic Probe	PMMA	Fluid Cracking Catalyst FCC	82	Increased measured voltage then decreased at 30% relative humidity.
Rojo et al.	1986	Electrostatic Probe	Acrylic	Glass Beads	350-420	Increased potential until onset of slugging.
Guardiola et al.	1992	Electrostatic Probe	Perspex	Glass Beads	500-590	Increased electrostatic potential
Guardiola et al.	1996	Electrostatic Probe	Perspex	Glass Ballotini	250-297 297-350 350-400	Increased potential until slugging with 297-350 μm particles.
Yao et al.	2002	Electrostatic probe	Plexiglas	Polyethylene	378, 318	Amplitude of voltage increased.
Revel et al.	2003	Faraday Cup	Acrylic	Polyethylene	801	Increased charge-to-mass ratio.

Table 5.1: Summary of previous studies performed on the effect of fluidizing gas velocity on electrostatic charge generation in gas-solid fluidized beds. (continued)

Authors	Year	Measurement Technique	Column Material	Particle Type	Particle Size μm	Effect of Increasing Gas Velocity
Escalante et al.	2003	Current probe	Teflon	Glass beads	210	Increased the measured current.
Murtomaa et al.	2003	Electrostatic probe	Acrylic	Glass beads	1130	Charge increased.
Moughrabiah et al.	2009	Electrostatic Probe	Carbon Steel	LLDPE	600	Increased cumulative charge.
Liu et al.	2010	Current probes	Carbon steel	Polyethylene	570-650**	Increased charge.

5.1. Experimental Conditions

Experimental conditions for this study are summarized in Table 5.2. The fluidizing particles were PE_A resin tested at seven fluidizing gas velocities, three of which were in the bubbling and four in the slugging flow regime.

Table 5.2: Experimental conditions used for testing the effect of fluidizing gas velocity.

Parameter	Value
Fluidizing Particles	
Type	PE_A
Size Range	10-1500 μm
Fluidizing Gas	
Velocity	1.5, 1.75, 2 u_{mf} (Bubbling) 2.5, 3, 3.5, 4 u_{mf} (Slugging)
Time	60 min
Temperature	22 °C
Relative Humidity	0 %
Fluidization Column	
Material	Carbon Steel
Additive	
Type	None
Quantity	-

5.2. Results and Discussion

Results shown in the following sections are presented for the particles mass collected, particles size distribution and the charge found in each region of the bed (i.e., Wall, Dropped and Fines). The error bars found in all figures represent one standard deviation from the mean value of the measurement.

5.2.1. Mass

The initial mass of the particles used in the experiments was consistent to maintain a bed height-to-column diameter ratio of 4. All other masses collected were normalized to the initial mass. The mass percent (m%) of the Fines, Dropped, Loosely Bound, and Wall particles at different

fluidizing gas velocities are shown in Figure 5.1. The range of gas velocities can be split into two different flow regimes: bubbling and slugging.

With the Fines, the m% collected increased as the fluidization gas velocity increased. This was expected since at higher velocities, larger particles can be elutriated from the bed. The mass of the Dropped particles represented between 92 to 98% of the particles initially placed into the system, which was to be expected as these particles contained the majority of the bed particles. For all fluidizing gas velocities investigated reactor wall fouling was observed. Overall it can be seen that the m% of the Wall particles was nearly a mirror image of that of the Dropped particles due to the migration of particles in the bulk of the bed to the column wall. In the bubbling flow regime, the amount of particles accumulated on the column wall was on average higher than those in the slugging regime indicating that as the fluidizing gas velocity increased less wall fouling was formed. There are possibly two mechanisms that could be present influencing the amount of particles mass. Firstly, particles are not charging as much since in the slugging regime particle-wall interactions are dominating over the particle-particle interactions resulting in less particles charging, and there is less likely as much migration from the centre of the bed to the wall. Secondly, the formation of slugs at the higher gas velocity will result in a larger drag force since the drag force is increased by the square of the gas velocity (Equation. 1.1). Higher drag force will then help either dislodge and/or impede particle-wall adhesion. Although a combination of both mechanisms could likely be present, but the first is likely dominating because by the formation of slugs, the particles are only frictionally charged close to the column wall. At the same time the slugs and the drag force make it more difficult for particles to coat the column wall. If there was less charging in general in the slugging flow then there should be less particle wall fouling closer to the distributor plate (below the formation of slugs). This will be further discussed in the following sections through the particles charge measurement results and wall coating images.

Evaluation of the results for the Loosely and Tightly Bound particles indicated that there was a transition between the masses collected between the two flow regimes. Although overall higher masses were collected in the Wall region in the bubbling flow, there were less Tightly Bound particles. This will be discussed further in the following sections.

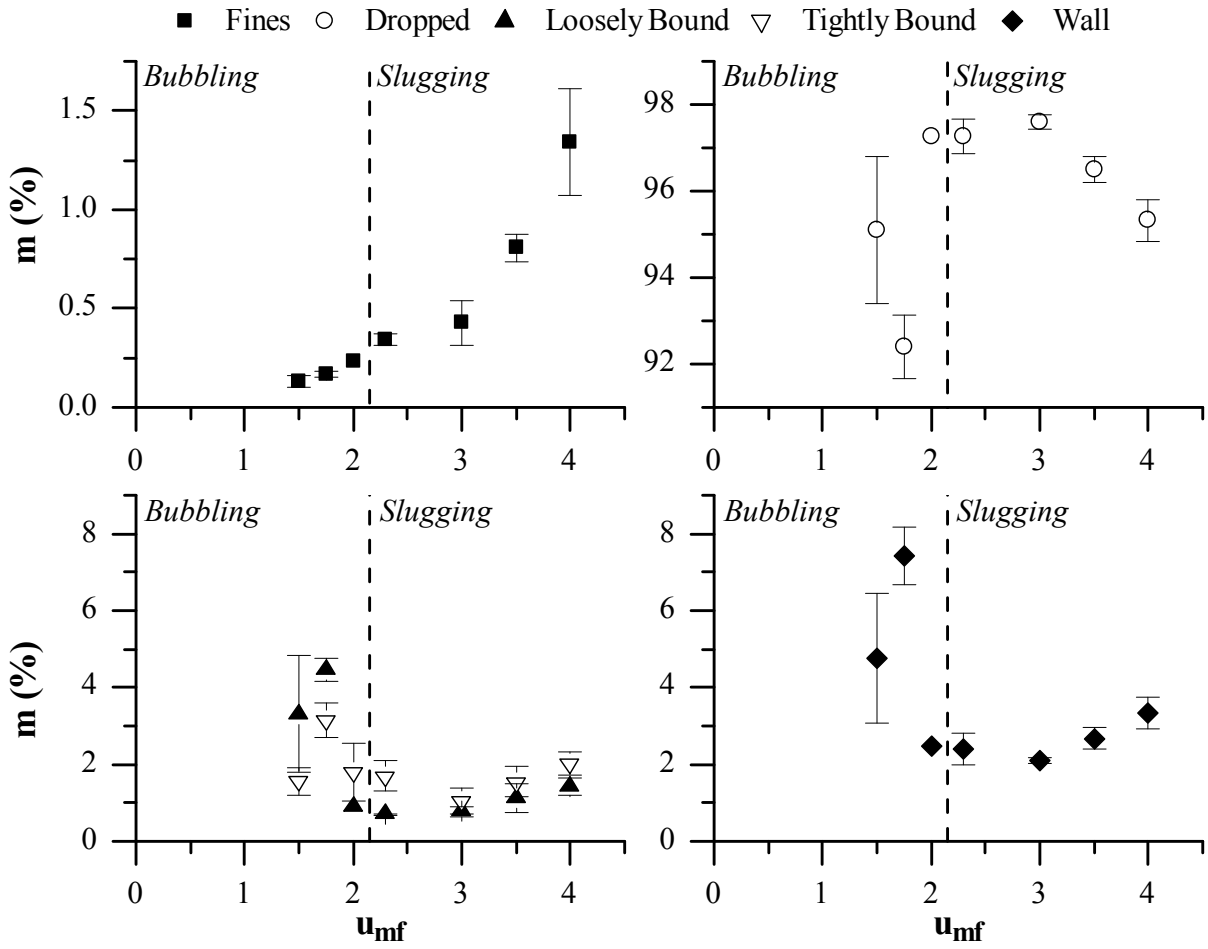


Figure 5.1: The m% of the PE_A particles collected from the Fines, Dropped, Loosely Bound, Tightly Bound, and Wall regions of the fluidized bed at different fluidization gas velocities.

5.2.2. Particle Size Distribution

Typical examples of the normalized particle size distributions from all regions of the bed are shown in Figure 5.2 for 1.5 and 4 u_{mf}. A similar trend was observed for all other fluidizing gas velocities and thus their results are not presented here. The normalized median particle diameters (d_P50_N) in all regions are shown in Figure 5.3. The Tightly Bound d_P50_N was only measured near the completion of these set of experiments and therefore results are only available for some of the fluidizing gas velocities. Overall in both flow regimes, the Fines were the smallest particles followed by Tightly and Loosely Bound particles, whereas the Dropped were the largest and had similar PSD to that of the Initial particles. This was expected as the Dropped particles consisted of at least 92% of the Initial particles. In all cases, it was found that particles of certain mean size, 350- 450 μm, were adhered to the column wall.

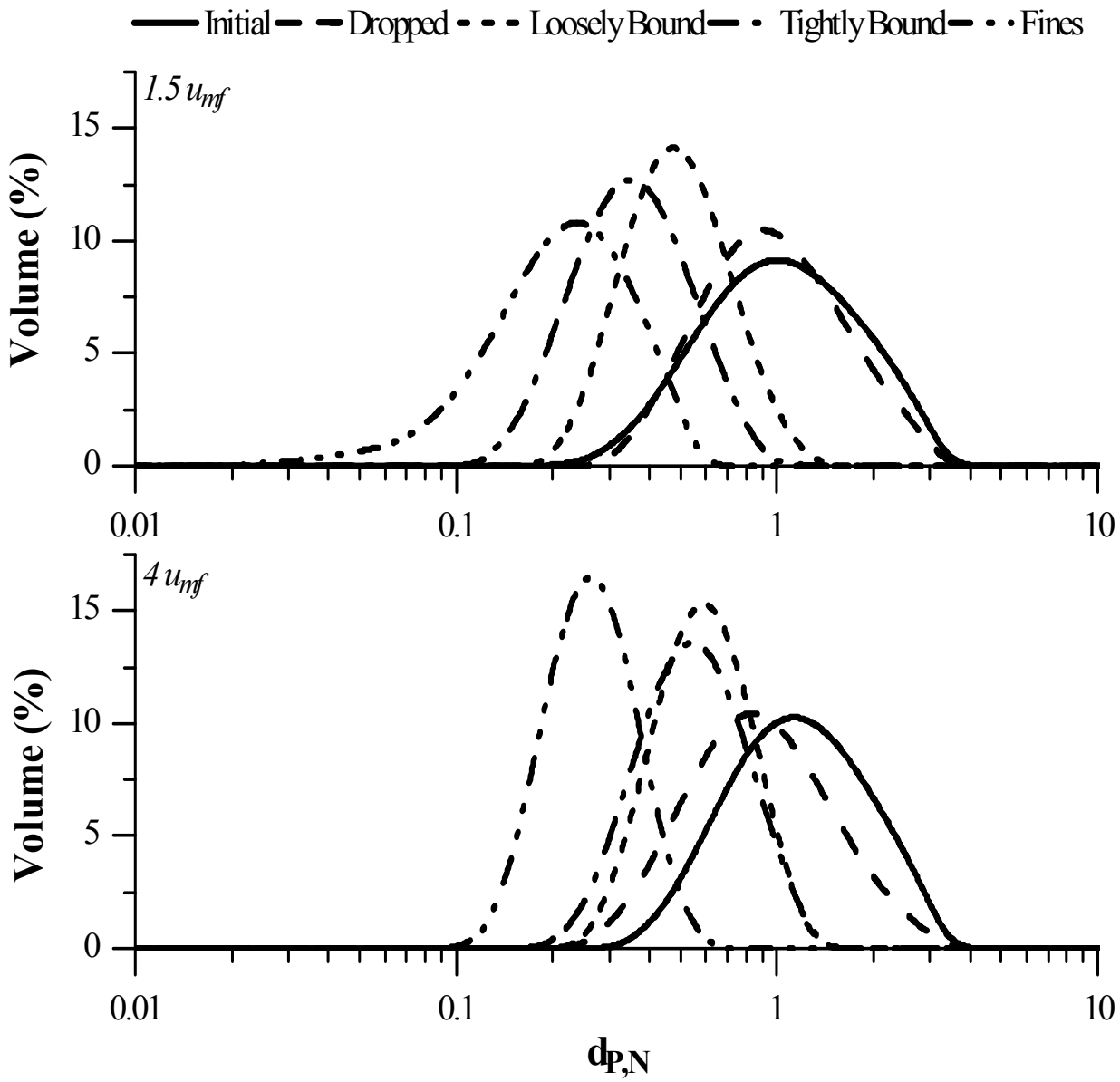


Figure 5.2: Examples of PSD in different regions of the fluidized bed at 1.5 and 4 u_{mf}.

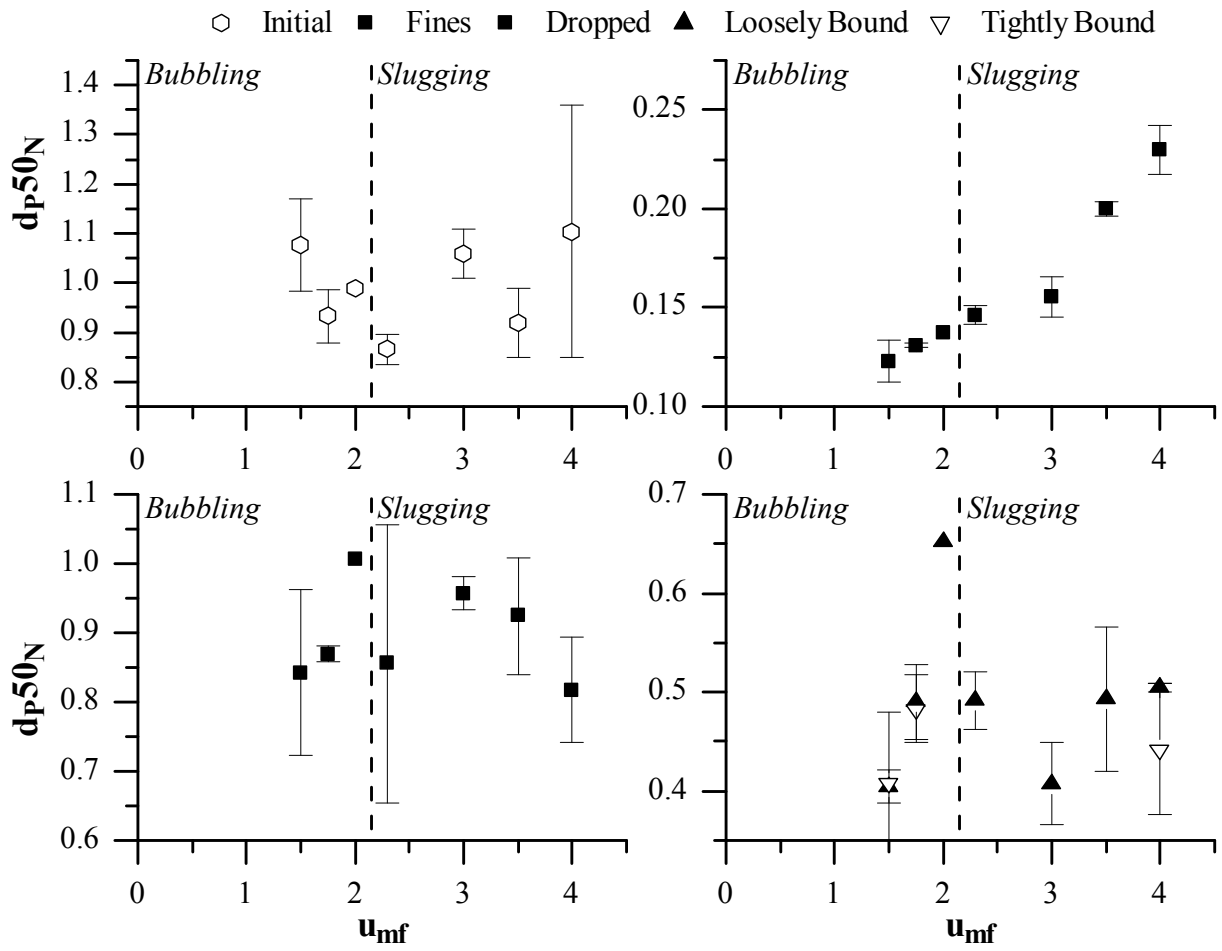


Figure 5.3: The d_P50_N of the PE_A particles from the Initial, Fines, Dropped, Loosely Bound, and Tightly Bound regions of the fluidized bed at different fluidization gas velocities.

The Fines displayed the smallest particle size and increased in size as the gas velocity increased, which was expected. As discussed in §5.2.1, this can be attributed directly to the terminal velocity of a certain particle diameter. The general equation for the terminal velocity (u_t) is shown in Equation 1.2. The drag coefficient (C_D) that can be calculated from Equation 1.2 is a function of the Reynolds number, which in turn is a function of the particle diameter.

$$u_t = \sqrt{\frac{4}{3}\frac{d_P(\rho_P - \rho_f)g}{\rho_f C_D}} \qquad [5.1]$$

Figure 5.4 shows the particle theoretical largest particle sizes that should be elutriated from the system as well as the median particle diameter of the Fines found in this work. The d_P50_N was always smaller than the theoretical maximum value as expected.

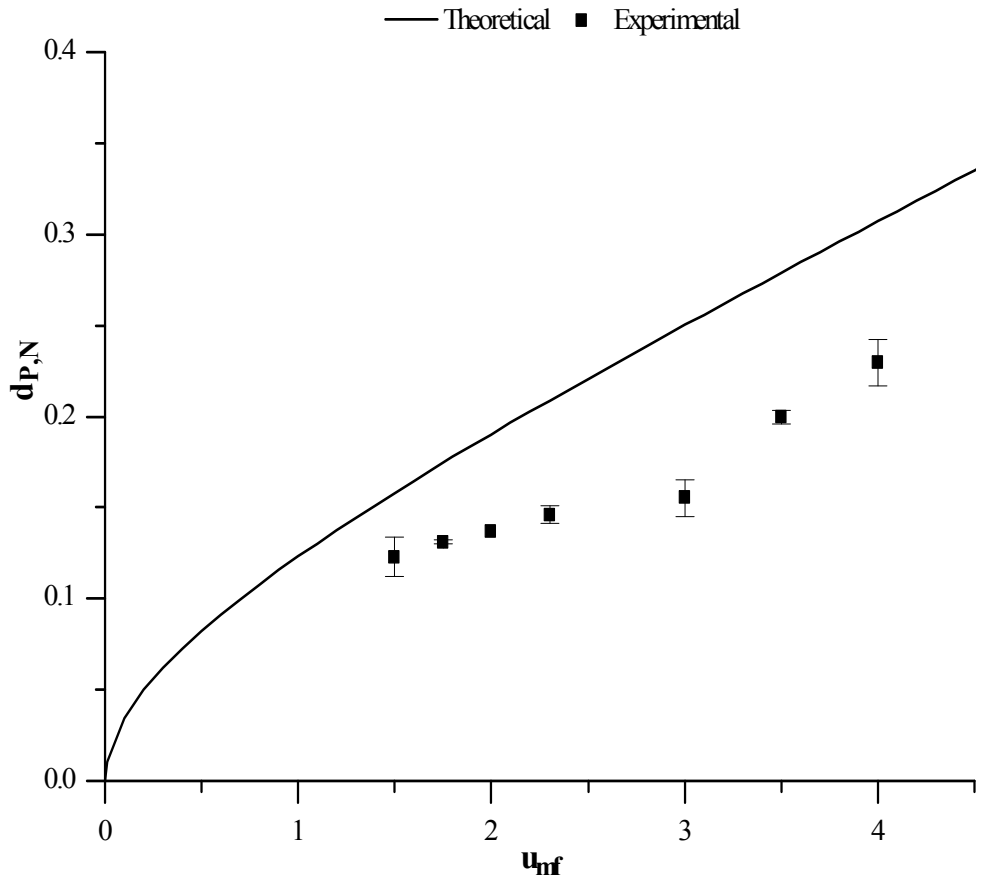


Figure 5.4: The theoretical largest diameter of particles estimated to be elutriated from the fluidization column, and the measured d_P50_N particle size of the Fines at different gas velocities.

From Figure 5.2 it is clear that the Loosely Bound particles were consistently smaller than the Dropped particles and were narrowly distributed. Also, the Tightly Bound particles were smaller than the Loosely Bound particles. Since the Tightly Bound particles were adhered directly to the column wall, this finding suggests that there is an overall increase in particle size moving from the column wall towards the centre of the column. This would also be explained well with the force balance on particles where these results show that the larger particle would have stronger gravitational forces, in comparison to electrostatic forces, and would be more easily removed from the wall. It should be noted that as can be seen in Figure 5.2 there was some overlap in size of the particles in all regions of the bed. In other words, there existed some particles of the size of the Fines in the Tightly Bound, Loosely Bound, and Dropped regions. Similarly, the Wall

particles (Loosely and Tightly Bound) were also found in the Dropped region. This indicates that although there is a distinct trend in the size of particles found in each region, the particle size does not exclusively dictate as where the particles will migrate inside the bed.

5.2.3. Particles Absolute and Specific Charge

The only transient charge measurement performed was with the entrained Fines. Examples of the cumulative charge (q) measured by the top Faraday cup at different fluidizing gas velocities are shown in Figure 5.5. In general, increasing the gas velocity increased the amount of particles that were elutriated from the system and therefore higher charges were measured. At the higher velocities it appeared as though the cumulative charge of the Fines began to plateau, suggesting that not many fine particles were leaving the bed near the end of the fluidization period. However, at the lower gas velocities (in the bubbling regime) Fines elutriated for the entire fluidization period. Giffin and Mehrani (2010) used the same system and fluidizing particles and studied the effect of fluidization time (between 15 to 360 min) in both the bubbling and slugging regimes. They showed that in the bubbling regime the q/m of the Fines increased over the entire period of six hours of fluidization whereas it reached steady state after approximately 60 min in the slugging regime. Results here showed that within the bubbling flow, the cumulative charge at 1.75 u_{mf} was lower than that at 1.5 u_{mf} and in the slugging flow it was also lower at 3 u_{mf} than 2.5 and 2 u_{mf}. This can be attributed to some degree of variability in the system. The amount of mass increased with fluidizing gas velocity; however, as the velocity is increased the residence time of the fine particles was effectively decreased which may also have resulted in the decrease in cumulative charge.

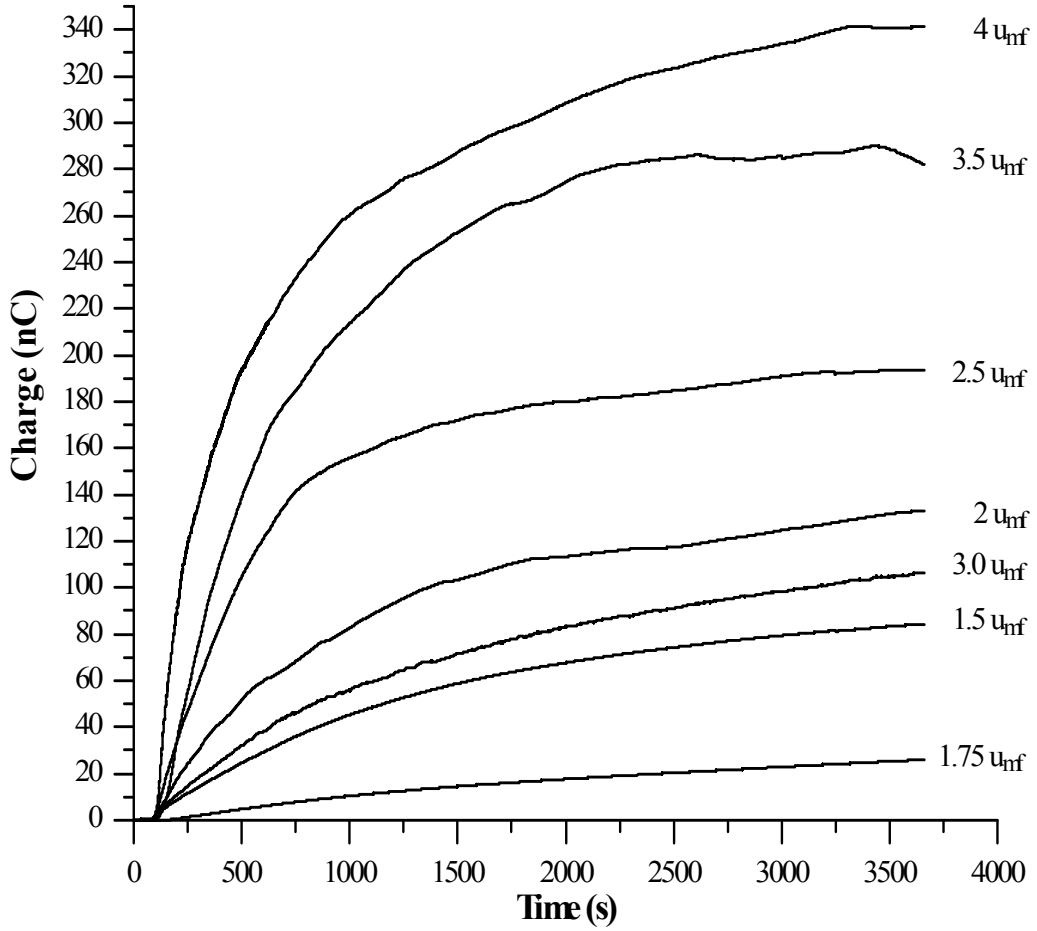


Figure 5.5: Examples of cumulative charge of the Fines measured during the 60 min of fluidization for different fluidizing gas velocities.

Figure 5.6 shows the specific charge (q/m) of the PE_A particles measured at different gas velocities for the Initial, Fines, Dropped and Loosely Bound regions of the fluidized bed. The Initial q/m ranged between -0.09 and -0.14 μC/kg and was relatively consistent for all trials. For all experiments, Fines were predominantly positively charged with the q/m of the experiments performed in the bubbling regime being overall more positively charged in comparison to the higher velocities. This can be attributed to two mechanisms. The first mechanism is the particles residence time. As shown in Figure 5.5 at the lower gas velocities there were still particles that were being elutriated from the system up to 60 minutes of fluidization. Therefore, there were some particles that were in constant contact with the bed particles and the column wall during 60 min of fluidization and could be subjected to more particle charging. Secondly, there was more mass collected at higher velocities, which means that the charge may not have increased as

rapidly as the mass of the Fines, which effectively lowered the q/m. The smaller standard deviation in q could also be attributed to the particles residence time in the bed.

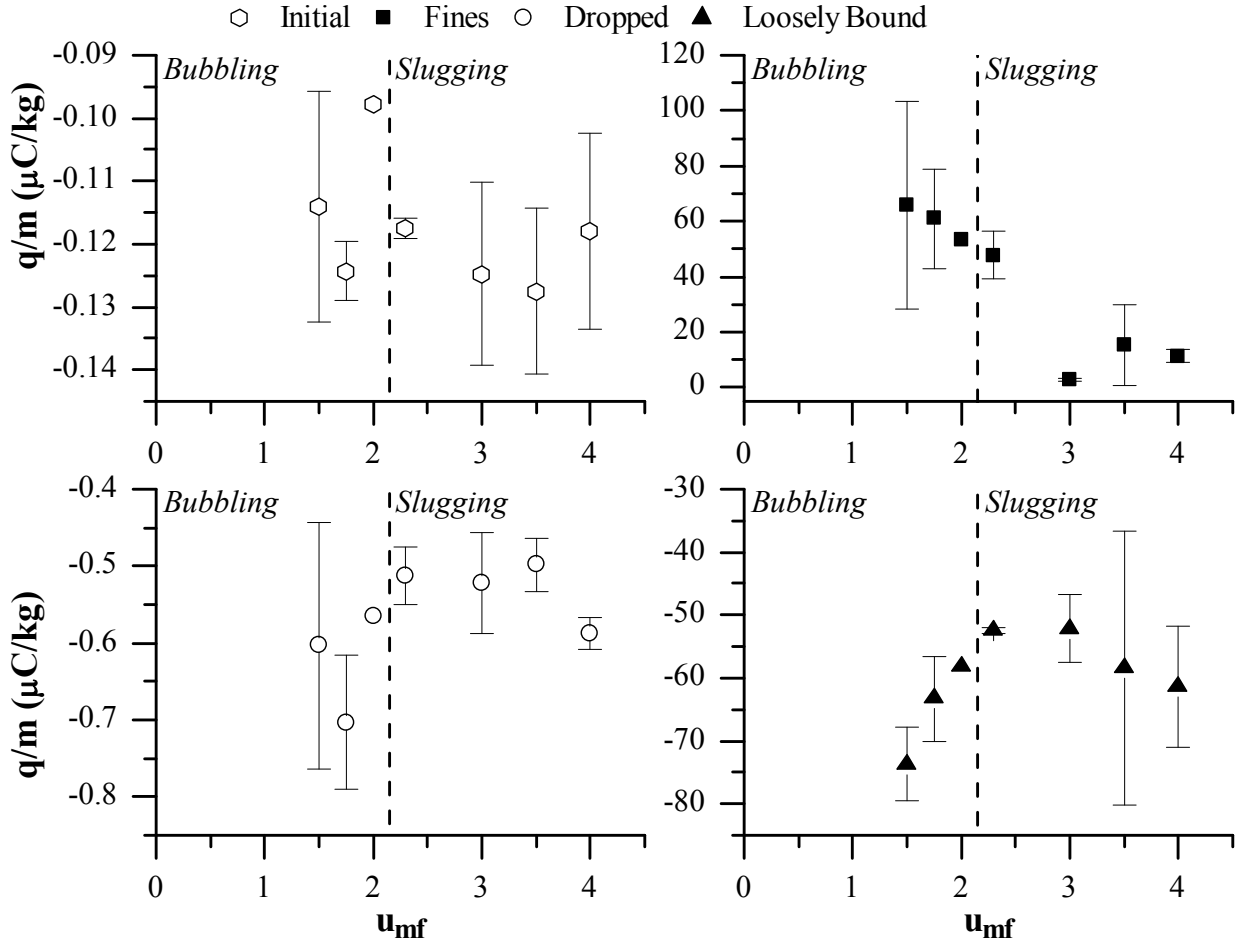


Figure 5.6: The q/m of the PE_A particles from the Initial, Fines, Dropped, and Loosely Bound regions of the fluidized bed at different fluidizing gas velocities.

The specific charge of the Dropped particles was predominantly negative and was approximately five times larger than that of the Initial particles, signifying charge generation due to fluidization. The q/m of the Dropped particles did not vary significantly with increasing gas velocity likely due to the type of particles interactions. Since the Dropped particles represented at least 92 m% of the total particles in the system, the interactions between them resulted in their triboelectrification. If all of these particles had remained in bulk and did not migrate to the wall, their net charge would have not change. There is definitely some charging of Dropped particles due to fluidization since the q/m of these particles is much larger than the Initial particles. This increase in negative charge can be attributed to the generation of negative charges due to

particles contact with the carbon steel wall, the large PE particles contacting the smaller PE particles, the elutriation of the positively charged Fines, the migration of positively charged particles to the column wall, or a combination of all above. The highly negatively charged particles within the bed would also migrate towards and adhere to the column wall, becoming Wall particles.

For all cases the Loosely Bound particles were highly negatively charged and were two orders magnitude more charged than the Initial particles. As shown in §5.2.2 there existed particles of the same diameter in both the Dropped and Loosely Bound regions but there is also clearly a large difference in these particles net q/m. As discussed in Chapter 4, as particles travel through the bed, some undergo contact charging through particle-particle or particle-wall interactions, or both, and become highly negatively charged. On the other hand, the column wall becomes positively charged due to particles contacts as well as acquiring a positive image charge in the presence of negatively charged particles. Thus, the attractive force between the positively charged column wall and the strong repulsive forces among the highly negatively charged particles within the bulk of the bed result in the migration and adhesion of these highly negatively charged particles to the column wall.

With increasing gas velocity the net q/m of the Loosely Bound particles became less negative until the onset of slugging where the q/m began to plateau, but also had a lot of variability. This transition agrees well with the findings of Gajewski (1985) and Ham et al. (1992). However, these authors measured the bed potential (via conductive rings and electrostatic probe, respectively) rather than the actual particles net q/m. The q/m of the Loosely Bound particles could have remained relatively constant in the slugging flow regimes if both the particles q and the mass increased or decreased at the same rate. Since the mass of the particles adhered to the column wall did not vary significantly within the slugging regime meaning that the charge did not vary significantly either. This could be attributed to the formation of the slugs that would dislodge the particles from the column wall maintaining a consistent mass. This will be discussed in more detail in §5.2.5.

5.2.4. Specific Charge-to-Specific Surface Area Ratio

Using the particles specific charge, and the specific surface area measured during the PSD analysis, the charge-to-specific surface area ($\hat{q}/\hat{A}$) was calculated. The $\hat{q}/\hat{A}$ gave an approximation of the average surface charge density (in units of μC/m^2) of particles in each region (Figure 5.7). The Loosely Bound particles had the largest $\hat{q}/\hat{A}$ which is another indication as to why these particles adhered to the column wall. Overall the $\hat{q}/\hat{A}$ of the Initial, Fines, Dropped, and Loosely Bound particles did not vary significantly with increasing gas velocity.

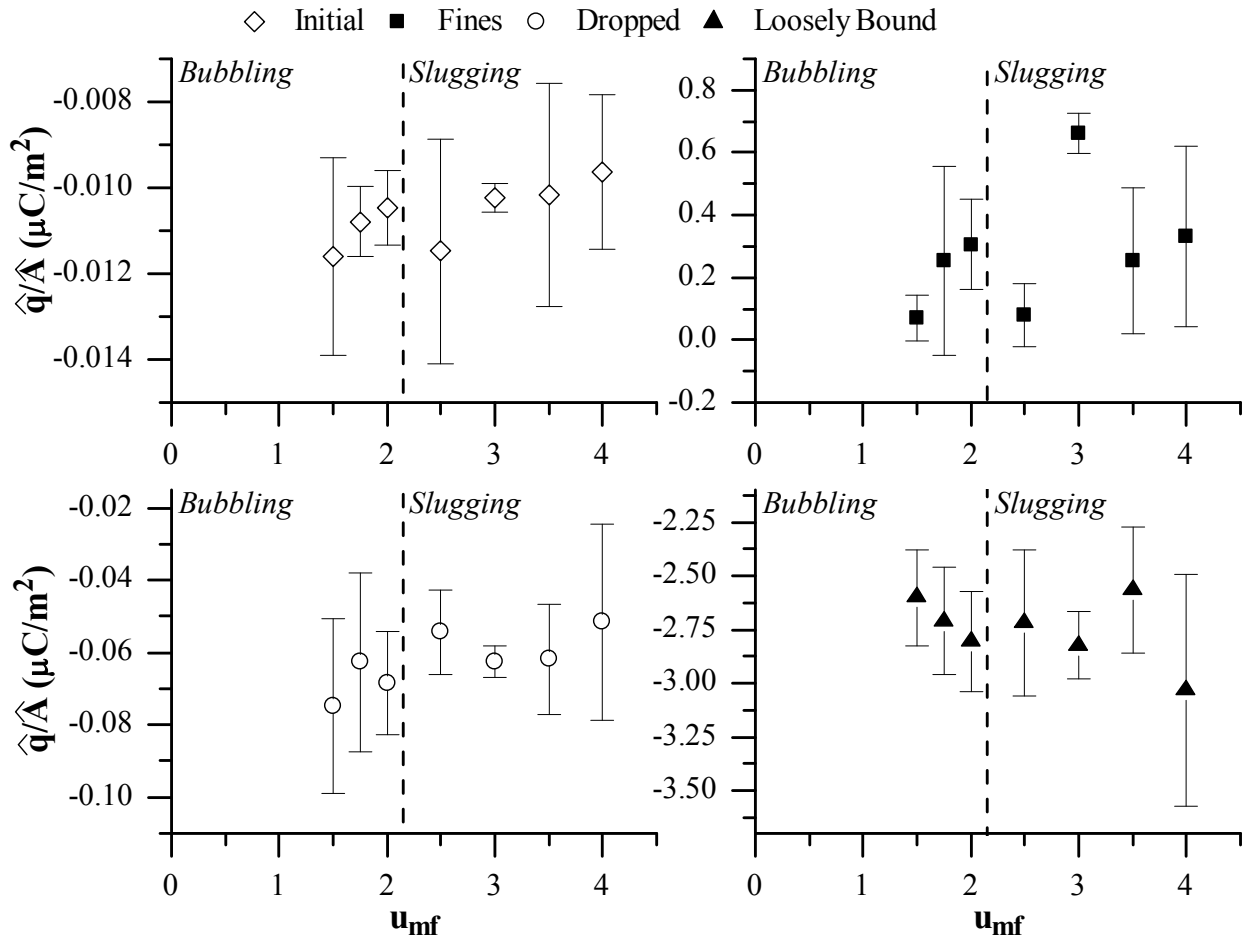


Figure 5.7: The $\hat{q}/\hat{A}$ of the PE_A particles from the Initial, Fines, Dropped, and Loosely Bound regions of the fluidized bed at different fluidizing gas velocities.

5.2.5. Wall Layer Coating

The magnitude of wall fouling was found for all trials by inspecting the inner column wall after the Dropped particles were removed. Examples of the wall layer coating pictures at 1.5 and 4 u_{mf}

are shown in Figure 5.8. A distinct difference was observed in the wall coating between the two flow regimes. In the bubbling regime there was a long and thin layer of particles that extended into the fluidization column. Whereas, in the slugging flow regime, the slugs caused the particles along the column wall to detach and migrate into the bulk of the bed, thus producing a shorter particle wall coating. This agrees well with the mass distributions found in §5.2.1. In both cases, a gap was observed in the particle coating where at 1.5 u_{mf}, it was located approximately at the static bed height. This suggests that the gap may be due to the oscillations in the bed surface in this flow regime which could potentially dislodge the particles from the wall. At 4 u_{mf}, the gap started at a much lower height, which was likely caused by the formation of slugs near that location that could have created enough force to dislodge the particles from the layer formed on the wall.

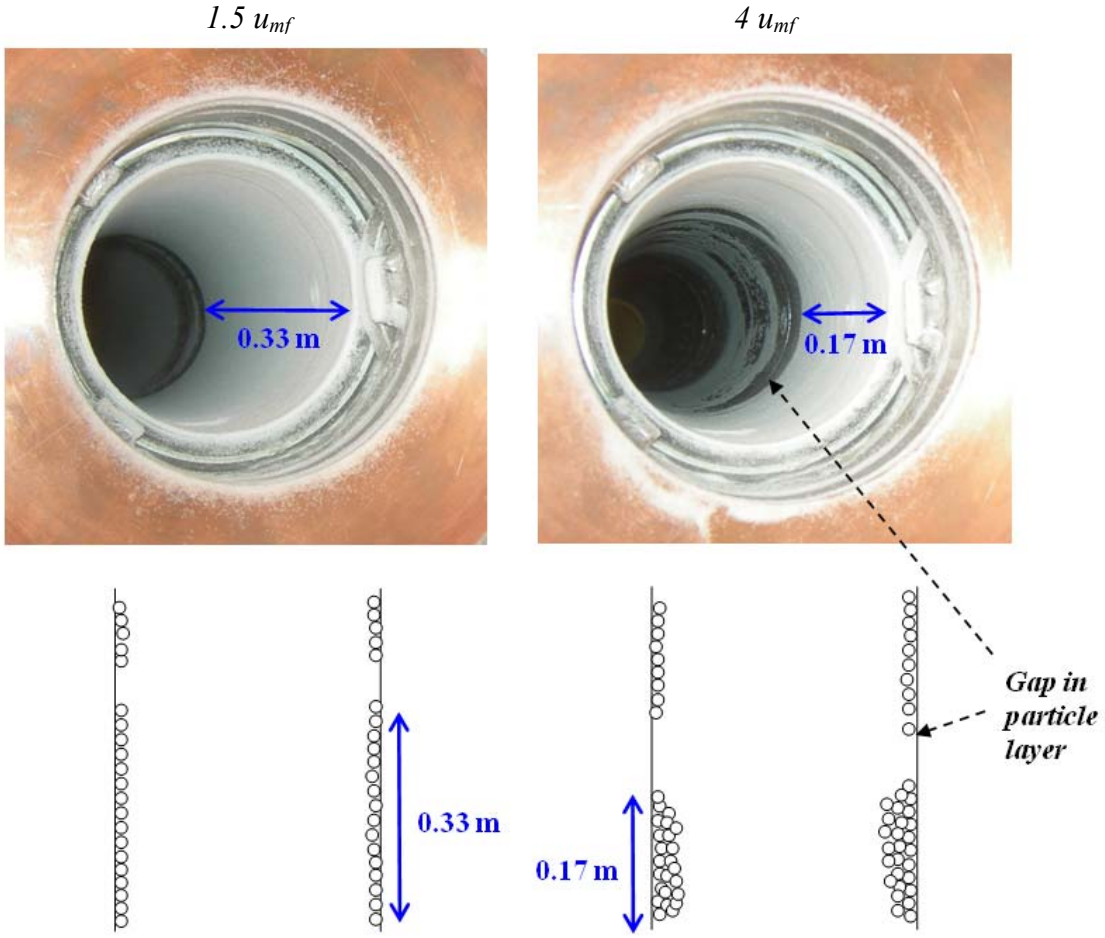


Figure 5.8: Examples of wall layer pictures for PE_A particles after 60 min of fluidization at 1.5 u_{mf} and 4 u_{mf}.

The average thickness and height of the wall coating at 1.5 u_{mf} were 0.6 x 10^{-3} m and 0.37 m, respectively, compared to 2 x10^{-3} m and 0.21 m at 4 u_{mf}. The short and thick particle layer found at 4u_{mf} agrees well with the discussion that the slugging flow regime helped remove particles from the column wall and that there was still a significant amount of charging in this flow regime. If there was not a significant amount of charging then there would not be any particle wall fouling below the formation of the slugs. Since there was a short particle wall layer, a significant amount of charges generated in the bed, but the presence of slugs dislodged many particles higher up in the fluidization column.

Although in all cases it had been found that the Loosely Bound and the Wall particles were predominantly negatively charged (§5.2.3), it was suspected that there must also be some positively charged particles present in the wall layer. It was previously shown (§5.2.2) that the

Tightly Bound particles were on average smaller than the Loosely Bound particles which suggested that the particles size increased from the wall to the centre of the column. Based on these results, a mechanism was proposed as how the wall coating was formed (Figure 5.9). First, the smaller bed particles adhere to the wall followed by the larger particles. As discussed in Chapter 4, contacts between the PE particles and the column wall would likely leave the column wall positively and the PE particles negatively charged. In addition, the generation of negatively charged particles will create a positive image charge on the conductive column wall. The highly charged particles must have some mechanism that drives them towards the column wall, either through the repulsion or attraction of these particles. Since the Dropped particles were predominantly negative, there would be a repulsion of the negative particles towards the column wall which, since the column wall is positively charged, would attract the negatively charged particles. Therefore, the first layer of particles was likely negatively charged. However, if all the particles were of the same charge polarity they would have eventually repulsed each other and the layer would not be able to grow. The negatively charged particles in the first layer would attract some of the positively charged particles. It was shown that there was an overlap in the PSDs of the Wall particles and Fines indicating that there was, to an extent, some Fines (which were found to be predominately positively charged) trapped within the wall coating.

The difference in the wall layer thickness and height could help explain the apparent positive increase in the q/m between the two fluidizing flow regimes shown in §5.2.3. As discussed above, the first layer of particles was likely highly negatively charged, and therefore the long and thin layer found at 1.5 u_{mf} composed of only a few layers of particles which were mostly negative. In the slugging regime, the layer was shorter but thicker, requiring the need of positively charged particles to produce the thicker layer. This agrees well with the consistent mass and q/m found within this flow regime. The formation of slugs removed a portion of the particles from the column wall. Below the presence of slugs, particle wall fouling was unhindered until it reached an equilibrium between the amount of particles could be attached to that small section of the column wall. However, this does not explain why the layer of particles at 1.5 u_{mf} does not build up with positively charged particles. At the lower gas velocity, after the initial coating of negatively charged particles, the positive particles may not be migrating towards the wall for the following reasons. Firstly, there are competing attractive forces between

the net negative charge of the bed particles, and those particles adhered to the column wall. Even though the charge present on the Wall particles is much larger than those present in the bed, the electrostatic force is inversely proportional to the square of the distance between charges. Therefore if the positive charges are already present within the negatively charged bed, then it may be difficult for these positively charged particles to migrate towards the column wall. Naturally, due to the vigorous mixing of a bubbling fluidized bed, some of these positively charged particles would migrate to the column wall due to the particle motions within the bed, but this migration would be limited.

It will be seen in the following chapters that further experimental work validate the proposed mechanism.

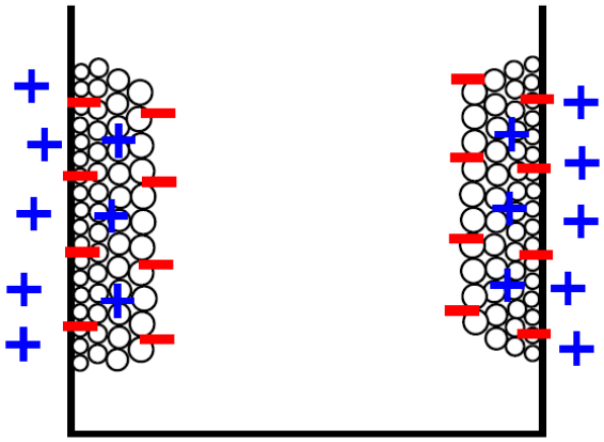


Figure 5.9: The diagram of the proposed wall particle layering mechanism.

5.2.6. Electrostatic Probe Measurements

Current measurement results from the electrostatic probe for experiments performed at 1.5 and 4 u_{mf} are shown in Figure 5.10. It is clear that the amplitude of the current measurements in the bubbling flow regime was much smaller than that generated with the slugging regime. Typically this would suggest that the bed electrification would be higher at 4 u_{mf}, but as shown in §5.2.3 the specific charge of the Loosely Bound particles was more negatively charged at the lower gas velocity and there were more particles adhered to the column wall for this condition. This indicates that the probe may not be given a correct measure of the electrostatic charges generated on the bed particles and the amount of particle wall coating. As described in §1.4.1.4 what the

electrostatic probe is actually measuring is not entirely understood. It may be possible that at the higher gas velocity, the particles were contacting the electrostatic probe at a higher frequency resulting in more charge transfer and thus increasing the amplitude of the current measured. However, this charge transfer is not a measure of the actual electrostatics charges on the bed particles, but rather simply is the result of contact charging between the probe and the particles.

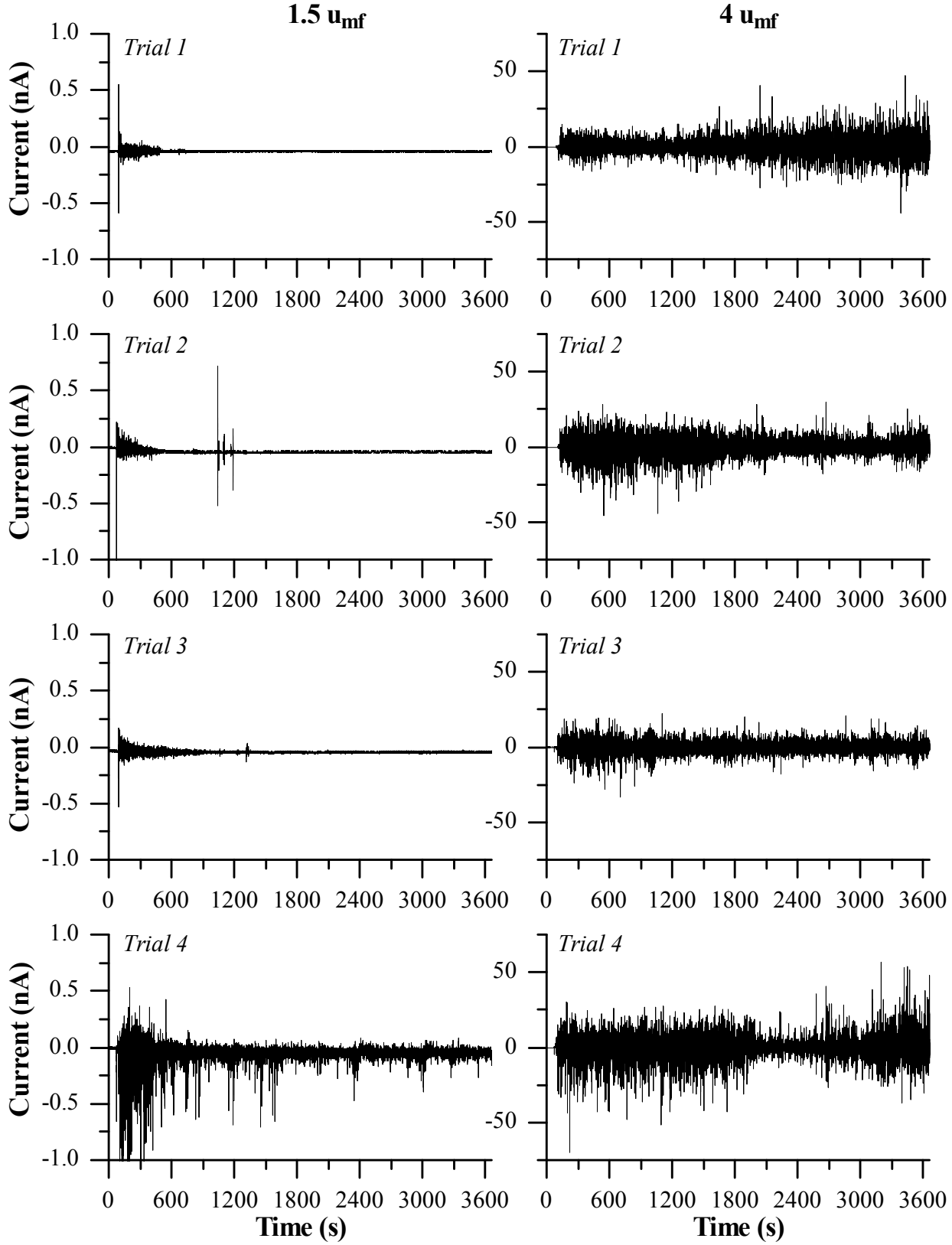


Figure 5.10: Examples of current measured by electrostatic probe for fluidization gas velocities of 1.5 and 4.0 u_{mf} over the period of 60 min of fluidization.

5.3. Summary

Regardless of the fluidizing gas velocity and initial particles size distribution, reactor wall fouling was observed for all trials. However, the magnitude of fouling was larger in the bubbling flow in comparison to the slugging flow. In addition, the entrained Fines and the bed particles (Dropped and Loosely Bound) were found to be mainly positively and negatively charged, respectively. This confirmed the theory of bi-polar charging in the gas-solid fluidized bed which had also been reported by other researches (Ali et al., 1989; Zhao et al., 2002; Mehrani et al., 2005). Furthermore, within the bed particles, the Loosely Bound q/m was more than 100 times and the $\hat{q}/\hat{A}$ results were about 50 times of that of the Dropped particles. The particles higher charge, and the smaller and narrower size distribution within the Wall region suggested that a certain size of particles were more susceptible to adhere to the column wall which with this system was found to be 350-450 μm.

Based on the data obtained, it was shown that the variations in the charge of different groups of particles inside a fluidized bed at different gas velocities may arise from the differences in particles flow patterns inside the bed in different fluidization flow regimes. The largest impact of the flow regime was on the types of the electrostatic charges generated (contact versus frictional charging) within the fluidization column, which in turn governed the migration of the particles throughout the system. The transition from bubbling to slugging resulted in Wall particles mass to decrease due to the formation of slugs at the higher gas velocities. The slugs were able to detach the particles that were adhered to the column wall due to the increase in drag force on the particles.

Within the bubbling flow regime, the Wall particles mass and net q/m increased with increasing the gas velocity which was projected due to the increase in particles interaction when the gas velocity is elevated resulting in more particles charging, and in turn more reactor fouling. However, within the slugging flow regime only a slight increase in Wall particles mass was obtained where their net q/m stayed relatively constant indicating that although the movement of the slugs increases with increasing the gas velocity, not a significant amount of change in charge is obtained, since the particles charging is limited to frictional charging along the column wall.

As expected, the PSD of the Fines was larger at a higher gas velocity, while their q/m was lower due to particles less residence time within the bed. The PSD, q/m and $\hat{q}/\hat{A}$ of the Dropped and Loosely Bound particles were comparable in both flow regimes; however, the $\hat{q}/\hat{A}$ for the Loosely Bound particles was much larger than that of the Dropped. The Tightly Bound particles were on average smaller in size than the Loosely Bound particles suggesting that smaller particles adhere to the column wall first, followed by larger particles. Even though the Loosely Bound particles were highly negatively charged, positively charged particles must also be present in order to form the particle layers.

The electrostatic probe results showed that at higher gas velocities, the current amplitude was larger. However, this did not agree well with the net q/m of the Loosely Bound particles and amount of particle wall fouling which were found to be lower at the higher gas velocities.

Chapter 6.
EFFECT OF PARTICLE SIZE

In continuation of studying the effect of fluidized bed hydrodynamics on the degree of bed electrification and reactor fouling, next the effect of fluidizing particle size was investigated. In addition to this general objective, earlier results related to the fluidization gas velocity presented in Chapter 5, had shown that particles of a certain narrow size were adhering to the column wall. This further highlighted the importance of understanding the influence of fluidizing particle size on particles charging and degree of reactor wall coating.

The results from previous studies that investigated the effect of particle size on bed electrification in gas-solid fluidized beds are summarized in Table 6.1. Overall it was found that increasing the particle size increased the amount of bed electrification. Gajewski (1985) reported a maximum limit to the bed electrification at 2500 μm diameter polypropylene particles with the system they used. However, none of these studies investigated the effect of particle size on reactor wall fouling, which is quite important to be examined for industrial operations. Although it was found that increasing the particle size increases the amount of bed electrification, it may not necessarily contribute to an increase in particles migration and deposition on the reactor wall since the gravitational forces will also be increased with particle size. Therefore, a comprehensives study was essential to investigate the migration behaviour of fluidizing particles of different size to various regions of the fluidized bed, specifically to the wall region. Since the fluidizing particles available for this thesis were polyethylene resin directly received from industrial reactors, they had a wide size distribution. Therefore, these particles were sieved into narrow sized batches for this investigation.

Table 6.1: Summary of previous studies on the effect of particle size on electrostatic charge generation in gas-solid fluidized beds.

Authors	Year	Measurement Technique	Column Material	Particle Type	Particle Size μm	Increasing Particle Size
Boland and Geldart	1971/ 72	Electrostatic Probe	Perspex	Lead Glass Ballotini	200-300	Increased the electrostatic potential.
Fasso et al.	1982	Faraday cup and Electrostatic Probe	Plexiglas	Glass Beads	30 to 55	Increased mean particle charge.
Gajewski	1985	Copper Rings	Organic Glass	Polypropylene	500 1000 2000 2500 3000 4000	Increased electrostatic potential up to 2500 μm particles and then decreased potential.
Guardiola et al.	1996	Electrostatic Probe	Perspex	Glass Ballotini	250-297 297-350 350-400	Increased the electrostatic potential.
Fang et al.	2008	Electrostatic probe	Plexiglas	LLDPE	185-1700	Amplitude of voltage increases with decreasing particle size up to a maximum point.
Moughrabiah et al.	2012	Electrostatic probes	Stainless Steel	Glass Beads	65-693	Charge increased slightly with decreasing particle size.

6.1. Experimental Conditions

The experimental conditions used in this study are summarized in Table 6.2. The PE_A resin was sieved into five different particle size ranges and the results were compared to the non-sieved industrial resin. For each particle size range, the u_{mf} was experimentally measured, and tests were performed at 1.5 and 4 times the u_{mf} of the respective particle size.

Table 6.2: The experimental conditions used for the experiments on the effect of particle size.

Parameter	Value
Fluidizing Particles	
Type	PE_A
Size Range	20-1500 µm (Non-sieved)
	300-425 µm
	425-500 µm
	500-600 µm
	600-710 µm
	710-1000 µm
Fluidizing Gas	
Velocity	1.5 u_{mf} (Bubbling)
	4 u_{mf} (Slugging)
Time	60 min
Temperature	22 °C
Relative Humidity	0 %
Fluidization Column	
Material	Carbon Steel
Additive	
Type	None
Quantity	-

6.2. Results and Discussion

Results shown in the following sections are presented for the particles mass collected, particles size distribution and the charge found in each region of the bed (i.e., Wall and Dropped). Since the particles were sieved, the amount of Fines collected was negligible and therefore not presented here.

6.2.1. Initial Particles Charge Distribution

The Charged Particle Separator was used on each narrow particle size range to determine if there were any bi-polar charges present in the particles prior to their fluidization. Results showed that for all particle size range there was definitely both positively and negatively charged particles even for a narrow particle size range (Figure 6.1).

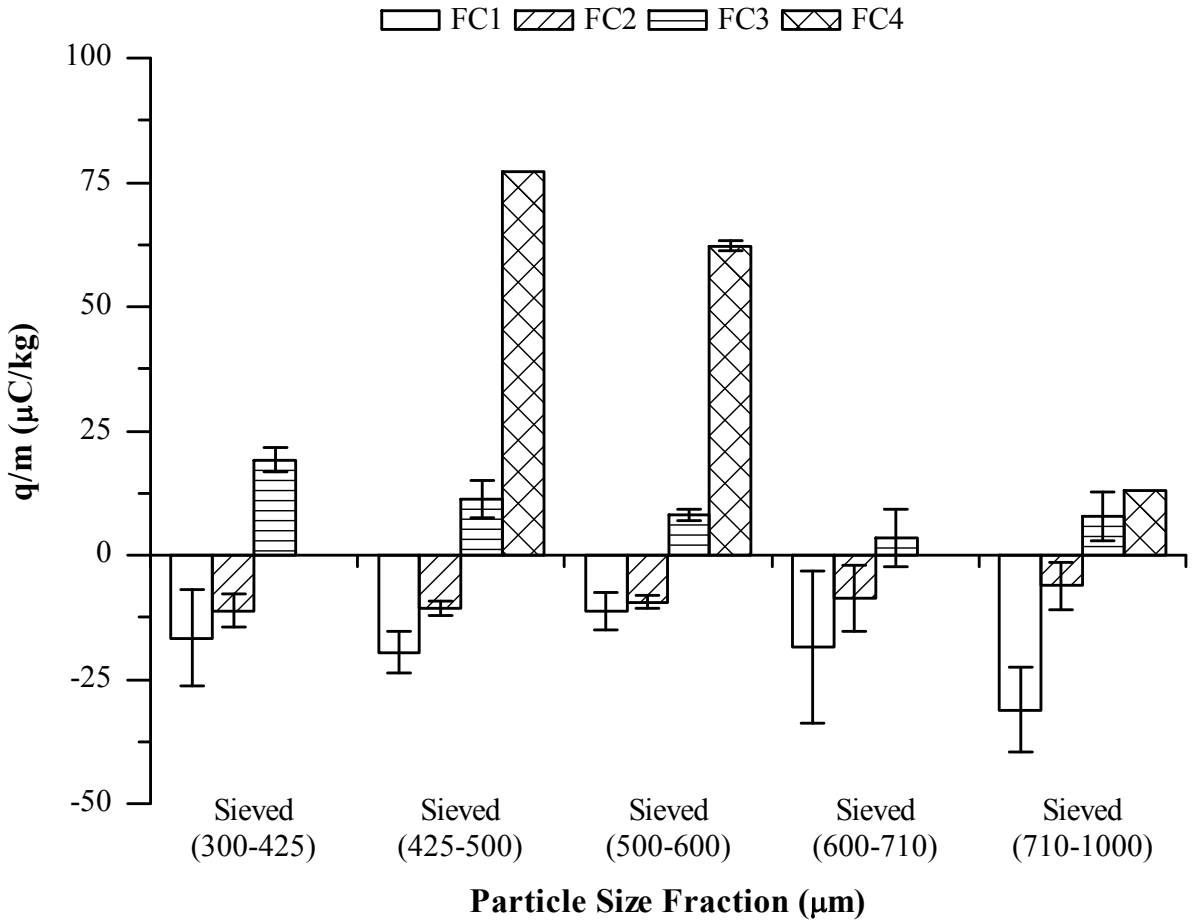


Figure 6.1: The initial net q/m of particles for different size ranges using the Charged Particle Separator in different Faraday cups (FC).

6.2.2. Mass

The m% of the Dropped, Loosely Bound, and Wall particles is shown in Figure 6.2 at 1.5 u_{mf} and Figure 6.3 at 4 u_{mf} for sieved and non-sieved conditions. At the lower fluidizing gas velocity, the mass of the Dropped particles with sizes smaller than 600 μm remained relatively constant and similar in magnitude as the non-sieved sample. However, at particle sizes greater than 600 μm,

the particles mass increased significantly. This is reflected by the amount of Loosely Bound and Wall particles collected which decreased significantly at this condition. Around this particle size, the gravitational forces dominated the adhesive forces (electrostatic, van der Waals, and image) and therefore few Wall particles were present. On average there were also more Tightly Bound particles with the non-sieved sample in comparison to those sieved in both fluidization flow regimes. This means that it was more difficult to remove the particles from the column wall when particles had a wide size distribution which was caused by the bi-polar layering effect described in Chapter 5.

The large standard deviation in the trials performed at 4 u_{mf} with particle size range of 600-700 μm was caused by large fluctuations in the amount of Wall particles. In some cases a large particle layer formed on the column wall and in other cases there was no particle coating. This represents a certain particle size where there was a near equality between the gravitational forces and the adhesive forces. In some trials the gravitational force was slightly larger and was able to dislodge the particles and in other cases the same behaviour was not found. More discussion on this issue will be presented in subsequent sections.

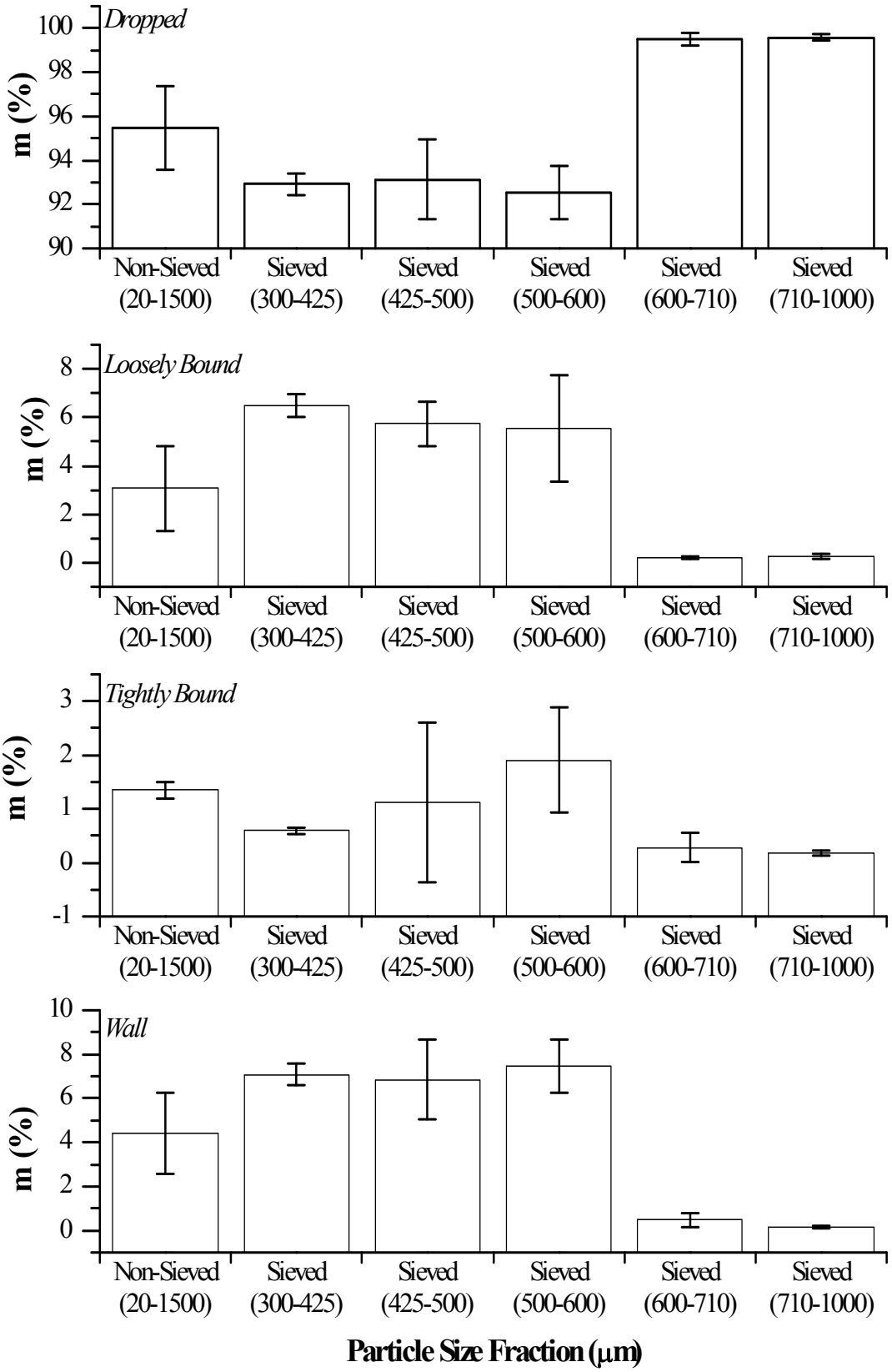


Figure 6.2: The m% of the Dropped, Loosely Bound, and Wall particles for different particle size ranges at 1.5 u_{mf}.

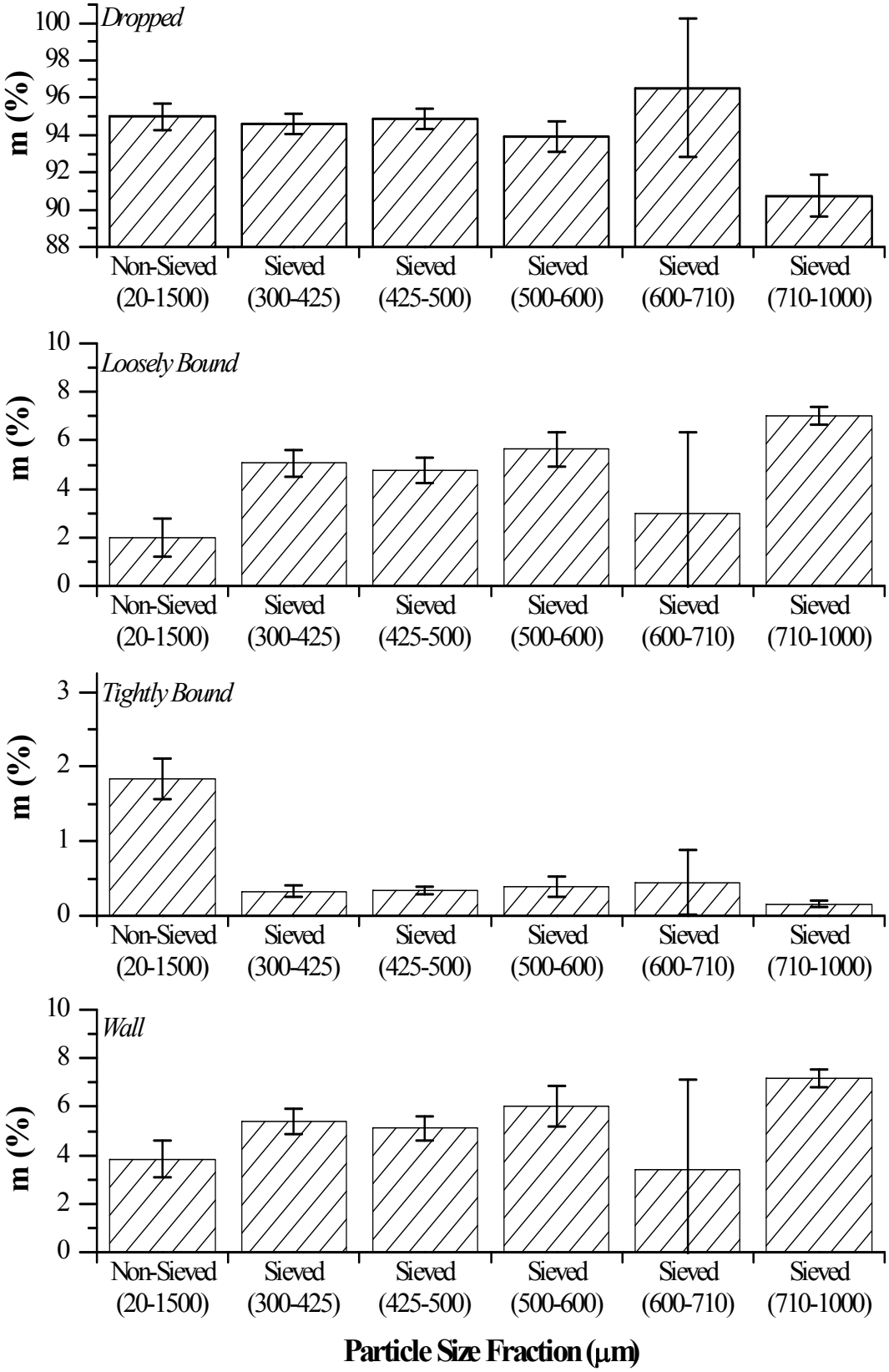


Figure 6.3: The m% of the Dropped, Loosely Bound, and Wall particles for different particle size ranges at 4 u_{mf}.

6.2.3. Particle Size Distribution

In order to be able to compare the particle size of the sieved particles, the d_P50 of each experiment was normalized (d_P50_N) to the average d_P50 of the non-sieved Initial particles. The results for the Initial, Dropped and Loosely Bound particles are shown in Figure 6.4. As can be seen in this figure even though the particles were sieved into a narrower particle size range, the particles that tended to coat the column wall were still on average smaller than the Initial sample for all particle size ranges and fluidizing gas velocities. This suggests the tendency for the smaller sized particles to adhere to the column wall.

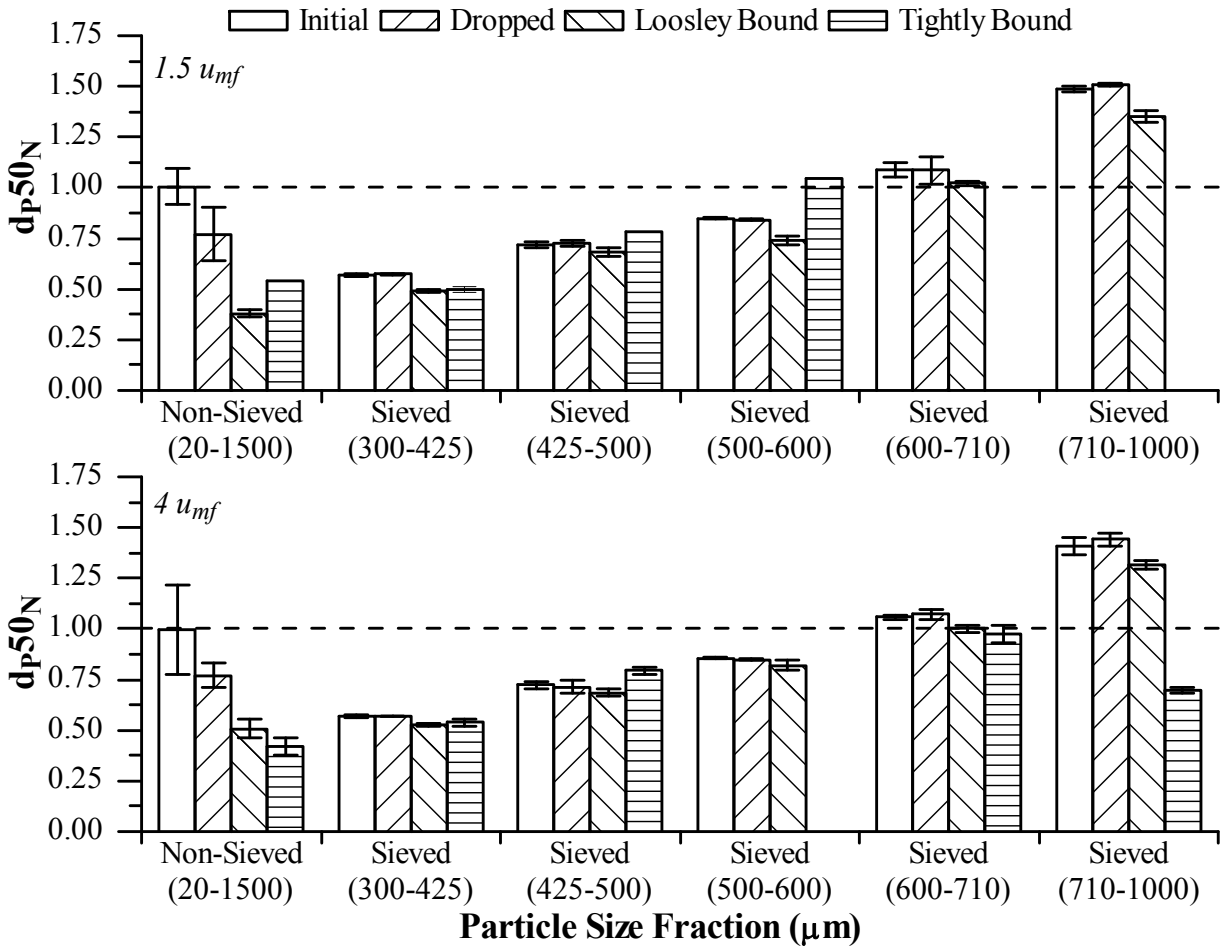


Figure 6.4: The d_P50_N of the Initial, Dropped, Loosely Bound, and Tightly Bound particles with different particle size ranges at 1.5 and 4 u_{mf}.

6.2.4. Particles Absolute and Specific Charge

Figure 6.5 shows the net specific charge of the particles in the Initial, Dropped, and Loosely Bound regions of the fluidized bed for particles of different size range at 1.5 and 4 u_{mf}. For both fluidizing gas velocities, for all particle size ranges, and in all regions, the Dropped and Loosely Bound particles were predominantly negatively charged. This can be attributed to the particle-wall contacts that occurred throughout the fluidization period. As shown in Chapter 4, polyethylene should charge negatively when in contact with the carbon steel column wall.

On average, the Loosely Bound particles were highly negatively charged with a specific charge of approximately -50 μC/kg. The sieved particles in the Dropped region were also predominantly negatively charged; however, not as charged as the Loosely Bound particles with a specific charge of approximately -1 μC/kg. Since with both the Loosely Bound and Dropped particles there was an overall increase in the amount of negative charge compared to the Initial particles, and the quantity of Fines was negligible, the positive charges would have been found on the column wall. The net q/m of the Loosely Bound particles did not vary with the particle size, yet only the smaller particle sizes (i.e., less than 600 μm) resulted in particle-wall adhesion. This again confirms that the measurement of the net q/m within a gas-solid fluidized bed is not necessarily an indication of reactor wall fouling.

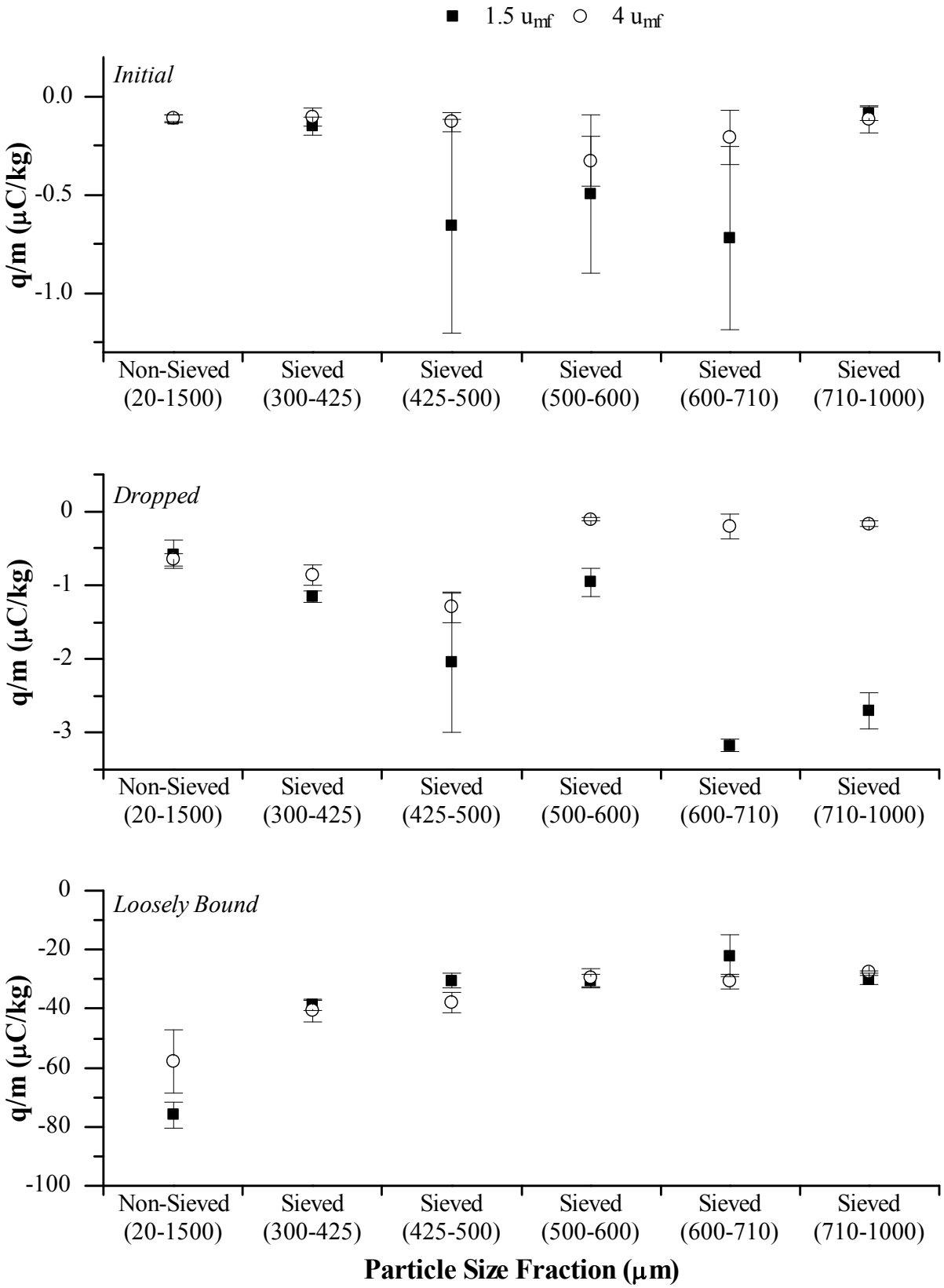


Figure 6.5: The particles net q/m in the Initial, Dropped, and Loosely Bound regions for different particle size ranges at 1.5 and 4 u_{mf}.

The fluidizing gas velocity did not have an impact on the specific charge of the Loosely Bound particles as the particle size increased. The fluidizing gas velocity did not affect specific charge of the Dropped particles up to approximately 600 μm, at which point there was a large difference in the q/m. This was caused by a fraction highly charged particles falling off the column wall. These particles would normally have been as part of Wall particles but the gravitational force was strong enough to detach them from the column wall. This can be justified by looking that the measurement of the cumulative net charge of the Dropped particles (Figure 6.6). During the measurement of the charge of the Dropped particles the electrometer records the signal background before the distributor plate is removed, at which point the Dropped particles fall down into the bottom Faraday cup. Normally there would only be one sudden drop in the measurement corresponding to the bulk of the particles dropped, however, in some cases after a short period, some of the Loosely Bound particles also fell off. This led to another sharp drop in charge measurement as can be seen in Figure 6.6. This resulted in a large increase in negative charges measured for the Dropped particles with only a small increase in the mass. Therefore the q/m of this region increased in magnitude; however, since there was such a large mass (> 90 m%), the magnitude of the q/m for the Dropped particles was not as large as for the Loosely Bound particles in general.

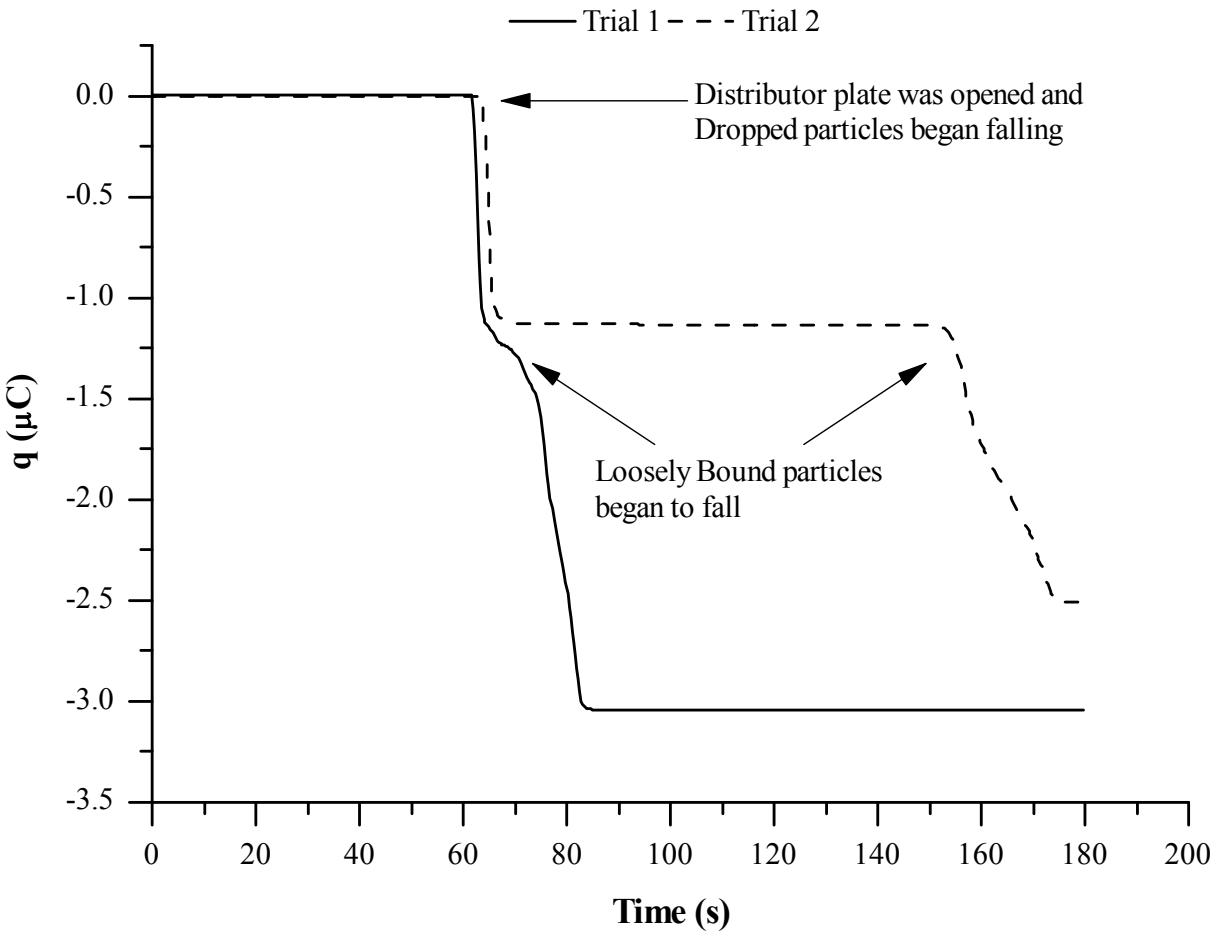


Figure 6.6: Examples of the Dropped particle measurement where Loosely Bound particles also fell with the Dropped particles. Results are presented for particles size range of 600-710 μm at 4 u_{mf}.

6.2.5. Specific Charge-to-Specific Surface Area Ratio

Figure 6.7 shows the $\hat{q}/\hat{A}$ for the sieved and non-sieved particles. Overall there was no effect on the particles surface charge density with increasing particle size. This comes from the migration of the highly charged particles to the column wall. If the particle does not have enough charge to remain bound to the column wall then it will return to the bulk of the particles. This surface charge density may be the limiting charge that will keep the particles bound to the column wall. There was an increase in magnitude of the $\hat{q}/\hat{A}$ of the sieved particle size range between 710-1000 μm at 4 u_{mf}, but this was likely attributed to some of the highly charged Loosely Bound particles falling off into the bottom Faraday up during the Dropped particle charge measurement as discussed in §6.2.4. Therefore, this means that overall the amount of charge on the surface of

these particles are similar. If the charges are similar, then as particle size increases, the electrostatic force and image forces (§ 1.3.1.2) would be decreasing since both are inversely proportional to the distances between the charges. At the same time, the gravitational force would be also increasing, which would result in the larger particles being less likely to adhere to the column wall. This was observed with the particles greater than 600 μm in diameter. Since it was determined that the column wall was positively charged and the Dropped and Wall particles were predominantly negatively charged, then the Dropped particles likely repulsed some highly negatively charged particles towards the wall while the positively charged wall and the image charge from the particles themselves attracted the particle to the column wall. This would have led to the column wall fouling for all particle size ranges.

It can also be observed that the $\hat{q}/\hat{A}$ for the Dropped particles was approximately one order in magnitude smaller than the Wall particles, meaning the charge on the narrow particle size ranges is not uniformly distributed for a certain particle size.

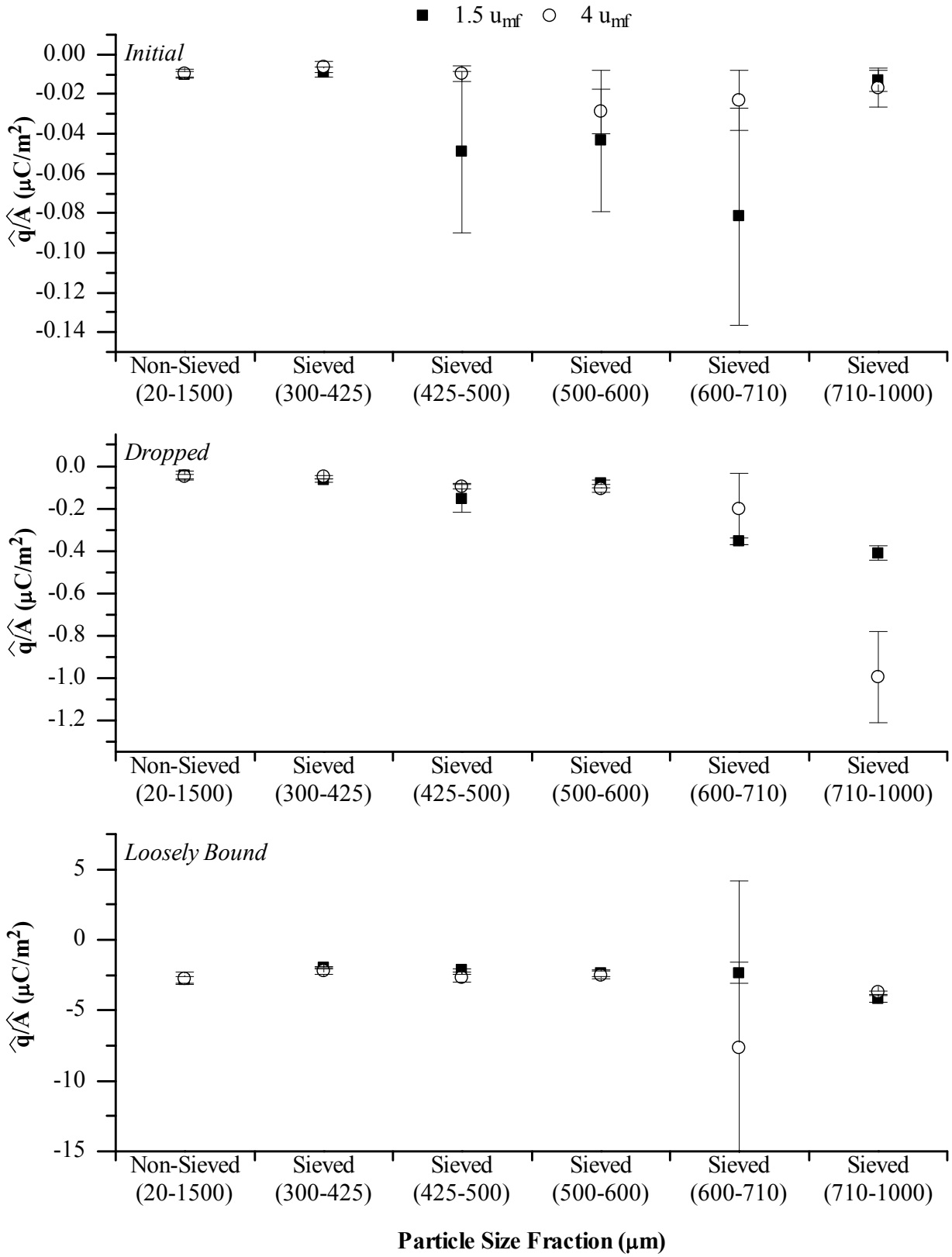


Figure 6.7: Particles $\hat{q}/\hat{A}$ in the Initial, Dropped, and Loosely Bound regions for different particle size ranges at 1.5 and 4 u_{mf}.

6.2.6. Wall Layer Coating

Pictures were taken from the particle fouling on the column wall before and after tapping off the Loosely Bound particles. Examples of pictures can be seen in Figure 6.8 for 1.5 u_{mf} and in Figure 6.9 for 4 u_{mf}. At both fluidizing gas velocities, there was a considerable amount of particle wall fouling up to 600 μm particle size. With the higher particle sizes, the gravitational force was able to overcome the adhesive forces at 1.5 u_{mf} consistently, and in the majority of cases at 4 u_{mf}. Examples of the observed inconsistency in the particle wall fouling formed with the sieved particles ranging between 600-710 μm fluidized at 4 u_{mf} can be seen in Figure 6.10. Pictures are shown for 4 of the 7 repeated trials performed. However at the same gas velocity, with the particles greater than 710 μm, consistent results were obtained with a layer of coating on the wall. This was likely caused by the presence of smaller particles that were not separated through sieving. Although not presented, but the only particle size ranges that showed any detectable amount of Fines were the larger particles giving rise to the possibility of other smaller particles being adhered to the column wall. The presence of these smaller particles would inherently affect the wall layer formation as described in Chapter 5.

In all trials, after tapping the column wall the majority of the particles easily fell off the column wall suggesting that the particles were mostly Loosely Bound. This can be attributed to the absence of the smallest particles due to sieving. Recall in Chapter 5, the Tightly Bound particles, those closest to the column wall, were on average smaller than even the smallest sieved particle size range (300-425 μm). The absence of these particles close to the column wall could mean that the adhesive forces could not overcome the gravitational forces, likely due to the larger particles present.

With the smaller particle size range (300-425 μm) as the gas travels through the bed the bubbles could be larger than with the larger particles size range (710-1000 μm). Since the force to move smaller particles would be smaller the gas travelling through the bed would more easily expand. The larger bubbles would increase their gas velocity and subsequently increase the amount of tribocharging of the particles. Therefore there is likely more charging with the smaller sized particles which would also aid in adhering this size range to the column wall.

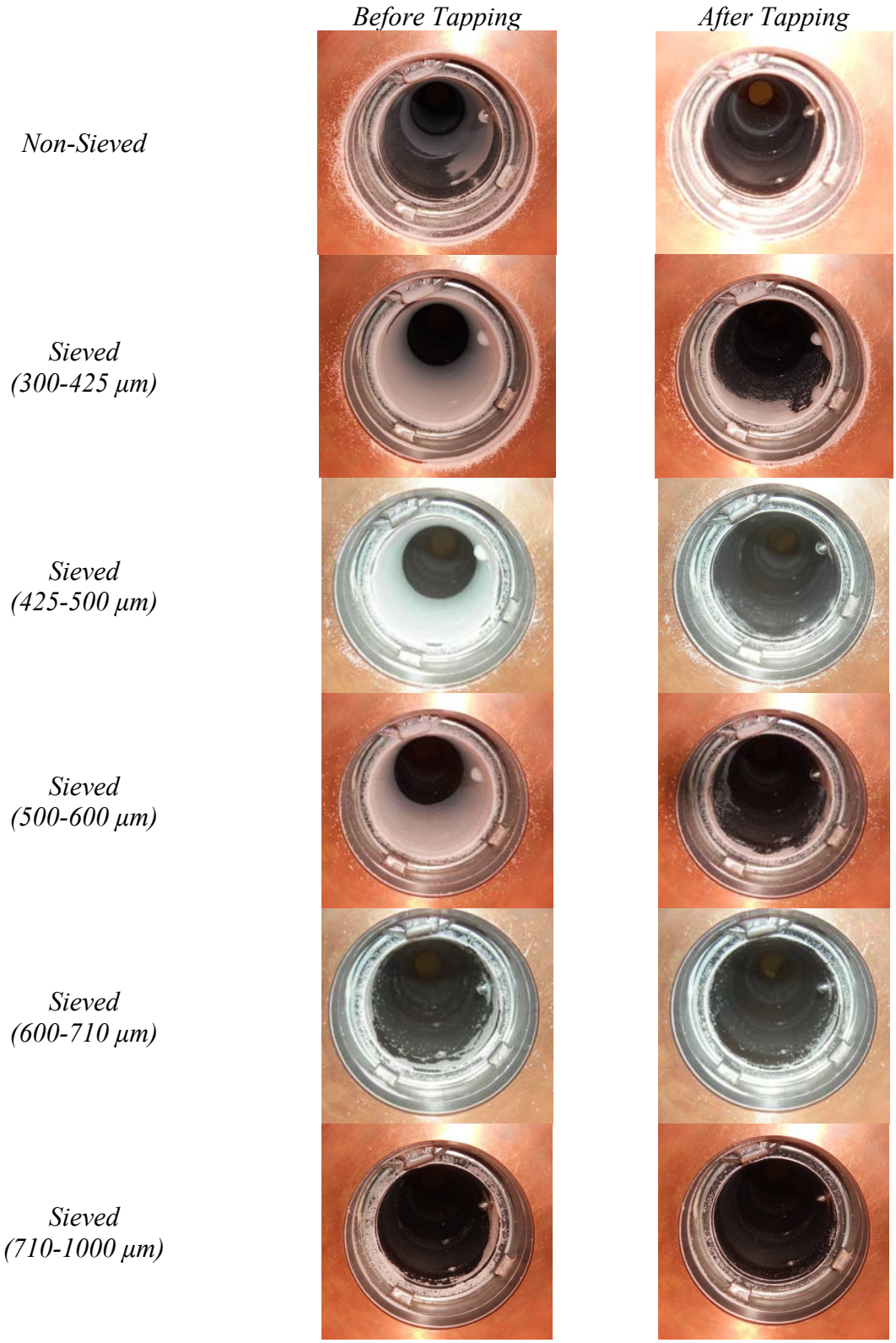


Figure 6.8: Images of the wall layer coating with different particle size ranges before and after tapping the column wall at 1.5 u_{mf}.

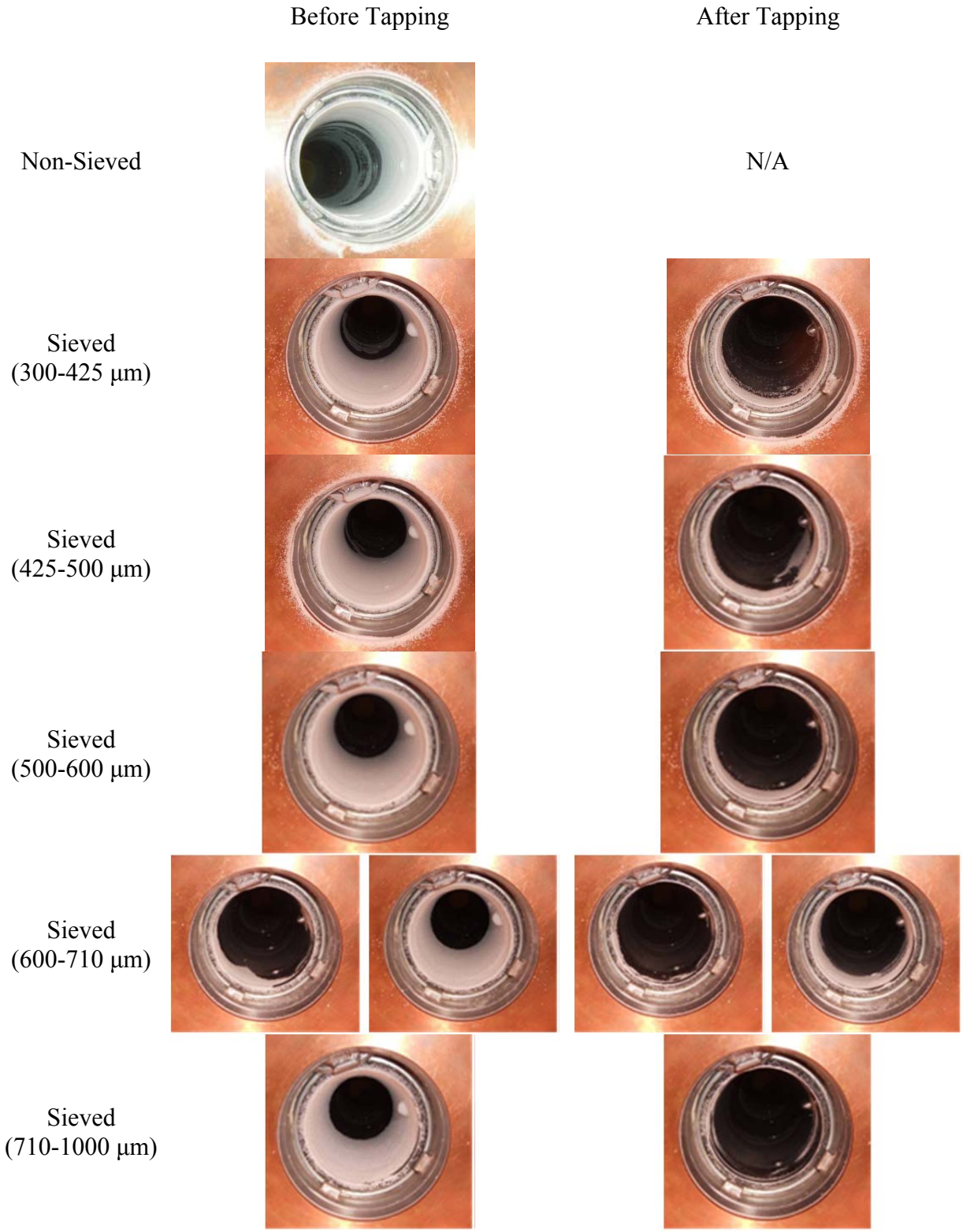


Figure 6.9: Images of the wall layer coating with different particle size ranges before and after wall tapping at 4 u_{mf}.

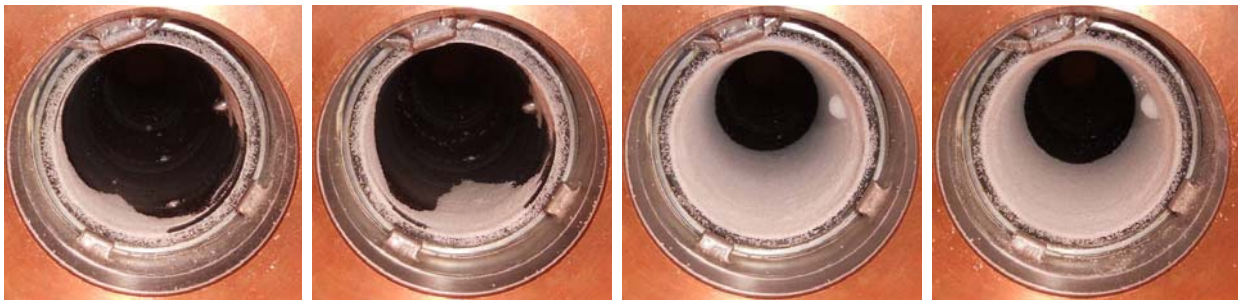


Figure 6.10: Images of the wall fouling of four out of seven repeated experiments with 600–710 µm particles at 4 u_{mf}.

6.2.7. Electrostatic Probe

The current measurements performed with the electrostatic probe at 1.5 and 4 u_{mf} are shown in Figure 6.11 and Figure 6.12, respectively. Overall, there were more negative peaks than positive peaks for all particle sizes tested. No clear trend was found with increasing the particles size although the 710-1000 µm range tended to have the largest signal fluctuations. Increasing the gas velocity did not significantly increase the amplitude of the current fluctuations; however, the frequency increased for the large negative fluctuations, particularly for the larger particles. Similar to results presented in §5.2.6, the increase in the frequency of these large fluctuations with increasing particle size and gas velocity did not necessarily mean that the electrostatic charges within the bed increased or that there was column wall fouling in the bed since the particles with the most particle fouling were those with the lower particle size range. Instead, the probe is likely measuring the charge transfer between the particles coming into contact with it during fluidization.

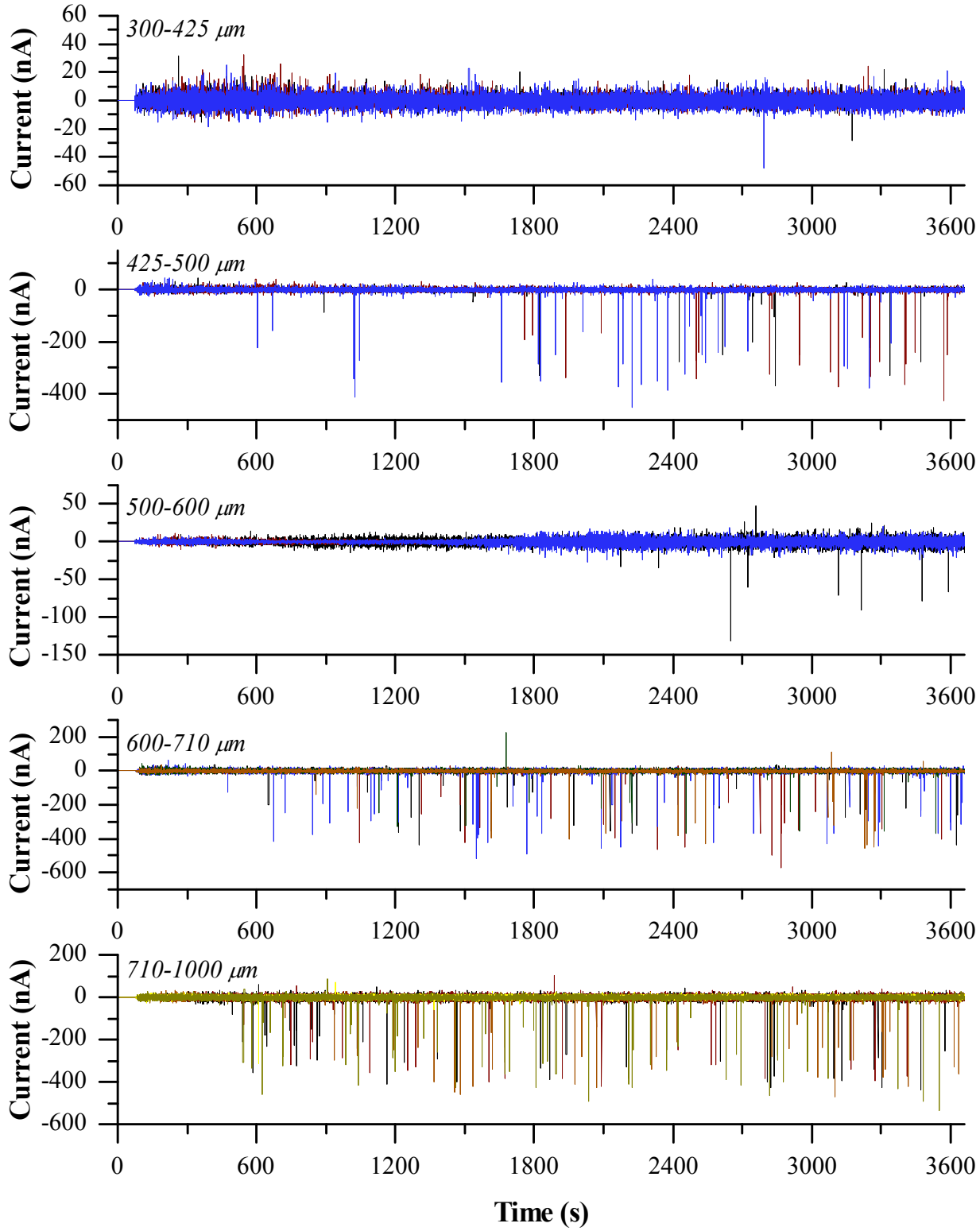


Figure 6.11: The current measurement from different sieved particle size ranges for 60 min of fluidization at 1.5 u_{mf}.

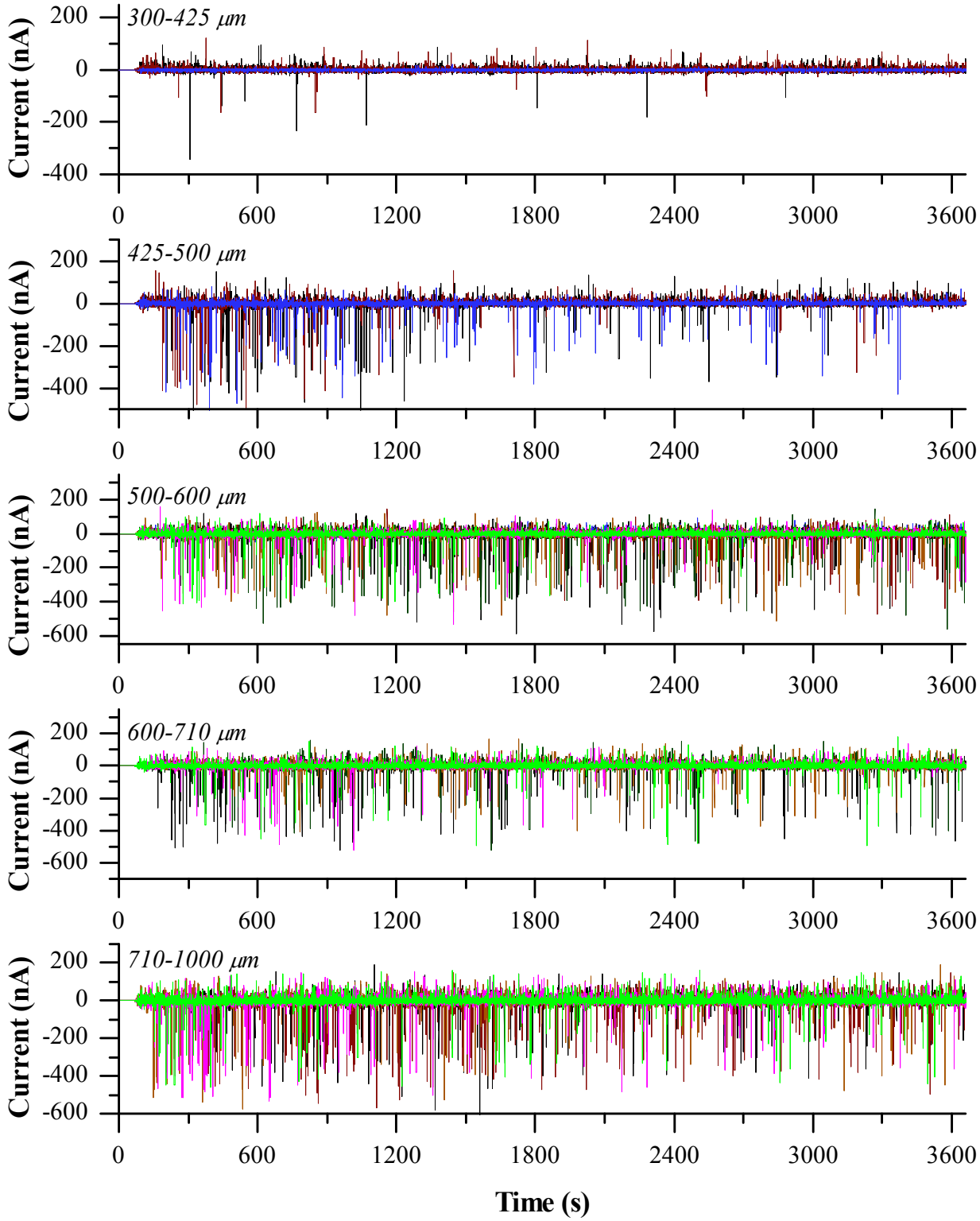


Figure 6.12: The current measurement from different sieved particle size ranges for 60 min of fluidization at 4 u_{mf}.

6.3. Summary

In the bubbling flow regime it was found that only particles with diameters less than 600 μm adhered to the column wall indicating that the smaller the fluidizing particle, the higher the tendency for wall fouling formation. This same effect occurred at the higher gas velocity with particle sizes ranging between 600-710 μm; however, particles of this particular size range either adhered to column wall or were easily dislodged with the Dropped particles prior to tapping the column wall. This was directly related to the amount of electrostatic charge generation within the fluidized bed. These results did not occur with the larger particles of 710–1000 μm, which may have been caused by the presence of smaller sized particles within the sample. These smaller particles may have been present due to the electrostatic charges generated during the sieving process which would bind them to the larger particles.

Overall, for both flow regimes, regardless of the particle size range used, the lower bound of the particle size within each size range would have a higher frequency of building up on the column wall. In addition, for the resin as received, which was of a wide particle size distribution, the portion attached to the column wall was of similar size to the lowest narrowed size range (i.e., 300-425 μm). This size range contained the highest charge which agrees well with the particle size ranges found in Chapter 5. For the majority of the parameters measured in the Wall region, similar trends were found in both flow regimes indicating that for particle wall adhesion, the fluidization regime may not have a large impact for sieved particles. Furthermore, the charge distribution within the fluidized bed was similar regardless of the particle size with the net q/m being the highest in the Wall region.

As expected, the Wall particles had the largest $\hat{q}/\hat{A}$ of any of the particles within the system regardless of particle size range which would have been a large factor for the particle-wall adhesion observed. Finally, it was found that the measurement of the overall q/m within the bed with fluidizing particles of narrowed size range was not an indication of the amount of reactor wall fouling since the q/m remained constant in spite of the amount of particles on the column wall. Finally, similar to results found in §5.2.6, the current measurements did not give a decisive measure of the actual bed electrification, nor the amount of particle wall fouling.

Chapter 7.
EFFECT OF COLUMN WALL MATERIAL

Electrostatic charging is a surface phenomenon; and thus it is highly dependent on the surface chemical and physical properties of objects at their point of contact. In gas-solid fluidized beds, particle-wall interactions can play an important role in generation of electrostatic charges. Therefore, it is critical to investigate the effect of fluidization column wall material on the magnitude of electrostatic charge generation and column wall fouling. Industrial polyethylene gas-solid fluidized bed reactors are generally made of carbon steel, however, in some reactors a polymeric coating containing chromium compounds has been applied in an attempt to reduce the electrostatic charges and the formation of sheeting (Mihan et al., 2002; Muhle et al., 2005). A summary of works found in literature that have focused on the effects of column wall material is shown in Table 7.1. Academically, there have not been many studies that have specifically focused on the effects of the column wall material in gas-solid fluidized beds, but there are a few that are related to pneumatic transport. Overall it was found that the material with the lowest electrical conductivity created the largest amount of bed potential. In relation to industrial applications, there have not been any studies that have focused on a column wall material being similar to that of the fluidizing particle; an example of the impact of insulator-insulator contact. In this work two extreme column materials (a conductor and an insulator) were tested. Since the fluidization column was made of carbon steel, for the other extreme case the bed charging was investigated against that of covering the inner column wall with a film made of the same polyethylene fluidizing particles. It was believed that if the column wall and the fluidizing particles were of the same material, the electrostatic charge generation would have been minimized and thus less column wall fouling would have occurred.

Table 7.1: Summary of previous studies on the effect of the column material on electrostatic charge generation in gas-solid fluidized beds.

Authors	Year	Measurement Technique	Column Material	Particle Type	Particle Size μm	Effect
Kisel'nikov et al.	1967	Electrostatic Probe	Metal Glass	Polymeric Resins Polyacrylonitrile Ammonium Sulfate	-	Glass column produced three times as much bed electrification.
Boland and Geldart	1971/ 72	Electrostatic Probe	Perspex Glass "Prectafilm"-lined walls	Lead Glass Ballotini	100-800	Perspex created most charge due to lowest conductivity.
Ally and Klinzing*	1985	Nickel Electrodes	Copper Plexiglas Glass	Copper Plexiglas Glass	196 75, 150, 345 145	Glass tube and copper particles had the most amount of pressure drop, which was associated to electrostatic effects.
Matsusaka et al.*	2006	E-SPART	316 Stainless Steel 304 Stainless Steel Aluminum Copper Brass	Alumina	3.3	Alumina against stainless steel resulted in positive charge, and against aluminum, copper and brass resulted in a negative charge.
Giffin	2010	Faraday Cup	Carbon Steel 316 Stainless Steel	Polyethylene	10-1500 μm	Similar charging effects in both columns, with the differences attributed to surface roughness.

* Pneumatic transport was studied.

7.1. Experimental Conditions

The operating conditions for the experiments performed for the effect of column wall material is shown in Table 7.2. The fluidizing particles were PE_B and were fluidized at 1.5 u_{mf} for a period of 60 minutes.

Table 7.2: The experimental conditions used for the experiments on the effect of the column material.

Parameter	Value
Fluidizing Particles	
Type	PE_B
Size Range	10-1500 μm
Fluidizing Gas	
Velocity	1.5 u_{mf} (Bubbling)
Time	60 min
Temperature	22 °C
Relative Humidity	0 %
Fluidization Column	
Material	Carbon Steel Polyethylene Film Sleeve
Additive	
Type	None
Quantity	-

In order to simulate a coated column wall composed of the same material as the fluidizing polyethylene particles, a 0.1 m diameter polyethylene film was made out of PE_B particles and supplied by industrial partners (Figure 7.1). In all experiments with the film, a new film was used with each trial.



Figure 7.1: A picture of the polyethylene film added to the interior of the fluidization column.

7.2. Results and Discussion

A thorough analysis of the effect of the column wall material is presented below. Results are presented for the particles mass, size distribution, q/m, and $\hat{q}/\hat{A}$ found in different regions of the fluidized bed. In addition, the wall layer particle coating charge distribution was investigated in detail with the Charged Particle Separator apparatus to determine whether there was any bi-polar charging within the Loosely Bound wall particles.

7.2.1. Charge of the PE Film

In order to better understand the charging behaviour of PE particles coming into contact with the film inside the gas-solid fluidized bed, first a few bench-scale tests were performed. The same apparatus discussed in Chapter 4 was used with the exception that the carbon steel plate was covered with a piece of the PE film. For each test and prior to mounting the film on the carbon steel angled plate, the film was first directly placed in the bench-scale Faraday cup to determine its initial charge where it was found to be negatively charged each time. For the charge measurement, the electrometer background signal was first recorded for approximately one minute before the PE_B particles were poured directly into the Faraday cup. Once the rate of change of the charge recorded as particles entered the Faraday cup was relatively constant, the beaker holding the particles was moved forward so that the particles would pour onto the film and fall into the Faraday cup. Again when the rate of the change of the charge was constant, the beaker was moved away so that the particles would fall directly into the Faraday cup. This procedure was repeated two times. Throughout the testing care was practiced to pour the

particles at a steady rate. At the end of the experiment, the charge accumulated on the film was measured by putting the film into the Faraday cup.

An example of the particles charge measurement is shown in Figure 7.2. From this figure it can be seen that as the particles started contacting the PE film there was a distinct difference in the charging of the particles as the rate of change of charge decreased every time the PE particles were contacted with the film indicating that the particles were becoming less negatively charged. This effect was not as noticeable as in the second period when the particles were contacted with the PE film, which may have been due to some charge built-up on the film reaching almost saturation. For this experiment, the charge of the PE film prior to the particles contact was found to be -0.55 nC and after was -1.45 nC, signifying that the PE film was charging negatively with contact with the particles.

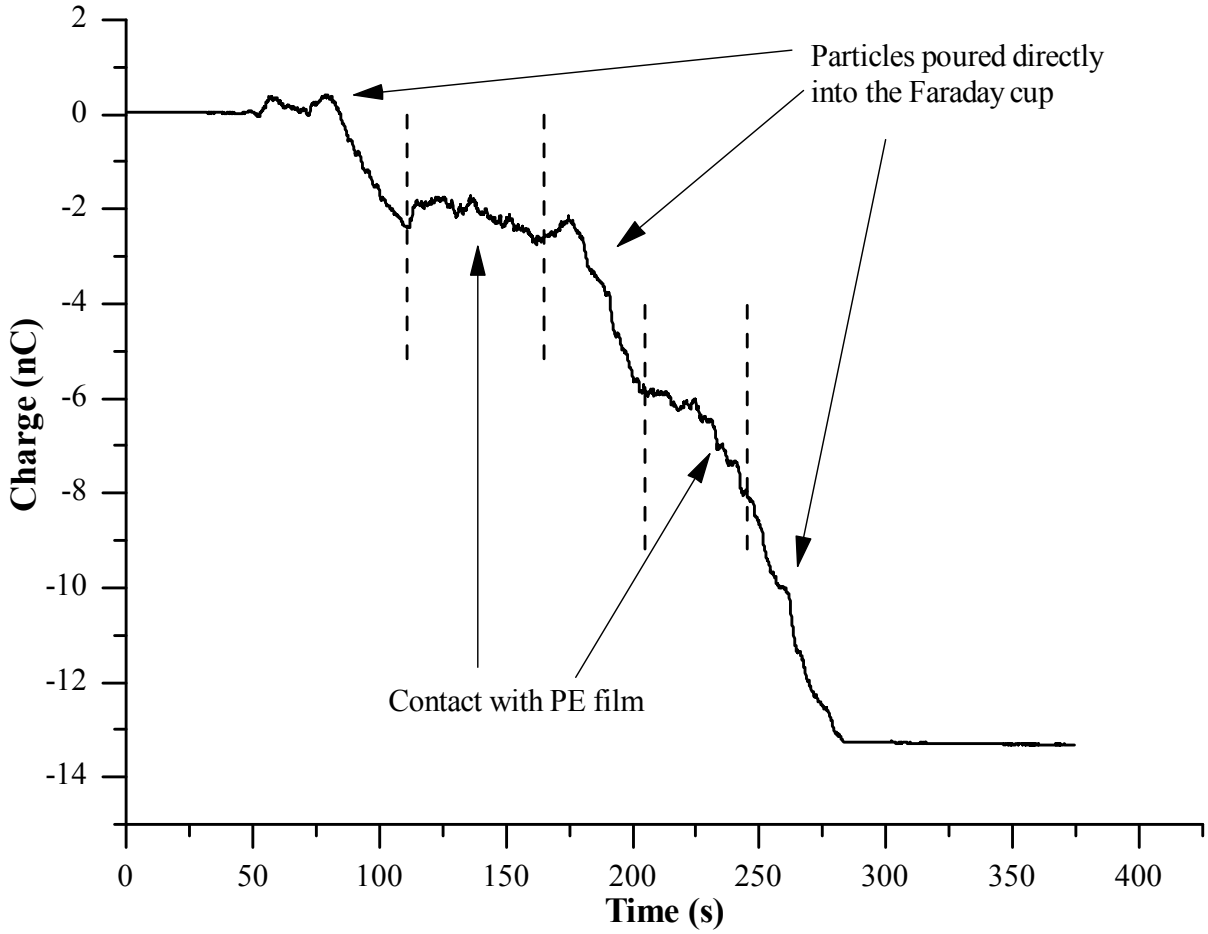


Figure 7.2: Example of the PE film charging PE_B particles.

7.2.2. Mass

The particles m% found in the Fines, Dropped, Loosely Bound, Tightly Bound, and Wall regions for both column materials are shown in Figure 7.3. Overall, the amount of Fines collected was very low for both cases and on average there was no significant difference in the amounts collected; however, there was a large standard deviation in results for the experiments performed with the PE film. The reasons for this large variation came from two trials having a very low mass (≈ 0.05 m%) and two trial having a larger mass (≈ 0.8 m%). This could either be caused by the smaller particles being trapped inside bed or the variation in the initial sample that originated from an industrial resin as received. The m% of the Dropped particles on average increased with having the PE film present; however, there was much variation suggesting that there was no significant difference in the results. On average the m% of the Loosely Bound particles decreased when using the PE film; however, there was a considerable amount of variation in the

amount collected, which is also seen for the Wall particles and therefore overall it was concluded that there was no significant difference in the magnitude of the wall fouling.

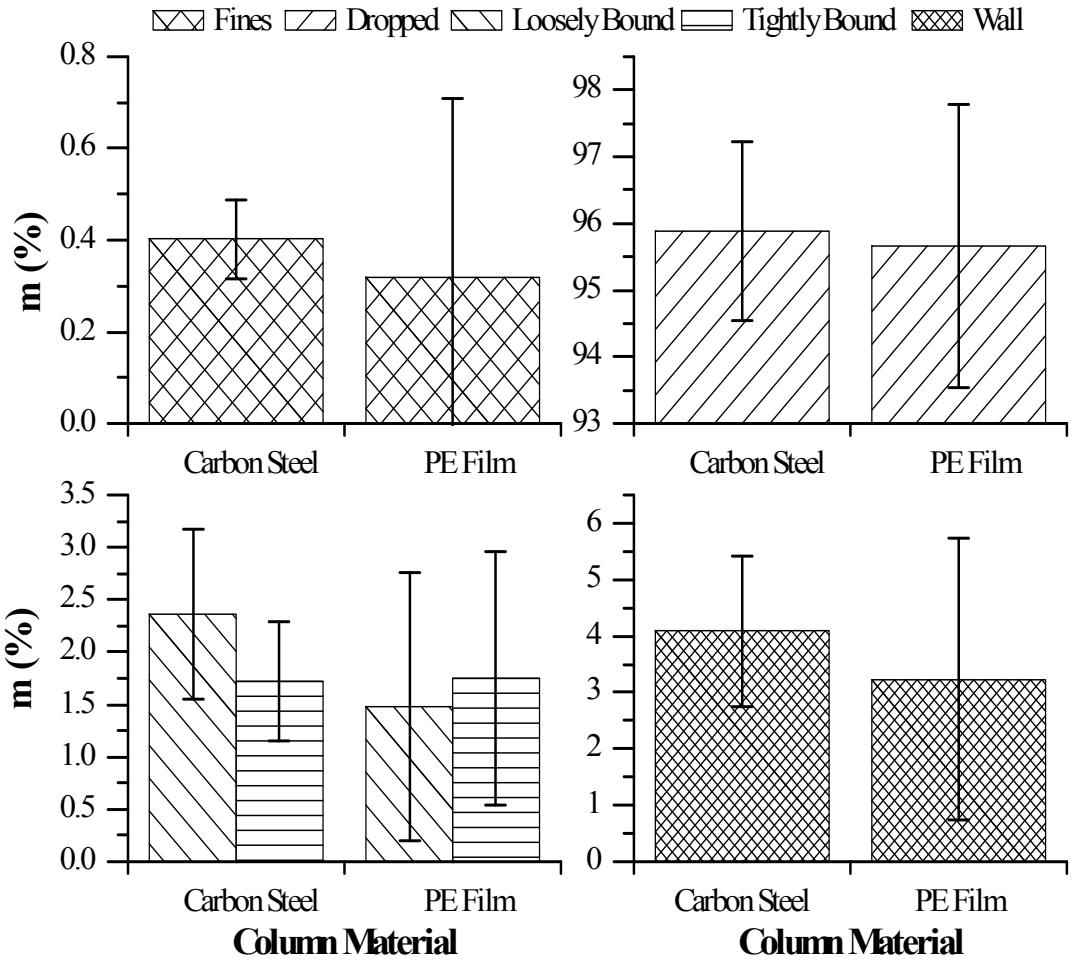


Figure 7.3: The m% of the PE_B particles in the Fines, Dropped, Loosely Bound, Tightly Bound, and Wall regions of the fluidized bed with different column materials.

7.2.3. Particle Size Distribution

An example of the normalized overall PSD found in different regions of the fluidized bed is shown in Figure 7.4 for the carbon steel and PE film column materials. As expected, the Dropped particles were nearly identical in size as the Initial particles as the Dropped particles contained at least 93% of the Initial particles. The Loosely Bound and Tightly Bound particles were smaller in size than the Dropped particles and more narrowly distributed in both columns. There was a small difference in the PSD of the Fines where it was much smaller in the carbon steel column. With the PE film, Fines consisted of some smaller particles and some larger

particles with sizes similar to those of the Wall particles. This may have been caused by the attraction of the finest particles to the PE Film, which in turn shifted the Fines PSD to slightly larger particles with a narrower particle size range. This will be discussed in more detail in the following sections.

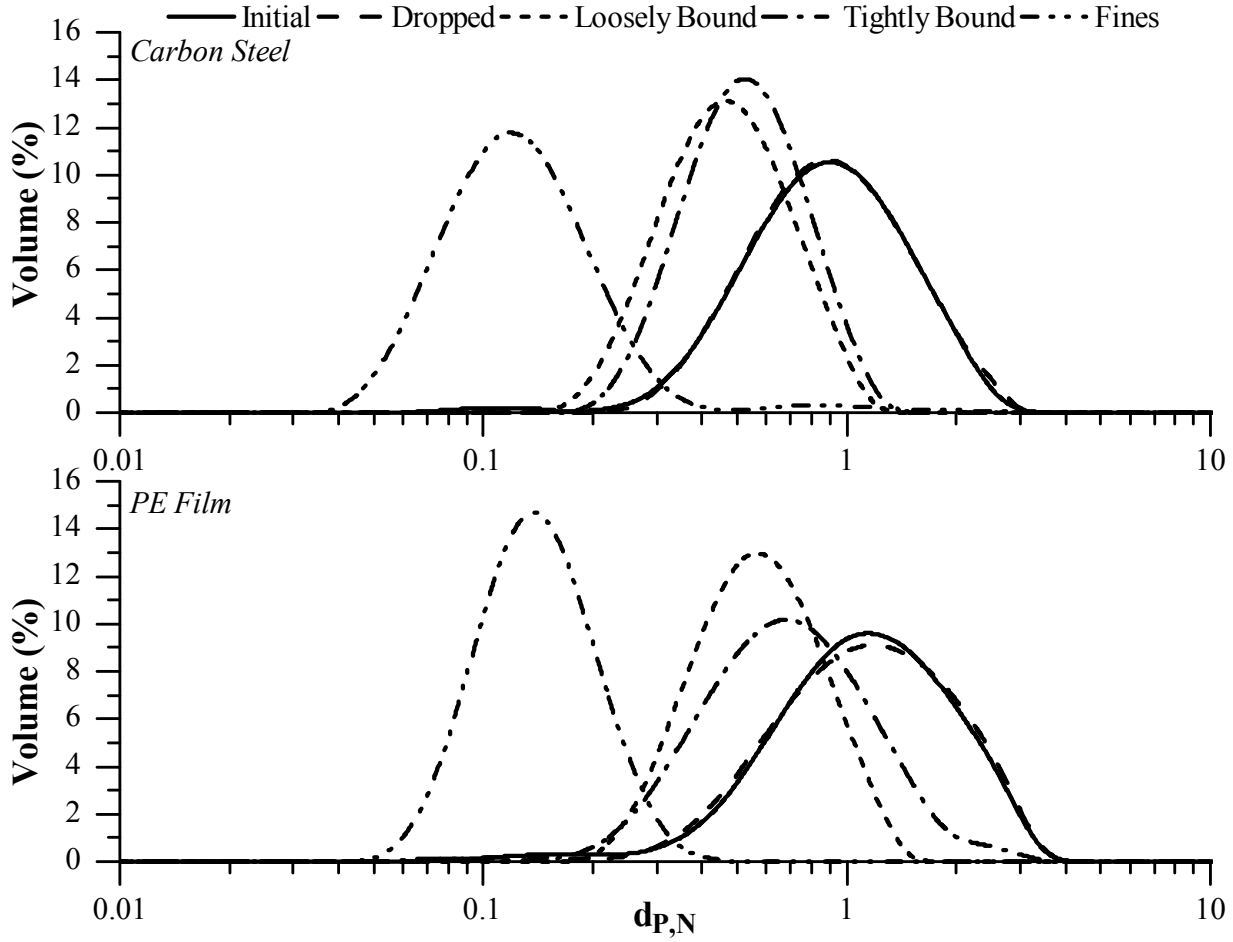


Figure 7.4: Examples of the normalized PE_B particles size distribution found in different regions of the fluidized bed with the carbon steel column and PE film sleeve.

The d_P50_N of the particles in different regions of the fluidized bed is shown in Figure 7.5. Overall in all regions of the bed, the particles d_P50 was larger in the presence of the PE film. Again this may have been caused by the Initial sample received directly from the industrial reactor, which was shown to be on average larger when the PE film experiments were performed.

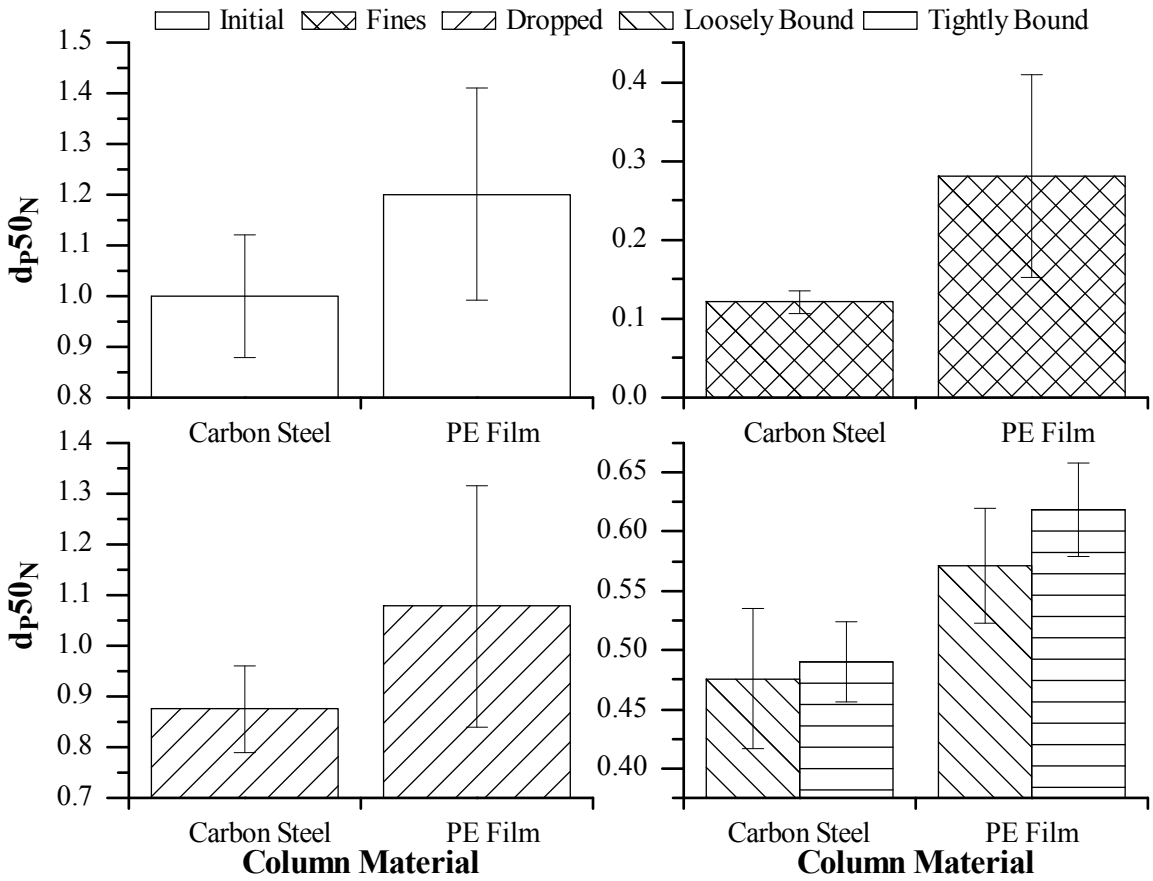


Figure 7.5: The d_P50_N of the PE_B particles in the Initial, Fines, Dropped, and Loosely Bound regions of the fluidized bed with different fluidization column wall material.

7.2.4. Particles Specific and Absolute Charge

The cumulative charge of the Fines entrained from the two types of columns is shown in Figure 7.6. It can be seen that in the carbon steel column the entrained Fines were predominantly positively charged for the duration of fluidization, whereas with the PE Film, the charge of the Fines was always predominantly negative.

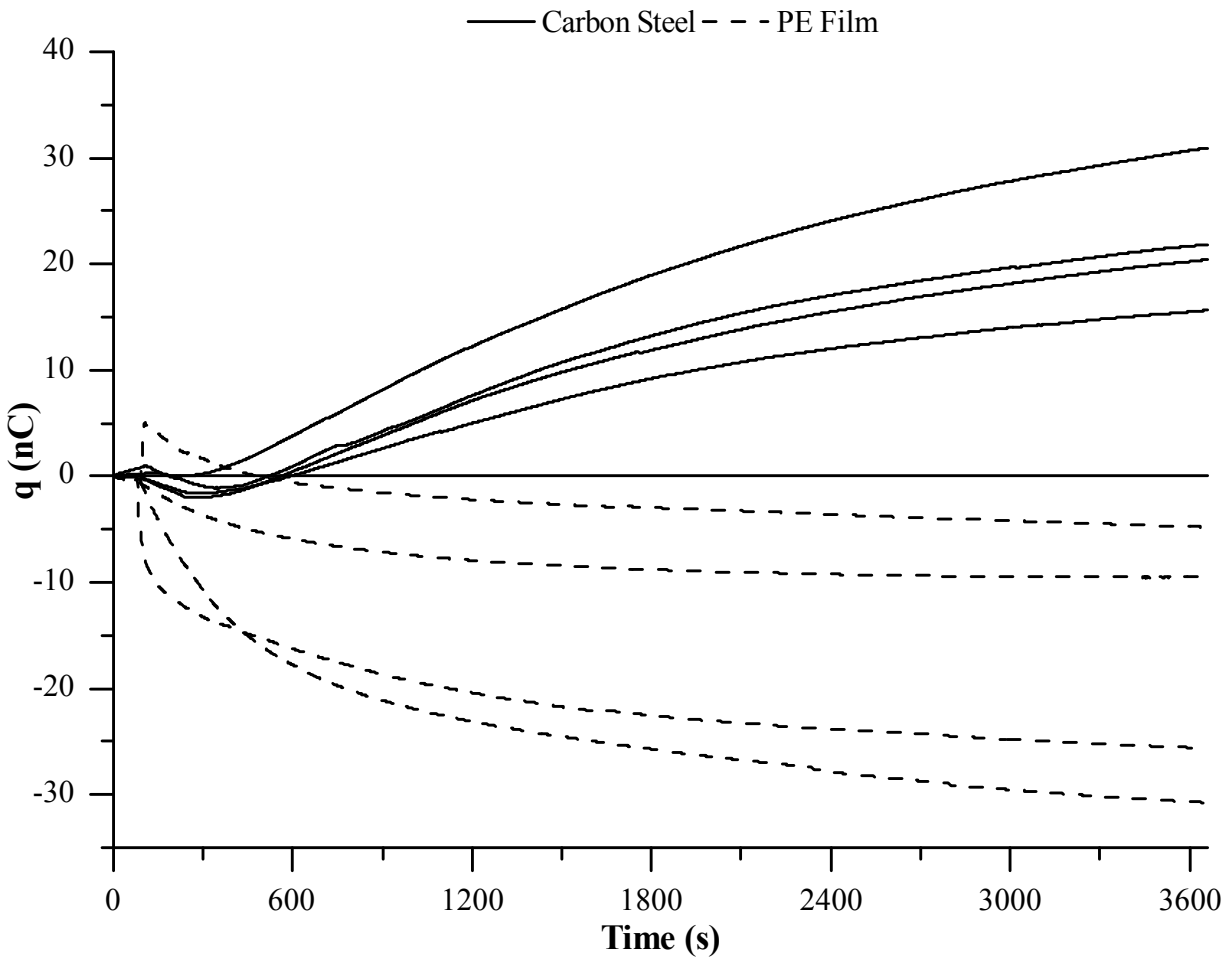


Figure 7.6: Cumulative charge of Fines measured for repeated trials for 60 min of fluidization with different column materials.

The specific charge of the Initial, Fines, Dropped, and Loosely Bound particles are shown in Figure 7.7. The net q/m of the Initial particles remained relatively the same whereas there was a large difference in the polarity and magnitude of the charge of the Fines, and the polarity of the Dropped particles. The large difference in the magnitude of the net q/m could be attributed to the lower mass collected in two out of the four trials with the PE film resulting in a significant increase in the q/m value.

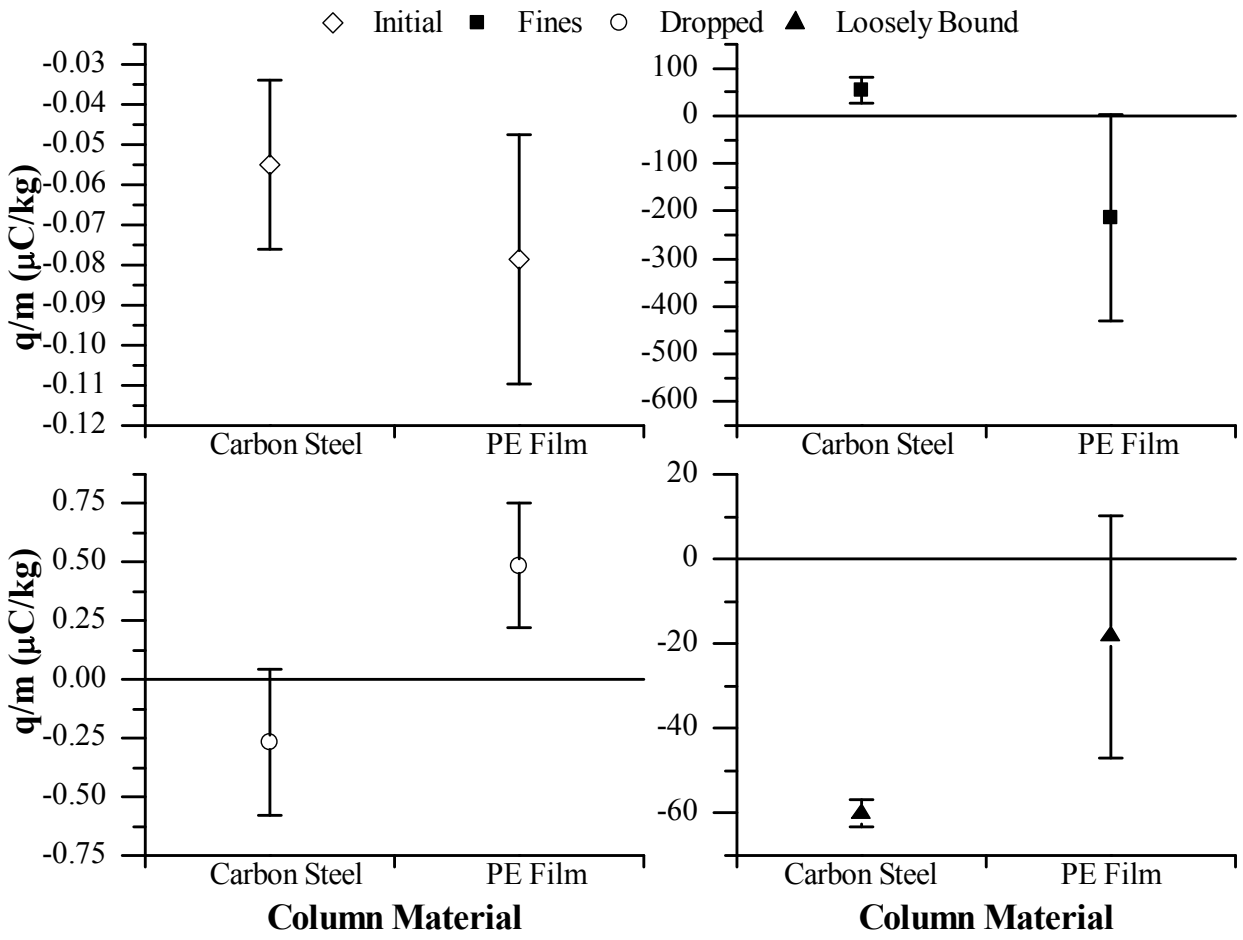


Figure 7.7: The net q/m of the particles in the Initial, Fines, Dropped, and Loosely Bound regions of the fluidized bed with different column wall materials.

The net q/m of the Dropped particle was of similar magnitude between the carbon steel and PE film experiments but the charge polarity was opposite. The polarity difference indicates that the contact between the PE particles and the PE film makes the PE film gaining electrons and becoming negatively charged whereas the PE particles donating electrons and becoming positively charged. This agrees well with the bench-scale testing results.as shown in §7.2.1. This may also explain as why the net q/m of the Loosely Bound particles was less negative with the PE film than the carbon steel wall. The negatively charged PE film would attract the positively charged particles. Negatively charged particles would then adhere to the positively charged particles and the wall layer would continue to grow, which could explain as why the mass of the Wall particles did not vary significantly between the two types of column. This would also decrease the net q/m of the Loosely Bound particles as there would be more positively charged

particles present. This also explains the negative polarity of Fines leaving the bed since the positively charged Fines were being attracted to the PE film.

7.2.5. Specific Charge-to-Specific Surface Area Ratio

The $\hat{q}/\hat{A}$ for the Initial, Dropped, Fines, and Loosely Bound particles are shown in Figure 7.8. There was no difference in the trends of the $\hat{q}/\hat{A}$ in comparison to that of the q/m; however, the Fines and the Loosely Bound particles were shown to have the most surface charge, which would contribute to the particle wall adhesion.

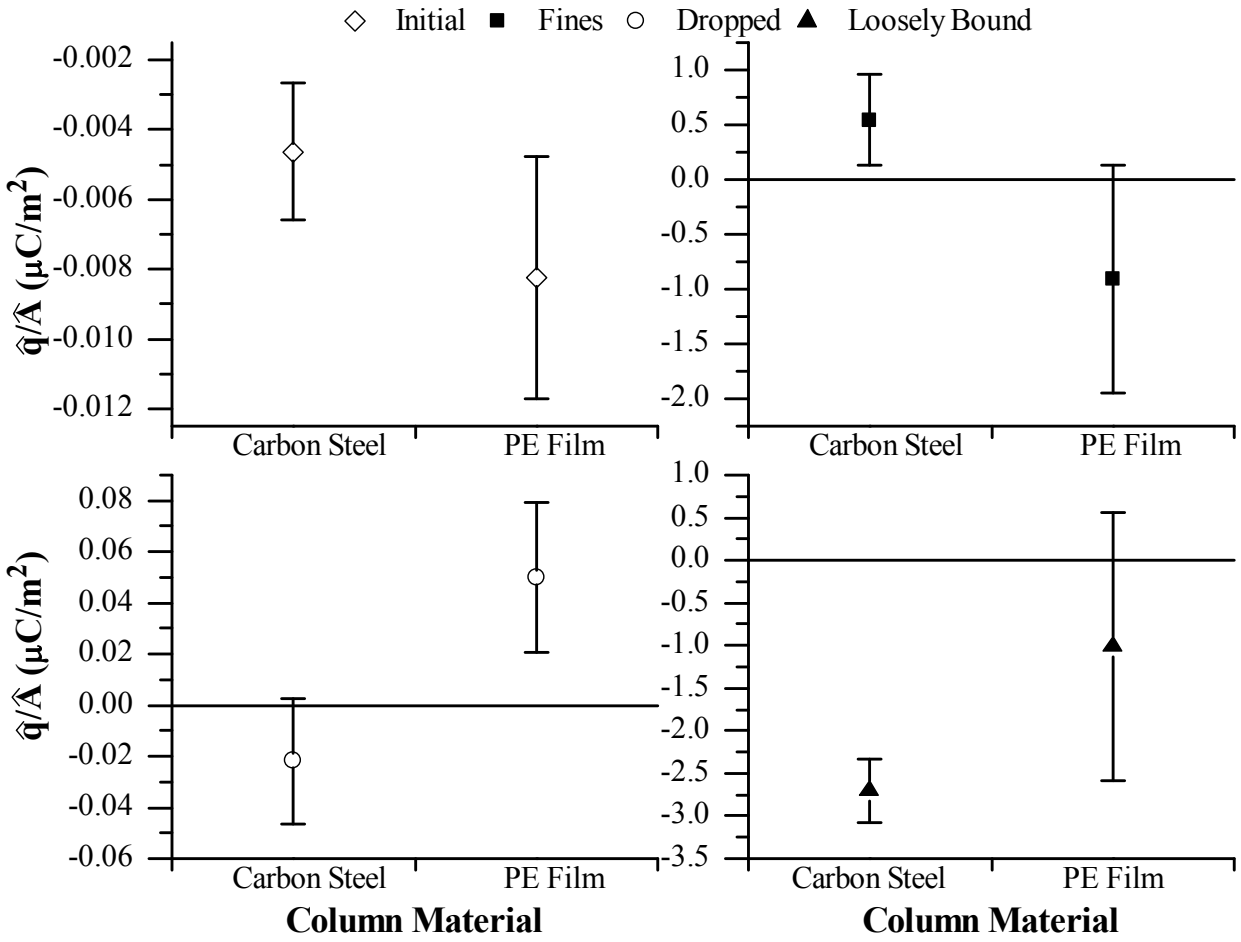


Figure 7.8: The $\hat{q}/\hat{A}$ of the particles in the Initial, Fines, Dropped, and Loosely Bound regions of the fluidized bed with different column wall materials.

7.2.6. Wall Layer Coating

Examples of images taken from the column wall coating in the carbon steel column and the column with the PE film are shown in Figure 7.9. In both cases there was a considerable amount of column wall fouling. With the carbon steel column there were fewer particles near the bottom of the column but more particles at the top of the bed compared to the experiments with the PE film.

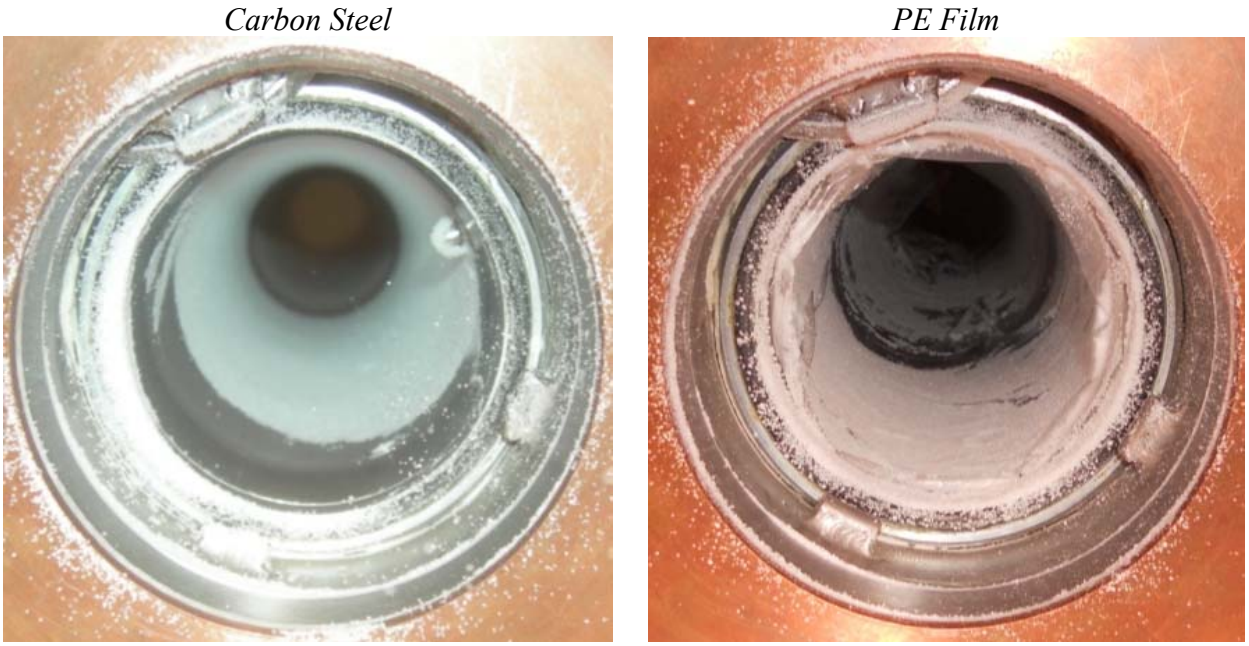


Figure 7.9: Examples of images from wall coating with carbon steel and PE film wall materials.

After all of the measurements were completed, the PE film was carefully removed from the column and pictures were taken of the particle fouling for the entire length of the film (Figure 7.10). Note that this picture was taken after some of the particles were removed from the bottom of the column for the PSD analysis of the Tightly Bound particles and therefore is not a complete representation of the entire wall fouling. As can be seen in the figure the majority of the adhered particles concentrated close to the static bed height, which would undergo many particle-film contacts when compared to the freeboard region of the column.

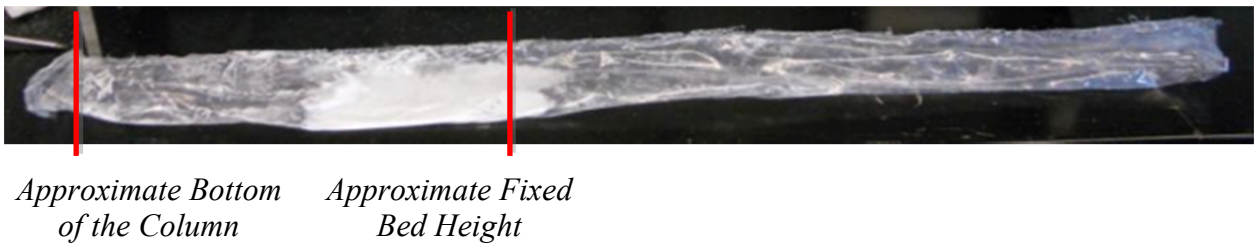


Figure 7.10: Example of particles coating on the PE film removed from column after the Wall particles were removed.

It was shown in previous sections that the mass of the particles forming the wall fouling was similar between the two column materials tested; however, on average the net q/m of these particles became less negative in the presence of the film. Therefore, these particles were less charged when the PE film was used. This was likely due to local charging on the PE Film. Since

the film was an insulator, the mobility of the electrons or ions is restricted meaning that when a certain region of the film undergoes contact or frictional charging, the charge generated remains in the same location. The continual particles contact in the same region of the film would cause a high electrostatic charge to form on the film, which would mean that the electrostatic charge on the particles do not need to be as high to make them attracted to the column wall. On the contrary, when the particles come into contact with the conductive carbon steel column wall electrons or ions are transferred, the charge is then distributed throughout the entire column. This would mean that charge density of the column wall does not increase as significantly due to the large surface area and therefore more highly charged particles are required in order to adhere to the column wall.

7.2.7. Charged Particle Separator

In order to determine charge distribution within the particles forming the wall fouling, in one trial the Charged Particle Separator apparatus was placed directly underneath the column in place of the bottom Faraday cup after the Dropped particles were removed. Unfortunately, due to the number of PE film sleeves available, only one experiment with the CPS apparatus could be performed. The results are shown in Figure 7.11.

The m% shown is the mass of particles collected in each of the four Faraday cups divided by the total mass of all four cups, and not divided by the initial mass as presented in the other sections. Overall results of particles m% and net q/m showed that bi-polarly charged particles existed within the Wall region with both column materials. This confirms the theory presented and discussed earlier that the wall coating is composed of layers of positively and negatively charged particles. For all Faraday cups, when using the PE film, the q/m of the Loosely Bound particles were equal to or more positive than the experiments performed without the CPS. This would either mean that the particles were not charging as negatively, there were more positively charged particles present within cups FC2 to FC4, or a combination of both. Since there was an overall increase in the charge for the cups then it is likely that a combination of both mechanism described above occurred but dominated by more positively charged particles presence. If there was less overall charging, then the q/m of FC3 and FC4 would have decreased as well. This would agree with the PE film being charged negatively from contact with the PE particles which

would attract more positively charged particles. The d_P50_N of the particles showed that when the PE film was used, the particles were consistently larger than when the carbon steel column was used which may be attributed to the positive particles present in the layer.

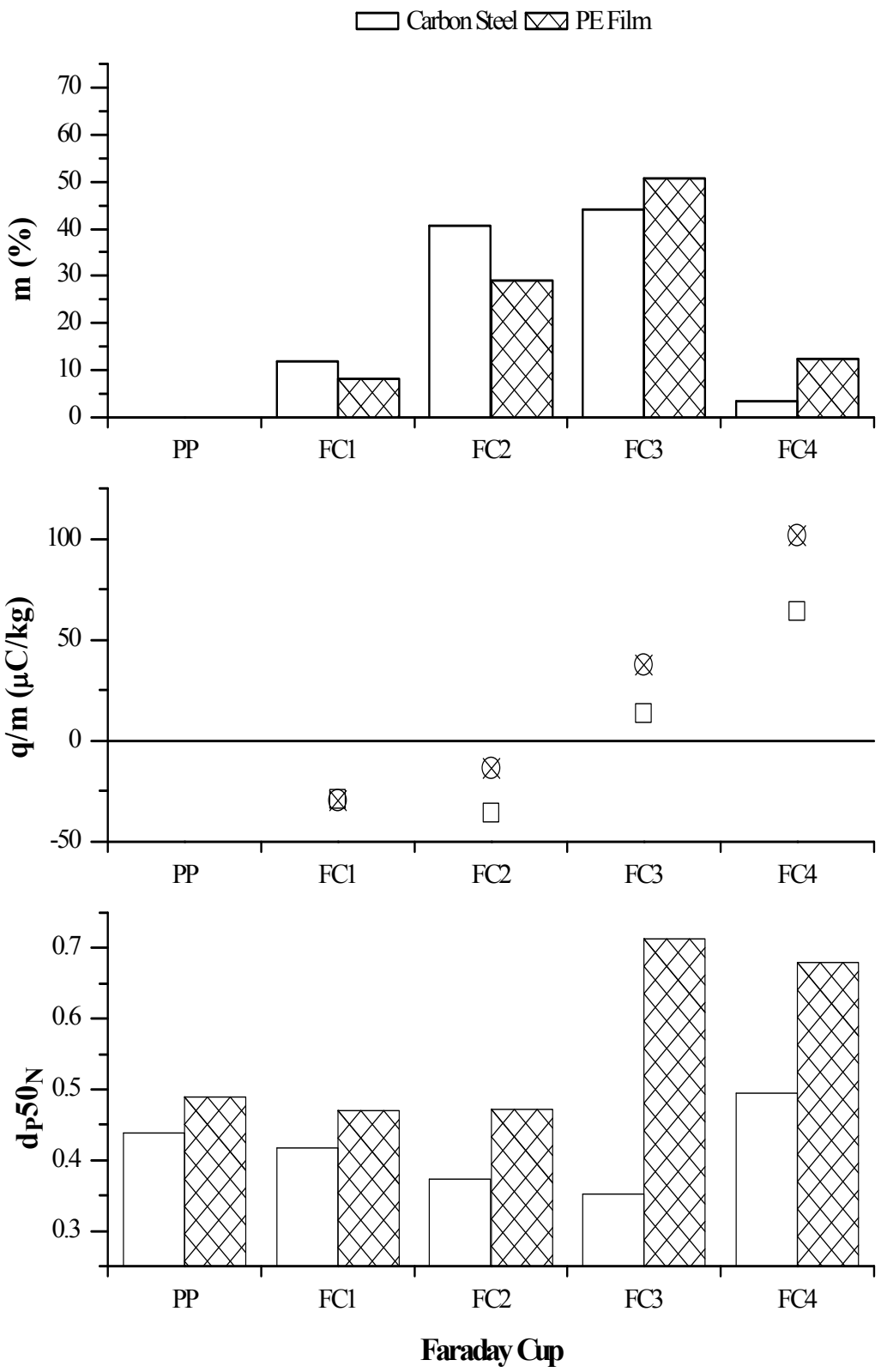


Figure 7.11: The m%, q/m, and d_P50_N results for the Loosely Bound particles using the CPS with the carbon steel and PE Film materials.

7.3. Summary

The projected influence of introducing the PE Film was to reduce the amount of bed electrification and subsequently the amount of particle wall fouling. It was hypothesized that since the particles and column wall were made out of the same material, then the triboelectrification would be reduced. Even though the q/m of the wall particles was reduced when the PE Film was used, the mass of the Wall particles remained consistent. A reduction in the q/m could be caused either from a decrease in particles charge, an increase in particles mass, or a combination of both. It was likely that the presence of positively and negatively charged particles in the Wall layer led to the decrease in the net charge. The positively charged particles were attracted to the column wall because the PE film was negatively charged by particles contacts. Local charging of the PE Film due to the inability of the film to distribute the charge equally throughout the column led to regions with large charge densities. This would in turn reduce the amount of charge required to bind particles to the fluidization column wall. Observations of the wall fouling on the PE films showed that the particles had a tendency to adhere to the column wall close to the fixed bed height.

Using the Charged Particle Separator, a charge distribution analysis was performed on the wall particles with the carbon steel and PE Film. With each scenario, bi-polar charging was present signifying that a wall layering effect of oppositely charged particles was present within the wall coating. The q/m of each of the Faraday cups for the trial performed with the PE Film was equal to or more positively charged than carbon steel q/m. This suggested the presence of more positively charged particles in the Loosely Bound region, which was likely caused by the PE Film charging negatively. With the PE Film charged negatively, the positively charged Fines that were normally elutriated from the bed were trapped within the bed and on the column wall and the negatively charged Fines were elutriated from the bed instead. This resulted in a difference in the particle size of the Fines. With the PE film charging negatively, the Dropped particles were predominantly charged positively, and the opposite effect was observed with the carbon steel column.

Chapter 8.
EFFECT OF SOLID ADDITIVE INJECTION

In gas-solid fluidized bed polymerization reactors more than one type of solid material is present within the system at any given time. Catalyst particles are continuously injected into the reactor while the polyethylene resin is formed through the polymerization reaction. Catalyst particles are fine powders as small as 1 to 5 μm and are recirculated through the reactor for multiple passes until completely consumed by the reaction. In addition to the electrostatic charging of the polyethylene resin, the catalyst particles also become electrostatically charged through contacts with the reactor wall and the polyethylene particles, as well as charging through their pneumatic transport while being recirculated within the system. Therefore, it is extremely essential to investigate the influence of the catalyst on reactor wall fouling formation and polyethylene particles charging within the fluidized bed reactor. Besides the presence of fine catalyst within the polymerization reactors, in some industrial cases, prostatic agents (which are fine powders with specific surface chemistry) are also injected into the reactor as a method of preventing or reducing electrostatic charges within the bed and any occurrences of sheeting.

Table 8.1 summarizes previous academic and industrial works that have focused on the introduction of different solid additives into gas-solid fluidized beds in an attempt to decrease bed electrification. However, no study was found in the open literature examining the influence of the catalyst itself on the magnitude of bed electrification and reactor wall coating. With the addition of prostatic agents, generally only a small amount of additive is introduced into the reactor. As stated by Hagerty et al. (2011) no more than 250 ppm of additive by weight of polymer produced may be required to contribute to a significant variation in the amount of bed electrification. The additives examined in the past are compounds that act as prostatic agents by introducing either positive charges (e.g., MgO, ZnO, Al_2O_3, and CuO) or negative charges (e.g., V_2O_5, SiO_2, TiO_2, and Fe_2O_3) when added to the fluidized bed of a known charge density (Song et al., 1995). The majority of the previous work has focused on measuring the bed electrification, and did not investigate the impact of the additives on level of reactor wall fouling, with the

exception of the industrial works by Song et al. (1995) and Hagerty et al. (2005, 2011) which claimed that these additives were effective at reducing the amount of wall sheeting incidences.

Having developed an online Faraday cup measurement technique in this research that is able to provide information on the particles charge distribution within the fluidized bed and most importantly the degree of reactor wall fouling, it was therefore very useful to apply this technique and to study the influence of some solid additives. Additives used in this work included two types of prostatic agents provided by industrial collaborators, a metallocene catalyst used to produced one type of PE resin used in this work, and silica which was the metallocene catalyst support.

Table 8.1: Summary of previous studies performed on the effect of addition of solid additives on electrostatic charge generation in gas-solid fluidized beds.

Authors	Year	Measurement Technique	Column Material	Particle Type	Additives	Additive Effect
Wolny and Opalinski	1983	Faraday Cup	Perspex	Polystyrene Particles	Active Coal Titanium Dioxide Pigment-A extract	All decreased the charge measured.
Wolny and Kazmierczak	1989	Capacitance Probe	Not known	Polystyrene Particles	Aluminum powder Sodium Chloride	Decreased the charge measured.
Guardiola et al.	1992	Electrostatic Probe	Perspex	Glass Beads	Steel particles	Decreased the bed potential.
Song et al.	1995	Voltage Probe	Not known	Polyethylene	MgO, ZnO, Al_2O_3, CuO, V_2O_5, SiO_2, TiO_2, Fe_2O_3, and carbon black	MgO, ZnO, Al_2O_3, and CuO increased positive charges. V_2O_5, SiO_2, TiO_2, and Fe_2O_3 increased negative charges. Carbon black decreased charges.
Yao et al.	2002	Electrostatic probe	Plexiglas	Polyethylene	Larostat 519 powder	Reduced voltage.
Hagerty et al.	2005	Electrostatic Probes	Not known	Polyethylene	Aluminum Stearate Aluminum Oleate Ethoxylated Amine Alkoxylated Amines Carboxylic Acid Polysulfones Polymeric Polyamines Sulfonic Acid	Claimed a reduction in charges.
Wang et al.	2009	Electrostatic Probes	Not known	LLDPE	Al_2O_3, ZnO, Fe_2O_3, TiO_2, MgO	Al_2O_3 was the most effective in bed potential reduction.

Table 8.1: Summary of previous studies performed on the effect of addition of solid additives on electrostatic charge generation in gas-solid fluidized beds. (continued)

Authors	Year	Measurement Technique	Column Material	Particle Type	Additives	Additive Effect
Yu et al.	2010	Electrostatic probe	Plexiglas	LLDPE	Fine LLDPE particles	Increased up to a maximum.
Moughrabiah et al.	2012	Electrostatic probes	Stainless Steel	Glass Beads	Larostat 519	Reduced charge below 1.5 wt% and increased it above that.

8.1. Experimental Conditions and Methodology

The operating conditions for the experiments performed for the effect of solid additive injection is shown in Table 8.2. The fluidizing particles were PE_A and PE_C, where PE_A was fluidized at 1.5 and 4 u_{mf} and PE_C was only fluidized at 1.5 u_{mf}. Fluidization was conducted for a period of 60 minutes with Additives A, B, C, and F. Additives A and B were known to be prostatic agents used in industrial reactors, and Additives F and C were a deactivated metallocene catalyst and the catalyst support, respectively. Due to experimental and safety limitations handling activated catalysts, a deactivated catalyst was used.

Table 8.2: The experimental conditions used for the experiments on the effect of solid additive injection.

Parameter	Value
Fluidizing Particles	
Type	PE_A, PE_C
Size Range	10-1500 μm
Fluidizing Gas	
Velocity	1.5 u_{mf} (Bubbling) 4 u_{mf} (Slugging)
Time	60 min
Temperature	22 °C
Relative Humidity	0 %
Fluidization Column	
Material	Carbon Steel
Additive	
Type	A B C F
Quantity	0.1 m% the total PE present

To be able to understand the complicated charging phenomena existing within a gas-solid fluidized bed reactor consisting of a multi-component particle mixture, a comprehensive study was necessary which was achieved by the following experiments.

1. The first step was to determine a pseudo-triboelectric series for all materials involved (i.e., the four additives used, polyethylene resin, and the carbon steel column wall). Such exercise enabled predicting and better understanding of the

charging mechanisms involved as these different materials came into contact with each other inside the fluidized bed.

2. Next, fluidization experiments were performed with each of the additives along with PE_A and PE_C resin at 1.5 u_{mf}. Two types of PE resins were used to allow determining whether there was a difference in effectiveness of the prostatic agents, and the influence of the catalyst and its support with different polyethylene particles.
3. Finally in order to identify the dominating mechanisms underlying the effectiveness of the prostatic agents in reducing reactor wall fouling, the effects of Additive B were investigated in more detail.
    a. Additional trials were performed where the additive was injected into the fluidization column prior to the presence of any PE particles in order to coat the column wall. This was performed to determine whether the additive was the most effective at reducing electrostatic charges and particle wall fouling due to its presence on the column wall or by coating the PE particles.
    b. In addition, trials were conducted with Additive B injected multiple times into the fluidized bed during fluidization period to simulate continuous additive injections. This type of experiment helped in determining whether it was necessary for the additive to be replenished to maintain a reduced amount of column wall fouling.
    c. Finally, a tertiary mixture of PE_C resin, and Additives B (prostatic agent) and F (deactivated catalyst) were examined to more closely simulate industrial polyethylene reactors, and also determine whether the prostatic agent has similar effectiveness in the presence of catalyst.

8.2. Results and Discussion

The results are presented here in the order of the experiments performed as described above.

8.2.1. Additive Charging

In order to better understand the charging effects and mechanisms involved as the additives passed through the injector prior to entering the fluidization column and coming into contact with the carbon steel fluidization column wall, different charging experiments were performed. Each experiment was repeated at least two times. The experiments included:

Initial: The initial charge of the sample of additives measured by dropping the sample directly into a bench-scale Faraday cup.

CS Plate: The charge of the sample of additives measured after being dropped onto an angled carbon steel plate and falling into a bench-scale Faraday cup similar to those described in Chapter 4.

Dry CS Plate: The same procedure as the CS Plate was followed; however, the additives were dried prior to the experiment to eliminate any moisture effects.

Injection: The injector unit was removed from the fluidization column and was loaded with the additive sample. The sample was then injected into a bench-scale Faraday cup (Figure 8.2). The injection was conducted with the same gas and at the same flow rate as the usual fluidized bed injections. This resulted in the measurement of the net q/m of each additive sample as it would go through the injector and entering the fluidization column.

Dry Injection: The same procedure as the Injection experiment was followed; however, additive samples where dried prior to the experiment.

Empty Column: Non-dried additives were injected into the empty fluidization column through the injector (i.e., no PE resin present). The filter bag and the top Faraday cup were mounted as per typical fluidization experiment to determine the mass and the cumulative charge of the additives as they were being entrained. The fluidizing gas was turned on prior to the injection to ensure no additive could drop down through the distributor plate and into the inlet gas line. The gas velocity was varied for different tests from 0.67 u_{mf} to 2.0 u_{mf} of

the PE_C resin. Upon the complete injection of the additive, the gas velocity was held constant for a few minutes and then turned off.

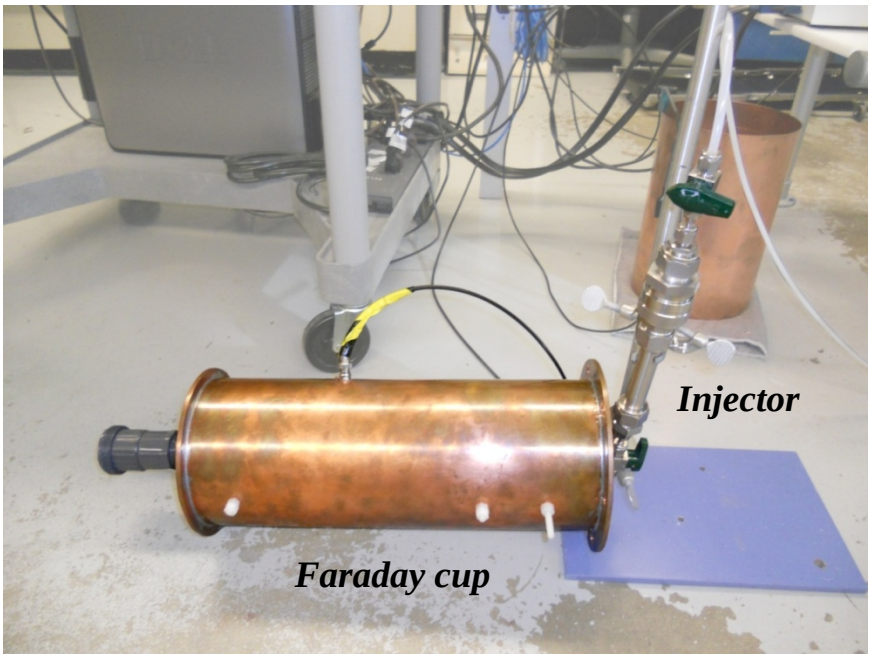


Figure 8.1: The Faraday cup set up used to measure the charge of additives passing through the injector unit.

For the dried testes, Additives B, C and F were dried in an atmospheric oven at 80 °C for 5 hours prior to the experiment. Additive A was dried in a vacuum oven at 40 °C for 3 hours since it had a low melting temperature; however, even at these settings some of the additive started to soften and melt and therefore not all of the charging experiments could be performed with this additive. The results of experiments conducted with additives are tabulated in Table 8.3 and shown graphically in Figure 8.2.

Table 8.3: The charging behavior of all additives found through experiments with carbon steel plate, stainless steel injector and empty fluidization column.

Test	Additives q/m (μC/kg)			
	A	B	C	F
Initial	-0.146 ± 0.05	0.51 ± 0.05	-11.55 ± 1.53	-0.51 ± 0.12
CS Plate	0.79 ± 0.28	0.39 ± 0.18	-8.03 ± 4.31	-8.88 ± 1.70
Dry CS Plate	0.69 ± 0.40	0.73 ± 0.03	-7.73 ± 0.72	-3.75 ± 0.71
Dry Injection	-	-122.13 ± 28.5	-249.20 ± 58.62	-110.20 ± 39.06
Injection	-35.51 ± 12.56	-40.80 ± 5.98	-186.50 ± 59.30	-83.54 ± 33.13
Empty Column	-235.72 ± 103.1	-30.78 ± 7.69	-47.36 ± 26.57	9.65 ± 1.93

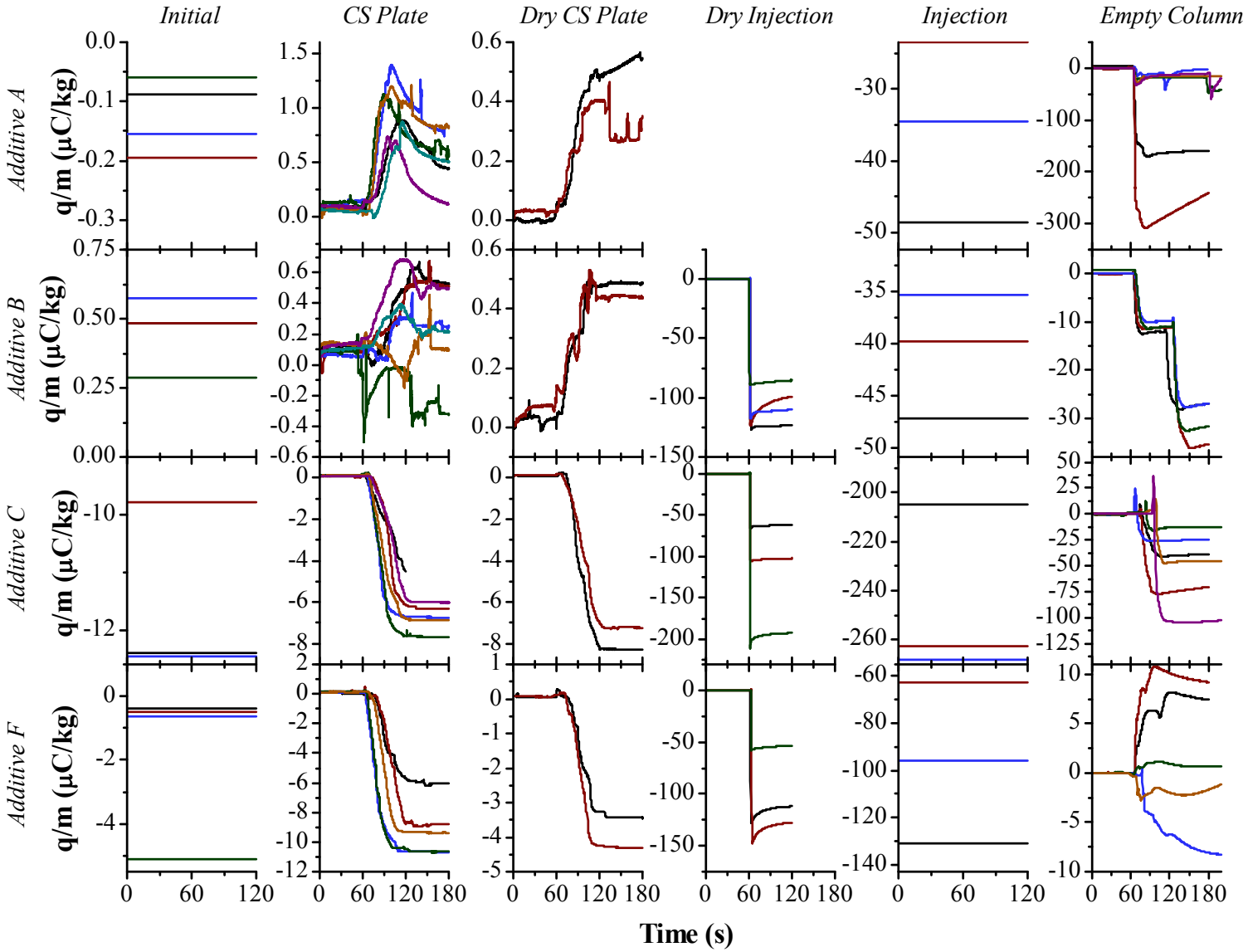


Figure 8.2: Charging behaviour of Additives A, B, C and F in contact with a carbon steel plate, passing through a stainless steel injector, and injected into an empty fluidization column.

Additives A, C, and F were initially negatively charged whereas Additive B was positively charged. The magnitude of the initial net q/m for all of the additives was relatively small in comparison to the other charging tests signifying some degree of charge generation with all the tests conducted.

When in contact with the CS plate, Additives A and B became positively charged whereas Additives F and C became negatively charged. When Additives A and B were not dried their net q/m was low and showed some bi-polar behaviour. However, with the dried samples, these additives showed more consistent positive charging. Therefore, this suggests that humidity was potentially playing a role in the dissipation of charges for tests performed with Additives A and B. With Additives C and F, there was no apparent difference between dried and non-dried samples charging. Additive C was hydrophilic and therefore it would absorb moisture very quickly. Since the actual tests were performed under ambient conditions, it is likely that Additive C absorbed moisture from surroundings after being removed from the dryer. This was likely the same case with Additive F since it is 90% composed of Additive C.

With the injector, all additives charged negatively and to significantly large magnitudes when subjected to a large particle velocity through a narrow tube (6.35 mm diameter). More charging seemed to have occurred when Additive B was dried prior to injection, which was similar to the CS Plate results. When Additive C and F were injected, there was no large difference in the q/m between dried and non-dried samples. The injection test with dried Additive A could not be performed due to issues of properly drying this additive as described previously.

With the Empty Column experiments approximately 20 m% (0.20 g) of total additive injected for all additives was entrained from the system when the gas velocity was 0.67 u_{mf}. This indicates that 80 m% was remained inside the fluidized bed, potentially deposited on the inner column wall and the distributor plate. The polarity of all additives collected at the top of the column was found to be negative with the exception of Additive F, which either charged positively or negatively. To determine whether a certain particle size range of each additive was being elutriated from the bed, more Empty Column tests were performed with all Additives where samples were taken from particles collected in the top filter bag and on the distributor plate for

PSD analysis. Results are presented in Figure 8.3 which clearly showed a biomodal distribution with Additive A but not with other additives. There was a difference in the charge between the additive passing through the injector and the additive being trapped in the top Faraday cup for the Empty Column experiments. Additive A became more negatively charged, the charge of Additive B remained relatively the same, while both Additives C and F became less negatively charged. The difference in charge measured came from the contact of some of the additive with the column wall, as well as a segregation of particles between those that were elutriated from the system and those that remained behind.

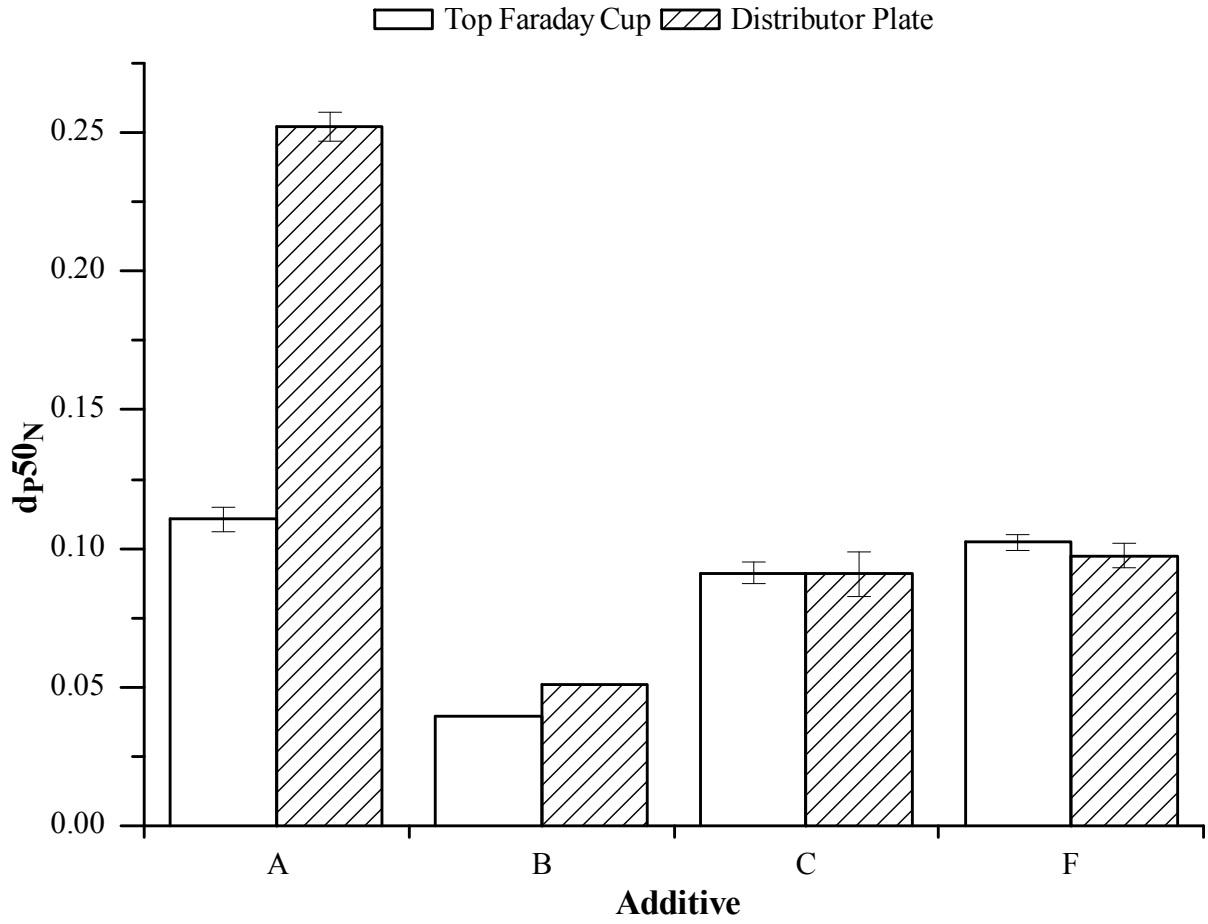


Figure 8.3: The d_P50_N of additives A, B, C and F found in the Top Faraday cup and on the distributor plate for the Empty Column experiment at 0.67 u_{mf}.

From Figure 8.2, it can be seen that Additive C appears to be bi-polarly charged as well. Therefore, it was suspected that all the additives could have been bi-polarly charged. This hypothesis was further investigated by using the Charged Particle Separator apparatus to determine the charge distribution of the additives prior to any testing. The voltage of the power

supply had to be varied per additive in order to achieve a suitable separation. When the voltage was too low, not much separation was achieved, and when the voltage was too high most of the negatively charged particles would stick to the positively charged plate and thus it was not possible to measure their charge. Regardless, as can be seen in Figure 8.4, Additive C and F, showed a clear bi-polar distribution whereas Additive A and B results were not as distinct. The d_P50_N of additives collected in each Faraday cup of the CPS apparatus is given in Table 8.4. In some cases there were not enough particles to perform a PSD, particularly in FC4. From the median diameter and the PSD results, it is difficult to see a definitive relationship between the particles size and their charge polarity; however, Additive F seemed to be decreasing in size from FC1 to FC4. The opposite is seen for Additives A, B and C where relatively smaller particles (those attached to the positive plate) were negatively charged.

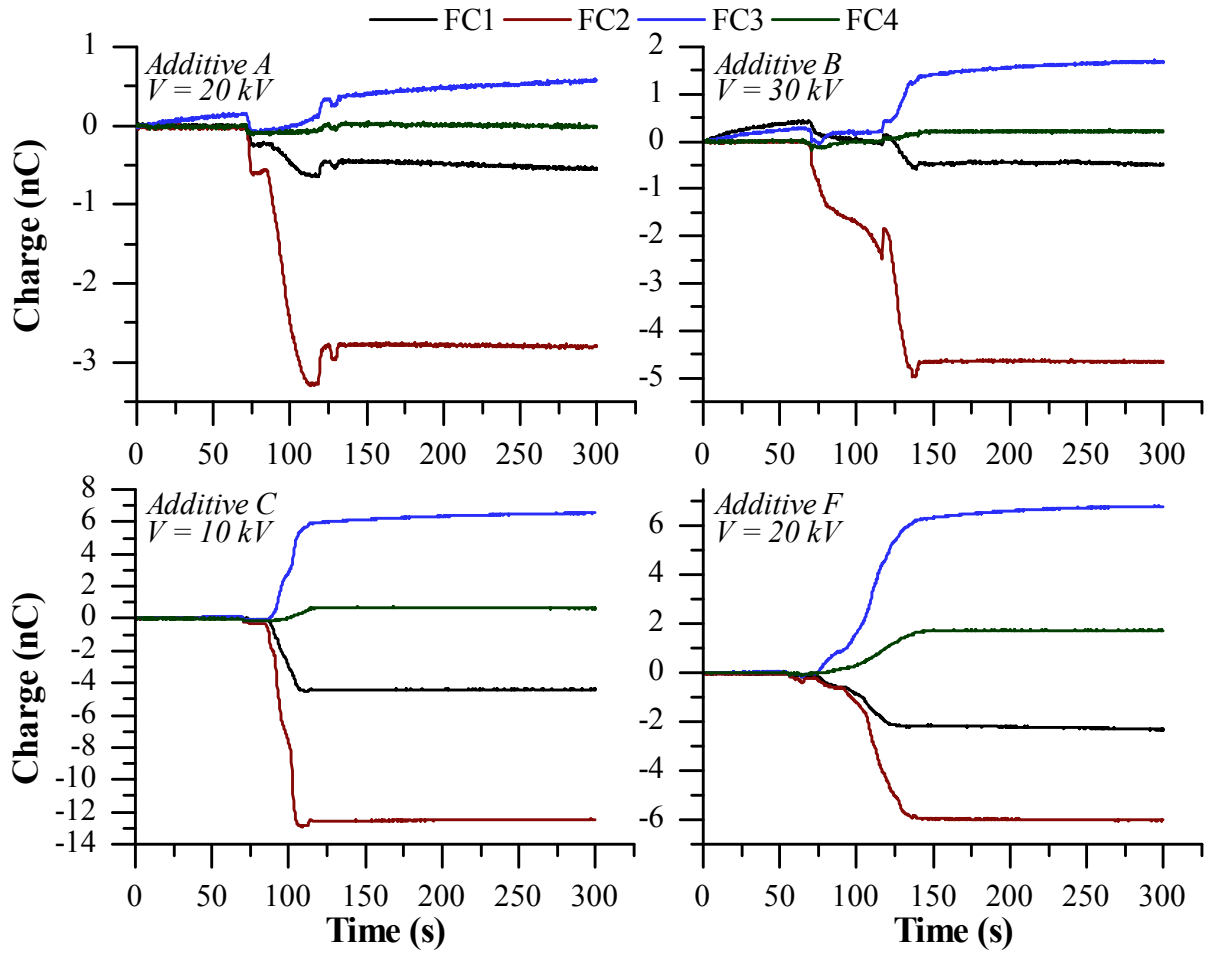


Figure 8.4: Typical charge distribution of Additives A, B, C, and F determined by the Particle Charge Separator at different applied voltage (V).

Table 8.4: The d_P50_N of samples taken from the CPS Faraday cups.

Additive	Positive Plate	FC1	FC2	FC3	FC4
A	0.088	0.211	0.254	0.188	-
B	0.040	0.050	0.042	0.054	-
C	0.087	0.112	0.099	0.093	-
F	0.105	0.102	0.095	0.092	0.087

In order to further confirm the bi-polar charging effects with smaller and larger additive particles, more experiments were performed. The gas velocity was increased to 1.5 and 2.0 u_{mf} in an attempt to entrain more fractions of the larger additive particles left behind inside the bed. If the above discussion and results on bi-polar charging was fully accurate, it was projected that by entraining more lager particles, the cumulative charge of these particles would become less

positively charged for Additive F and less negatively charged for Additives A, B and C. Only one trial could be performed with Additive B due to limited amount of this additive available at the time of testing. This test was run at 1.5 u_{mf} to represent a normal fluidization experiment. For each experiment, samples were taken from the top Faraday cup and the distributor plate for PSD analysis. As can be seen from results presented in Figure 8.5, Additive A was bi-polarly charged since as the gas velocity was increased more positively charged particles were entrained resulting in a net charge close to zero. The PSD analysis of this additive (Figure 8.6) showed a distinct distribution with the larger particles found on the distributor plate and smaller particles in the top Faraday cup. With Additive B, the net specific charge was predominantly negative as the gas velocity was increased. The PSD at the top and bottom of the column for this additive did not show any distinct difference meaning that Additive B was relatively uniformly sized, similar to that found in Table 8.4. The PSDs of Additives C and F showed only a slight difference in the size of particles found at the bottom of the column and those at the top. With Additive C, at all gas flow rates, the net specific charge remained predominantly negative; however, there were also some positive particles present at the beginning of the injection. With Additive F, as the gas velocities increased (1.5 and 2.0 u_{mf}) the additive became predominantly negative which agrees well with hypothesis that this additive was bi-polarly charged. The first time the experiment was performed there were only two trials which were both predominantly positive. The second time the experiment was performed, one trial was predominantly positive while the other two were predominantly negative. This suggests that it is likely that Additive F at the lower velocity could be either positively or negatively charged. During the normal experiment at 1.5 u_{mf}, the polarity of Additive F would be predominantly negative which agrees well with the CS Plate tests described above.

From results shown in Figure 8.2 it can also be seen that for all cases using the injector the additives became more negatively charged. Therefore, at the beginning of any normal fluidization experiments, all of the additives are negatively charged as they enter the fluidization column and fluidize along with the PE resin. Since the plate tests had shown that Additives A and B became positively charged whereas Additives C and F became negatively charged, then during fluidization similar charging would occur as these additives come into contact with the carbon-steel column wall.

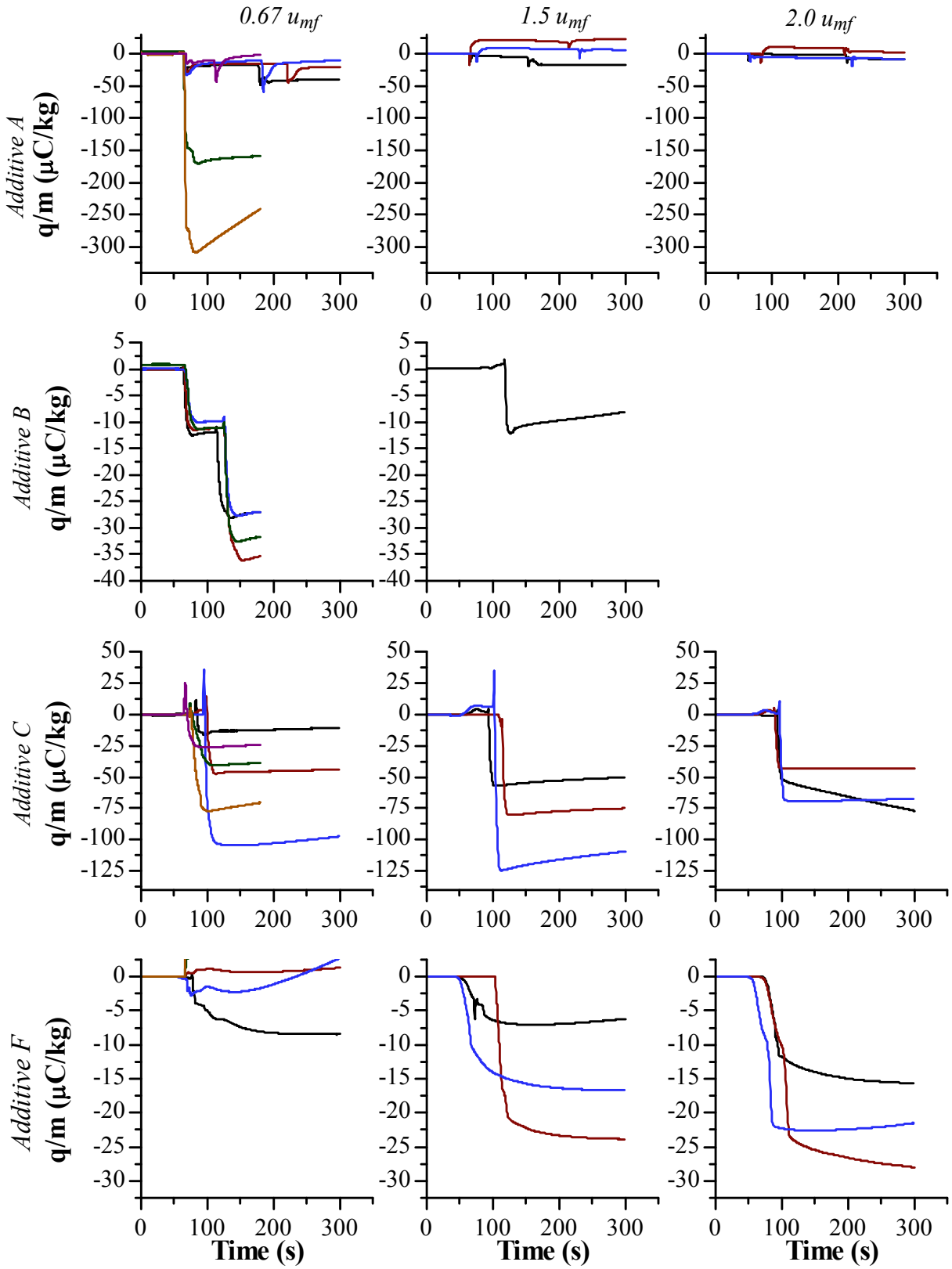


Figure 8.5: Empty column experiments performed with Additive A, B, C, and F at different gas velocities.

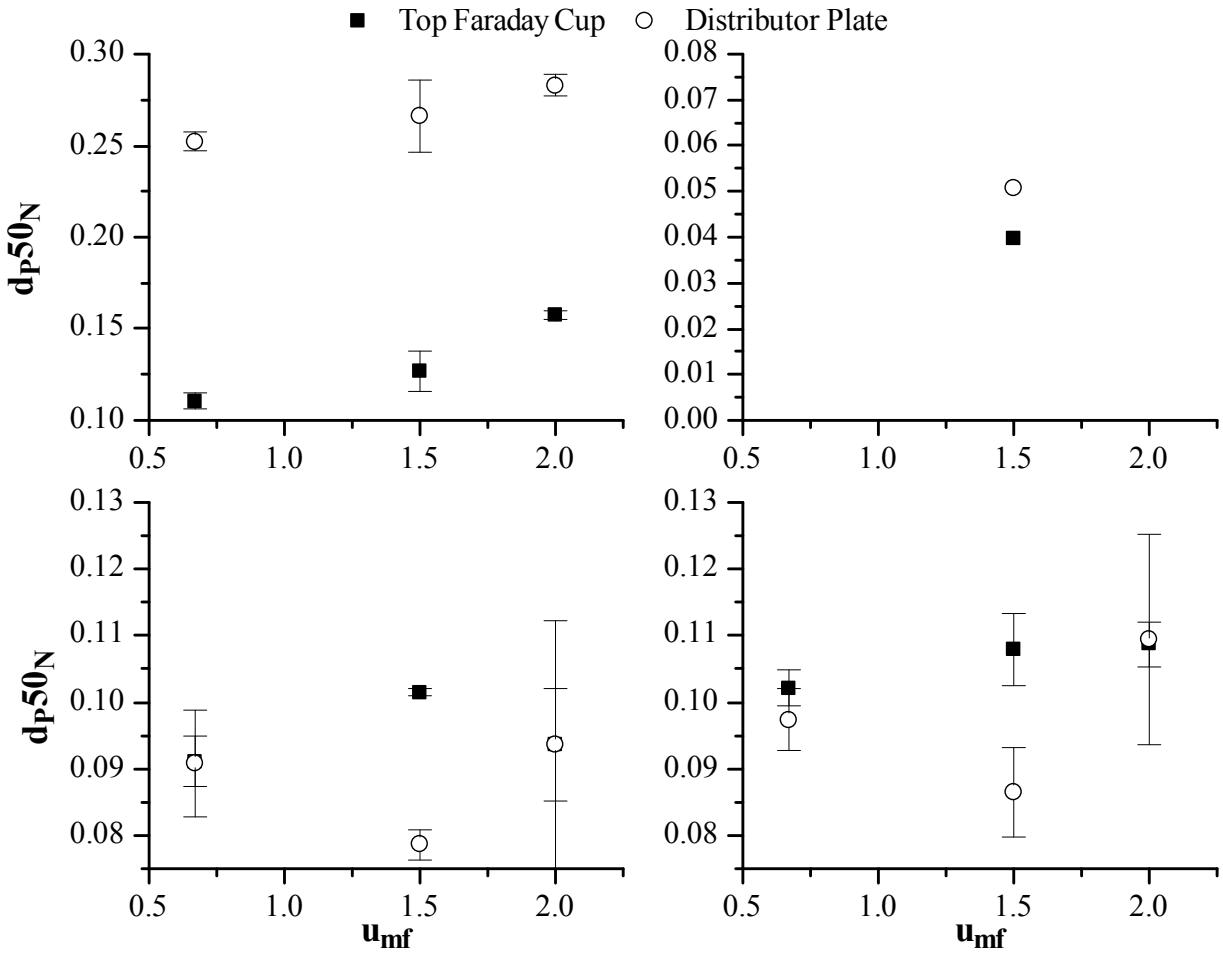


Figure 8.6: The d_P50_N of additives A, B, C and F found in the Top Faraday cup and on the distributor plate for the Empty Column experiments at different fluidizing gas velocities.

8.2.1.1. Pseudo-Triboelectric Series

A pseudo-triboelectric series (Table 8.5) was created based on the CS Plate experiment and also compared with the work function of some of the materials found in literature. The work functions of the polyethylene, Additive C, and carbon steel were estimated from a list of work functions found by Masuda et al. (2006). Since the work functions found in literature were estimations for ideal cases and also the exact composition of Additives A, B, and F were unknown, the bench-scale CS Plate test results were found to be more accurately representing the current system.

Table 8.5: Pseudo-triboelectric series for all materials in the fluidized bed.

	Material	Work Function eV
+ Positive	Additive A	-
	Additive B	-
↓	Carbon Steel	4.5
	Additive F	-
	Additive C	5
	Small Polyethylene Particles	
- Negative	Large Polyethylene Particles	5.3

8.2.1.2. Proposed Charge Generation Mechanism

Based on Table 8.5 the interactions between all objects within the fluidized bed tested in this work can be characterized as presented in Table 8.6 and Figure 8.7.

Table 8.6: Predicted surface polarity due to triboelectrification between different surfaces coming into contact inside the fluidized bed. The left value corresponds to the column on the left and the right value corresponds to the row on the top.

	Large PE	Small PE	Additive A	Additive B	Additive C	Additive F	CS Wall
Large PE		-\+	-\+	-\+	-\+	-\+	-\+
Small PE	+\-		-\+	-\+	-\+	-\+	-\+
Additive A	+\-	+\-					+\-
Additive B	+\-	+\-					+\-
Additive C	+\-	+\-					-\+
Additive F	+\-	+\-					-\+
CS Wall	+\-	+\-	-\+	-\+	+\-	+\-	

Using Table 8.5, all additives except C and F would obtain a similar charge polarity by coming into contact with the polyethylene particles or the column wall. Between any two solids in contact, the solid with the lower work function would most likely become positively charged.

As discussed in Chapter 4 the polyethylene particles displayed bi-polar charges, and therefore would behave differently for both polarities. Therefore, as they come into contact with any additive particles, provided that the electrostatic forces are not strong enough to bind the particles and additive together, two scenarios can occur:

1. **Additive - fine polyethylene particle contact:** Since the smaller polyethylene particles, as will be seen in the following sections are predominantly positively charged (while fluidized in the absence of any additive) they would become less positively charged when additives present, whereas any additive particle would become less negatively charged.
2. **Additive - large polyethylene particle contact:** Since the larger polyethylene particles, as will be seen in the following sections, are predominantly negatively charged through fluidization, they would become more negatively charged when contacting the additives, whereas any additive particle would become less negatively charged.

It was expected that if either the polyethylene or Additive C or F come into contact with the conductive column wall, they would become more negatively, and the wall becomes positively charged (Figure 8.7). When either Additive A or B comes into contact with the wall, the additive would transfer some of its electrons to the wall effectively becoming more positively charged and the wall more negatively charged.

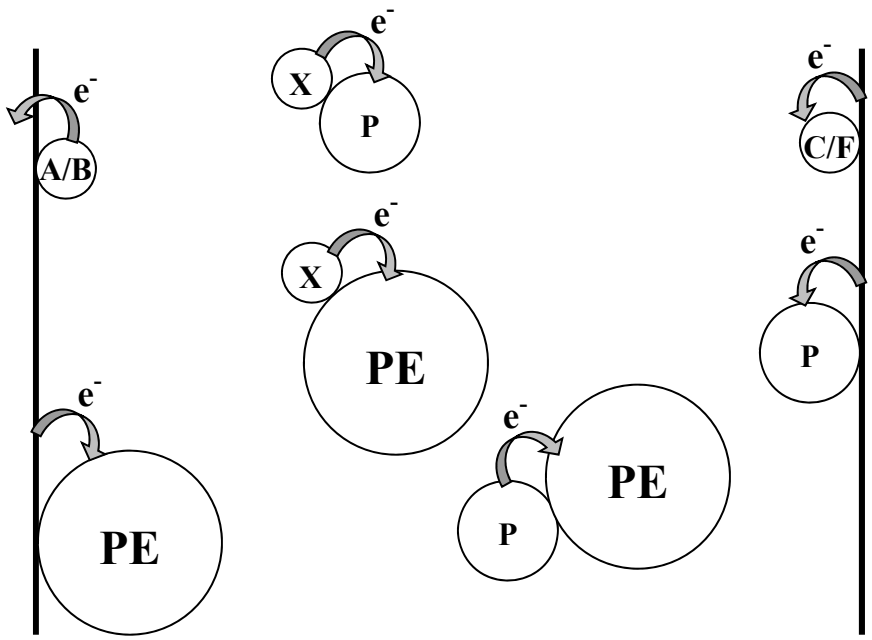


Figure 8.7: Proposed charging mechanisms found inside the fluidized bed between the polyethylene particles (PE), all additive particles (X), and the column wall.

The surface morphology of the particle can also play a role in the magnitude of charging. If the surface of the particles, additives or carbon steel column is rough, then there would be more

contact area between the particles and other particles, additives, or the column wall. More contact area would result in more opportunity for charge to be transferred between the two objects. Thus, more charging would occur with an increase in surface roughness.

8.2.1.3. Proposed Charge Dissipation Mechanisms

Charge dissipation is an important factor that can sometimes be forgotten in many processes. It is believed that the presence of moisture in this system, as well as conductive elements would help increase the rate of charge dissipation from the particles to the fluidization column. Both water molecules and the conductive elements would help increase the overall surface conductivity of the particles which could lead to charge dissipation. However, it is important to note that the fluidized bed used in this study was electrically isolated for all experiments and therefore any charge dissipation would have only occurred from the particles or additive to the column wall. The total net charge of the entire fluidization system should remain constant throughout the entire fluidization process.

In this work, the fluidizing gas used in all trials was dry air (0% RH) and therefore any moisture present in the system would have been from particle handling prior to fluidization. Since polyethylene is a non-polar molecule it is considered to be hydrophobic and therefore would not adsorb a significant amount of moisture. The additives; however, have some constituent groups that could undergo hydrogen bounding and adsorb some water from the ambient air. As stated previously, it is believed that all of the additives were to some magnitude hydrophilic in nature. Additives A and B, displayed a large amount of agglomeration during preparation which was likely caused by cohesive forces and the presence of moisture. The presence of a metal element could act as a path to transfer and distribute electrons on a surface and effectively reduce some of the charge present on the particle. Additives B and F were the only additives that contained a metallic element. Additive B had an aluminum atom per molecule present; however, the composition of Additive F was not known due to confidentiality reasons.

Looking at the functional groups of Additive A in Table 3.4, they consist of tertiary amine and hydroxyl groups. Amines have been used in many antistatic agents in the past due to their conductive properties. Primary amines are effective antistatic agents, whereas secondary amines are not. However, with tertiary amines it depends on the presence of hydroxyl alkyl groups

where having two hydroxyl groups has been shown to be an efficient antistatic agents (Chanda and Roy, 2006). This agrees well with the chemistry of Additive A used in this work. Also, the presence of OH groups makes the agent less dependent on humidity due the formation of a chain from hydrogen bonding. This type of hydrogen bonding from OH as well as NH_2 (which is not present with prostatic agents tested in this work), can display antistatic behaviour at low humidities which is not present with compounds that only form intramolecular hydrogen bonding (Chanda and Roy, 2006). With Additive B, the functional groups consisted of aluminum atom, OH group, and double bonded O from ester groups. The aluminum atom could help contribute to the surface conductivity of the compound since aluminum itself is conductive. The OH group likely has the same antistatic properties through the hydrogen bonding similar to Additive A. Overall, it is likely that Additive B has a high conductivity thus helping in the dissipation of charge in the system. Even with these antistatic properties, Additives A and B behaved more as prostatic agents for the system studied.

Conductivity is likely not the only property that dictates the efficiency of antistatic agents. Wu and Bi (2011) found that aluminum particles used in their bench-scale charging experiments did not necessarily have a large effect on charge reduction. Oguchi and Tamatani (1993) found a correlation between the amount of alumina present and the amount of charging found in their system. It was found that as the quantity of alumina within the particle used was increased, the amount of charge generated increased positively. This agrees well with the CS plate charging tests in this work shown in Figure 8.2 where Additive B, containing an aluminum atom, became more positively charged.

Oguchi and Tamatani (1993) also found that an increase in the amount of Si present in particles subjected to contact charging experiments created more negative charge, which also agrees well with Additive C and F charging behaviour shown in Figure 8.2. The large negative charge could be seen as a negative driver in the system. Since the majority of the polyethylene particles were negatively charged, the addition of Additive C or F could ultimately be the cause for more wall fouling since it does not decrease the net charge of the particles in the system but rather increasing it. This could mean that the presence of these additives could repel more polyethylene particles towards the column wall and therefore increase the amount of wall fouling.

Based on the above discussion it was assumed that the rate of charge dissipation in descending order is as follows: Additive B, Additive A, Additive F, and Additive C.

8.2.1.4. Proposed Additive Coating and Mechanism

During the empty column injection experiments images were taken from different regions of the inside of the fluidization column to estimate the amount of coating that the additives produced inside the fluidized bed. Pictures were taken of the electrostatic probe, the distributor plate, and the top of the column as shown in Figure 8.8.

All additives showed some degree of coating with Additive B exhibiting the largest amount throughout the entire fluidized bed. With all Additives there was a layer of coating present along the column wall. Additive B being the smallest additive studied and due to its surface chemistry had a waxy nature which made it smearing on surfaces resulting in significant coating on different surfaces within the bed. In all cases, there was still a significant amount of additive present on the distributor plate that was not elutriated from the system. No pictures from the most recent empty column experiments are shown in Figure 8.8, but coating was still observed at all gas flow rates.

In addition, Additives A and B were likely to be able to coat more of the polyethylene particles and the column wall due to their small particle size and high surface area which would then reduce the amount of polyethylene-polyethylene and polyethylene-carbon steel column wall contacts but increasing the amount of additive-additive contacts. Although the additives cannot completely cover the surface of all of fluidizing polyethylene particles or the column wall, it is believed that a small amount would be sufficient. In this work some coating was observed with Additive A, and more so with Additive B (Figure 8.8). Similarly, since Additives A and B were shown to provide higher conductivities from their functional groups, any additive/additive contact would likely results in a minimal amount of charge transfer and/or charge dissipation effectively reducing the amount of net charge in the system and the amount of reactor wall fouling.



Figure 8.8: Images of additive coating in different areas of the gas-solid fluidized bed upon the completion of the Empty Column experiments.

It has long been believed that one of the major mechanisms behind electrostatic charge reduction in a gas-solid fluidized bed comes from the addition of fine additive particles to coat the fluidizing particles (polyethylene in this case) and also the column wall. The coating is known to

reduce the fluidizing particles contacting each other and the reactor wall. Using the specific surface area ($\hat{A}$) found by the Malvern Mastersizer 2000 and typical masses collected in an experimental trial, the total available surface area for each particle as well as the surface area for the fluidization column was calculated (Table 8.7).

It is clear that for the amount of total available surface for the additives, they cannot cover all of the polyethylene particles. It is definitely not possible for the additives to cover even a fraction of the Dropped particles; however the presence of even some of the additive on the PE particle may reduce the likelihood of PE-PE particle contact. It should also be noted that if theoretically all of the additive particles were to migrate to the column wall, there would still not be a sufficient amount of particles to coat the entire wall. Since the additive particles are partly spherical in nature, at best only half of the total available surface area for the additives would be able to coat the column wall. Since the additives need to only cover the area where the PE resin comes into contact with the column walls approximately the expanded bed height), the actual surface area that would be required to be coated is reduced. Using half of the total available surface area for any additive, Additives A, B and C could potentially coat the expanded bed section provided that the additives do not adhere to any of the bed particles. Additive C was calculated to have the largest $\hat{A}$ and therefore would cover the column wall the most. However, this is due to how the Malvern Mastersizer calculates the $\hat{A}$ which is based on the density and absorption index as discussed earlier. From the analysis it is believed that any additive can be present within any region of the fluidized bed; and will affect different regions depending on the amount of additive coating present.

Table 8.7: The particles specific surface area ($\hat{A}$), and total available surface area within each region of the fluidization system.

Region	$\hat{A}$ m^2/g	Particles Mass Per Experiment G	Total Available Surface Area m^2
Dropped Particles	0.0133	994.98	13.233
Loosely Bound Particles	0.0225	34.58	0.7781
Fines	0.147	0.02	0.0036
Additive A	0.379	1.06	0.4017
Additive B	0.363	1.06	0.3848
Additive C	0.439	1.06	0.4653
Additive F	0.179	1.06	0.1865
Carbon Steel	-	-	0.131*

*Calculated based on the inner diameter and the length of the fluidization column to the maximum measured expanded bed height.

8.2.2. Fluidization Experiments with PE_A and PE_C Resin

Both PE_A and PE_C resins were tested with all the additives at 1.5 times of their respective u_{mf} to determine whether each additive had a different effect no electrostatic charge generation and particle wall fouling for different resins. Experiments with PE_A was also performed in the slugging flow regime at 4 u_{mf}; however, not a significant effect on the bed electrification and particle wall fouling was observed due to the decreased residence time of the additives in the bed. More information on this flow rate is presented in Appendix D.

8.2.2.1. Mass

The particles mass distribution in different regions of the bed with and without additives with both resins is presented in Figure 8.9. No difference was observed between the magnitudes of Fines entrained with or without any additive with the PE_A resin; however, there was a large difference between trials with the PE_C resin. This was due to the low amount of fine particles present within the PE_C resin. Therefore, the majority of the Fines mass collected for experiments with this resin was likely from the additive particles.

With the PE_A resin, only Additive B showed a consistent decrease in the amount of particle wall fouling in the system. Additive A had more Wall particles; however, the majority of these particles were Loosely Bound, meaning that Additive A likely aided in minimizing the adhesives

forces along the column wall. With Additives C and F, the amount of Wall particles increased particularly in the presence of Additive F. With Additive F there was a considerable amount of Tightly Bound particles, meaning that Additive F likely contributed to strong adhesive forces within the column wall. Additive C and F were both shown to be highly negatively charged when passing through the injector and entering the fluidization column as shown in Figure 8.2. This high negatively charged particles would be attracted to the column wall where the first layer of the particle fouling would be formed. This in turn would attract the positively charged particles and the coating layer would grow. This will be discussed in more detail below.

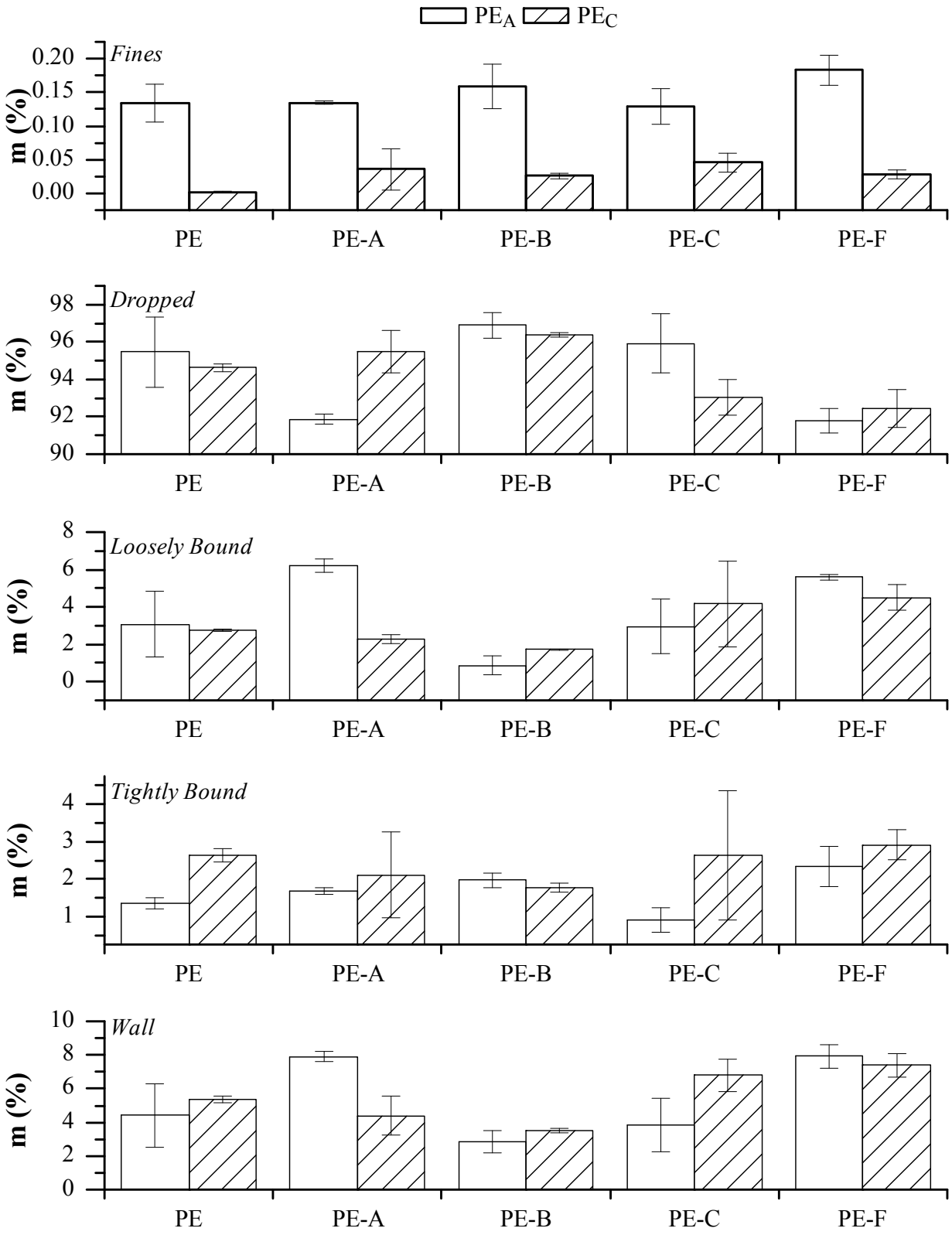


Figure 8.9: The m% of the Fines, Dropped, Loosely Bound, Tightly Bound, and Wall particles for experiments performed with and without additives with both PE_A and PE_C resin.

8.2.2.2. SEM Pictures

Numerous SEM pictures were taken of samples collected from the Fines, Dropped, Loosely Bound, and Tightly Bound regions for the PE_A resin in an attempt to determine whether the additives coated the PE resin. Figure 8.10 to Figure 8.13 show examples of SEM pictures taken. Some image analysis was performed to determine an equivalent particle diameter for particles that may looked to be an additive. The equivalent diameter was calculated by finding the area of a particle and equating it to the equation for the area of a circle. The normalized particle diameter is also presented on the figure.

In the backscatter images (pictures on the right) Additives A, C, and F, were mostly white which is caused by the presence of heavier atoms. The shade difference between the PE particles and Additive B was more difficult to distinguish.

It was difficult to detect the presence of Additive A within the Fines (Figure 8.10). In the Dropped, Loosely Bound, and Tightly Bound regions, there were some small white particles attached or embedded into the PE particles; however, the size of these particles appeared to be smaller than the pure Additive A particles shown in Table 3.4, therefore this was likely already part of the polyethylene particles, or some contaminant. This may also be additive attrition; however, some of these particles were also found in the Initial SEM pictures as well suggesting the possible presence of some contaminants.

It was also difficult to detect Additive B within the Fines sample (Figure 8.11). However, this additive was found to be coating some of the larger particles in the Dropped region, although not a substantial amount of them. In the Loosely Bound and Tightly Bound regions, there was also the possibility that some of the particles found were Additive B particles due to their irregular shape.

Additive C was present to some extent within all regions of the fluidized bed (Figure 8.12) but mostly within the Loosely Bound and Tightly Bound regions. The presence of only a single small particle of Additive C on the Dropped particle may also mean that there may not be much Additive C present in this region.

Additive F was also definitely found in the Fines and Tightly Bound regions of the bed (Figure 8.13). There was also the presence of white particles in the Dropped and Loosely Bound regions; however, these particles are likely too small to be Additive F.

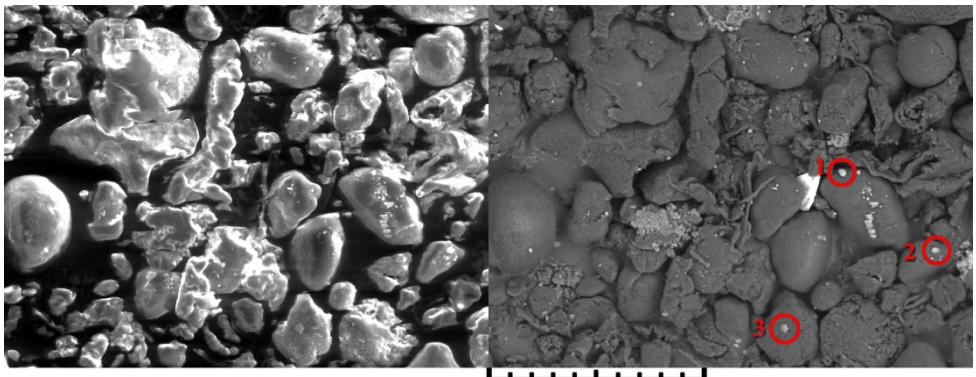
It should be noted that even though the presence of some additives were not detected within different regions, this does not necessarily mean that the additives were not present. There was approximately three orders of magnitude more mass of PE particles present than the additives, and since only a small sample was used per region for SEM analysis, the probability of finding additives on the particles was low. The purpose of this study was to attempt to prove the presence of the additives in different regions of the fluidized; not to disprove their presence.

Fines

$d_{P,N1} = 0.006$

$d_{P,N2} = 0.006$

$d_{P,N3} = 0.007$



SEM Magnification: 500x

200 µm

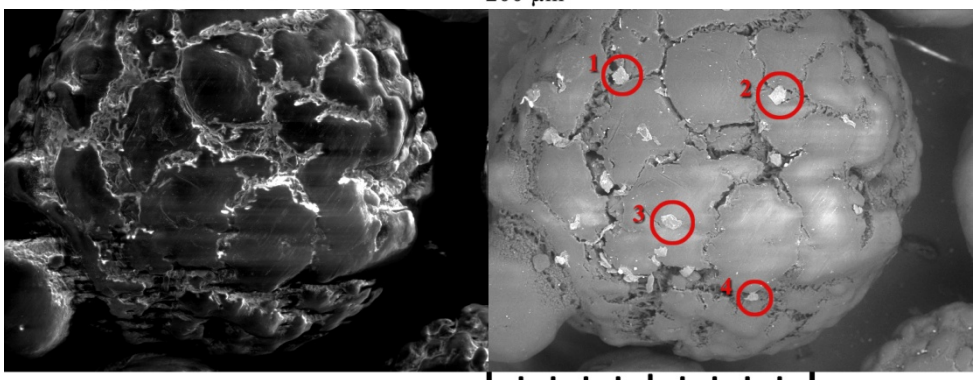
Dropped

$d_{P,N1} = 0.021$

$d_{P,N2} = 0.021$

$d_{P,N3} = 0.021$

$d_{P,N4} = 0.012$



SEM Magnification: 300x

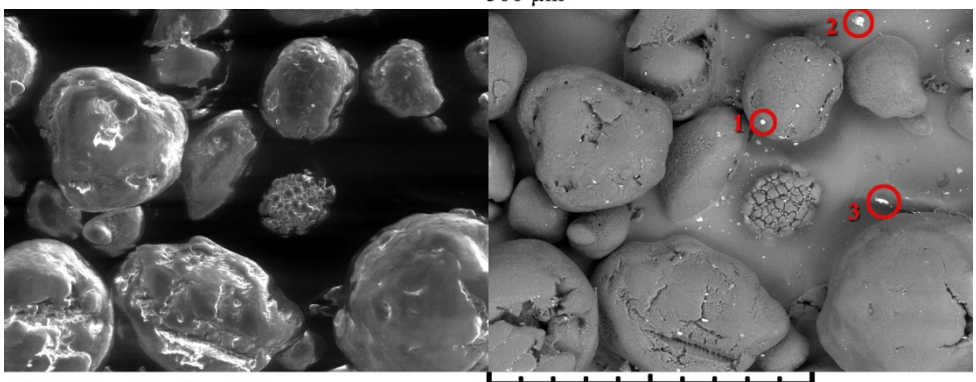
500 µm

Loosely Bound

$d_{P,N1} = 0.007$

$d_{P,N2} = 0.013$

$d_{P,N3} = 0.010$



SEM Magnification: 300x

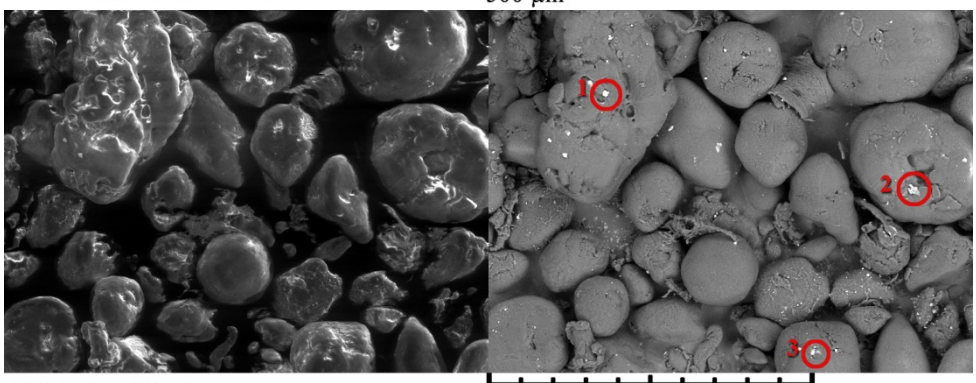
500 µm

Tightly Bound

$d_{P,N1} = 0.009$

$d_{P,N2} = 0.013$

$d_{P,N3} = 0.006$



SEM Magnification: 300x

500 µm

Figure 8.10: SEM Pictures of the Fines, Dropped, Loosely Bound, and Tightly Bound particles when Additive A was present with the PE_A resin.

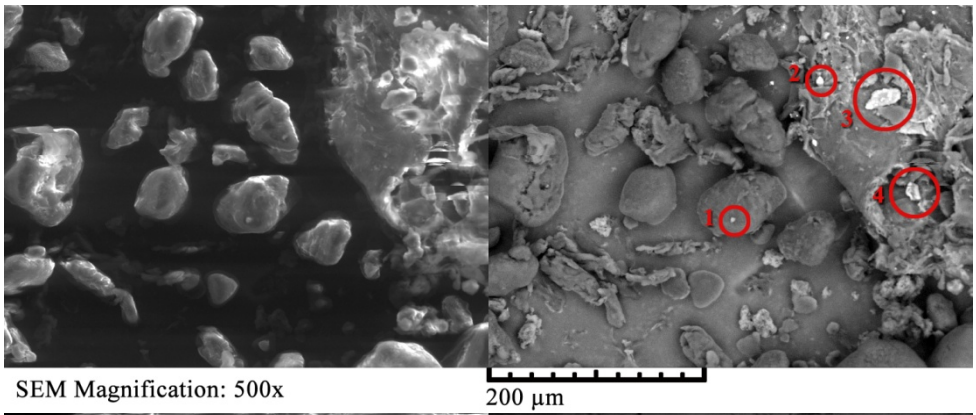
Fines

$d_{P,N1} = 0.004$

$d_{P,N2} = 0.006$

$d_{P,N3} = 0.019$

$d_{P,N4} = 0.012$

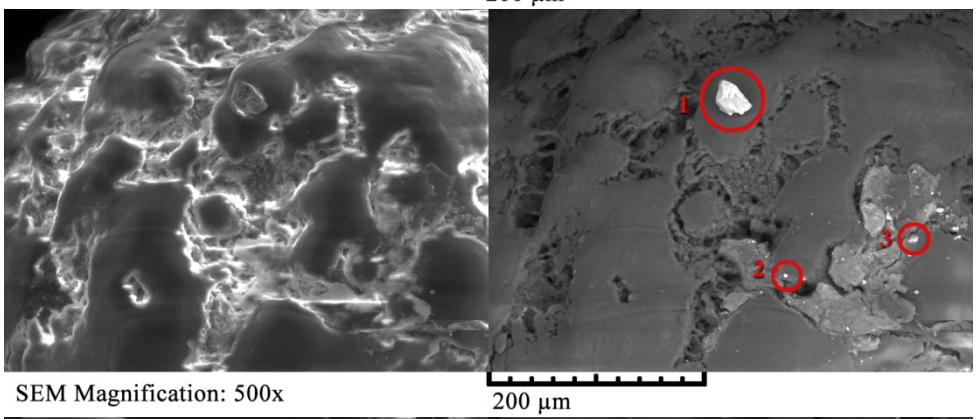


Dropped

$d_{P,N1} = 0.024$

$d_{P,N2} = 0.003$

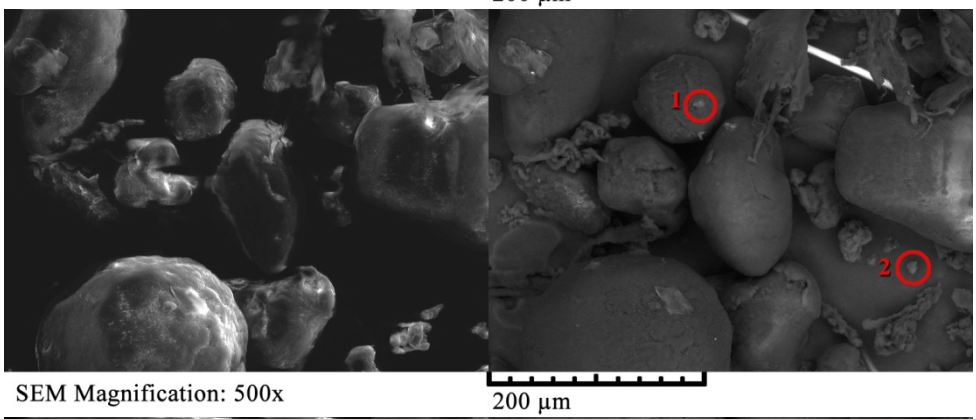
$d_{P,N3} = 0.007$



Loosely Bound

$d_{P,N1} = 0.008$

$d_{P,N2} = 0.009$



Tightly Bound

$d_{P,N1} = 0.007$

$d_{P,N2} = 0.005$

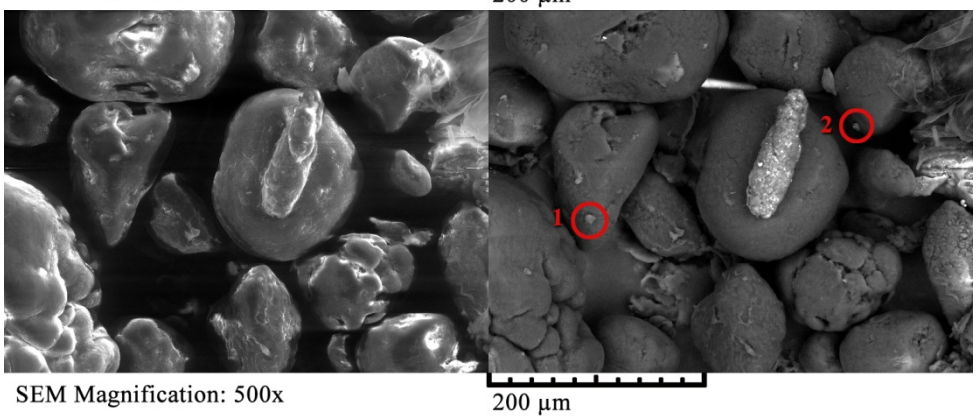


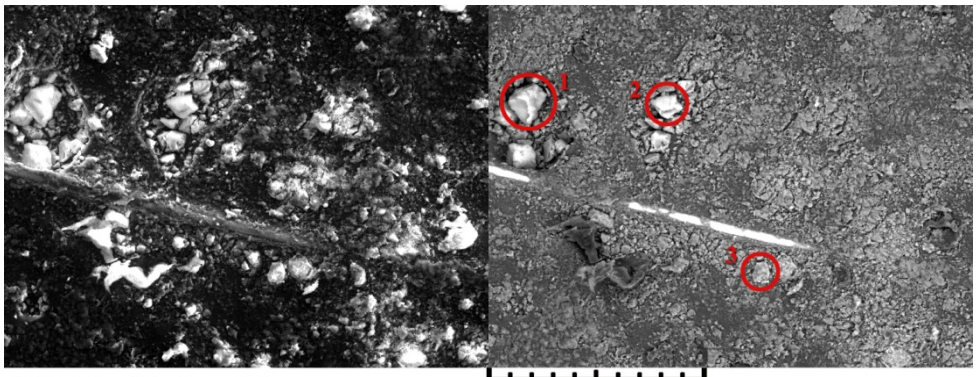
Figure 8.11: SEM Pictures of the Fines, Dropped, Loosely Bound, and Tightly Bound particles when Additive B present with the PE_A resin.

Fines

$d_{P,N1} = 0.026$

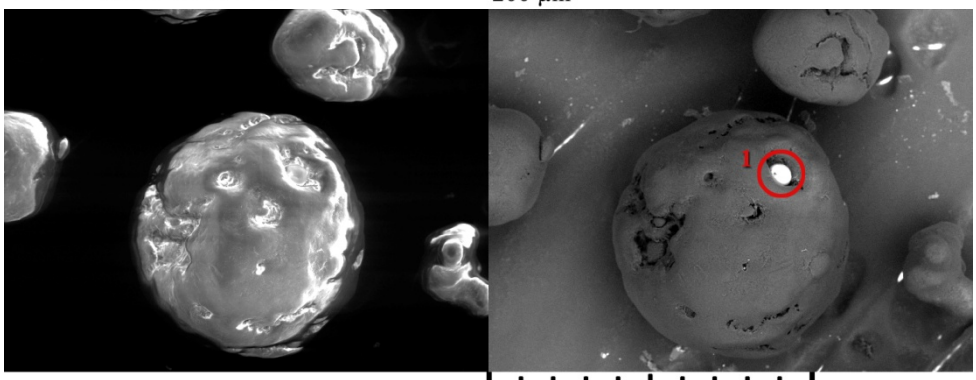
$d_{P,N2} = 0.019$

$d_{P,N3} = 0.014$



Dropped

$d_{P,N1} = 0.030$

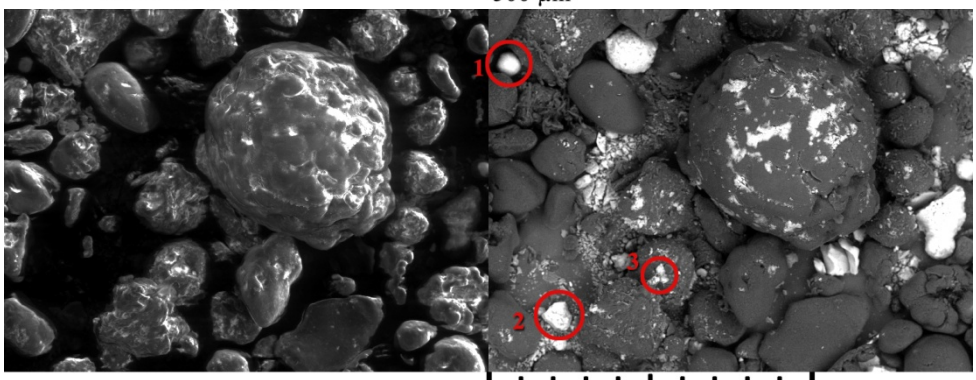


Loosely Bound

$d_{P,N1} = 0.028$

$d_{P,N2} = 0.034$

$d_{P,N3} = 0.014$



Tightly Bound

$d_{P,N1} = 0.022$

$d_{P,N2} = 0.063$

$d_{P,N3} = 0.008$

$d_{P,N4} = 0.034$

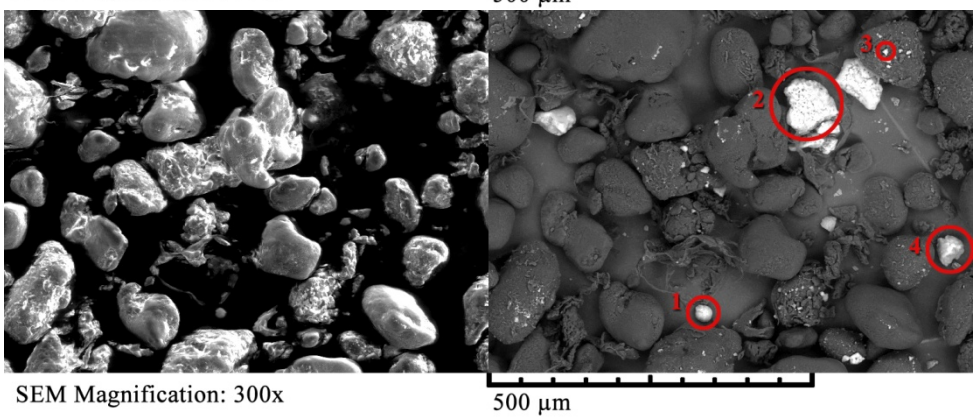


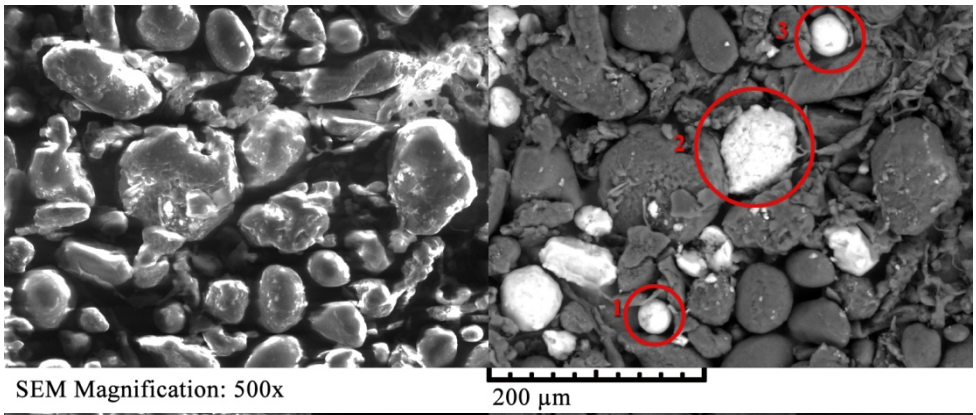
Figure 8.12: SEM Pictures of the Fines, Dropped, Loosely Bound, and Tightly Bound particles when Additive C present with the PE_A resin.

Fines

$d_{P,N1} = 0.025$

$d_{P,N2} = 0.059$

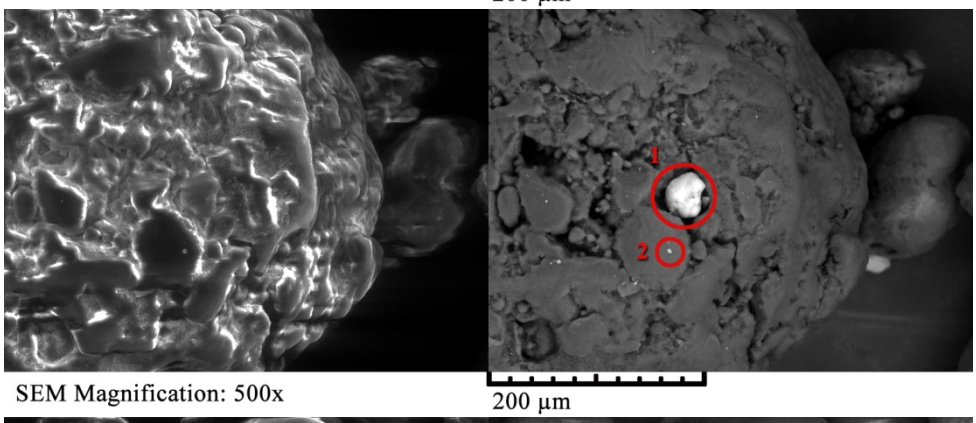
$d_{P,N3} = 0.030$



Dropped

$d_{P,N1} = 0.031$

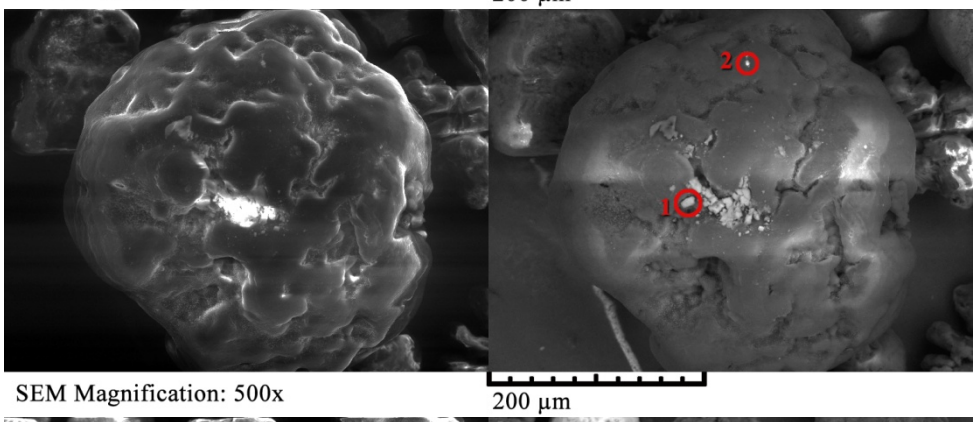
$d_{P,N2} = 0.004$



Loosely Bound

$d_{P,N1} = 0.009$

$d_{P,N2} = 0.004$



Tightly Bound

$d_{P,N1} = 0.048$

$d_{P,N2} = 0.005$

$d_{P,N3} = 0.006$

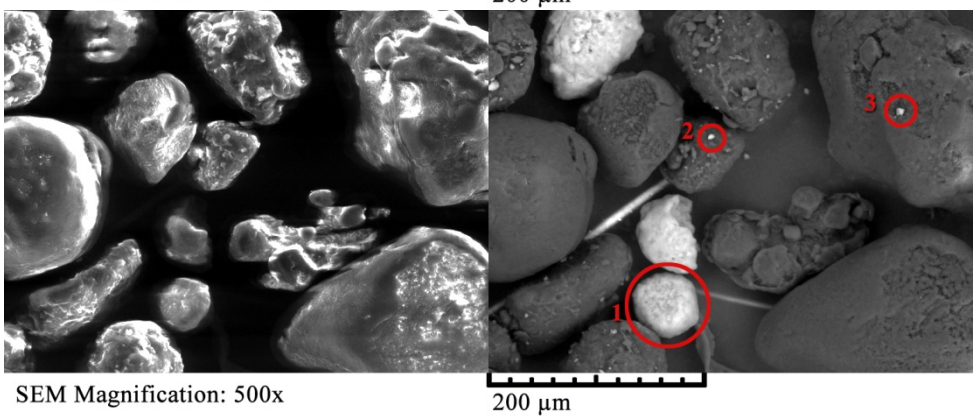


Figure 8.13: SEM Pictures of the Fines, Dropped, Loosely Bound, and Tightly Bound particles when Additive F present with the PE_A resin.

SEM analysis was also performed with the PE_C resin on sample of particles taken from different regions of the fluidized bed. The samples were also taken when the Charged Particle Separator was used from FC1 and FC3. These two cups were chosen to determine whether any of the additives would be present in predominantly negatively (FC1) or predominantly positively (FC3) charged fractions of the Loosely Bound particles. The SEM pictures were only taken for 60 min fluidization time experiments in the presence of Additives A, B, C, and F (Figure 8.14 to Figure 8.17).

Additive A was detected in the Fines region meaning that there was definitely Additive A particles being elutriated from the bed, which agrees well with the mass of the Fines collected in Figure 8.9. There was no Additive detected in the Dropped region, in FC1 or FC3. There were some large spherical particles found in FC3; however, these did not match the particle size and surface morphology of Additive A shown in Table 3.4 and were therefore assumed contaminants.

Additive B was found to be present in elutriated Fines. The additive; however, was not detected in the Dropped, FC1, and FC3 regions of the bed. There was one particle in FC1 that was not polyethylene; however, the particle did not match the size and surface morphology of Additive B found in Table 3.4.

Additive C was found to be present in significant quantities in the Fines, Dropped, FC1, and FC3 regions (Figure 8.16). This means that Additive C migrated throughout the entire bed.

Additive F had a similar migration pattern as Additive C where there were significant quantities found in the Fines, FC1 and FC3 regions but none were detected in the Dropped region (Figure 8.17). With both resins, Additive C and F, which promoted column wall fouling, were definitely found close to the column wall, suggesting a connection between the presence of these additives near the column wall and the wall fouling.

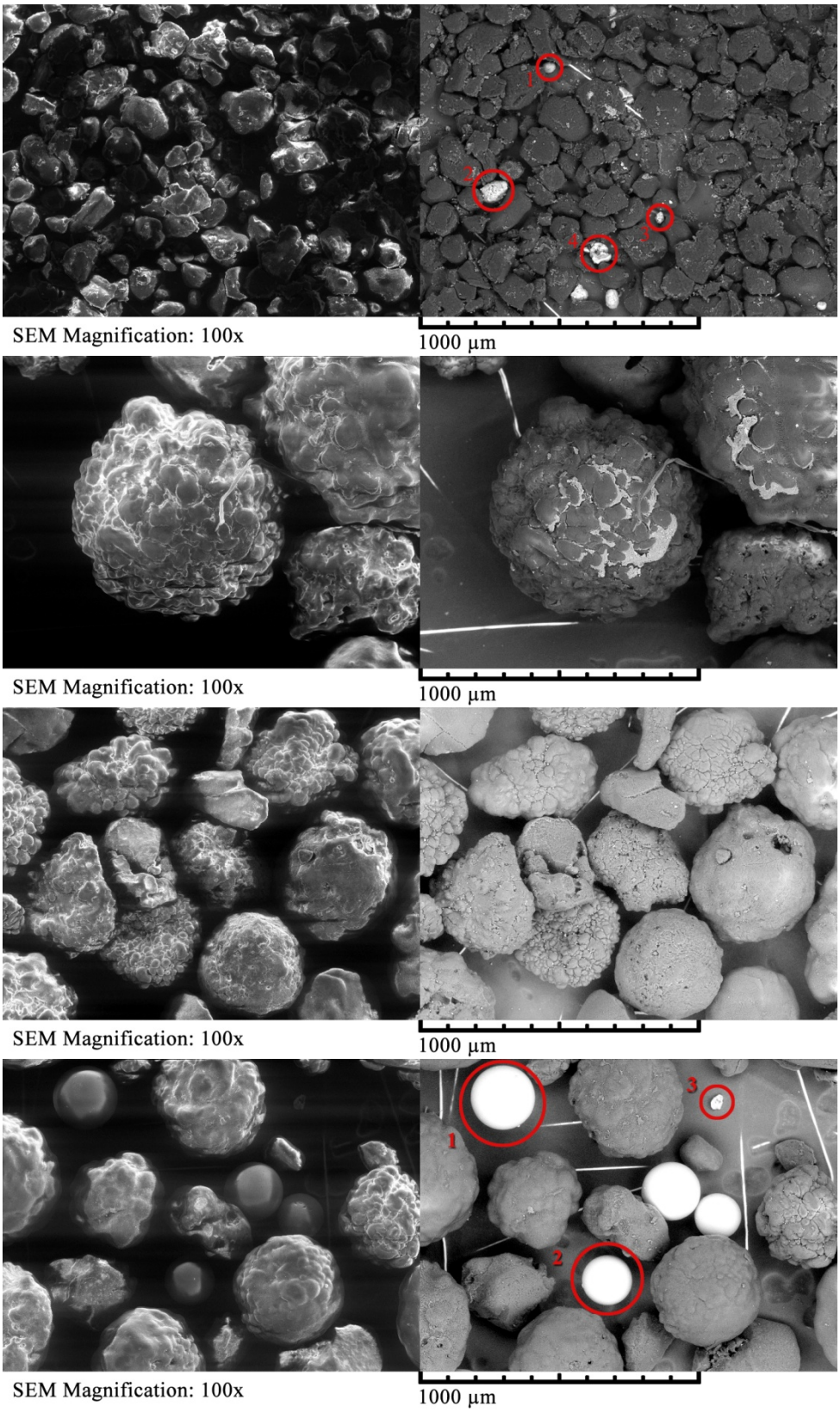


Figure 8.14: SEM pictures of PE_C particles from the Fines and Dropped regions, and FC1 and FC3 with Additive A for 60 minute fluidization.

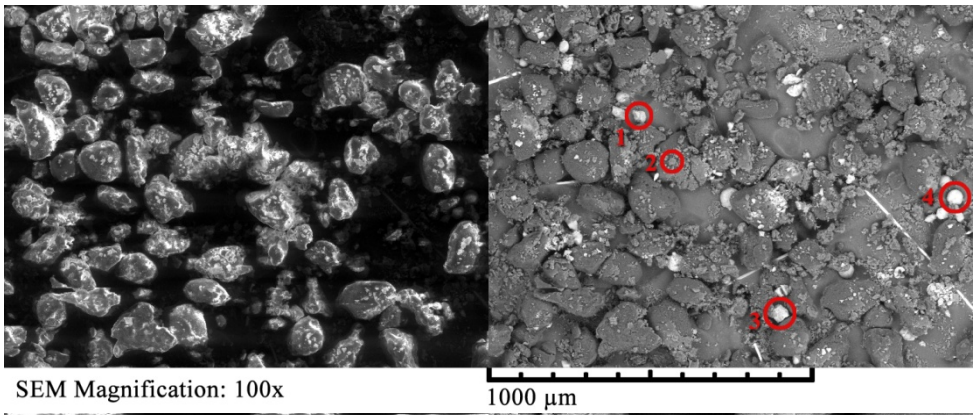
Fines

$d_{P,N1} = 0.033$

$d_{P,N2} = 0.019$

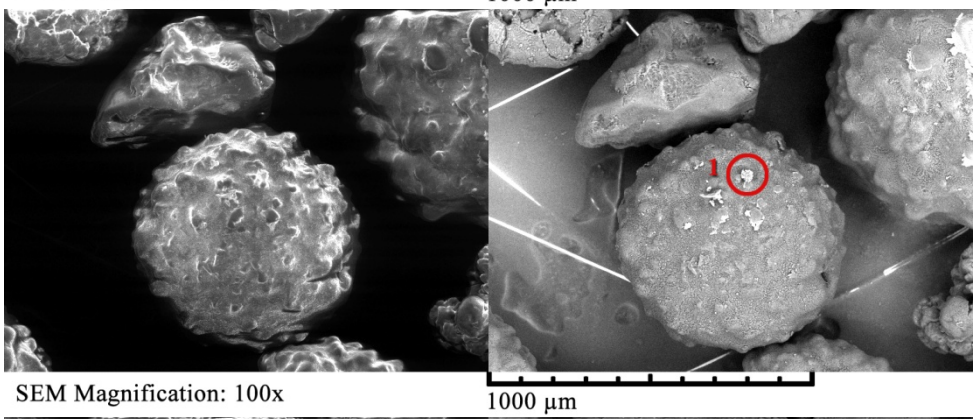
$d_{P,N3} = 0.043$

$d_{P,N4} = 0.039$



Dropped

$d_{P,N1} = 0.034$

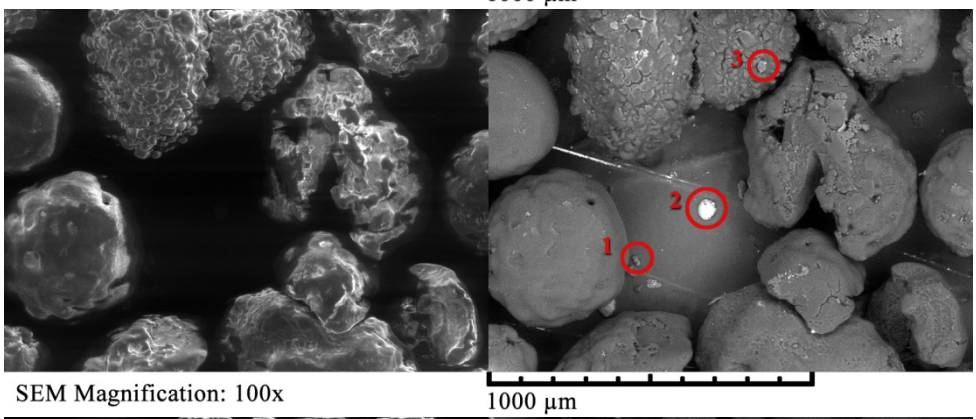


FC1

$d_{P,N1} = 0.002$

$d_{P,N2} = 0.005$

$d_{P,N3} = 0.003$



FC3

$d_{P,N1} = 0.025$

$d_{P,N2} = 0.013$

$d_{P,N3} = 0.015$

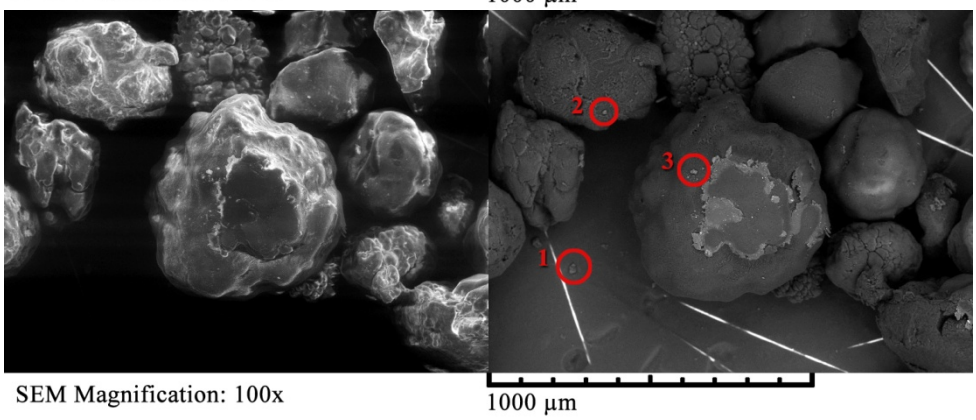


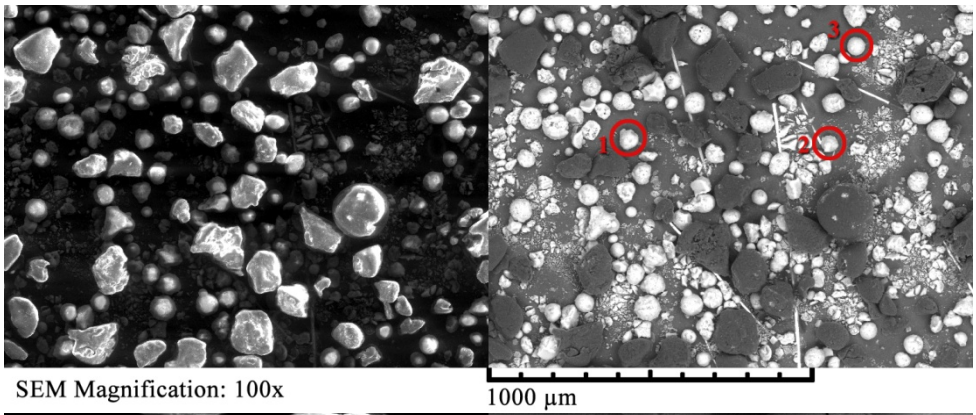
Figure 8.15: SEM pictures of PE_C particles from the Fines and Dropped regions, and FC1 and FC3 with Additive B for 60 minute fluidization.

Fines

$d_{P,N1} = 0.048$

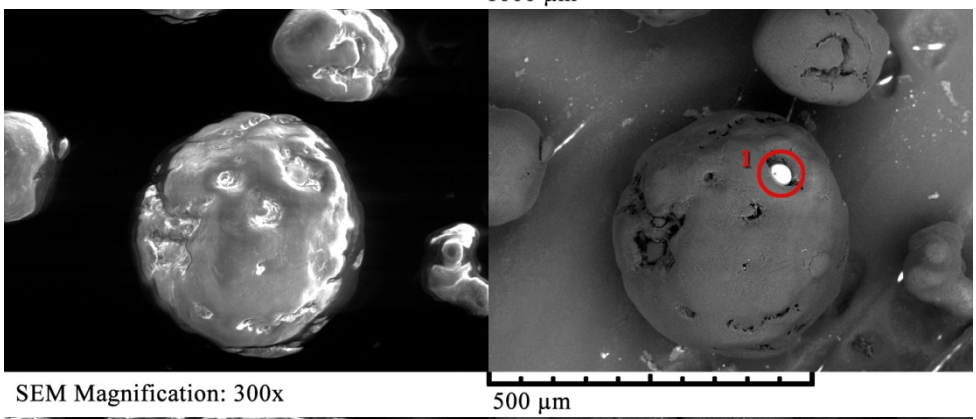
$d_{P,N2} = 0.041$

$d_{P,N3} = 0.043$



Dropped

$d_{P,N1} = 0.032$

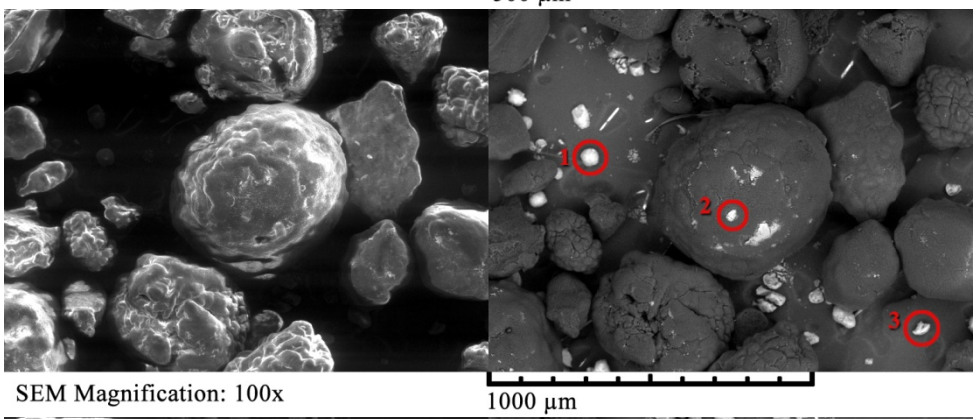


FC1

$d_{P,N1} = 0.044$

$d_{P,N2} = 0.028$

$d_{P,N3} = 0.036$



FC3

$d_{P,N1} = 0.037$

$d_{P,N2} = 0.046$

$d_{P,N3} = 0.072$

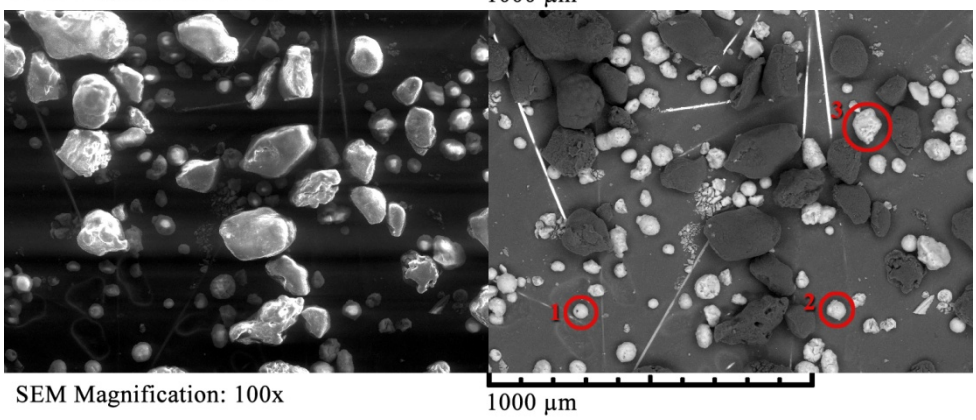


Figure 8.16: SEM pictures of PE_C particles from the Fines and Dropped regions and FC1 and FC3 with Additive C for 60 minute fluidization.

Fines

$d_{P,N1} = 0.068$

$d_{P,N2} = 0.046$

$d_{P,N3} = 0.045$

Dropped

$d_{P,N1} = 0.036$

$d_{P,N2} = 0.020$

FC1

$d_{P,N1} = 0.035$

$d_{P,N2} = 0.045$

$d_{P,N3} = 0.052$

FC3

$d_{P,N1} = 0.066$

$d_{P,N2} = 0.038$

$d_{P,N3} = 0.179$

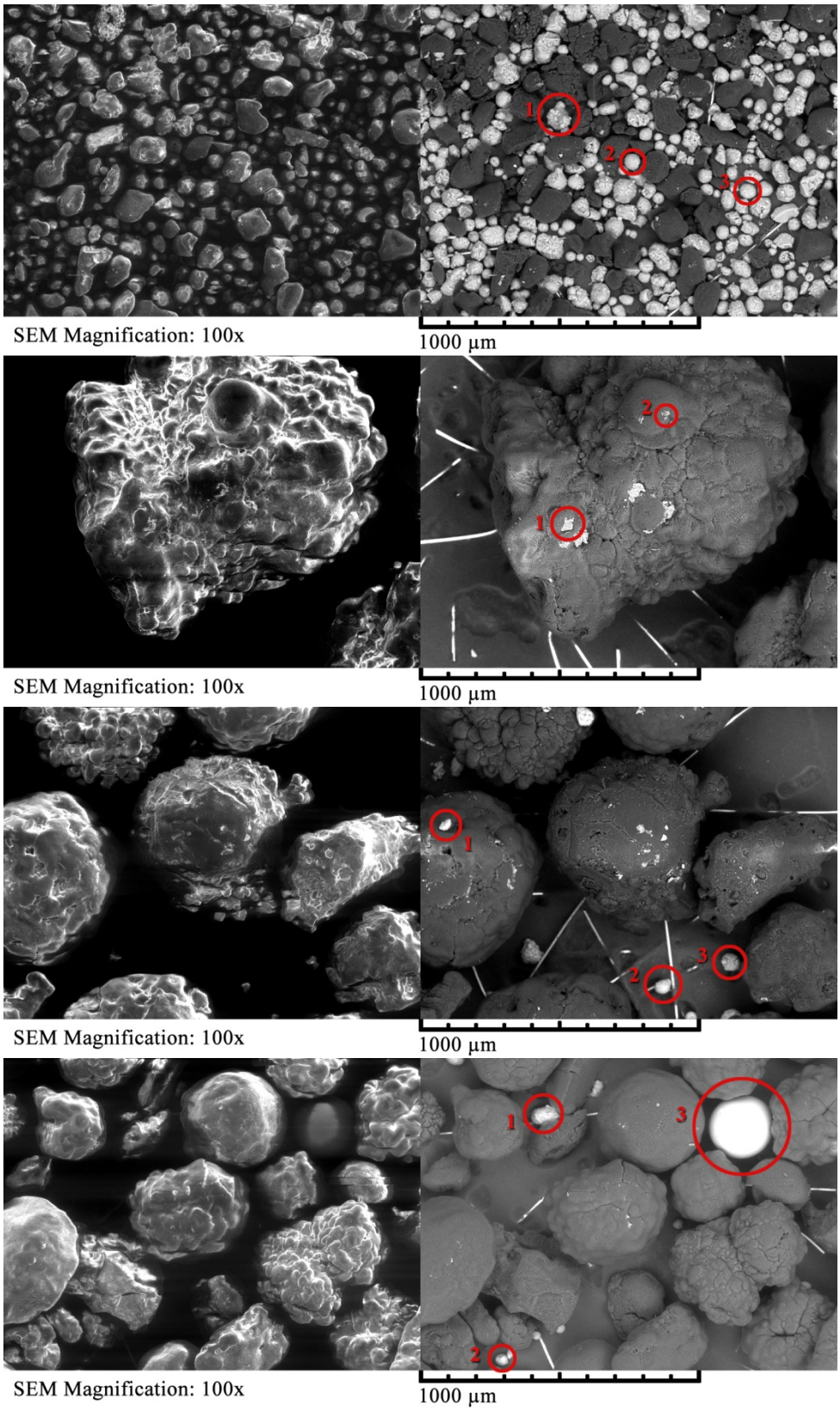


Figure 8.17: SEM pictures of PE_C particles from the Fines and Dropped, regions, and FC1 and FC3 with Additive F for 60 minute fluidization.

8.2.2.3. Particle Size Distribution

The d_P50_N of the particles found in different regions of the bed with and without any additive with both resins is shown in Figure 8.18. There was some large deviation in the median particle diameter with the Initial particles which would be due to the small sample size used to perform the PSD analysis, and the uncontrolled resin size. Between the two resins it is clear that PE_C had a larger median particle size.

With the PE_A resin, the Dropped region appeared as though there was a decrease in the particles d_P50_N in the presence of only Additive B. However, there was a large amount of variation in the results and therefore this was likely due to the samples taken for the PSD measurement, similar to the Initial particles, and as discussed with the repetitions test perform in §3.3.2.2. The d_P50_N for the Loosely Bound particles showed that the particle size did not change when Additive A was injected and were the smallest sizes measured. With all of the other additives; however, the d_P50_N was approximately twice the particle size as without any additives. From Chapter 5, it was found that at the higher gas velocity the particle wall fouling layer was shorter and thicker. As the layer became thicker, larger particles were present within the layer. This effect was likely happening at 1.5 u_{mf} but due to the presence of Additives B, C, or F. This will be discussed in more detail in §8.2.2.4.

With the PE_C resin, the d_P50_N of the Fines was influenced by the presence of the additive particles since these particles contributed to the majority of the Fines entrained. For all other regions (Dropped, Loosely Bound, and Tightly Bound), there was no distinct effect of additives on the size of the particles. There was likely no noticeable effect on the size of the particles present on in the Loosely Bound region with the PE_C resin in contrast to the PE_A resin due to the larger particle size. The Malvern Mastersizer measures the volume distribution of the sample, and therefore is more biased to larger particles (i.e., one large particle takes up more volume than numerous smaller particles). Therefore the larger PE_C particles found in the Loosely Bound likely shifted distribution towards the larger size.

It should be noted that the size of the PE particles adhering to the column wall was larger with the PE_C resin than PE_A resin. However, with both resins, these particles were still smaller than

their respective Initial particles, which agree well with the results of different particle size range adhering to the column wall found in Chapter 6.

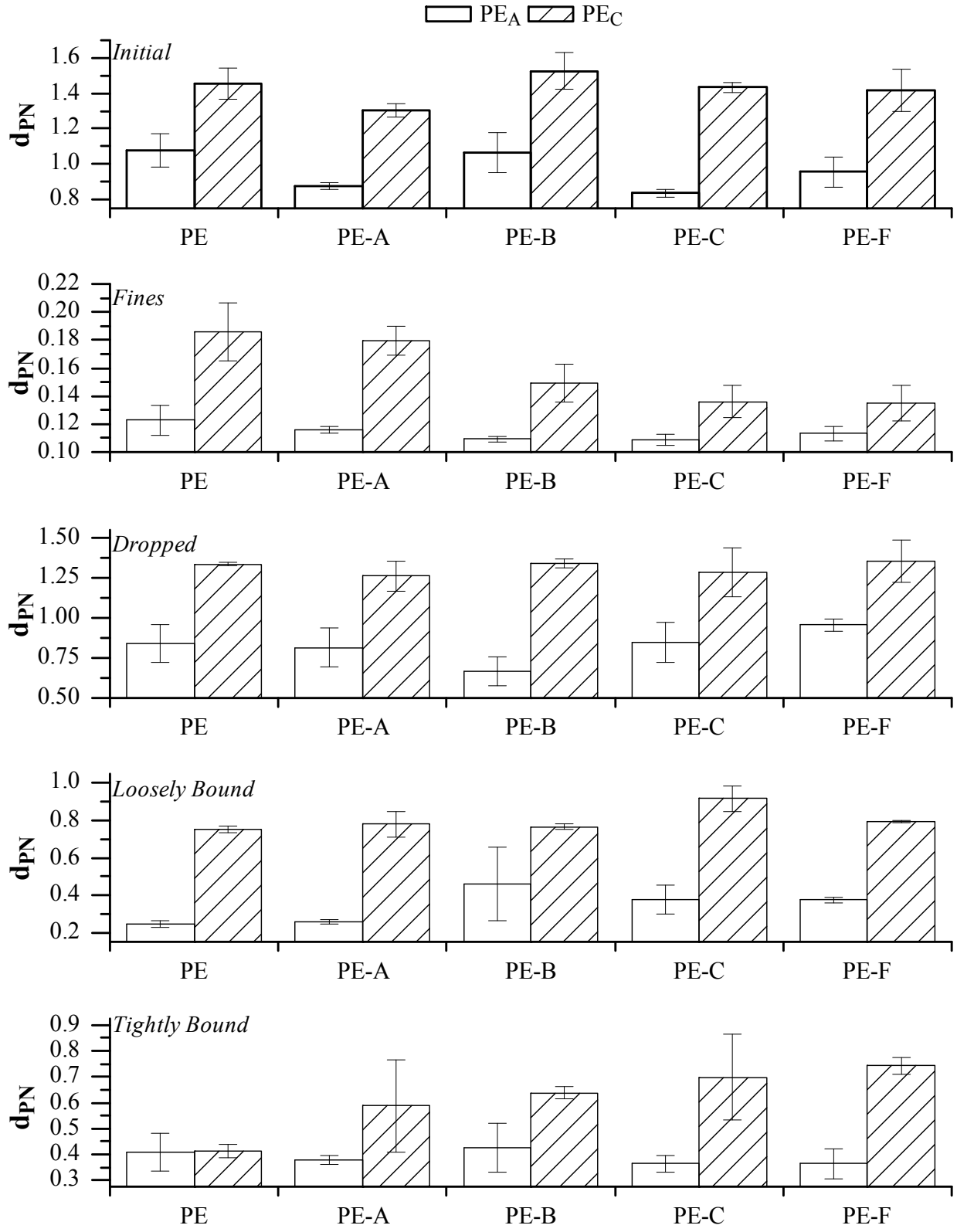


Figure 8.18: The d_P50_N of the Initial, Fines, Dropped, Loosely Bound, and Tightly Bound particles for experiments performed with and without additives with PE_A and PE_C resins

8.2.2.4. Particles Absolute and Specific Charge

A typical example of the cumulative charge of the elutriated Fines with both resins with and without any additives is shown in Figure 8.19. Without any additive, the Fines were predominantly positively charged with both resins.

With PE_A resin, only Additive B seemed to have the most notable effect during the course of fluidization as the charge of the entrained fines increased positively before starting to decline. There was no evident trend when the other additives were present.

PE_C resin did not have many fine particles that could be elutriated and thus as can be seen a significantly small charge was detected for the case without any additive. The presence of the prostatic agents (Additives A and B) altered the Fines polarity to negative whereas the deactivated catalyst and its support (Additives F and C) resulted in a positive charge. With Additives C and F injected into the bed of PE_C resin, the charge of the Fines was consistently positive; however, as shown in Figure 8.2, both these additives were negatively charged passing through the injector and became less negatively charged passing through the empty column. Thus, the reasoning for the positive Fines in the fluidization system likely comes from the PE particle-additive interactions within the bed. Since Additives C and F were placed above PE in the pseudo-triboelectric series found in Table 8.5, these particles become more positively charged when in contact with the PE particles.

The difference between the cumulative charges of the Fines between the resins due to the presence of additives was caused by the presence of an abundant amount of fine particles in the PE_A resin itself. Since there were so many fine PE_A particles leaving the fluidized bed over the fluidization period, any charge of the additive was not as noticeable. With the other resin, the Fines were dominated by the presence of additives, which ultimately dictated the cumulative charge of the Fines. Regardless of the polarity of the particles leaving the system, the entrained Fines would leave an opposite polarity within the bed, or on the reactor wall. Therefore, with Additives A and B, there should be an increase in the amount of positive charges found in the bulk of particles. Similarly, Additives C and F should increase the amount of negative charges found in the bulk of particles.

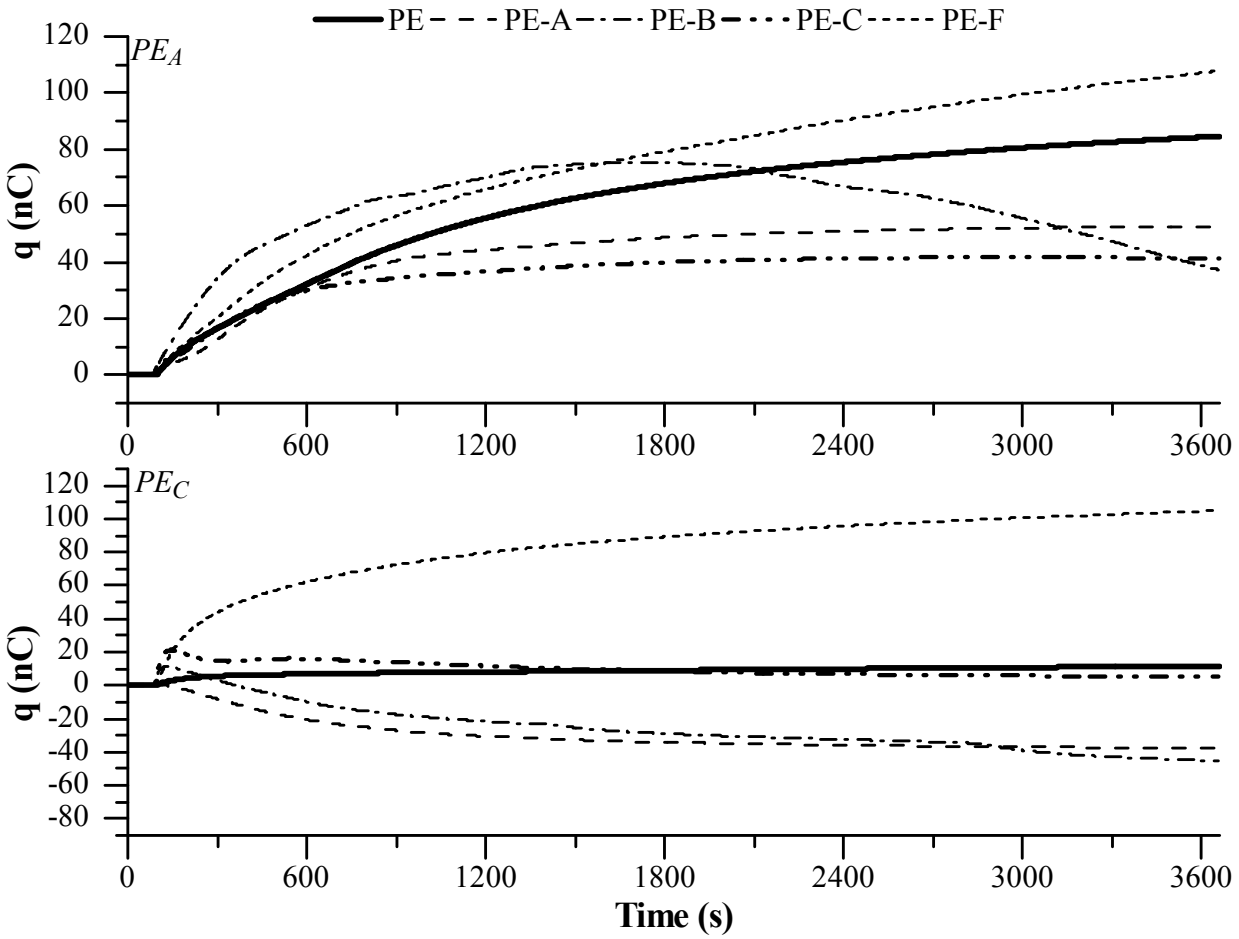


Figure 8.19: Examples of the cumulative charge of the Fines measured during 60 min of fluidization with and without the additives with both PE_A and PE_C resin.

The specific charge of the Initial, Fines, Dropped, and Loosely Bound particles with and without an additive with PE_A and PE_C resin are shown in Figure 8.20.

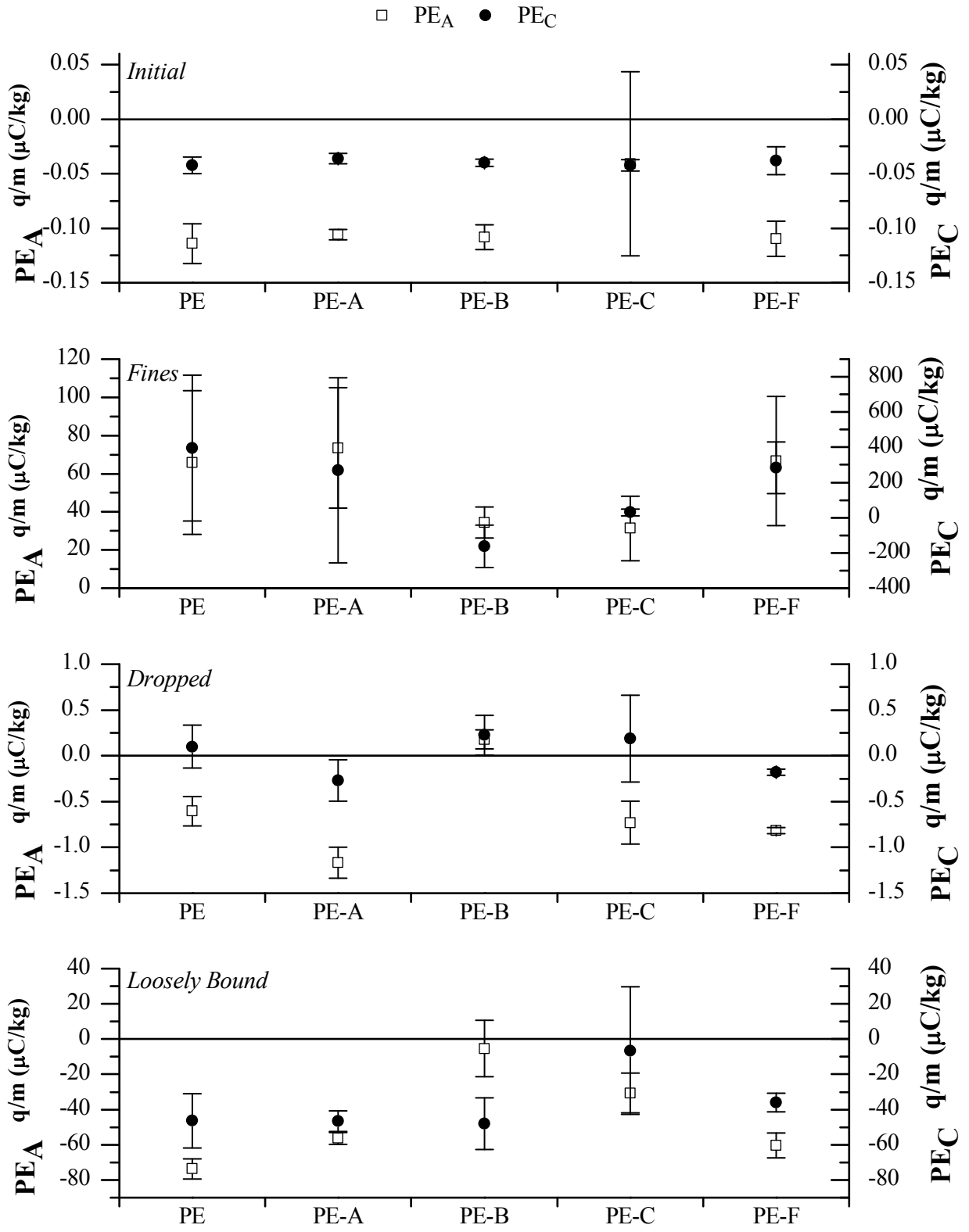


Figure 8.20: The net q/m of the Initial, Fines, Dropped, and Loosely Bound particles for experiments performed with and without additives with both PE_A and PE_C resin.

The Initial q/m of the particles did not vary for given resin, but the PE_A resin was always more negatively charged than the PE_C resin. The q/m of the Initial particles for the PE_A resin had some variation but was on average approximately -0.1 μC/kg whereas the q/m of the PE_C resin was approximately -0.5 μC/kg.

With the PE_A resin, the q/m of the Fines was predominantly positively charged and the Loosely Bound particles were always negatively charged with any of the additives. With the Dropped particles, they were predominantly negatively charged and did not vary significantly with different additives injected, with the exception of the experiments with Additive B. Additive B appeared to have altered the particles charge in all regions of the fluidized bed as the net q/m of Fines decreased (but remained positive), the Dropped particles became more positively charged, and Loosely Bound particles became less negatively charged in general. In comparison to no additives used, the net q/m of the particles shifted towards zero for all regions. From the pseudo-triboelectric series, Additive B was assumed to on average charge positively when in contact with the polyethylene, or with the carbon steel column. When Additive B is initially injected into the bed, the particles are negatively charged and therefore some of Additive B would migrate to the column wall, some would coat the PE particles, and during fluidization some would elutriate from the bed. If Additive B does not come into contact with many of the PE particles in the bed before being elutriated, then they would exit the column negatively charge, effectively reducing the amount of charge for the Fines. The presence of Additive B on the column wall and on some of the PE particles would limit the amount of PE-column wall contact and would increase the amount of Additive B-PE and Additive B-Additive B contacts. Additive B-PE contacts would increase the amount of positive charges on the Additive B particles, which could alter the net q/m of the Dropped particles to be positive and effectively decrease the q/m of the Loosely Bound particles. With the other Additives, not a large difference was found in the net q/m of the Loosely Bound particles. There was also a similar amount of Wall particles present with Additive A, C, and F meaning that there was a similar amount of particle wall coating and charge for these additives.

With the PE_C resin, the magnitude of the net q/m of Fines was significantly large due to the low mass of Fines collected. With the additive injection, the majority of the Fines captured was found to be additive; therefore, through interactions between the column wall, other additives, and PE particles, Additive A and B were charged negative, and Additive C and F were charged positive. The charging behaviour of Additives C and F agreed well with the pseudo-triboelectric series (Table 8.5) whereas Additives A and B did not match. However, with Additive B at the beginning of fluidization there was a sharp positive increase in cumulative charge of the Fines (Figure 8.19) suggesting that there were at least some Additive B particles there were positively charged. However, over time the Fines became negatively charged, which could be caused by interactions between the additive and the PE particles. This could also be attributed to negatively charged Additive B when it was injected into the bed also being elutriated from the bed of particles if there were not many particle interactions. The net q/m of the Dropped particles did not differ significantly compared to the q/m of the experiments performed without any additive, suggesting that there was not much of an influence from additives. With the Loosely Bound particles, with any Additive present, the q/m was less negatively charged compared to without any additive present. It is known that all of the additives were negatively charged when being injected into the bed (§8.2.1). If some of these negatively charged additives were attracted to the column wall at the beginning of the fluidization then this could attract the positively charged particles to the wall, effectively reducing the q/m of the Loosely Bound particles. Similarly, these particles are likely to remain adhered to the column wall as Tightly Bound particles, leaving some negatively charged particles on the wall. It should be noted that even though there was no significant difference in the q/m of the Loosely Bound particles in the presence of the additives, there was a difference in the mass of the adhered particles. Therefore the q/m of the Loosely Bound particles may not be a good measure of the amount of particle wall fouling.

8.2.2.5. Specific Charge-to-Specific Surface Area Ratio

The $\hat{q}/\hat{A}$ of the particles for different regions in the fluidized bed with and without additives with both resins is shown in Figure 8.21. Overall with both resins, the results did not vary significantly with the Initial, Fines, Loosely Bound, and Dropped particles with the presence of any of the Additives.

Between the two resins there was no significant difference between the Initial particles suggesting a similar surface charge was present on both. There was a difference in the magnitude of the $\hat{q}/\hat{A}$ of the Fines where the $\hat{q}/\hat{A}$ for the PE_C particles was much larger than that of the PE_A resin. This was caused by two factors, the first being the larger q/m of the PE_C Fines due to much smaller mass collected, and the smaller specific surface area due to larger particles being present in the PE_C Fines.

It should be noted; however, that on average the magnitude of the Loosely Bound particles for both resins was always larger than all other regions of the bed, which would be one reason why these particles were prone to adhering to the column wall. The $\hat{q}/\hat{A}$ of the Loosely Bound particles was also found to be the largest in the previous chapters as well.

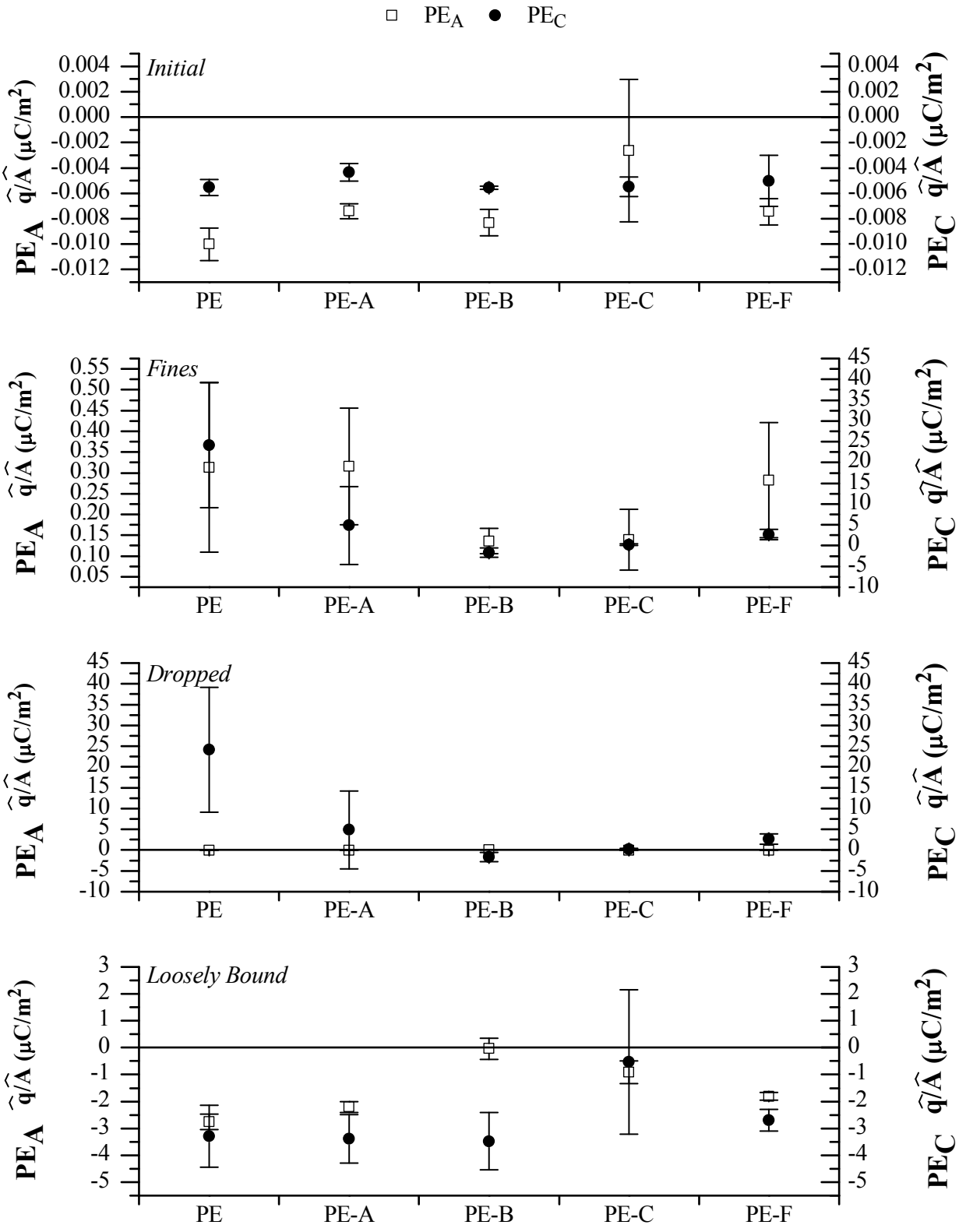


Figure 8.21: The $\hat{q}/\hat{A}$ of the Initial, Fines, Dropped, and Loosely Bound particles for experiments performed with and without additives with both PE_A and PE_C resin.

8.2.2.6. Wall Layer Coating

Examples of wall layer pictures with and without any additive with both resins are shown in Figure 8.22. Between the two resins, it is clear that there was more particle wall fouling with the PE_A resin compared to the PE_C resin.

With the PE_C resin Additive A was effective at reducing the amount of particles adhered to the column wall near the bottom of the column, but not with PE_A. This may be directly related to the presence of finer particles with the PE_A resin. It has been shown in previous chapters that the smaller PE particles had a tendency to adhere more easily to the column wall. With PE_A resin and Additive A less Tightly Bound particles were found and therefore it is possible that Additive A had an effect on the particle wall layer, but due to the presence of the smaller particles, there simply was not enough Additive A to have a significant effect.

From images it is clearly evident that Additive B had the largest impact on reducing the amount of particle build up on the column wall for both resins. In addition, the removal of the polyethylene particles off the wall was the easiest with this additive. This was likely caused by additive adhering to the PE particles, reducing the number of contacts between the particles and thus reducing the particles charging and their adhesion to the column wall. As presented in §8.2.1.4 Additive B resulted in the largest amount of reactor wall coating as well, resulting again in less PE particle and carbon steel column wall contacts. Also it was believed that Additive B would be the most effective at any sort of charge dissipation due to its functional groups, which would likely help remove any of the bound particles. Charge dissipation from Additive B to the column wall may help in reducing the amount of particle-wall layering as well as releasing some of the PE fines that may be trapped within the layer. Indeed, the m% of the Fines collected was the largest when Additive B was injected into the system (Figure 8.9) with the PE_A resin.

Additive B may have been more effective than Additive A due to differences in the particle size, and surface chemical properties. Additive A had a bimodal particle size distribution with some significantly larger particles. Additive B overall was the smallest particle meaning that it can more easily bind to the larger PE particles. It is also possible that the larger fraction of Additive A is not as effective at reducing the particle wall fouling as the smaller particles. Additive A

contained a tertiary amine with hydroxyl group whereas Additive B contained the aluminum atom. It was assumed that Additive B was the most effective at charge dissipation from the additive to the column wall followed by Additive A. Therefore, for these reasons Additive A may not have been as effective as Additive at reducing the amount of particle wall fouling.

When Additive C was present, it appeared as though the entire column wall was completely covered with polyethylene particles with PE_A and still a significant amount of particle wall fouling with PE_C resin, showing a large effect on electrostatic charges within the system. This increase in the particle-wall adhesion could be caused by Additive C particles becoming negatively charged in contact with the column wall, increasing the positive charging on the column wall, in addition to positive charges generated due to polyethylene contacting the wall. On the other hand, additive particles contacting polyethylene particles cause the polyethylene particles to become more negatively charged. The two charging mechanisms mentioned above would then increase the electrostatic forces between the carbon steel wall and the PE resin and thus promotes the reactor wall fouling. Additive F also showed an increase in the amount of particle wall fouling with both resins. Similar charging effects discussed above apply to this additive as well.

It is clear that all of additives played an important role in the amount of particle wall fouling. However, the presence of the fine polyethylene particles also clearly has a large impact on the amount of particle wall fouling in the system.

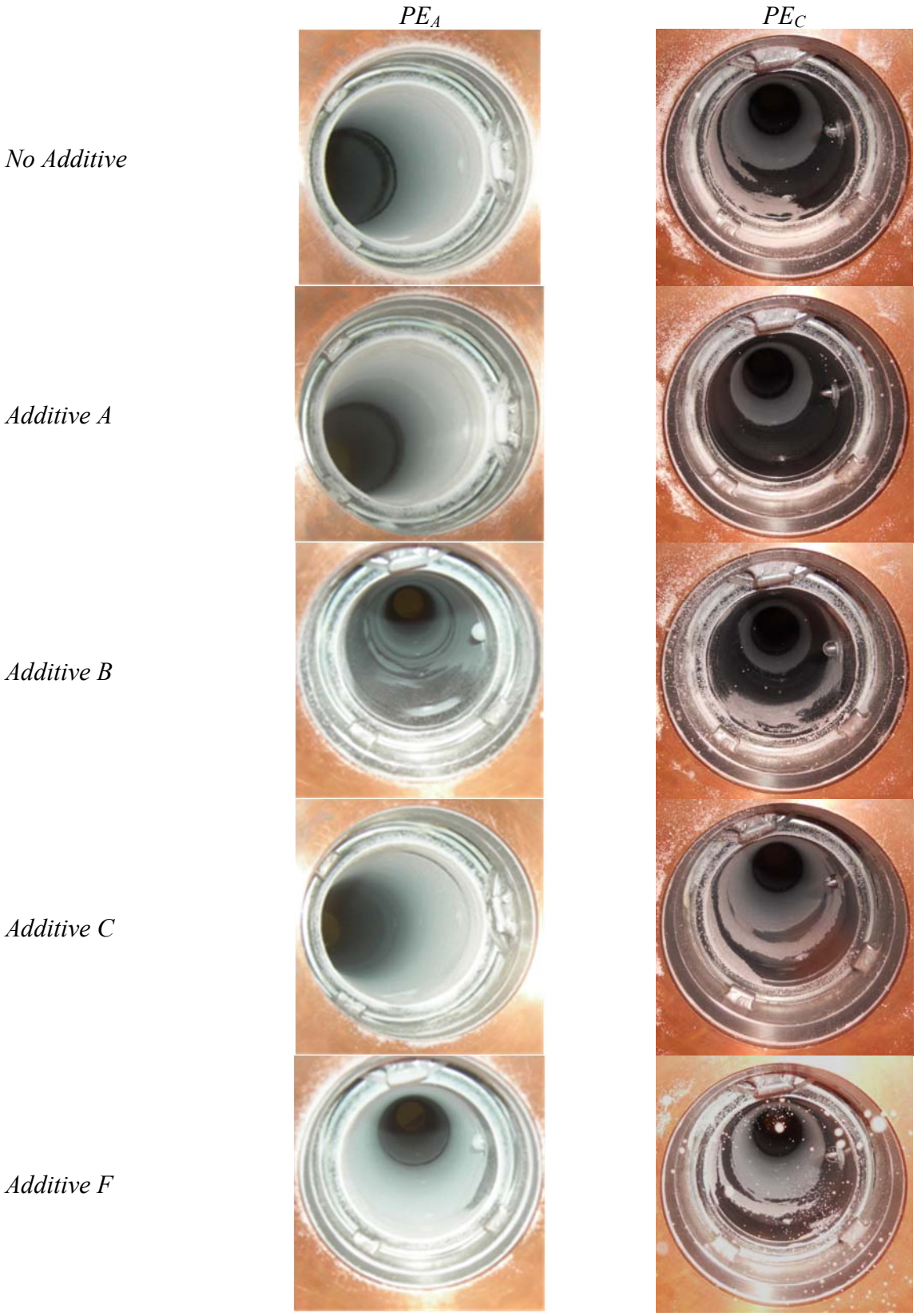


Figure 8.22: Pictures of the wall particle layer with and without additives with both PE_A and PEC resin.

8.2.2.7. Charged Particle Separator

For each set of experiments with the PE_C resin, one extra experiment was performed where the bottom Faraday cup was replaced with the CPS to obtain the charge distribution of the Loosely Bound particles. Results of all of these trials are summarized in Figure 8.23. Only one trial was performed for each type of experiment. Overall, for all experiments performed with and without any additive, the Loosely Bound Wall particles were composed of both of negatively and positively charged particles. The d_P50_N of all the additive experiments were relatively consistent throughout all of the Faraday cups with a few exceptions. The d_P50_N of highly charged particles deposited on the positive plate (PP) was relatively smaller in size than those collected in Faraday cups. Another exception was the small particle size found in FC4 for experiments performed with Additives C or F. Assuming that Additives C and F each retained their positive charge found in §8.2.1, then this decrease in size could be the separation of the positively charged particle into FC4, effectively reducing the d_P50_N of the Faraday cup.

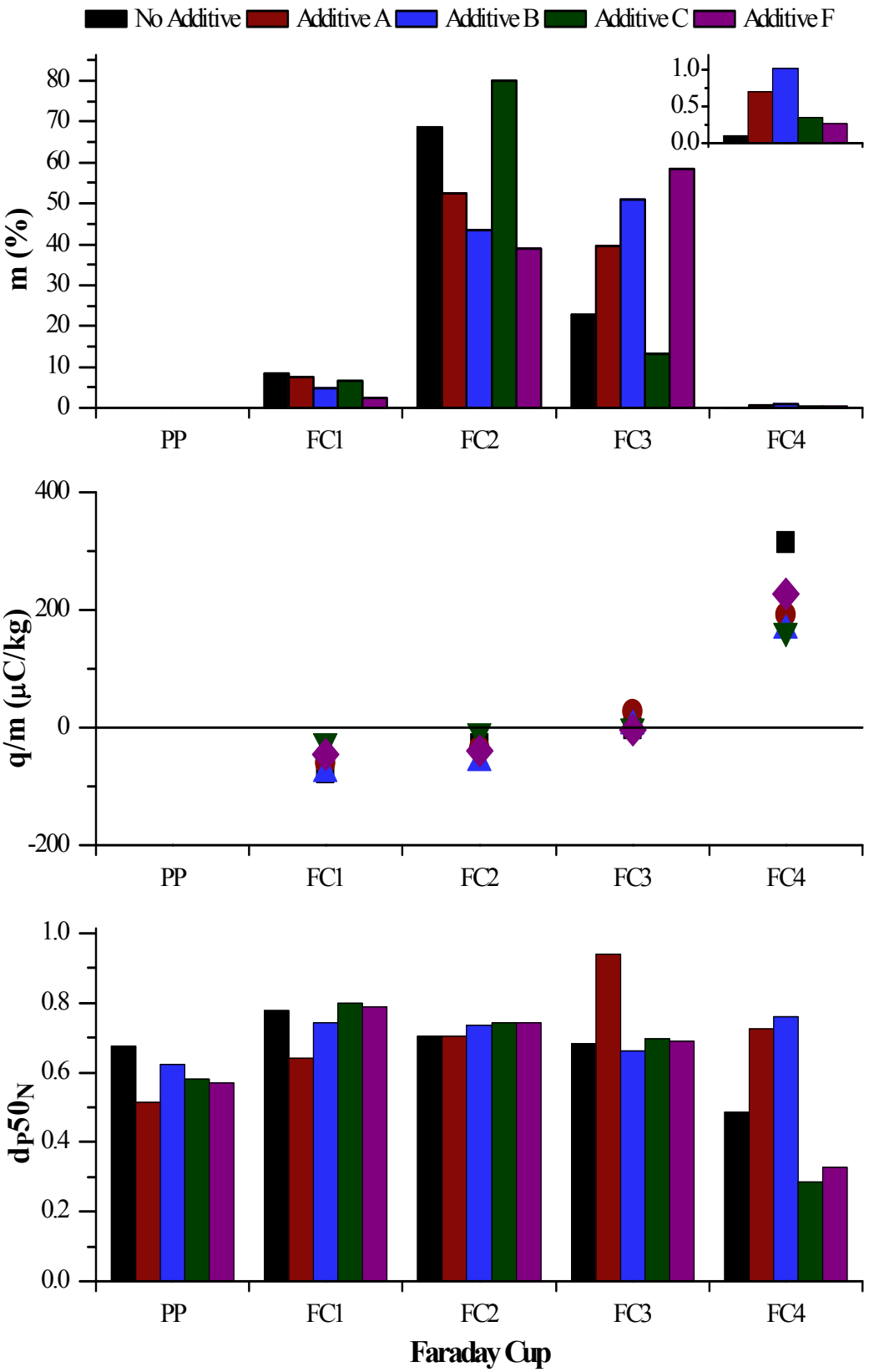


Figure 8.23: The CPS results for the Loosely Bound PE_C particles with and without any additive after 60 min of fluidization.

8.2.2.8. Electrostatic Probe

The probe was not available when the Additive A and Additive C experiments were performed with PE_A; therefore no measurements are available. However, the current measurements for the trials with PE_A and both current and charge measurements with PE_C are shown in Figure 8.24. The current measurements showed varying results even with the same repetitions with the same resin. A comparison of the current measurement for PE_C showed larger amplitude than that measured with the PE_A resin; however, the amount of particle wall fouling was overall greater with the latter resin. The cumulative charge measured by the probe was always positive with the PE_C resin but the magnitude of the charge differed significantly between trials, making it difficult to correlate these results with the column wall fouling.

The current and charge measurements for Additives A, B, C, and F are plotted in Figure 8.25 to Figure 8.28, respectively. Where available, both measurements for both resins are plotted.

For all charge measurements with the PE_C resin, the cumulative charge measured was always positive, which is opposite to the net charge of the Loosely Bound particles discussed in §8.2.2.4. With Additive A the current measurements were not reproducible as one of trials started with large fluctuations in the amplitude, before decreasing significantly, while the other trial did not exhibit this behaviour. Additive B, which resulted in the least amount of particle wall fouling with both resins, consistently resulted in small current amplitude. However, this also occurred without any additive present with the PE_C resin, which that had more particle wall fouling. With the PE_C resin there was a distinct drop in the measured current after a period of time which was not observed with the other resin. With Additive C, the amplitude of the current measurement also did not show consistent results. This was also seen with Additive F and the PE_A resin in which one trial had a much larger current amplitude than the other three trials; however, the amount of particle wall coating remained the same. This inconsistency makes it difficult to correlate these results to the extent of column wall fouling.

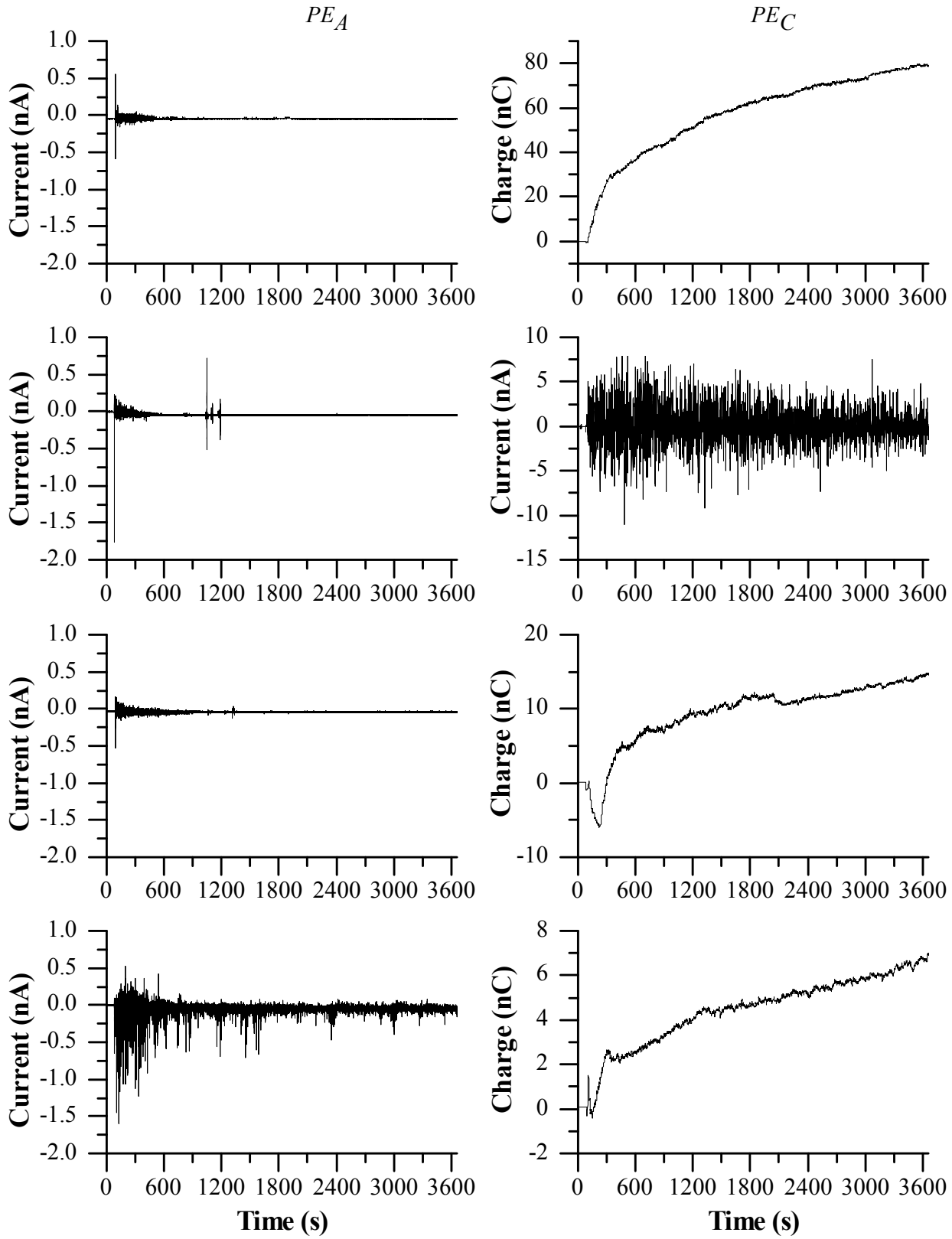


Figure 8.24: The current and charge measurements for trials with no additive for 60 min of fluidization with PE_A and PE_C resin present.

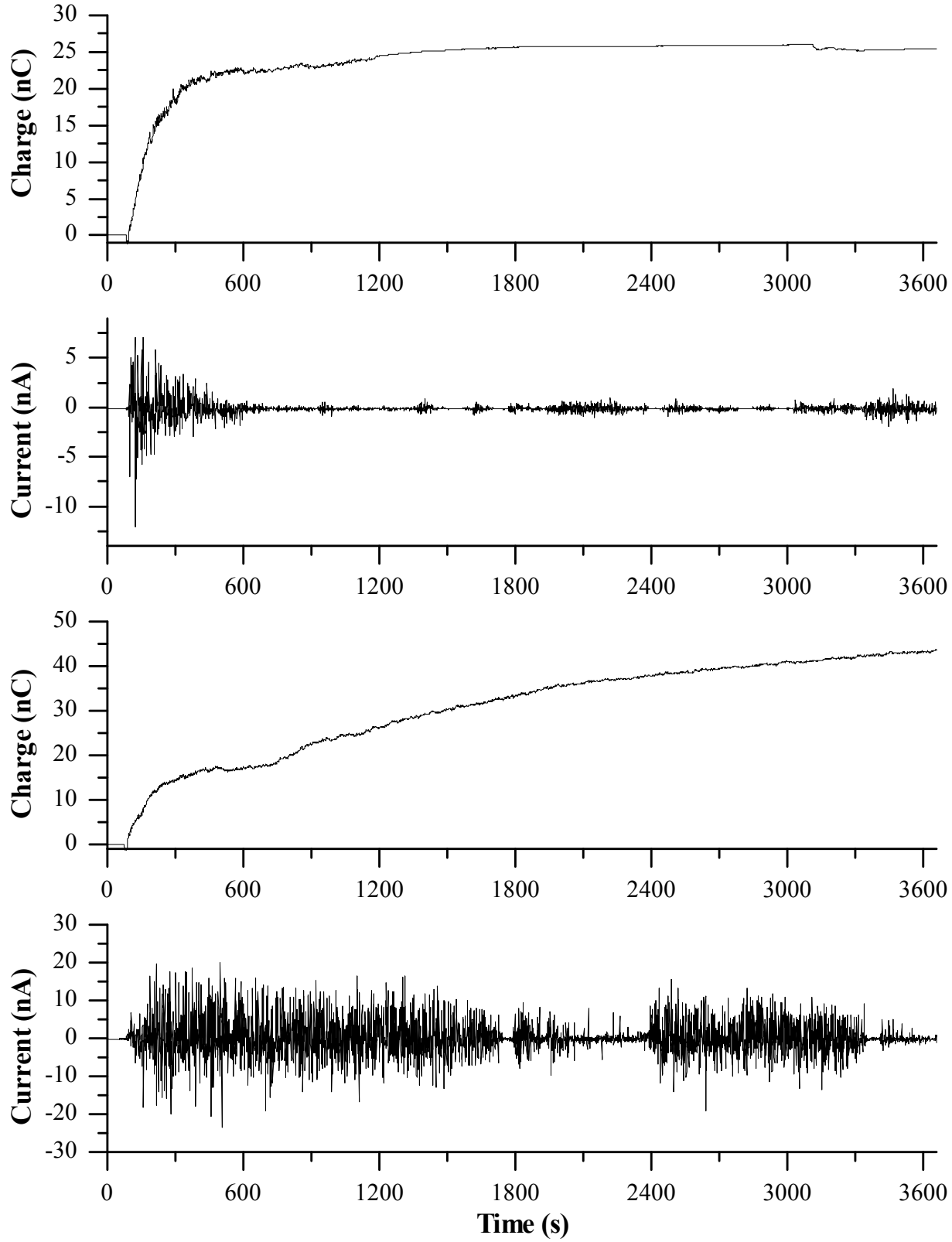


Figure 8.25: The current and charge measurements for trials with Additive A for 60 min of fluidization with PE_C.

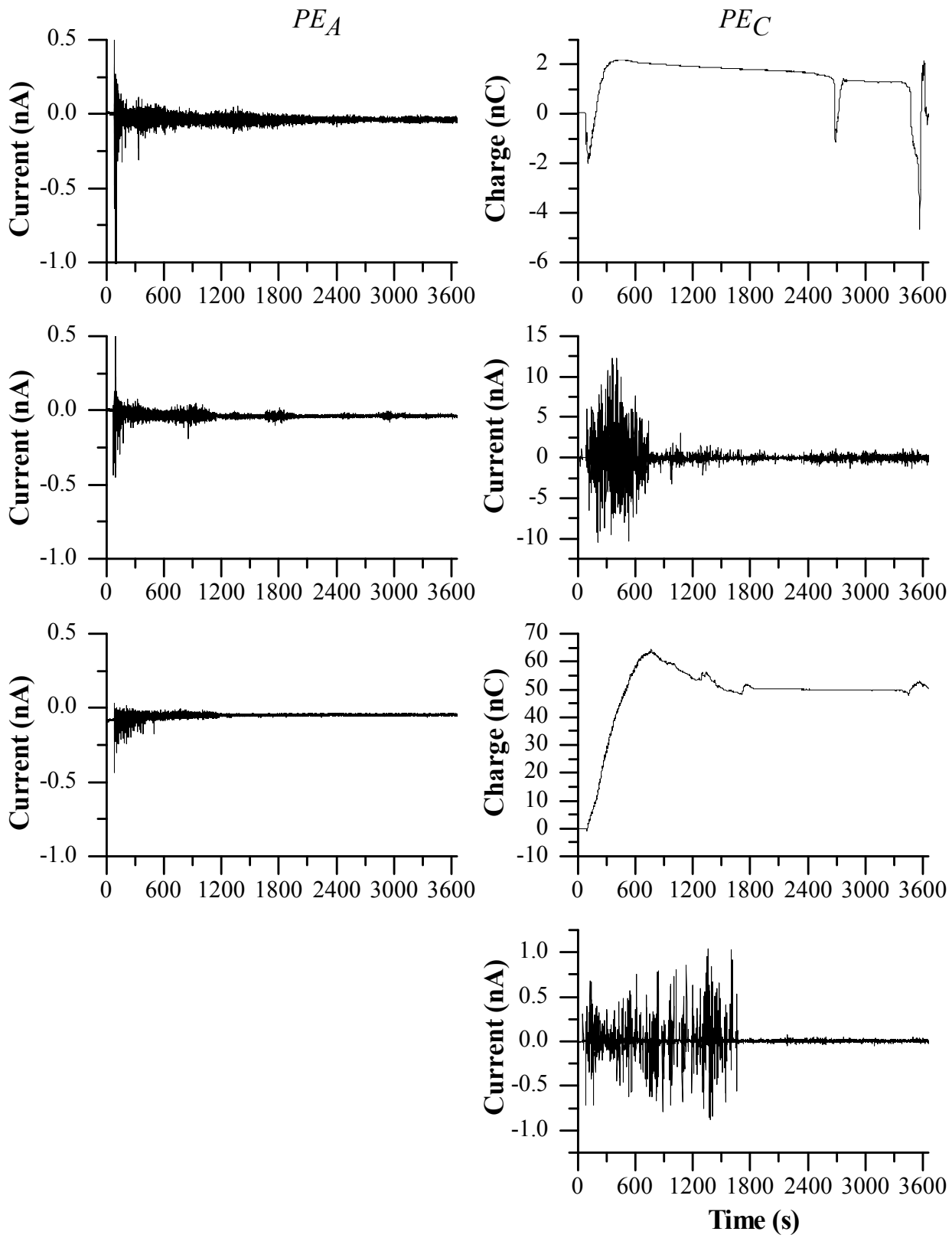


Figure 8.26: The current measurements for trials with Additive B for 60 min of fluidization with PE_A and PE_C resin.

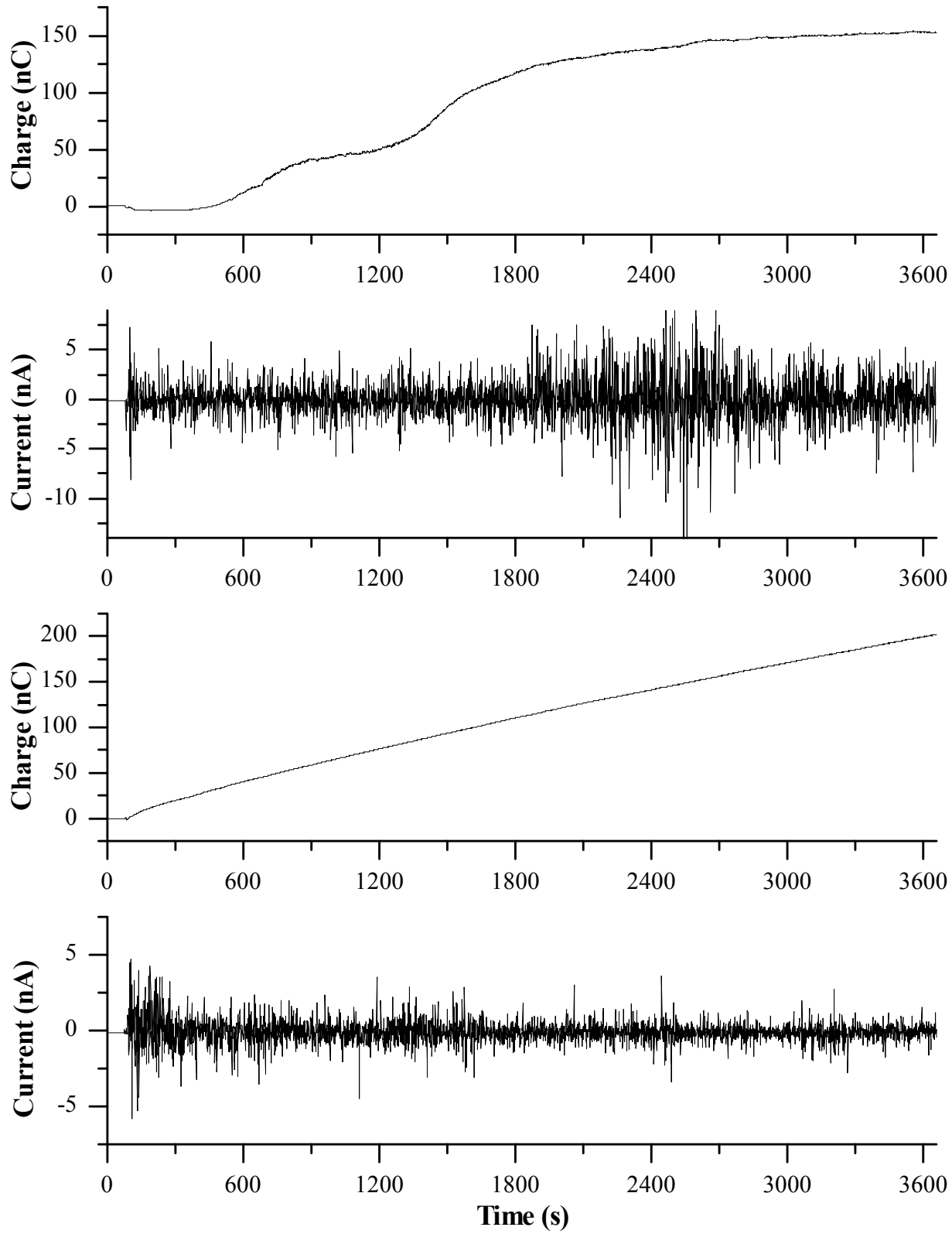


Figure 8.27: The current measurements for trials with Additive C for 60 min of fluidization with PE_C resin.

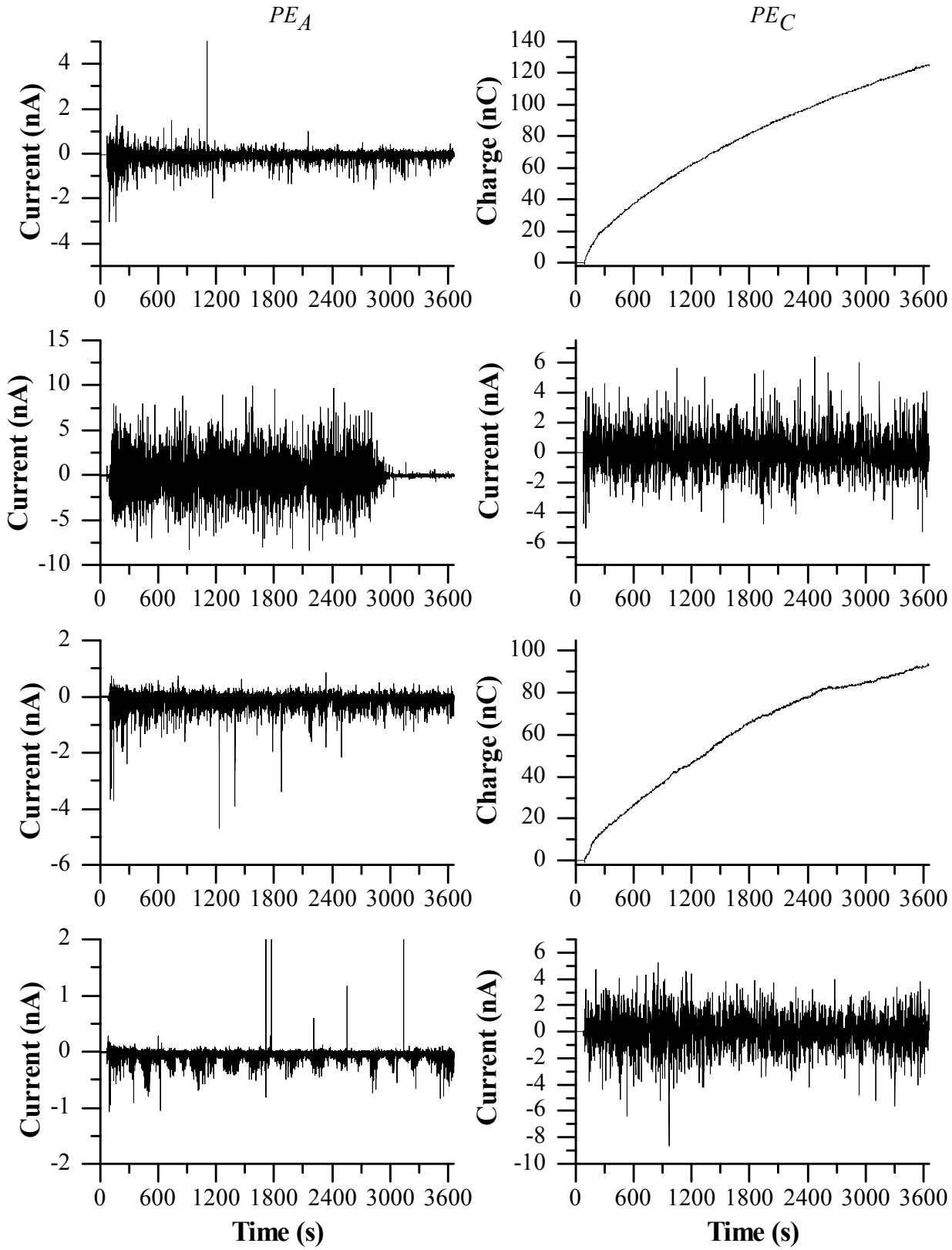


Figure 8.28: The current measurements for trials with Additive F for 60 min of fluidization with PE_A and PE_C resin.

8.2.3. Additional Experiments with Additive B

Additional experiments were performed with PE_C particles using Additive B in order to determine the underlying mechanisms that made this additive the most effective in reducing electrostatic charges and reactor wall fouling. Specifically, experiments were conducted to identify as whether its influence was due to its coating the column wall or coating of the PE particles and thus reducing the interactions between these surfaces. This was achieved with the following experiments:

1. First the effect of Additive B coating the column wall was examined. Additive B was injected into an empty column while the fluidizing gas was sent through the system. Additive B was then entrained through the system and some of the particles coated the column wall as could be seen in Figure 8.8. After the additive coated the column wall, three types of fluidization experiments were performed:

   B_C-PE: The PE resin was added to the fluidized bed and a typical 60 minutes fluidization experiment was conducted. This experiment had Additive B on the column wall and some on the distributor plate.

   B_C-PE-B-I: After Additive B coated the column wall, any additive particles that remained on the distributor plate (those seen in Figure 8.8) were removed by vacuuming the particles out through a port at the bottom of the column, without disturbing the wall coating. The PE resin was then added to the fluidization column followed by another 0.1 m% of Additive B injected into the bed of the particles. A typical 60 minutes fluidization experiment was then conducted. This experiment effectively had Additive B present on the column wall and within the bed of particles.

   B_C-PE-B-II: After Additive B coated the column wall, any additives that remained on the distributor plate were subsequently removed. PE resin was then added to the fluidized bed and a typical 60 minutes fluidization was performed. This experiment had Additive B only present on the column wall.

2. The effect of multiple injections of Additive B (**PE-B_{MI}**) was also investigated to determine whether a continual addition of the additive was an effective way of reducing the particle wall fouling in the system. A portion of the 0.1 m% of Additive B was injected into the fluidization column prior to fluidization, at 15 min, 30 min, and 45 min into fluidization. This would be similar to more continuous additive injection in industrial applications.

3. To determine whether the effectiveness of the additive had any time dependency, experiments with were performed for 15 minutes of fluidization in comparison to the usual trials conducted for 60 minutes. Similarly, experiments with no additive were performed, as a control, for 15 minutes. If Additive B has a finite amount of effective time then this effect may be shown in only the first 15 minutes of the fluidization. As time progresses, the influence of the additive could be diminished, leading to the increase in the wall coating up to 60 minutes of fluidization.

4. Finally, to mimic more of an industry-like setting where both the catalyst and the static control agents are present, both Additive B (prostatic agent) and Additive F (deactivated metallocene catalyst) were each added at 0.1 m% to the system (**PE-B-F**). As shown in §8.2.2, Additive F promoted reactor wall fouling. In the current experiments, prior to fluidization, Additive B was injected into the bed of PE resin in three radial positions. Additive F was then injected all at once into the bed close to the column wall. The particles were then fluidized for 15 and 60 min to test for time effects as well. Since the deactivated catalyst had a light beige colour, it was possible to visibly detect these particles in the Fines, Loosely Bound, and Tightly Bound regions, signifying the extent of its migration to different locations of the bed.

8.2.3.1. Mass

Figure 8.29 presents the particles mass collected in different regions of the bed for different types of experiments performed. From the comparison of results it was evident that injecting Additive B into the bed of PE particles (i.e., PE-B, B_C-PE-B, B_C-PE-B-I) had the most effect on the reduction of the degree of reactor wall fouling. With the pre-coating of the column wall, the results were very similar to tests done without any additive present. This suggests that either the

coating was not effective enough, or the major influence of Additive B was through particle-particle interactions.

Multiple injections of Additive B into the bed were only slightly better at reducing the amount of wall fouling compared to injecting no additive. This might be attributed to the amount of additive that was injected each time that may not have been enough. Only a fraction of the total 0.1 m% (approximately 0.25 g) of additive was injected at a time. This amount could perhaps not be sufficient to make a large enough difference in the particle-particle interactions in the system as less PE particles would subsequently be coated. In addition, over time some of the additive would leave the system such that when the next injection occurs, there would still not be enough additive to make a large impact.

Next set of experiments was performed to approximately represent the real system where a binary mixture of Additives F and B was injected into the bed of PE resin. Overall, the binary additive mixture injection resulted in the least amount of particle wall fouling. Since Additive B and Additive F charged oppositely when in contact with the carbon steel column wall as shown in §8.2.1, likely caused for the positively charged Additive F to adhere to negatively charged PE particles and negatively charged Additive B to adhere to positively charged PE particles, effectively reducing the net charge of the particles and ultimately the electrostatic force attracting the PE particles towards the column wall. This can also be seen with the insignificant mass of the Tightly Bound particles when them the mixture of the additives was used.

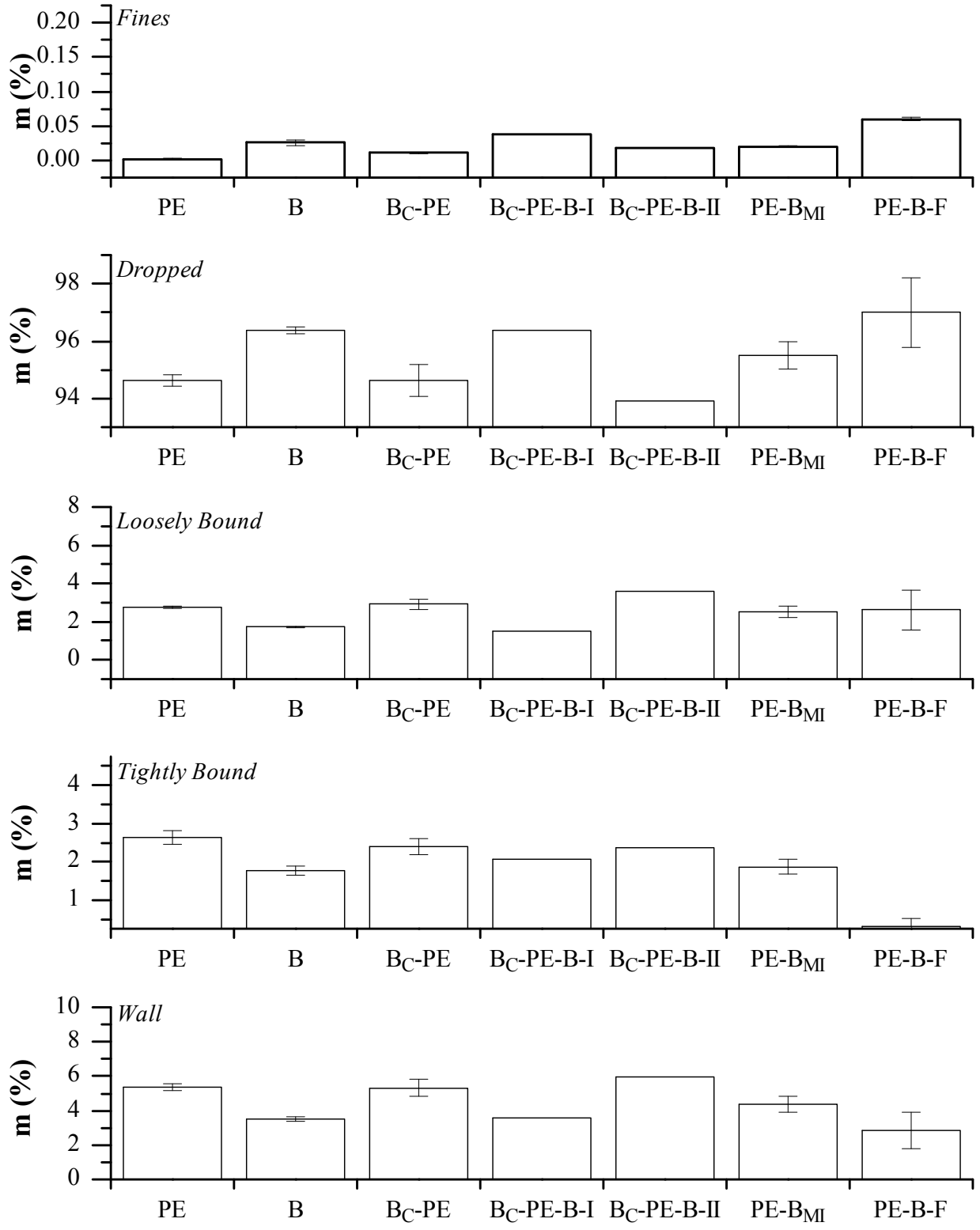


Figure 8.29: The m% particles in the Fines, Dropped, Loosely Bound, Tightly Bound, and Wall regions of the fluidized bed after 60 min of fluidization with different Additive B experiments.

Next the effectiveness of time on injecting Additive B, and mixture of B and F were investigated. Figure 8.30 shows the m% of the particles found in various regions of the fluidization system with and without additive for different fluidization periods of 15 and 60 minutes. Results clearly indicated that the fluidization time did not influence the magnitude of particles mass collected in the Dropped and Wall regions for any of the additives mixtures injected. However, there was a decrease in the amount of Loosely Bound particles with Additive B present at the longer fluidization period translating to presence of more Tightly Bound particles adhering to the column wall. Overall, this signifies that Additive B was effective at reducing the total amount of particles bound to the wall by making the majority of the particles easily removable from the wall when the column was tapped. However, over time Additive B did lose some of its effectiveness as the amount of Tightly Bound particles increased (nearly doubled) between 15 and 60 min experiments. The reason could be that over the full 60 minutes some of the Additive B was already elutriated from the system and thus the system became less effective. The binary additive mixture of Additives B and F reduced the amount of wall fouling in the system as well as the amount of Tightly Bound particles, more so than with Additive B alone. This may have been caused by the presence of both Additive B and F in the Wall region of the bed. This will be further discussed in more detail in §8.2.3.3.

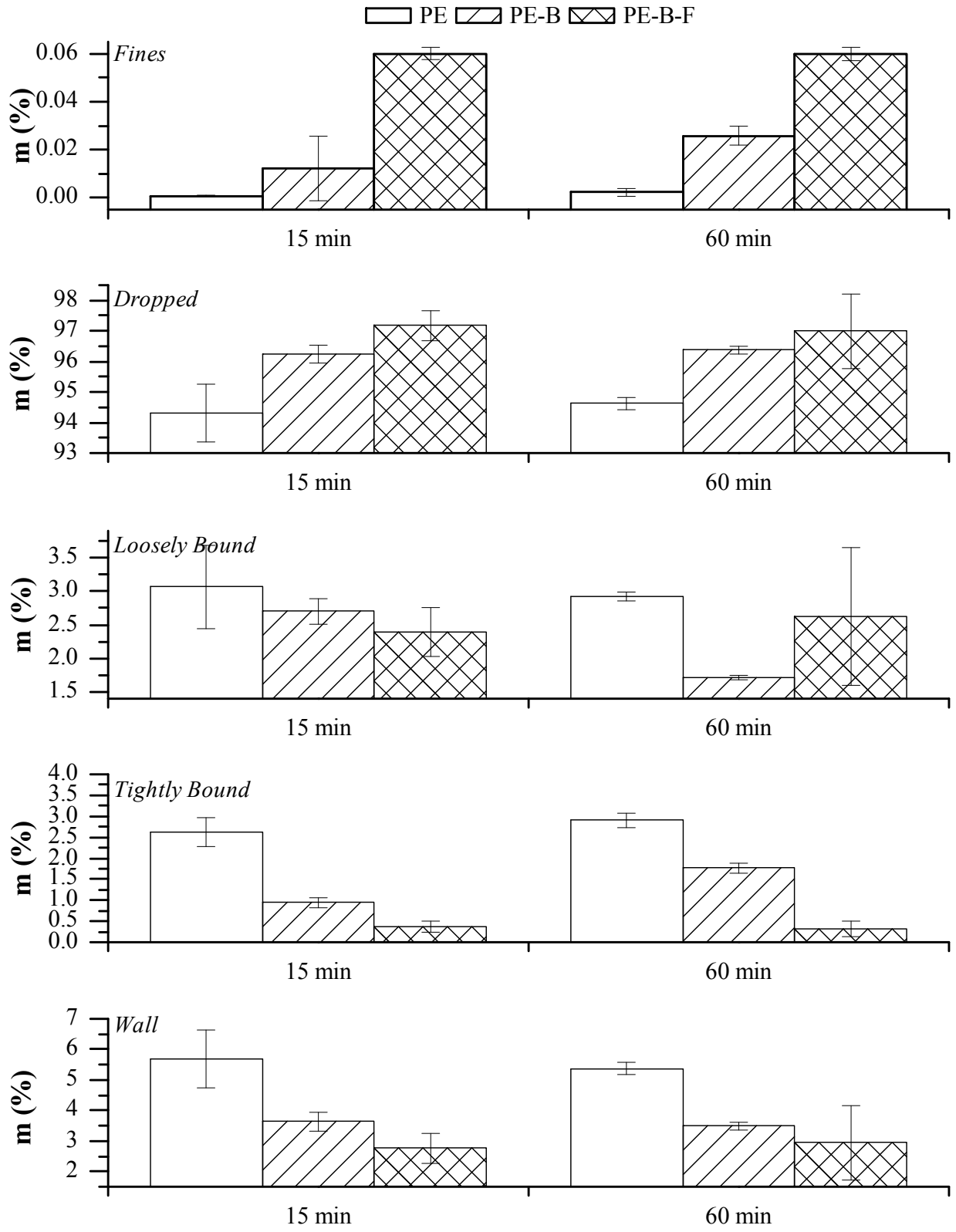


Figure 8.30: The particles m% found in the Fines, Dropped, Loosely Bound, Tightly Bound, and Wall regions of the fluidized bed after 15 and 60 min of fluidization with different Additive B experiments.

8.2.3.2. PSD

Figure 8.31 presents the d_P50_N of the particles for the Initial, Fines, Dropped, Loosely Bound, and Tightly Bound regions of the fluidized bed different experiments. The Fines had relatively the same normalized median diameter for all types of experiments suggesting that although the majority of the Fines were additives, some fine PE particles were present. The PSD performed on the Dropped particles showed very little difference regardless whether or not any additive was added. It is important to note that the presence of any additive within these particles is not detectable because of the quantity and size of the additive which was significantly smaller in comparison to those of the PE particles. Similar to the Dropped particles, the Loosely Bound particles showed very little variation. There was a decrease in the size of the Tightly Bound particles in the tertiary mixture compared to the other Additive B experiments. Due to the low mass of Tightly Bound particles, these particles were the first layer of particles and therefore on average the smallest, as discussed in Chapter 5. Overall however, the presence of Additive B along the column did not affect the size of the particles that migrated to the wall.

The effect of fluidization time on the particles d_P50_N results is shown in Figure 8.32. Overall, the d_P50_N remained relatively constant over time and in the presence of a combination of both additives.

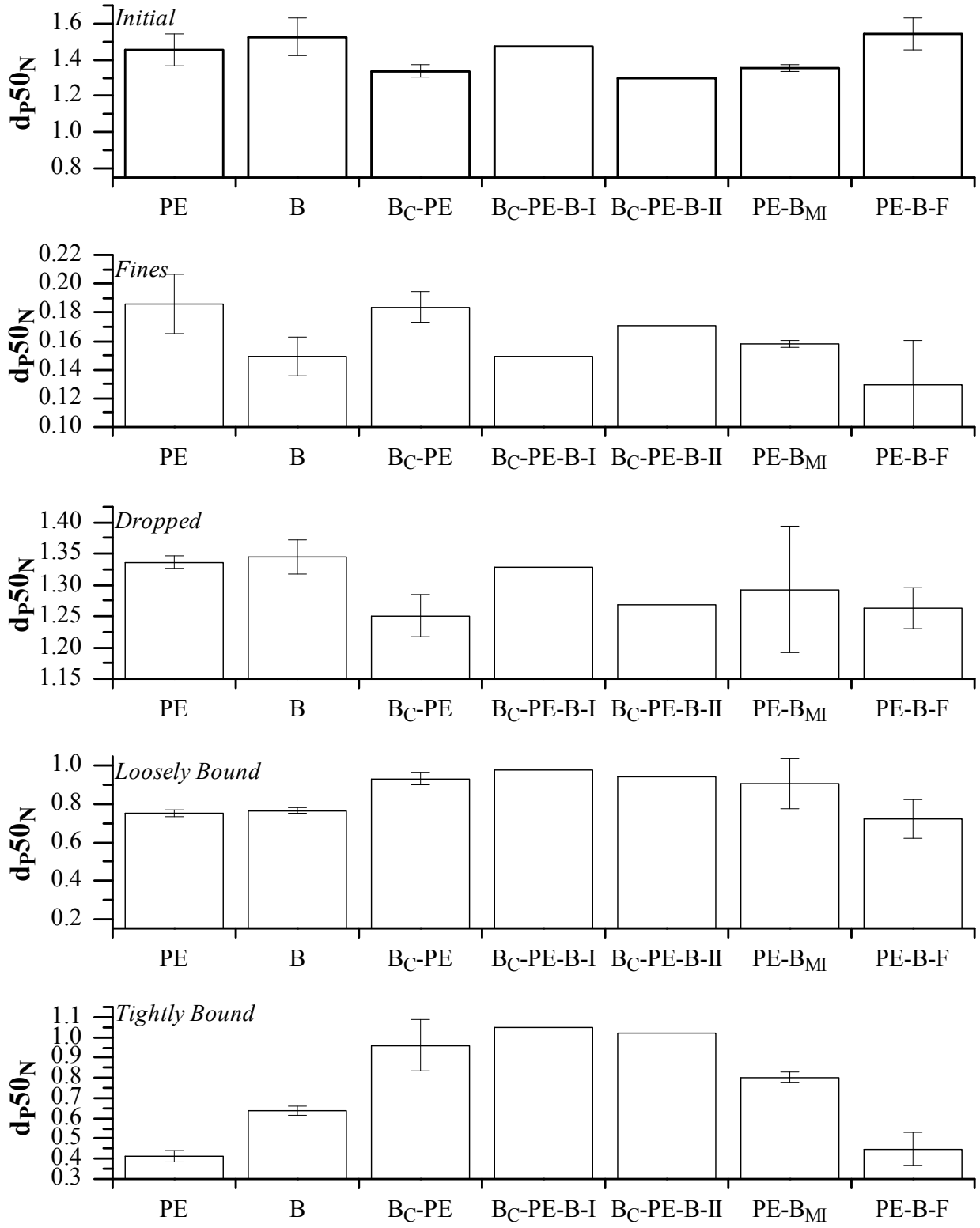


Figure 8.31: The d_P50_N of particles collected from the Initial, Fines, Dropped, Loosely Bound, and Tightly Bound regions of the fluidized bed after 60 min of fluidization with different Additive B experiments.

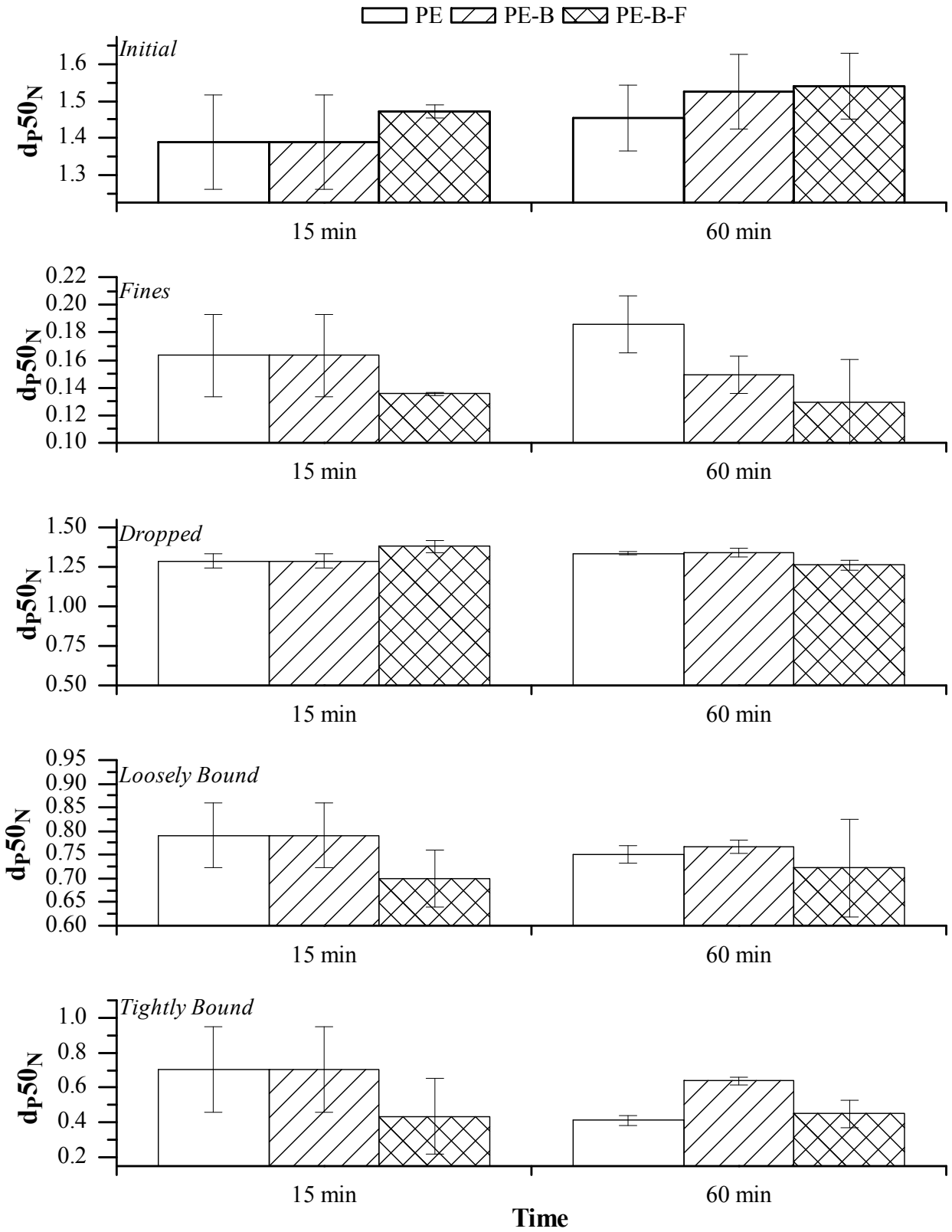


Figure 8.32: The d_P50 of particles from the Initial, Fines, Dropped and Loosely Bound regions of the fluidized bed after 15 and 60 min of fluidization with different Additive B experiments.

8.2.3.3. Particles Absolute Charge and Specific Charge

Figure 8.36 shows examples of the cumulative charge of Fines for experiments with and without any additive. Without any additive, results showed that the entrained Fines were predominantly positively charged and the cumulative charge increased during fluidization.

With the pre-coating experiments as shown in Figure 8.34 the q of the Fines were usually predominantly negatively charged with the exception of the B_C-PE trial which behaved similarly to when no additive was present. This was caused by the additive being only present on the column and therefore not likely to be entrained from the system. With the presence of the mixture of Additives B and F, the cumulative charge of the particles increased similar to the Additive F only experiments shown in Figure 8.19 and then decreased over time. Additive B alone also showed this initial increase in charge before decreasing. Therefore the initial increase in positive charges were likely caused by some of the positively charged Additive B being quickly entrained from the bed followed by some positively charged Additive F being entrained from the bed. Then negatively charged Additive B particles were elutriated from the fluidization column, which effectively decreased the cumulative charge.

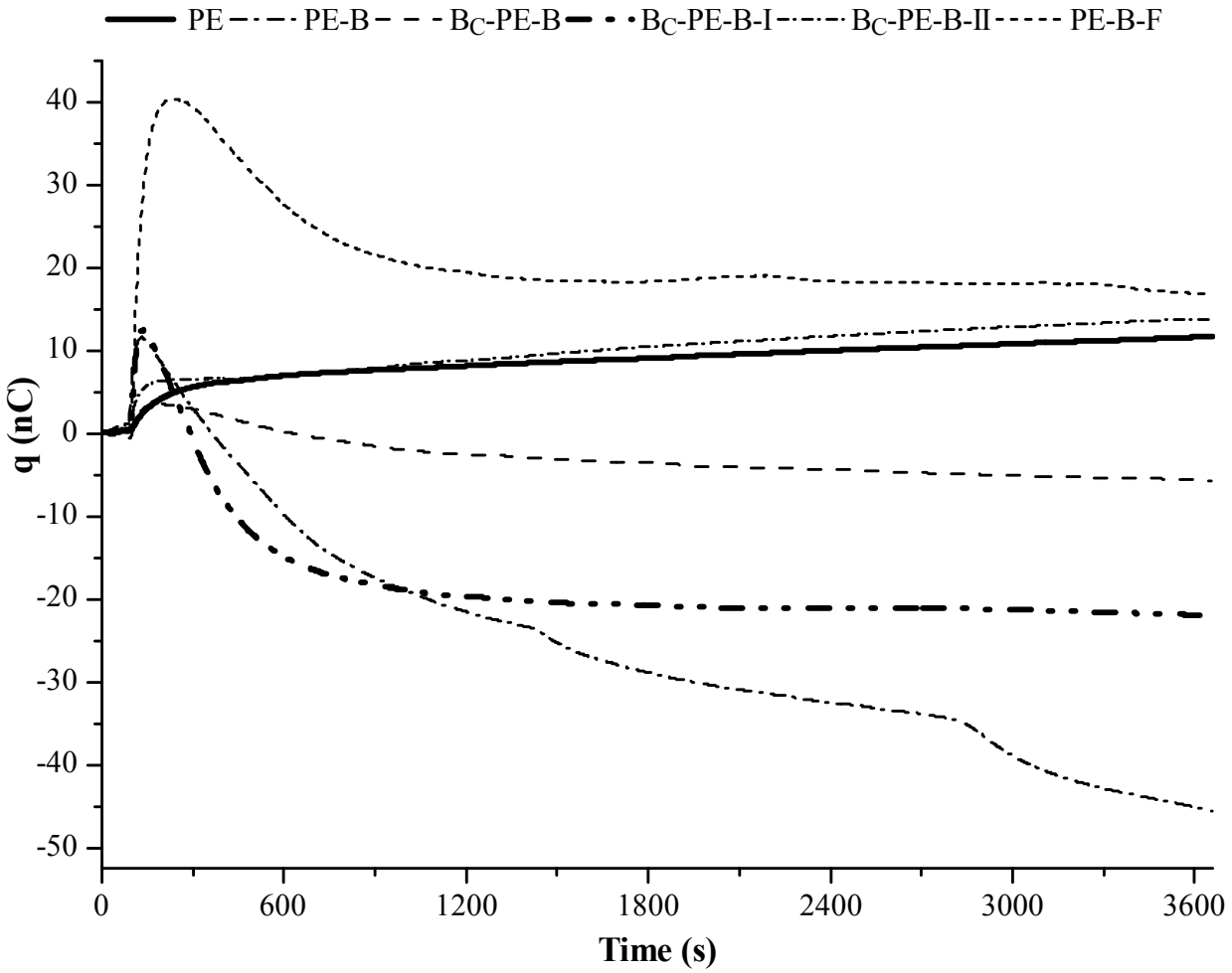


Figure 8.33: Examples of the cumulative charge of Fines under different Additive B experiments for 60 min of fluidization.

With multiple injections of Additive B it was expected that there would a noticeable difference in the cumulative charge measurement of the Fines in comparison to other cases. This was found to be true as shown in Figure 8.34 where every time Additive B was injected into the bed a slight increase in positive charge was obtained before a sharp decrease was followed. An example of the cumulative charge for a PE-B trial was also plotted with the PE-B_{MI} trialed for comparison purposes. It can be seen that there was a larger initial peak with the PE-B trial than with the multiple injections. With the PE-B experiment, the entire 0.1 m% of Additive B was injected into the bed prior to fluidization, which means that more Additive B would have been elutriated from the bed. With the multiple injections, only a fraction of Additive B was present prior to fluidization and therefore there was less of a peak. From Figure 8.34, it can be seen that there was a positive peak in the measured charge upon each injection, but the magnitude of positive

charge was reduced every time the injection was performed. This was possibly due to a decrease in the amount of Fines that were released even though the quantity of Additive B on each injection was approximately equivalent. Since there were less of a cumulative charge leaving the bed, this either means that either the particles being elutriated from the bed were less charged, or there were less particles being elutriated.

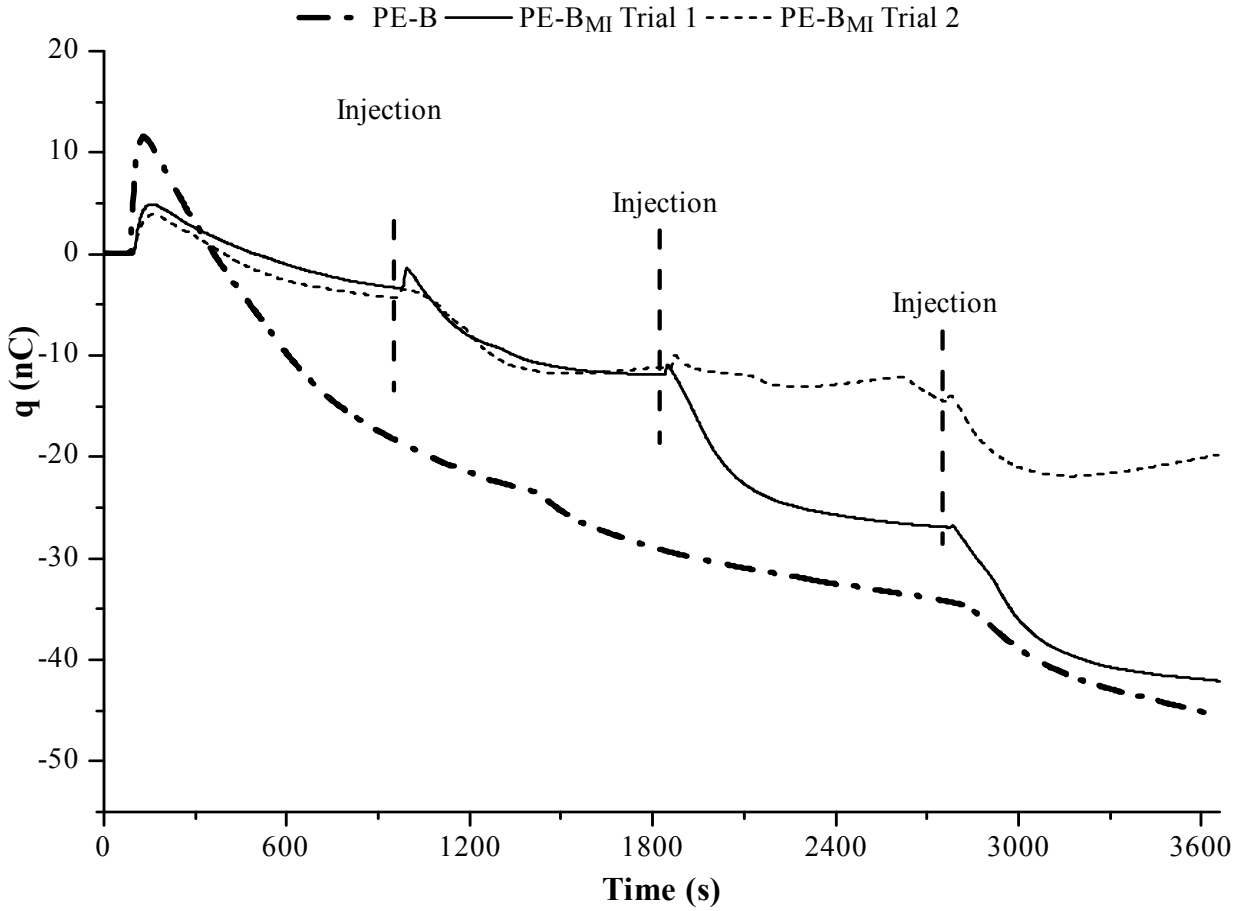


Figure 8.34: Examples of the cumulative charge of Fines with Additive B injected every 15 minutes into the fluidized bed over 60 minutes of fluidization and Additive B injected prior to fluidization (PE-B).

The net q/m of the Initial, Fines, Dropped, and Loosely Bound particles for different Additive B experiments are presented in Figure 8.35. Overall, the q/m of the Initial particles was relatively constant with the exception of two trials with pre-coating which deviated from the average. This would be caused by the uncontrollable nature of the initial charge of the industrial resin. The Fines had mostly a negative net q/m with different Additive B experiments, with the exception of the B_C-PE-B-II experiment where Additive B was only present on the column wall, therefore

none of the additive particles were elutriated from the bed. The reason for the large variation in q/m when no additive was present was caused by the low mass of Fines collected during the 60 min of fluidization as discussed previously.

Interestingly, the experiments with pre-coated column wall with Additive B resulted in Dropped particles becoming more positively charged, while the Loosely Bound particles became less negatively charged which will be discussed in more detail below. With the pre-coating experiments the q/m of the Loosely Bound particles was slightly less negative than with Additive B alone. Coating the column wall prior to fluidization would reduce the number of PE particle-carbon steel wall interactions and increase the number of PE particle-additive interactions. If some of the additive also coated the PE particles, then there would also be more additive-additive contacts, which would reduce the amount of charging close to the column wall. As seen in Figure 8.29, the mass of Loosely Bound particles was similar for the case of the pre-coated column wall and no additive trials. However, the q/m results of particles for the former case were less negative. This translates to particles from the pre-coated trial being less negatively charged, confirming the hypothesis that pre-coating reduced the PE particle-metal wall interactions. The q/m of the Loosely Bound particles is similar with and without Additive B present. However, Figure 8.29, showed that the mass of these particles was smaller when Additive B present, indicating that their charge must have been less negative as well.

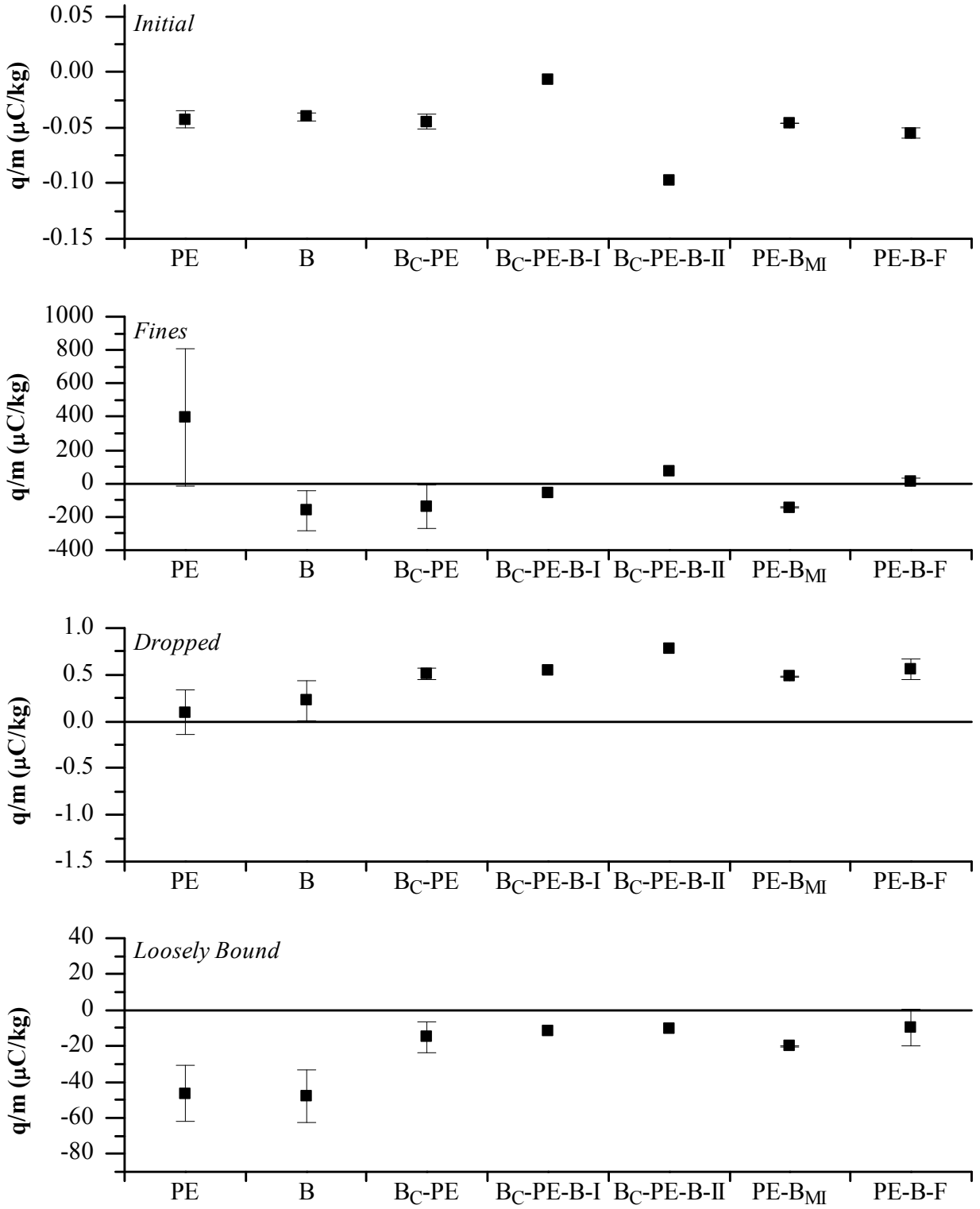


Figure 8.35: The net q/m of the particles found in the Fines, Dropped, Loosely Bound, and Wall regions of the fluidized bed after 60 min of fluidization with different Additive B experiments.

Multiple injections of Additive B also led to a decrease in the negativity of the Dropped particles as well as the Loosely Bound particles. The injections were to attempt to maintain a constant amount of Additive B in the system throughout the fluidization period. It appeared as though that this method was effective in altering the particles net charge in the Dropped and Loosely Bound region but was not effective in reducing the amount of fouling in the system. This may be caused by only approximately 0.025m% of Additive B was added at a time and therefore may not have been enough in the system at one given point of time.

The mixture of Additive B and F also resulted in a smaller q/m, likely from the presence of the positively (Additive F) and negatively (Additive B) particles in the wall layers. This is discussed in more detail with the fluidization time experiments below.

Figure 8.36 shows the cumulative q of entrained Fines during 15 min of fluidization where results show a similar trend for the cumulative charge with and without Additive B suggesting that both fluidization periods behaved similarly as well. Without Additive B after approximately 200 s, the cumulative charge started to plateau signifying that the PE fines were likely completely entrained from the system. With Additive B present after approximately 200 s the cumulative charge started to decrease rapidly. This likely constitutes to the elutriation of Additive B from the bed. This also happened with the mixture of the additives where the cumulative charge increased rapidly before decreasing with the elutriation of additives. These two trends also agree well with the 60 min fluidization experiments (Figure 8.33). From the m% of the Fines (Figure 8.30) it is clear that more Fines exiting the system with Additive B present so it is likely that the sudden decrease in charge in the Fines is due to the elutriation of Additive B.

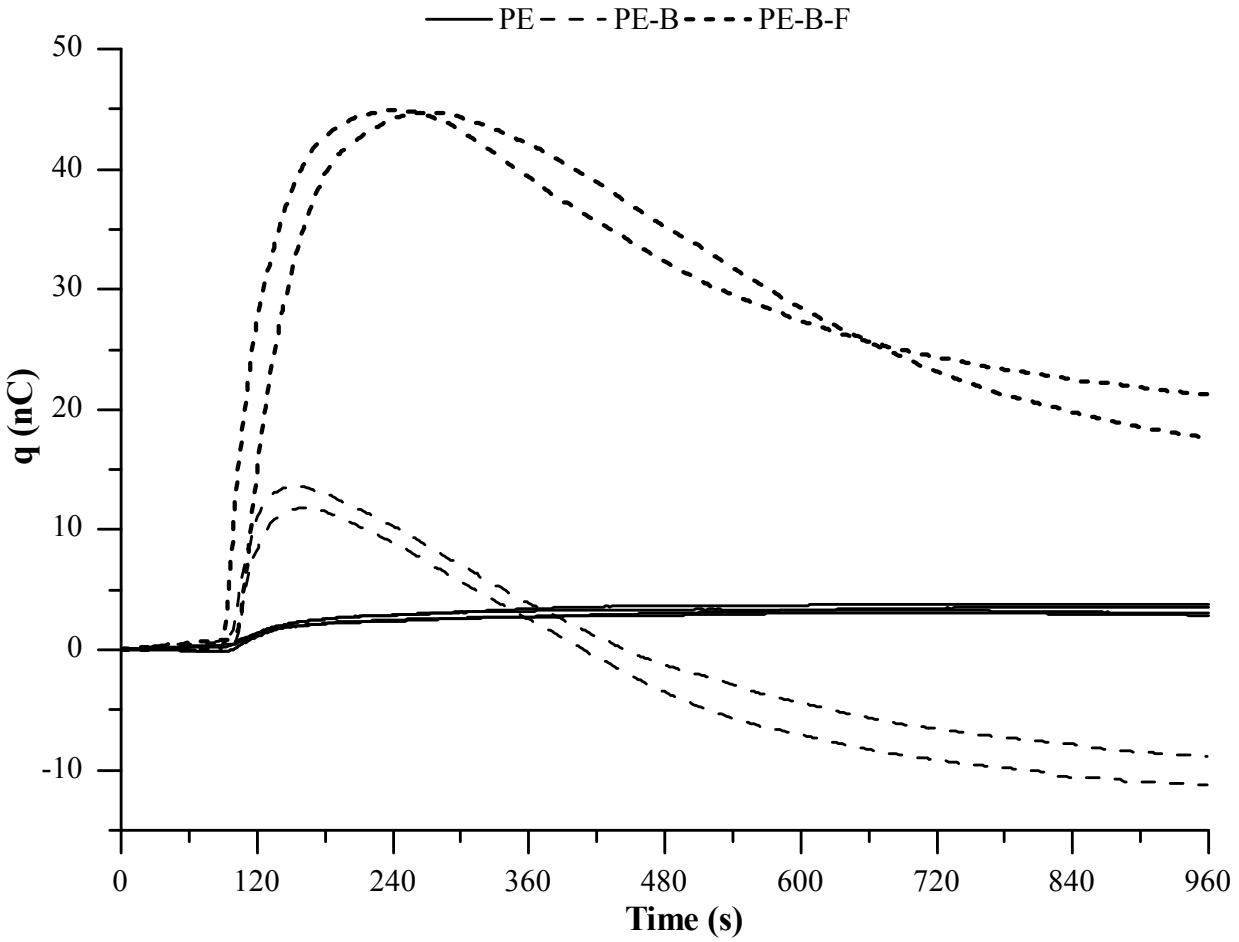


Figure 8.36: Examples of the cumulative charge of the Fines under different Additive B experiments during 15 min of fluidization.

The q/m of the particles in different regions of the fluidization column for different fluidization times are shown in Figure 8.37. In the presence of the mixture of Additives B and F, the charge of the Fines was close to neutral, suggesting that Additive B and F could be oppositely charged. This is true as can be seen from individual additive injection experiments in §8.2.2.4 where Additive F fines were positively charged and Additive B Fines were negatively charged. Similar to Additive B injection, the q/m of the Dropped and Loosely Bound particles with the mixed additive became more positive after 60 min of fluidization. This suggests that the combination of Additives B and F helped reduce the amount of charging in the system. This could have been from the additives coating the larger particles (both B and F) and since it appears as though they are oppositely charged, would not add a significant increase in charge to the system. This could reduce the amount of attractive/repulsive charges provided by the additives in the system. Another factor that could play a role is the amount of additive used. In total 0.2 m% additive (0.1

m% Additive B, 0.1 m% Additive F) exists in the system. The largest impact that may occur with the binary mixture of Additives B and F may come from the bi-polarity of the mixture. Additive B has been shown to charge negatively whereas Additive F was positively charged based on the interactions in the system, meaning that there existed highly mobile small positively and negatively charged particles that could adhere to difference oppositely charged areas on polyethylene particles and reduce the overall charge of the particles. This would in turn affect the amount of particles that would migrate and adhere to the column wall effectively reducing the amount of wall fouling in the system.

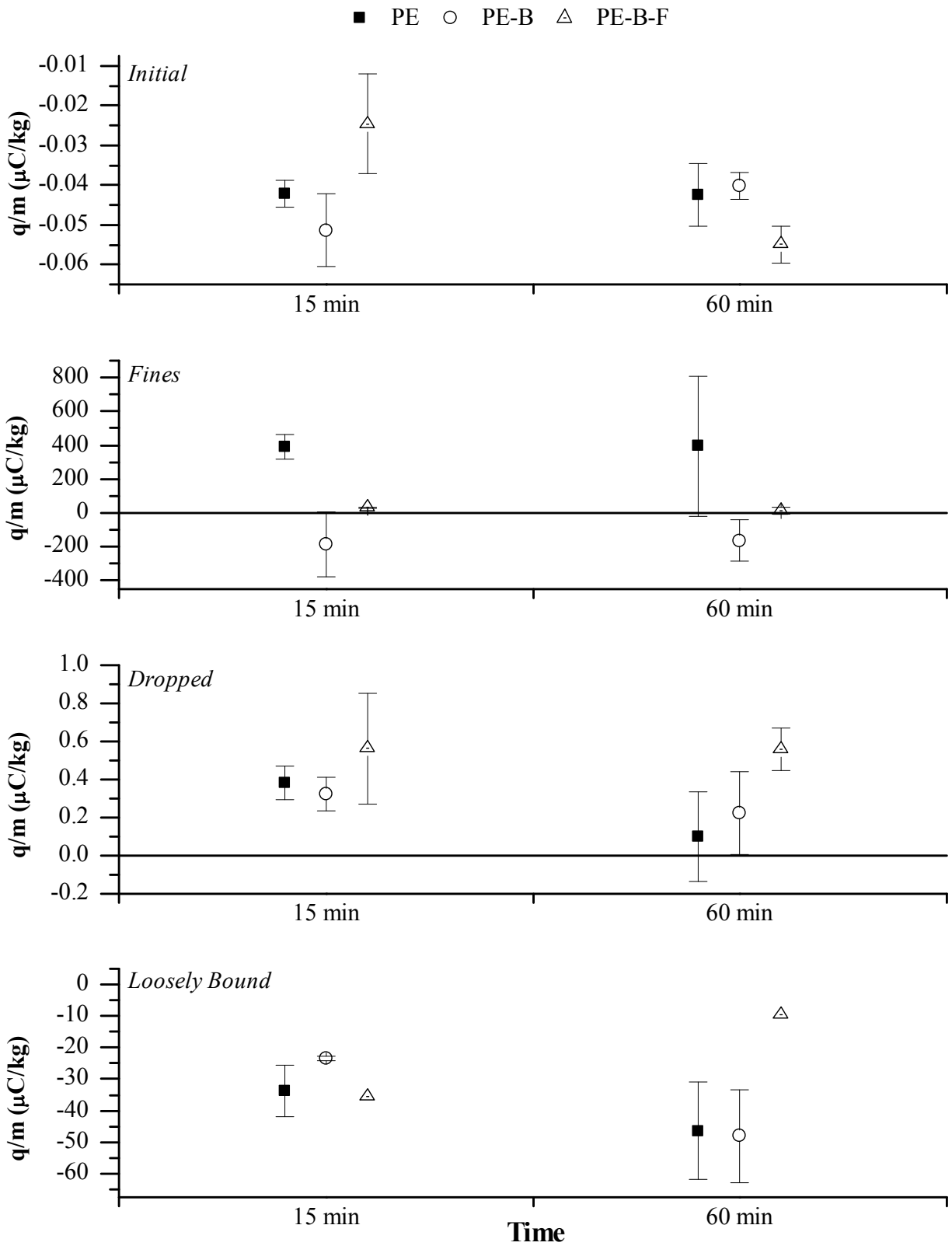


Figure 8.37: The particles net q/m in Initial, Fines, Dropped, and Loosely Bound regions of the fluidized bed after 15 and 60 min of fluidization with different Additive B experiments.

8.2.3.4. Specific Charge-to-Specific Surface Area Ratio

The $\hat{q}/\hat{A}$ of particles in different regions of the fluidized bed for different additive experiments are presented in Figure 8.38 for 60 min of fluidization. The $\hat{q}/\hat{A}$ for the Initial particles was relatively consistent and small in comparison to the magnitude of the other particles sizes. With the Fines, there was definitely a decline in the magnitude of $\hat{q}/\hat{A}$ when any of additive was used. This was most likely caused by the mass collected. Since the q/m was used to calculate the $\hat{q}/\hat{A}$ and there was very little mass with PE resin only, the q/m was very large, which caused the large $\hat{q}/\hat{A}$. The magnitude of the $\hat{q}/\hat{A}$ of the Dropped particles was on average approximately 10 times larger than the Initial particles, signifying the presence of some charging. The magnitude of the $\hat{q}/\hat{A}$ of the Loosely Bound particles in turn was on average approximately 10 times larger than the Dropped particles, which agrees well with the findings from the other chapters. The $\hat{q}/\hat{A}$ of the Loosely Bound particles was found to be less negatively charged in the pre-coating experiments and the binary additive mixture; however, on average the values were relatively similar, meaning that the additive experiments did not have a large effect $\hat{q}/\hat{A}$ in the different regions.

Figure 8.39 shows the $\hat{q}/\hat{A}$ of the Initial, Fines, Dropped, and Loosely Bound regions for PE, PE-B, and PE-B-F experiments at 15 and 60 min fluidizing gas velocity times. Overall the effect of fluidization time did not significantly alter the $\hat{q}/\hat{A}$ of PE particles in each of the regions.

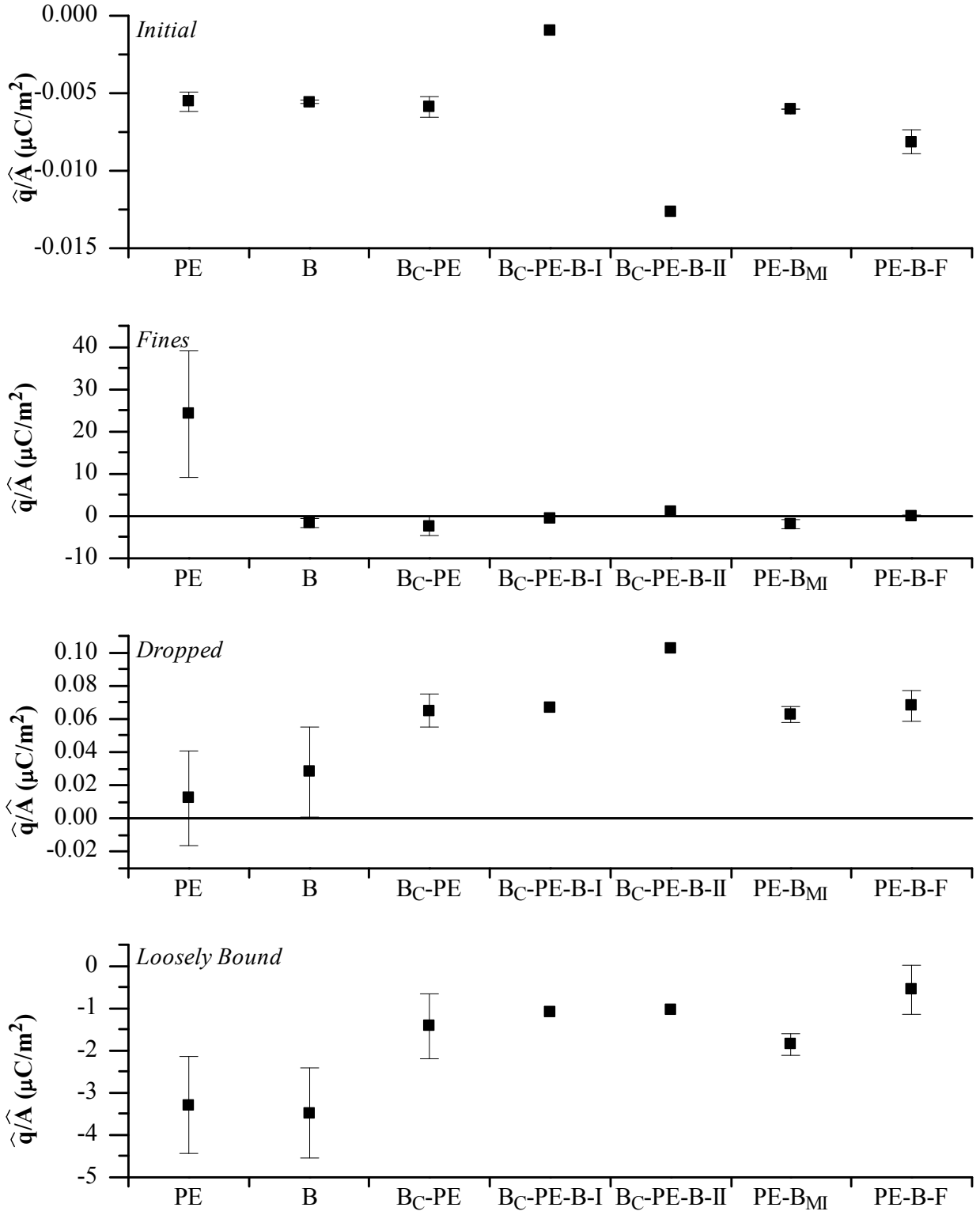


Figure 8.38: The net $\hat{q}/\hat{A}$ of particles in Fines, Dropped, and Loosely Bound regions of the fluidized bed after 60 min of fluidization with different Additive B experiments.

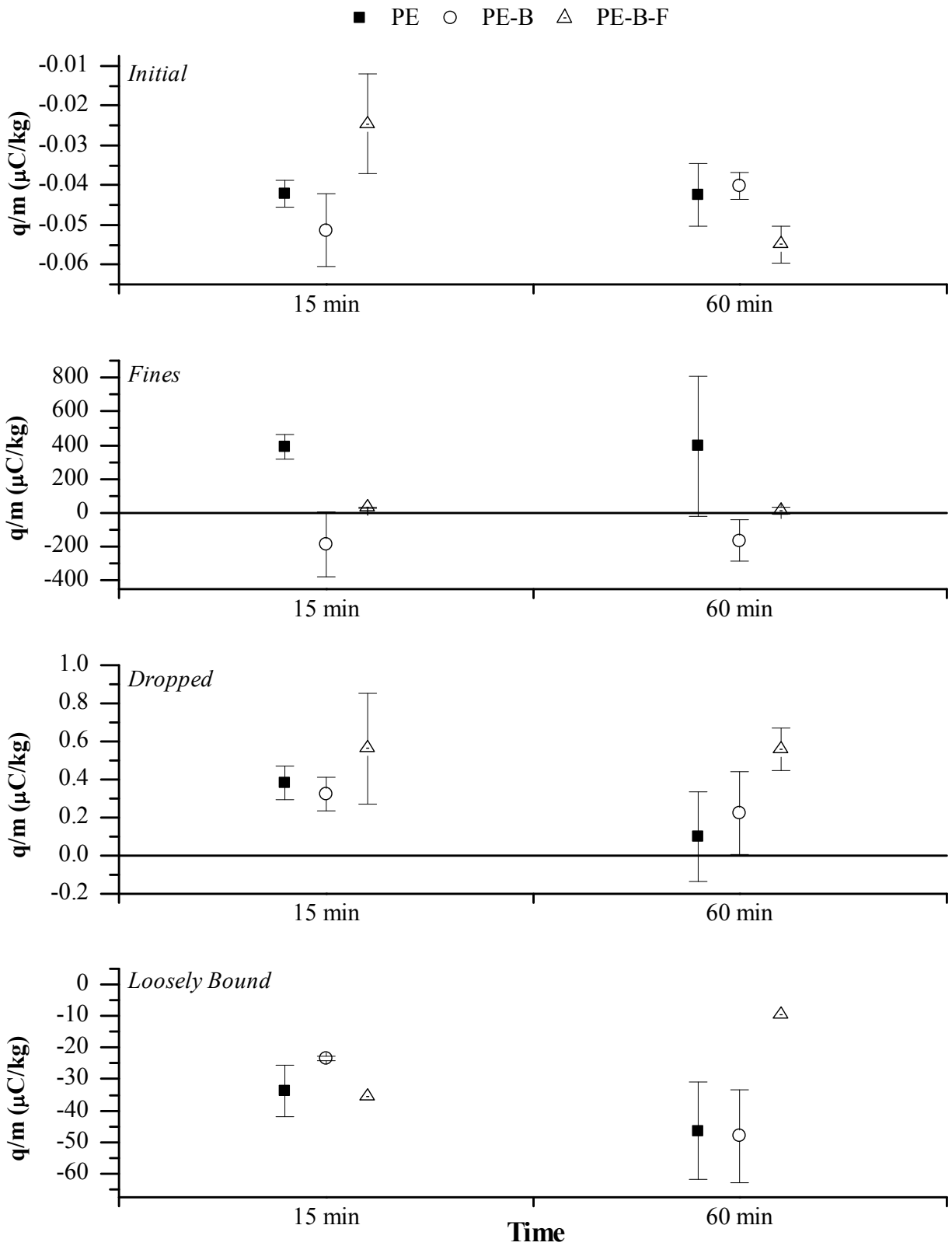


Figure 8.39: The net $\hat{q}/\hat{A}$ of different Additive B experiments in the Fines, Dropped, Loosely Bound and Wall regions of the fluidized bed after 15 min of fluidization.

8.2.3.5. Wall Layer Coating

Figure 8.40 shows some typical column wall pictures for trials with PE resin only, resin and Additive B, all three types of pre-coating and the multiple injection experiments. It can be seen that experiments with Additive B injected into the bed of particles had the least amount of particles adhered to the column wall, whereas no additive and the pre-coating experiments had similar amounts of wall fouling. Injecting Additive B multiple times also did not show any significant reduction in the amount of column wall fouling.

Figure 8.41 shows the wall fouling pictures without any additive, with Additive B, with Additive F, and with mixture of additives at 15 and 60 min fluidization times. It is evident that the magnitude of wall fouling was minimized in the presence of mixture of additives and the pictures agree well with the m% of the Wall particles shown in Figure 8.30. Overall, the amount of wall coating was relatively similar regardless of fluidization time indicating that the coating was formed within the first 15 minutes of fluidization. The effect of the additives would likely be the most effective during this time period, before some of the additive is elutriated from the fluidization column.

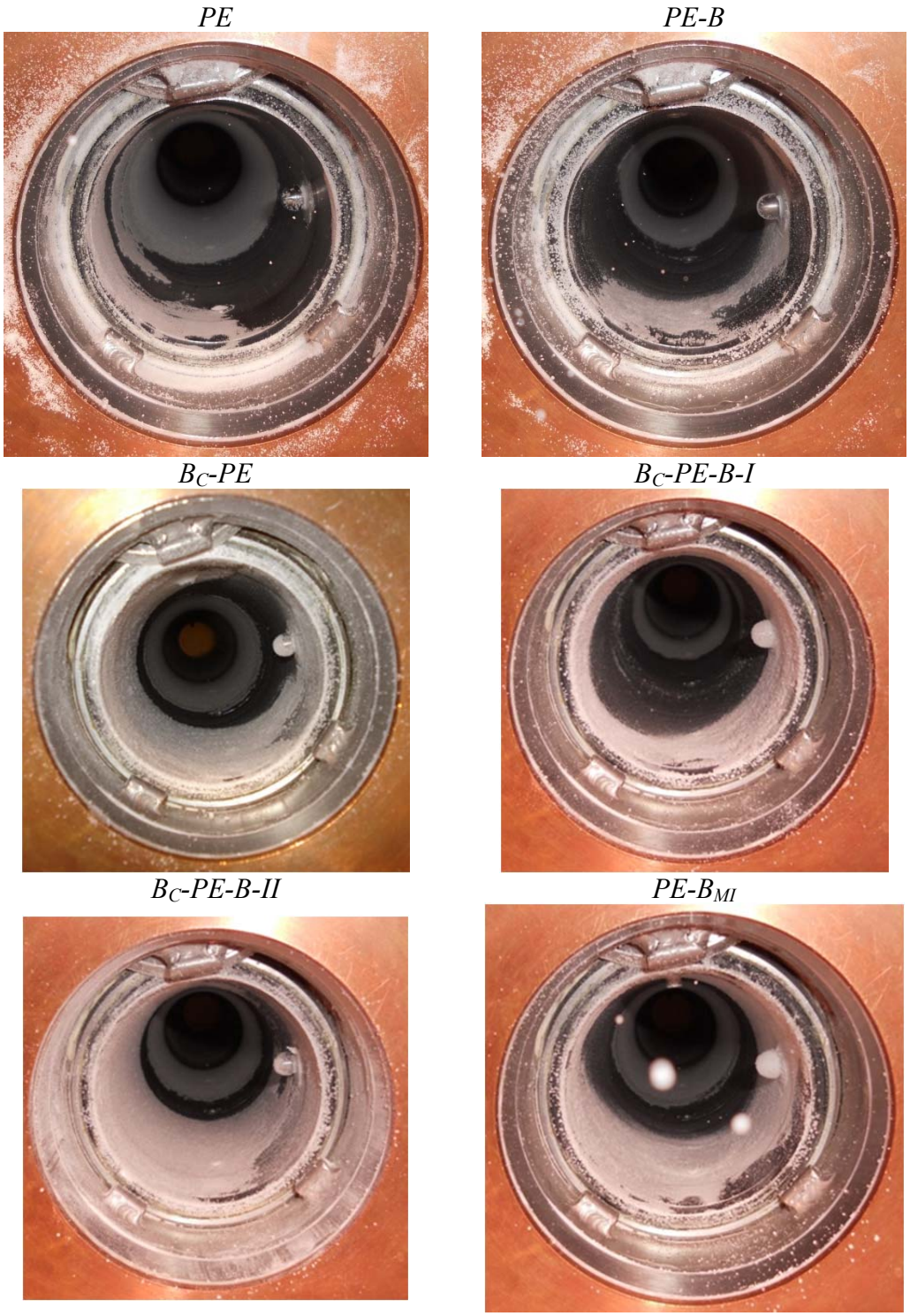


Figure 8.40: Typical pictures of the wall particle layer before removing the Loosely Bound particles with different Additive B conditions after 60 min of fluidization.

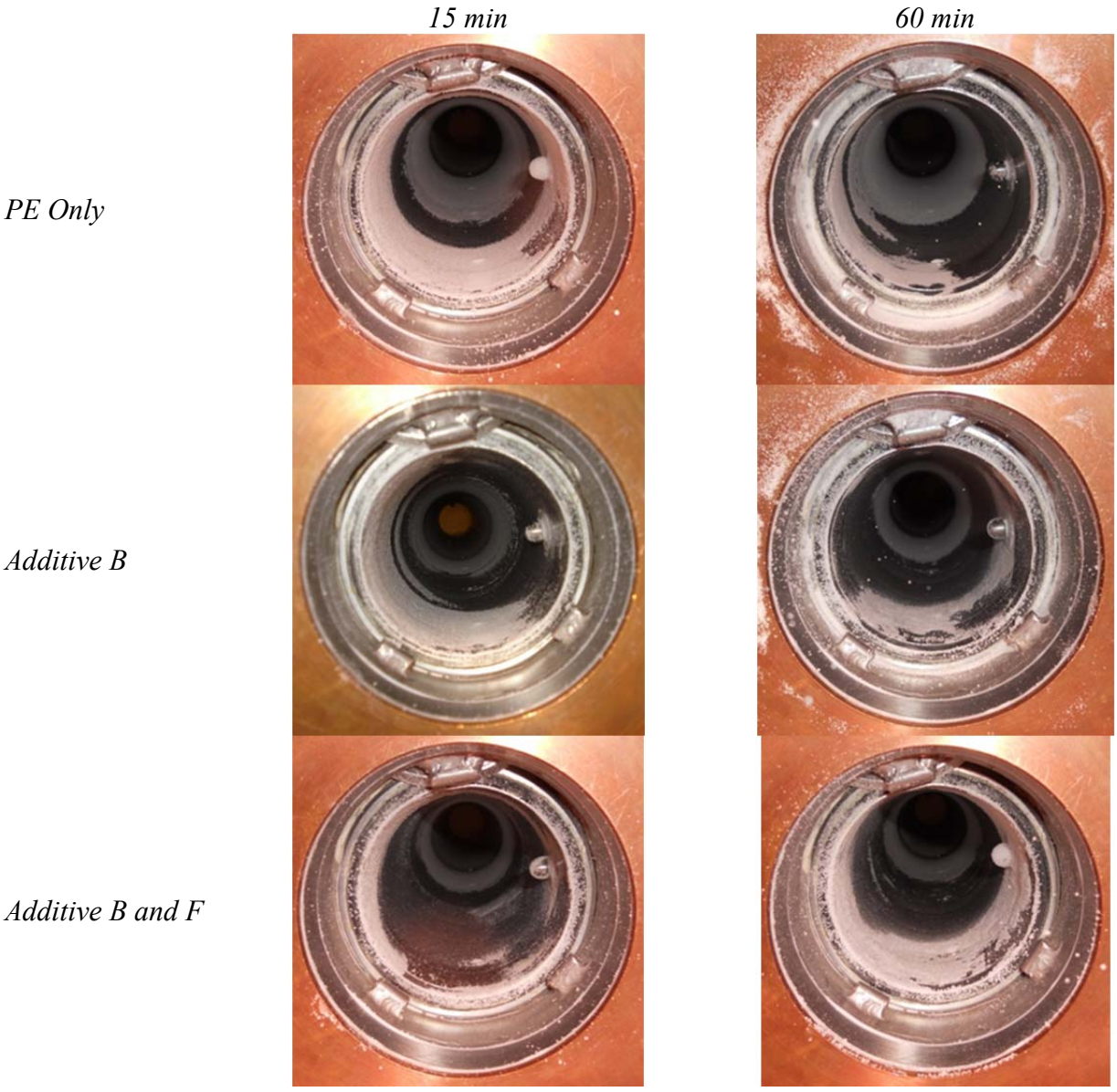


Figure 8.41: Typical pictures of the wall particle layer before removing the Loosely Bound particles with different Additive B conditions for different fluidization periods.

8.2.3.6. Electrostatic Probes

The current and cumulative charge measurements for the Additive B injected directly into the fluidization column and the pre-coating experiments are shown in Figure 8.42. Looking only at the current measurements, it is clear that pre-coating the column wall seems to have reduced the magnitude of the current measured. This would likely be attributed to Additive B coating the probe prior to fluidization as shown in Figure 8.8. It should be noted that injecting Additive B into the bed of particles was consistently better at reducing the amount of wall fouling in the

system than only pre-coating the column wall even though the magnitude of the current with the pre-coating was significantly smaller. This suggests that using the electrostatic probe to monitor the wall fouling for this system may not be a good measure of the amount of wall fouling.

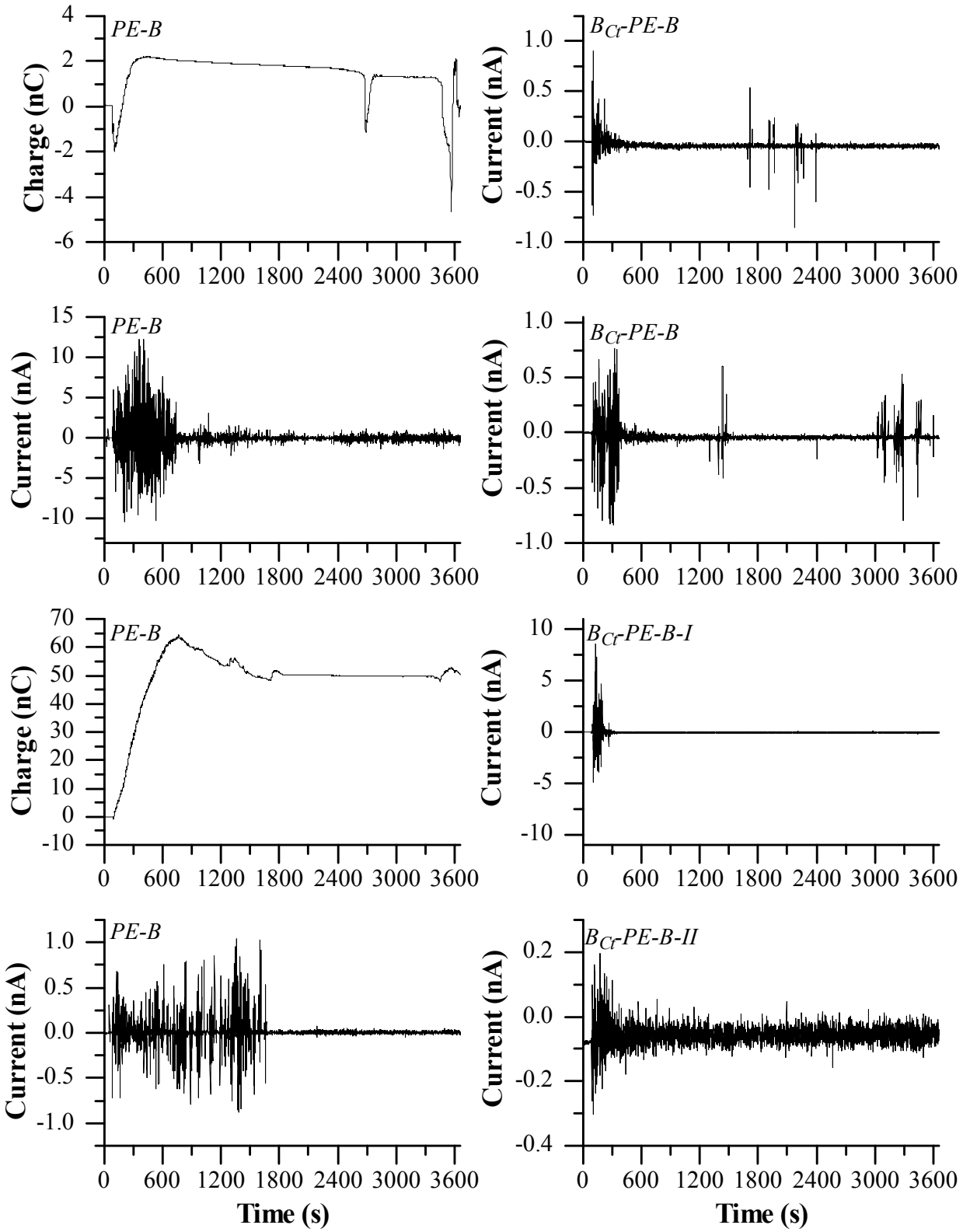


Figure 8.42: The electrostatic probe measurements (in both current and charge modes) for PE resin fluidization experiments performed with Additive B injected into the bed and Additive B pre-coating the column wall.

Figure 8.43 shows the current measurements from the bottom probe and the top Faraday cup cumulative charge measurements for multiple injections of Additive B. When Additive B was injected into the bed after 15 minutes of fluidization, the current measurement from the electrostatic probe dramatically decreased in magnitude. When Additive B was injected into the bed at 30 min there was a slight increase in magnitude of the current measured but this magnitude quickly decreased. The same effect can be seen at the 45 min injection as well. The increase in the magnitude of the charge at the injection was likely due to Additive B being injected into the system near the probe since the height of probe and the injector was equal, ultimately affecting the probe measurement for a short time. Afterwards Additive B may coat the probe and the measured current would subsequently decrease. Although injecting Additive B multiple times into the fluidization column did have some effect on the amount of particles that were adhered to the column wall, this effect was less than that found by simply injecting Additive B into the bed. Therefore, similar to pre-coating the column wall, a reduction in the measured current may not signify a reduction in the amount of wall fouling in the fluidization system.

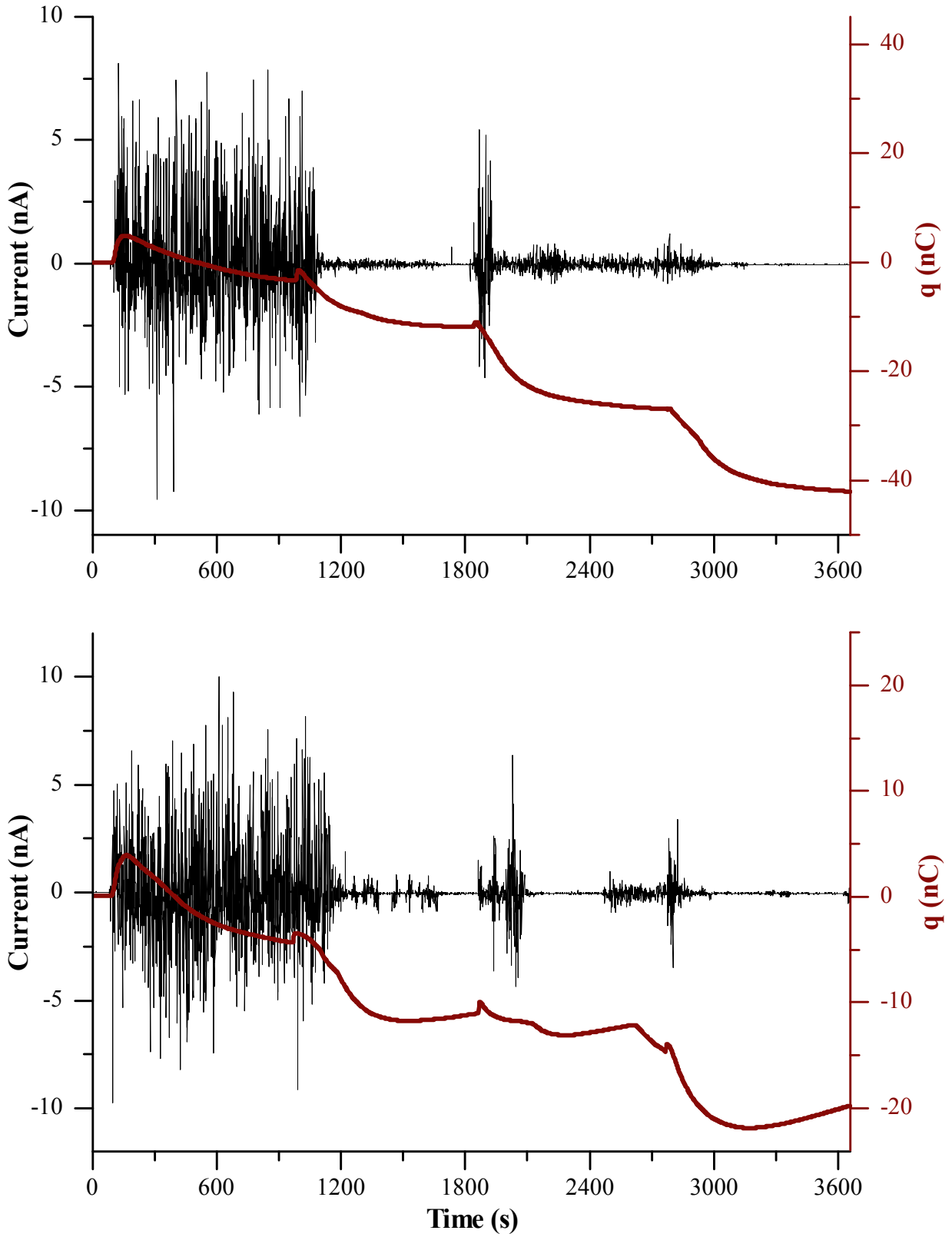


Figure 8.43: The electrostatic probe measurements (current mode) for experiments performed with Additive B injected into the bed multiple times during fluidization and the cumulative charge simultaneously measured by the Top Faraday cup.

The electrostatic probe measurements for no Additive, Additive B, Additive F, and the mixture of Additives B and F are shown in Figure 8.44 at both 15 and 60 min fluidization periods. The sudden drop in the current magnitude was also apparent for the 15 min fluidization experiments. In the second trial with Additive B present, the magnitude of the current measurements significantly dropped after only approximately 550 seconds of fluidization corresponding well with experiments performed at 60 min. Similarly with the 60 min fluidization periods the magnitude of the current varied significantly between experiments. One possible reason for the sudden drop in signal after approximately 500 seconds of fluidization could be attributed to particles, namely Additive B, adhering to the electrostatic probe, effectively reducing the measured signal from the probe. With both Additives B & F present, the amount of time for the magnitude of the current measurement to greatly reduce was always less than 500 s which is a better response than with Additive B. Even though the mixture of Additives B and F was the most effective at reducing the amount of wall fouling in the system and had the smallest current fluctuations, the multiple injections and pre-coating experiments also showed similar current results but with more column wall fouling. Therefore, for this system, it is unclear if the current probe measurements actually give a good indication of the particle wall fouling.

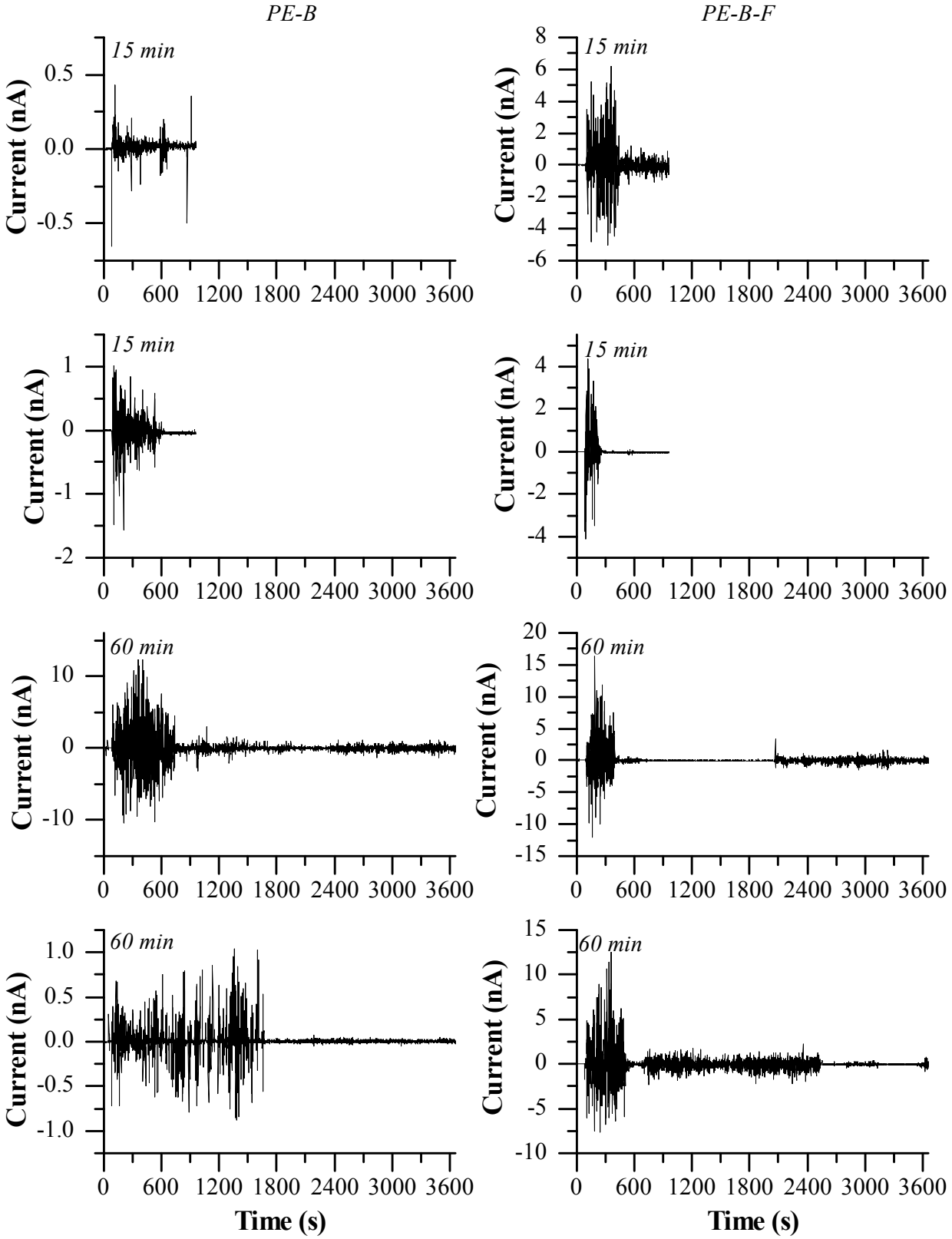


Figure 8.44: The electrostatic probe measurements (in current and charge mode) for experiments performed with and without Additive B during 15 min of fluidization.

8.3. Conclusions

Since the additives all differ in chemical composition, surface morphology, size, sphericity, and work function, it is challenging to compare their effects on the charge build up or dissipation inside the fluidized bed and to effectively determine the true charging mechanism involved. A study on the interactions between the additives and the column wall was performed to determine a pseudo-triboelectric series for materials existed inside the fluidized bed. It was found that when Additives A or B contacted a carbon steel plate, the additives became more positively charged, while Additive C or F became more negatively charged. However, after passing through the injector, all of the additives were negatively charged by the time they entered the bed of particles.

Additive B was the most effective in reducing the degree of reactor wall fouling for both polyethylene resins tested whereas Additive A was only effective with the PE_C resin. This shows the difficulty in producing an additive to be effective for a broad range of polyethylene resins and catalysts. Additive A was likely ineffective with PE_A particles due to the overall smaller particle size range of this resin and the large amount of fines in the system studied. In addition, Additive A was overall larger in size than Additive B and would be less effective at coating the PE particles. It was also believed that Additive B would exhibit the most amount of charge dissipation from the additive to the column wall due to its functional group. Overall PE_A resin generated more particle wall coating than PE_C resin where the lower number of smaller particle in the system with PE_C resin was likely one of the contributing factors. It is possible that Additive A could not overcome the charging of all of the smaller particles in the system which would readily adhere to the column wall and promote particle wall fouling.

With the PE_C particles it was found that injecting Additive B directly into the bed was more effective than pre-coating the column wall or injecting the additive multiple times into the fluidized bed. This signifies the fact that Additive B was the most effective when present within the bed of PE particles, and a certain quantity of this additive must be present within the fluidized bed at one given time. Overall, the fluidization time did not have a significant effect on the magnitude of bed electrification or column wall fouling.

Combining both Additive B and Additive F led to the largest drop in the amount of particle wall fouling in the system. This was attributed to the positively charged Additive F particles adhering to negatively charged PE particles and negatively charged Additive B particles adhering to the positively charged PE particles, effectively reducing the amount of charge within the bed. This effect ultimately reduced the magnitude of electrostatic forces required for attracting the PE particles towards the column wall.

The electrostatic probe measurements of the probe submerged directly into the bed on charge mode was always positive for all additives but was not completely reproducible; however, the cumulative charge was larger when there was more particle wall fouling, i.e, in the presence of Additive C or F. The results on current mode were not completely reproducible, and it was found that when Additive B was injected into the bed, the fluctuations decreased significantly, even though in some cases the amount of particle wall fouling did not decrease. Therefore, the current probe measurements may not be a good indication of the amount of particle wall fouling at least for the system studied.

Chapter 9.
CONCLUSIONS AND RECOMMENDATIONS

Reactor wall fouling is a serious problem found in some gas-solid fluidized bed reactors. It occurs due to build-up of electrostatic charges within the fluidized bed from particle-particle and particle-reactor wall interactions. The significant drawback of this phenomenon is observed in industrial polyethylene reactors which results in frequent reactor shut downs for clean-up and economic loses. In order to find ways of reducing or preventing the generation of electrostatic charges in gas-solid fluidized beds, it is vital to gain a better understanding of the relevant phenomenon by identifying the contributing factors and the underlying mechanisms. However, to achieve these goals an appropriate measurement technique is necessary. Thus, the primary goal of this thesis was to develop an improved measurement technique that would allow the investigation of the charge generation and distribution within the fluidized bed and the extent of reactor wall fouling.

9.1. Conclusions

The main goal of this thesis was achieved where a unique on-line measurement technique was developed based on the Faraday cup method where the fluidized bed was housed with two Faraday cups located at the top and the bottom of the fluidized bed. The bottom Faraday cup replaced the windbox of the fluidization column and the top Faraday cup was located at the exit of the column. The distributor plate was designed in a unique way to be able to open and close allowing the bulk of the bed particles to be dropped into the bottom Faraday cup. The top cup housed a filter bag to capture the entrained fines for their charge measurement. This method not only overcame many weaknesses of previous techniques such as particle handling, measurement accuracy reduction, very small local measurements, indirect measurement of particles charge, etc., but it enabled the investigation of particles charge distribution within the gas-solid fluidized beds. This is the first study which provides information on particle charging in three key areas within a gas-solid fluidized bed simultaneously: the bed particles, the particles adhered to the column wall, and those entrained. Most importantly, this system is the first of its type to provide

information on the extent of reactor wall fouling where not only it permits the measurement of the particles mass and charge in this region, but also it allows images to be taken from the inner reactor wall to examine the particle coating thickness and height.

The new method was successfully implemented in a custom-made pilot-scale atmospheric gas-solid fluidized bed, 0.1 m in diameter and fabricated out of carbon steel to simulate the industrial reactors. Upon the successful testing of this system, a comprehensive experimental program was undertaken in which the effects of different parameters including bed hydrodynamics (fluidizing gas velocity and particle size), the column wall material, and addition of solid additives on the level of bed electrification and most importantly the degree of particles build-up on reactor wall were investigated. Although the results obtained in this thesis could apply to any gas-solid fluidization process, the main focus of the experimental work performed was on polyethylene reactors and therefore different types of polyethylene resins (made from metallocene catalyst), directly received from commercial reactors, were used as the fluidizing particles. Extra dry air was used as the fluidizing gas.

The charge measurements conducted by the top and bottom Faraday cups represented the net charge of the particles found within each region of the bed. Therefore, even if one charge polarity dominated the overall net charge, both positive and negative charges could exist within a sample of particle. Therefore, with the aim of further identifying the charge distribution of particles within those that formed the wall fouling, an additional apparatus (Charged Particle Separator) was designed and built in-house. Two inclined copper plated were placed above four Faraday cups, each attached to a separate electrometer. A voltage was applied to the inclined plates that created an electric field which helped separation of the oppositely charged particles as the particles dropped between the plates. The particles mass, charge, and PSD collected in each of the four Faraday cups could then be measured. The apparatus was designed in a unique way so that it could easily be placed below the fluidization column by replacing the bottom Faraday cup allowing direct collection of the bed particles into the apparatus, thus eliminating any particle handling. This unit was successful at detecting bi-polar charging within each initial sample of the polyethylene resin as received, as well as the Loosely Bound particles.

In addition to fluidization experiments, simple bench-scale triboelectric charging tests were performed with the polyethylene resin contacting an inclined carbon steel plate. Tests were performed with non-sieved polyethylene resin as well as seven narrowly sieved particle size ranges. With the smallest sieved particles there was clear evidence that the polyethylene particles were charging negatively against the carbon steel plate. With the larger particle size ranges and the non-sieved resin this result was not as evident, likely due to the short contact time between the particles and the plate.

The range of parameters that were investigated included: a) 1.5 to 4 u_{mf} for the fluidizing gas velocity which allowed the study to be conducted in both the bubbling and slugging flow regimes; b) polyethylene resin as received with a wide size distribution of 20-1500 μm, and sieved particles with size ranges of 300-425 to 710-1000 μm, which helped determine whether certain sized particle adhered to the column wall and their degree of influence; c) two extreme cases of column wall materials of carbon steel (a conductor) and polyethylene film (an insulator) were used to simulate the industrial column material and the case where the column material was the same as the polyethylene fluidizing particles; and d) solid additives included two static drivers known to be particle wall fouling reducing agents, a deactivated catalyst, and the catalyst support; all of which simulated similar industrial conditions.

A few general conclusions were determined based on all of the experiments performed in this thesis, regardless of the operating condition. They include:

– With all three different polyethylene resins used (of different particle size distributions) and with all different operating conditions tested, bi-polar charging was found within the fluidized bed where the elutriated fines were predominantly oppositely charged in comparison to the bed particles (bulk of the bed and those adhered to the column wall). The bi-polar charging was not limited to a difference in particle size since all particles, even having a uniform particle size distribution, showed a degree of bi-polar charging. This was proven both with the Charged Particle Separator and the bench-scale carbon steel plate contacting experiments, both for a sample of the resin as received as well as smaller sieved particle size ranges. In addition, bi-polar charging was identified within each region of the

fluidized bed; specifically it was measured for the particles that formed the reactor wall coating.

- Between all three resins, PE_A displayed the most amount of column wall fouling followed by PE_B then PE_C. All three resins were produced from metallocene catalysts and their surface morphology was very similar. From Figure 3.3, the PE_A resin was shown to have the most amount of Fine particles while PE_C had overall larger and less fine particles. Therefore there is a connection between the amount of fine particles present and the degree of particles fouling the wall. The smaller particles are more likely to migrate around through the bed and come into contact with the wall. These particles are smaller and therefore would not be as susceptible at remaining adhered to the column wall, effectively increasing the amount of particle wall fouling. The Charged Particle Separator tests with the initial sample of each resin shown in §3.1.2.4 found that the smallest particles were negatively charged; however, for the majority of the fluidization experiments with any resin, the entrained Fines were positively charged. This means that either these negatively charged particles were becoming positively charged during the course of fluidization, or they were trapped within the Dropped and Wall particles, or both.

- In all experiments some degree of reactor wall fouling was observed, where the net q/m of the particles within the coating was the highest found among all regions of the fluidized bed. Regardless of the magnitude of the fouling, the net q/m of the Loosely Bound particles remained relatively similar between experiments, indicating that knowing the particles charge near the column wall cannot predict the extent of the reactor wall fouling. The net q/m could be saturated from an equilibrium of oppositely charged particles found as the layer of particles builds up on the column wall, effectively maintaining a similar q/m with increasing the wall layer thickness.

- Tests conducted with polyethylene resins as received (i.e., not sieved), with all operating conditions examined, concluded that a certain sized particles tend to adhere to the column wall. With the PE_A and PE_B resin the range was 350-450 μm and with PE_C resin was 475-575 μm. In addition, the Loosely Bound particles were found to have net charge density that were

more than 100 times, and the surface charges ($\hat{q}/\hat{A}$) that were approximately 50 times higher than that of the Dropped particles.

- The particle size distribution analysis for all conditions tested showed that the Initial and Dropped particles were of approximately similar particle size, followed by the Loosely Bound and then Tightly Bound particles, and the Fines were the smallest. It was overall concluded that within the reactor wall coating the particles size increased in the radial direction, from the wall to the centre of the bed.

- The electrostatic probe measurements did not present much reproducibility with both the current and charge measurements. The cumulative charge measured was always positive, which was opposite to charges found from the Loosely Bound particles, raising a question as what the probe was actually measuring. When the current was measured, there were more fluctuations in the amplitude of the measurement with cases such as high gas velocity or while additives were present, which intuitively would correspond to higher bed electrification and particle wall fouling. However, this was not found to be true with measurements conducted with the Faraday cup and images taken from the reactor wall coating.

The influence of the fluidizing gas velocity was studied to investigate the effects of bed hydrodynamics on the electrostatic charge generation within the fluidized bed. Experiments were performed in both the bubbling and slugging flow regimes where in the bubbling regime particles charging would likely be dominated by particle-particle collisions due to the vigorous mixing of the bed, while in the slugging flow regime the particle-wall interactions were dominating as portions of the particles slide and rubbed along the column wall. Within each flow regime, elevating the gas velocity promoted the reactor wall fouling which agreed well with the fact that increasing the gas velocity would increase the particle-particle and particle-wall collisions and thus creating more particle charging. However, the wall coating mass in the slugging flow was overall found to be smaller than that in the bubbling regime. In the slugging flow the drag force generated from the movement of the slugs was able to overcome the adhesive forces found on the particles attached to the column wall, reducing the amount of particle wall fouling. In the bubbling flow regime, the particle wall layer was thin and long with a small gap

near the bubbling bed height, whereas in the slugging regime, the wall layer was thicker and shorter, and the gap in the particle layer was near the formation of the slugs. Overall, increasing the gas velocity resulted in an increase in the net q/m of the Wall particles up to the slugging flow where further increase in gas velocity did not alter the particles specific charge. Although a particle wall layer still formed in both flow regimes, the type of the flow did affect height and thickness of the particle wall layer, none of the velocities were found to be effective at reducing the coating. This suggests that both contact and frictional charging had a large impact on the electrostatic charge generation in the system studied.

The effect of fluidizing particle size was investigated as it was previously shown in this work that a narrow particle size range was more prone to adhere to the column wall. With both flow regimes, particles with a diameter less than 600 μm were more likely to adhere to the column wall; however, with particles ranging between 600-700 μm the particles either remained adhered to the column wall or were easily removed. This was due to the degree of the strength of the electrostatic forces versus gravitational force. Also for both flow regimes, the lower bound of the particle size within each size range had a larger tendency of accumulating on the column wall. The lowest sieved particle size range (300-425 μm) was also similar in size to the particles that adhered to the column wall when the non-sieved resin was tested. Overall, it was shown that even though there was a tendency for smaller particles to readily adhere to the column wall, the smaller particles did not need to be present in order to have particle wall fouling as even particles as large as 600 μm were able to accumulate on the column wall.

In the gas-solid fluidized bed used in this work there were continuous contacts between the insulating polyethylene particles and the conductive carbon steel column wall. Due the large difference in the work function of these materials, electrostatic charges would ultimately be generated within the bed through the contact between these surfaces. To minimize this effect, the column wall was covered with a polyethylene film, made from the same fluidizing polyethylene resin, creating contacts between similar materials in an attempt to reduce the degree of particle wall fouling. This case also provided information on particles charging behaviour while in contact with a conductive versus a non-conductive fluidization column wall. In the presence of the polyethylene film, opposite charge polarity distribution within the bed was found in comparison to the carbon steel column where the Fines charged negatively whereas the Dropped

particles were always positively charged and the Loosely Bound particles were either negatively or positively charged. This confirmed the results of the bench-scale testing that was concluded that the contacts between the polyethylene particles and the film result in the particles and the film being positively and negatively charged, respectively. It was found that the net q/m of the Loosely Bound particles was reduced in the presence of the PE film; however, the mass of Wall particles remained consistent. Using the Charged Particle Separator, it was determined that there were more positively charged particles within the Loosely Bound region with the presence of the film, likely due to the negative electrostatic field generated from the negatively charged film. Visual observations showed that the wall fouling on the film was primarily close to the fixed bed height where particle contacts would be higher. This was likely due to the presence of local charging on the film. The continual particle contacts would generate charges within that region but since the film is an insulator, the mobility of the electrons/ions is restricted and therefore a large surface charge is built up within that region, effectively promoting the adhesion of charged particles along the column wall. Overall, it was concluded that the reactor wall fouling was not influenced by applying the same material as the fluidizing particles on the extent of the reactor wall coating.

Since the system developed in this thesis, for the first time enabled the determination of particles charge distribution and level of reactor wall fouling within the gas-solid fluidized bed simultaneously, the impact of solid additives injected into the bed of polyethylene particles was investigated. Both static drivers known to reduce the amount of particle wall fouling in some industrial reactors and a catalyst were used to simulate industrial conditions. Initial charging tests were performed to determine a pseudo-triboelectric series between the additives, the carbon steel column wall, and the fluidizing polyethylene particles. While in contact with a carbon steel plate, both Additives A and B charged positively whereas Additives C and F charged negatively. Injection tests were also performed to determine the charging behaviour of the additives as they passed through the injection set-up and entered the fluidization column. It was found that overall all of the additives charged negatively after passing through the injector at the high gas velocity. Furthermore, additive injection tests were conducted into an empty fluidization column to determine the charging of the additives as they come into contact with only the carbon steel column wall. In this case, Additive A became more negatively charged, Additive B charge

remained the same, while both Additives C and F became less negatively charged. Visual observations indicated that Additive B coated the column wall the most. With usual fluidization experiments where various additives were injected into the bed of polyethylene resin, it was found that Additive B was most effective at reducing the extent of reactor wall fouling while Additives F and C (the deactivated catalyst and its support) significantly promoted wall fouling for both PE_A and PE_C resins tested. This finding is of quite significant importance as it suggests that the catalyst used in the polyethylene production process is itself a source of increase in bed electrification and a promoter of reactor wall fouling. Between the two static drivers, it was found that the surface chemistry of the additive is of importance in affecting the extent of bed charging. Additive B with having an aluminum atom was more effective than Additive A which contained a tertiary amine and hydroxyl functional groups.

Knowing the effectiveness of Additive B in reduction of particles charging and wall fouling, additional tests were performed with this additive to better understand the underlying mechanism involved. It was determined that coating the column wall with Additive B particles was not as effective as injecting the additive directly into the bed of the polyethylene particles in reducing the amount of particle wall adhesion. This concluded that Additive B was most effective by coating the polyethylene particles and thus reducing these particle-particle interactions and their contacts with the carbon steel column wall. Similarly multiple injections of a portion Additive B over the course of 60 min of fluidization was not as effective at reducing the amount of particle wall fouling in the system as simply injecting the whole amount of Additive B into the bed of particles prior to fluidization. This was likely caused due to the insufficient amount of Additive present within the bed at a given period of time suggesting that there is a minimum amount of Additive B required to be effective. Overall there was no discernible effect of Additive between fluidizing periods of 15 minutes versus 60 minutes. The tertiary experiments where the mixture of Additives B and F were used to simulate a similar case as an industrial operation showed the least amount of reactor wall coating, likely due to the presence of positively and negatively charged additives which in turn reduced the amount of charges within the bed.

9.2. Recommendations for Future Work

The charge measurement system developed in this work is able to provide immense amount of information regarding the electrostatic charge generation within gas-solid fluidized beds and the degree of reactor wall coating which potentially can lead to identifying adequate charge reduction/elimination techniques. Therefore, based on the experimental results obtained in this thesis the following recommendations are proposed for future work:

1. Continue the work on the additive injection to examine the following:

    a. In this work numerous experiments were performed with Additive B to identify whether the additive was effective due to coating the column wall or the fluidizing particles. This study should be further extended to other additives (Additive A, and both the catalyst and its support) to gain a better understanding of the relevant phenomenon. In addition, other additives, particularly carbon black, could be tested which would allow for the visual detection of the migration pattern of the additive particles within the fluidized bed.
    b. Since previous works reported in open literature have only provided information on the effect of additives on bed electrification (i.e., bed potential) and not the level of wall fouling, conduct testing with additives used in these studies to further provide information on the relationship between the degree of bed electrification and the extent of reactor wall coating.
    c. To better understand the mechanisms involved in the influence of prostatic agents in the reduction of wall coating, create a matrix of experiments where different additives to be examined and their effects to be related to their surface chemistry and morphology.
    d. To further study the effect of presence of catalyst within the bed on wall coating, examine different systems composed of the different types of polyethylene resin and their corresponding catalyst, and to characterise the results based on the catalyst chemistry.
    e. Finally to continue the works on the multicomponent mixtures composed of numerous additives with different polyethylene resins.

2. Study different types of polyethylene resins manufactured from different catalysts such as Ziegler-Natta or chromium oxide, and compare the results with those found in this work to ultimately relate the fluidizing particles differences such the surface morphology to extent of reactor fouling or particles charging behaviour. In addition, blends of different catalyst based resins could be used to help simulate product transition in industrial gas-solid fluidized bed reactors.

3. Conduct similar experiments in larger column diameters and compare results to those found in this work to further examine the effect of particle-wall interactions on the bed charging behaviour.

4. Investigate the effects of operating pressure and temperature to also more closely mimic industrial operations.

5. Mimic industrial polyethylene operations, by performing a study where the catalyst particles could be re-circulated within the fluidized bed. This will allow the determination of the effects of pneumatic transport of the catalyst as it goes through the system via multiple passes.

6. Conduct a comprehensive study of the electrostatic probes to determine whether the measurements can be correlated to those found by the Faraday cups. This will allow the industries in better understanding the signals obtained from electrostatic probes and the exact particles charging occurring within the reactor.

REFERENCES

Ali, F.S., Ali, M.A., Ali, R.A., Inculet, I.I., 1998. Minority Charge Separation in Falling Particles with Bipolar Charge. Journal of Electrostatics, 45, 139-155.

Ali, F.S., Inculet, I.I., Tedoldi, A., 1999. Charging of polymer powder inside a metallic fluidized bed. Journal of Electrostatics, 45, 199-211.

Bafrnec, F., Bena, J., 1972. Quantitative data on lowering of electrostatic charge in a fluidized bed. Chemical Engineering Science, 27, 117-1181.

Bailey, A.G., 1984. Electrostatic phenomena during powder handling. Powder Technology, 37 (1), 71-85.

Barber, P.W., Hill, S.S., 1990. Light scattering by particles: Computational methods. Advanced Series in Applied Physics 2. World Scientific. Singapore.

Bartilucci, M.P., Davis Jr., E.R., Egan, B.J., Hagerty, R.O., Husby, P.K., 2003. Method and Apparatus for reducing static charges during polymerization of olefin polymers. US Patent 6,548,610.

Baytekin, H.T., Patashinski, A.Z., Branicki, M., Baytekin B., Soh, S., Grzybowski, B.A., 2011. The mosaic of surface charge in contact electrification. Science, 333, 308-312.

Boland, D., Geldart, D., 1971/72. Electrostatic Charging in Gas Fluidized Beds. Powder Technology, 5, 289-297.

Briens C.L., Bergougnou, M.A., Inculet, I.I., Baron, T., Hazlett, J.D., 1992. Size Distribution of Particles Entrained from Fluidized Beds: Electrostatic Effects. Powder Technology, 70, 57-62.

Chen A.H., Bi, H.T., Grace, J.R., 2003. Measurement of particle charge-to-mass ratios in gas-solids fluidized bed by a collision probe. Powder Technology. 135-136, 5181-191.

Chirillo, J.R., Kimbrough II, K.C., McHattie, P.E., 1989. Method for reducing sheeting during polymerization of alpha-olefins. US Patent 4855370.

Ciborowski, J., Wlodarski, A., 1962. On electrostatic effects in fluidized beds. Chemical Engineering Science, 17, 23-32.

Cross, J., 1987. Electrostatics: Principles, Problems and Applications. Adam Higler, Bristol, U.K.

Davies, D.K., 1969. Charge generation on dielectric surface. Journal of Physic D: Applied Physics. 2, 1533.

Ducati, T.R.D., Simoes, L.H., Galembeck, F., 2010. Charge partitioning at gas-solid interfaces: humidity causes electricity buildup on metals. Langmuir, 26, 13763.

Duff, N., Lacks, D.J., 2008. Particle dynamics simulations of triboelectric charging in granular insulator systems. Journal of Electrostatics, 66 (1-2), 51-57.

Escalante, S.G.L, Dominguez, G., Touchard, G., 2004 Electrostatic phenomena in fluidized beds and new method for measuring the minimum fluidization velocity in the powder materials. Journal of Electrostatics, 60, 1-13. French Title: *Phénomènes électrostatique dans les lits fluidisés et nouvelle méthode pour la mesure de la vitesse minimale de fluidisation dans les matérieux pulvérulents.*

Fang, W., Jingdai, W., Yongrong, Y., 2008. Distribution of Electrostatic Potential in a Gas-Solid Fluidized Bed and Measurement of Bed Level. Separator. Industrial Engineering and Chemistry Research, 47, 9517-9523.

Fasso, L., Chao B.T., Soo S.L., 1982. Measurement of Electrostatic Charges and Concentration of Particles in the Freeboard of a Fluidized Bed. Powder Technology, 33, 211-221.

Feng J.Q., 2000. Electrostatic interaction between two charged dielectric spheres in contact. Physical Review E 62, 2891

Fenzel-Alexander, D., Brock, P., Diaz, A., 1994. Control Contact Charge in Polymers with Ionomers. Langmuir, 10, 3323-3327.

Forward, K.M., Lacks, D.J., Sankaran, R.M., 2009a. Charge segregation depends on particle size in triboelectrically charged granular materials. Physical Review Letters, 102, 028001-4.

Forward, K.M., Lacks, D.J., Sankaran, R.M., 2009b. Methodology for studying particle-particle triboelectrification in granular materials. Journal of Electrostatics, 67, 178-183.

Fujino, M., Ogata, S., Shinohara, H., 1985. The electric potential distribution profile in a naturally charge fluidized bed and its effects. International Chemical Engineering, 25, 149-159.

Fulks, B.D., Sawin, S.P., Aikman, C.D., Jenkins III, J.M., 1985. Process for reducing sheeting during polymerization of alpha-olefins. US Patent 4532311.

Gady, A., Schleef, D., Reifenberger, R., Rimai, D., DeMejo, L.P., 1996. Identification of electrostatic and van der Waals interaction forces between a micrometer-size sphere and a flat substrate. Physcial Review B, 53, 8065-8070.

Gajewski, A., 1985. Investigation of the Electrification of Polypropylene Particles during the Fluidization Process. Journal of Electrostatics, 17, 289-298.

Geldart, 1973. Types of Gas Fluidization. Powder Technology, 7, 285-292.

Giffin, A., Mehrani, P., 2010. Comparison of influence of fluidization time on electrostatic charge build-up in the bubbling vs. slugging flow regimes in gas-solid fluidized beds. Journal of Electrostatics 68, (6), 492-502.

Goode, M.G., Hasenberg, D.M., McNeil, T.J., Spriggs, T.E., 1989. Method for Reducing Sheeting During Polymerization of Alpha-Olefins. US Patent 4,803,251.

Goode, B.D., Williams, C.C., Hussein, F.D., McNeil, T.J., Lee, K.H. 2000. Static control in olefin polymerization. US Patent 6,111,034.

Grace, J.R., 1982. Fluidized-bed hydrodynamics, in Handbook of Multiphase Systems, G. Hetsroni, Ed. Hemisphere, Washington.

Guardiola, J., Ramos, G., Romero, A., 1992. Electrostatic behaviour in binary dielectric/conductor fluidized beds. Powder Technology, 73, 11-19.

Guardiola, J., Rojo, V.,Ramos, G., 1996. Influence of particle size, fluidization velocity and relative humidity on fluidized bed electrostatics. Journal of Electrostatics, 37, 1-20.

Gupta, C.K., Sathiyamoorthy, D., 1999. Grouping of Gas Fluidization. Fluid Bed Technology in Materials Processing. CRC Press LLC, 16.

Hagerty, R.O., Muhle, M.E., Agapiou, A.K, Kuo, C.-T., Goode, M.G., Hussein, F.D., Pannell, R.B., Szul, J.F., 2005. Method for Controlling Sheeting in Gas Phase Reactors. US Patent 2005/0148742 A1.

Hagerty, R.O., Stevens, K.B., DeChells, M.L., Fischbuch, D.B., Farly, J.M., 2007. Polymerization process. US Patent 7300987 B2.

Hagerty, R.O., Muhle, M.E., Agapiou, A.K, Kuo, C.-T., Goode, M.G., Hussein, F.D., Pannell, R.B., Szul, J.F., 2011. Method for Controlling Sheeting in Gas Phase Reactors. US Patent 7985811 B2.

Haider, A., Levenspiel O., 1989. Drag coefficient and terminal velocity of spherical and non-spherical particles. Powder Technology, 58, 63-70.

Ham, R.W.,Gauthier, P.A., Bergougnou, M.A., 1992. Electrostatic in an Air/Catalyst Fluidized Bed at Ambient Temperature and Pressure. Fluidization VII, eds. O.E. Pother and D.J. Nicklin, Engineering Foundation, NY, 611-620.

Harper, W.R., 1967. Contact and Frictional Electrification. Oxford University Press. Oxford.

Hendrickson, G., 2006. Electrostatics and gas phase fluidized bed polymerization reactor wall sheeting. Chemical Engineering Science, 61, 1041-1064.

Hindermann-Bischoff, M., Ehrburger-Dolle, F., 2001. Electrical conductivity of carbon black–polyethylene composites: Experimental evidence of the change of cluster connectivity in the PTC effect. Carbon, 39, 375-382.

Jones, T.B., 1997. Electrostatic and Dust Explosions in Powder Handling, in Selected Topics on Fluidization, Solids Handling, and Processing. Noyes Publications, Park Ridge NJ, 817-871.

Katz, H.M., 1957. Studies of particle size distributions in fluidised beds. Argon National Laboratory, US Atomic Energy Commission. ANL-5725.

Kisel'nikov, V.N., Vyalkov, V.V., Filatov, V.M., 1967. On the problem of electrostatic phenomena in a fluidized bed. International Chemical Engineering, 7, 428-431.

Komatsu, T.S., Hashimoto, M., Miura, T., Arakawa, I., Nasumo, S., 2004. Static electrification by asymmetric rubbing. Applied Surface Science, 235, 60-64.

Kunii, D. Levenspiel O., 1991. Fluidization Engineering. Butterworth-Heinemann, Newton, USA , pp. 1-478.

Lacks, D.J., Levandovsky, A. 2007. Effect of particle size distribution on the polarity of charging in granular insulator systems.

Lacks, D.J., Duff, N., Kumar, S.K., 2008. Nonequilibrium accumulation of surface species and triboelectric charging in single component particulate systems. Physical Review Letters, 100 (18), 188305.

Lacks, D.J., Sanakaran, R.M., 2011. Contact electrification of insulating materials. Journal of Physics D, 44, 453001, 1-15.

Lowell, J., Rose-Innes, A.C., 1980. Contact electrification. Advances in Physics, 122, 947 - 1023.

Lowell, J., Truscott, W.S., 1986. Triboelectification of identical insulators: II. Theory and further experiments. Journal of Physics D: Applied Physics, 19, 1281.

Li W., Li, D.Y., 2005. On the correlation between surface roughness and work function in copper. Journal of Chemical Physics, 122, 064708.

Liu, Z., Bi, X.T., Grace, J.R., Electrostatic charging behaviour of dielectric particles in a pressurized gas-solid fluidized bed. Journal of Electrostatics, 68, 321-327.

Masuda, H., Gotoh, K., Higashitani, K., Matsusaka, S., 2006. Adhesive Force of a Single Particle in Powder Technology Handbook. Third Edition. CRC Press. Florida.

Mastusaka S., Masuda, H., 2003. Electrostatics of particles, Advanced Powder Technology, 14 (2), 143-166.

McCarty, L.S., Winkleman, A., Whitesides, G.M., 2007. Electrostatic self-assembly of polystyrene microsphere by using chemically directed contact electrification. Angewandte Chemie International Edition, 119, 210-213.

Mehrani, P., Bi, H.T., Grace, J.R., 2005. Electrostatic charge generation in gas-solid fluidized beds. Journal of Electrostatics, 63, 165-173.

Mehrani, P., Bi, H.T., Grace, J.R., 2007. Electrostatic behaviour of different fines added to a Faraday cup fluidized bed. Journal of Electrostatics, 65, 1-10.

Montgomery, D.J., 1959. Static electrification of solids. Solid State Physics, 9, 136-196.

Moughrabiah, W.O., Grace, J.R., Bi, H.T., 2009. Effects of Pressure, Temperature, and Gas Velocity on Electrostatics in Gas-Solid Fluidized Beds. Industrial Engineering and Chemistry Research, 48, 320–325.

Moughrabiah, W.O., Grace, J.R., Bi, X.T., 2012. Electrostatics in gas-solid fluidized beds for different particle properties. Chemical Engineering Science, 75 , 198-208

Murtomaa, M., Räsänen, E., Rantanen, J., Bailey, A., Laine, E., Mannermaa, J.-P., Yliruusi, J., 2003. Electrostatic measurements on a miniaturized fluidized bed. Journal of Electrostatics, 57, 91-106.

Nase S.T., Vargas W.L., Abatan A.A., McCarthy, J.J., 2001. Discrete characterization tools for cohesive granular material. Powder Technology, 116, 214-223

Newton, R.E., Day, D.R., Swartzentruber, R.L., 1999. Apparatus and Methods for Measuring Conditions in Fluidized Beds. US Patent 6,008,662.

Ohara, K., 1979. Contribution of molecular motion of polymers to frictional electrification. Electrostatics (Oxford)., Institute of Physics Conference Series. 48, 257-264.

Oguchi T., Tamatani M, 1993. Contact electrification phenomena and powder surface treatments. Wear, 168 (1-2), 91-98.

Park, A.-H., Bi, H., Grace, J.R., 2002. Reduction of electrostatic charges in gas-solid fluidized beds. Chemical Engineering Science, 57, 153-162.

Pham, R., Virnleson, C.R., Sankaran R.M., Lacks, D.J., 2011. Contacting charging between surfaces of identical insulating materials in asymmetric geometries. Journal of Electrostatics, 69, 456-460.

Pulsifer, A.H., Wheelock, T.D., 1978. The electrical resistance of gas fluidized beds. Fluidization. Cambridge. Cambridge University Press, 76-80.

Pryer, D.W., Gale, P.F., 2003. Cables, in Electrical engineer's reference book. Edited by Laughton, M.A., Warne, D.F., Eds. Newnes, Oxford, 31-39.

Revel, J., Gatumel, C., Dodds, J.A., Taillet, J., 2003. Generation of static electricity during fluidisation of polyethylene and its elimination by air ionisation. Powder Technology, 135-136, 192-200.

Rojo, V., Guardiola, J., Vian, A., 1986. A Capacitor Model to Interpret the Electric Behaviour of Fluidized Beds. Influence of Apparatus Geometry. Chemical Engineering Science, 41, 2171-2181.

Schaeffer, D.M., Carpenter, M., Gady, B., Reifenberger, R., DeMejo, L.P., and Rimai, D.S, 1995. Fundamentals of Adhesion and Interfaces in Surface roughness and its influence on particle adhesion using atomic force techniques. Edited by Rimai, D.S., DeMejo, L.P., and Mittal, K.L., VSP, Utrecht, The Netherland) pp. 35–48.

Servais, T., Bernot, C., 2000. Measurement of electrostatic effects in a fluidized bed reactor. First European Conference on the Reaction Engineering of Polyolefins, Lyons, July 3-6, 2000.

Song, G.-H., Rhee, A.S., Lowder, G.R., 1995. Method for Reducing Sheeting and Static Charges during Polymerization of Ethylene Polymers. US Patent 5,391,657

Tanue, K., Masuda, H., 2006, Electrostatic Separation, Powder Technology Handbook. 3rd Editions. Editors: Hiroaki Masuda, H., Higashitani, K., Yoshida, H., CRC Press LLC, 656.

Tardos, G., Pfeffer, R., 1980. A Method to Measure Electrostatic Charge on a Granule in a Fluidized Bed. Chemical Engineering Communications, 4, 665-671.

Trigwell, S., Mazumder, M.K., Pellissier R., 2001. Tribocharging in electrostatic beneficiation of coal: Effects of surface composition on work function as measured by x-ray photoelectron spectroscopy and ultraviolet photoelectron spectroscopy in air Journal of Vacuum Science and Technology A, 19(4), 1454-1459.

van Krevelen, D.W., te Nijenhuis, K., 2009. Properties of Polymers: Their Correlation with Chemical Structure; their Numerical Estimation and Prediction from Additive Group Contributions, 4th Edition. Elsevier Science.

Valverde, J.M., Quintanilla, M.A.S., Espin, M.J., Castellanos, A., 2008. Nanofluidization electrostatics. Physical Review E - Statistical, Nonlinear, and Soft Matter Physics, 77 (3), 031301.

Wang, J., Xu, Y., Li, W., Yang, Y., Wang, F., 2009. Electrostatic potentials in gas-solid fluidized beds influenced by the injection of charge inducing agents. Journal of Electrostatics, 67(5), 815-826.

Williams, M.W., 2012. Triboelectric charging of insulators – mass transfer versus electrons/ions. Journal of Electrostatics, 70, 233-234.

Wolny, A., Opalinski I., 1983. Electric Charge Neutralization by Addition of Fines to a Fluidized Bed Composed of Coarse Dielectric Particles. Journal of Electrostatics, 14, 279-289.

Wolny, A., Kazmierczak, W., 1989. Triboelectrification in Fluidized bed of Polystyrene. Chemical Engineering Science, 44, 2607-2610.

Yamaguchi, Y., Suga, S., Morikawa, Kubo, K., Watanabe, M., Sano, Y., 1995. Method of producing polyolefin. US Patent 5,385,991.

Yao, L., Bi, H.T., Park, A.H., 2002. Characterization of electrostatic charges in freely bubbling fluidized beds with dielectric particles, Journal of Electrostatics, 56(2), 183-197.

Yu, H.X., Wang, F., Wang, J.D., Yang, Y.R., 2007. Progress in study of electrostatics and wall sheeting in gas phase polymerization fluidized bed reactor. Petrochemical Technology, 36, 206-211.

Yu, X., Li, W., Wang, J., Yang, Y., Xu, N., Wang, H., 2010. Effect of polymer granules on the electrostatic behaviour in gas-solid fluidized beds. Industrial & Engineering Chemistry Research, 49, 132-139.

Zhao, H., Castle G.S.P., Inculet, I.I., Bailey, A.G., 2000. Bipolar Charging in Polydisperse Polymer Powders in Industrial Processes. Conference Record of the 2000 IEEE, 2, 835-841.

Zhao, H., Castle, G.S.P., Inculet, I.I., 2002. The measurement of bipolar charge in polydisperse powders using a vertical array of Faraday pail sensors. Journal of Electrostatics, 55, 261-278.

Zhao, H., Castle G.S.P., Inculet, I.I., Bailey, A.G., 2003. Bipolar Charging of Poly-Disperse Polymer Powders in Fluidized Beds. IEEE Transactions on Industry Applications, 39, 612-618.

Zimmer E., 1970. Die elektrostasche aufladung von hochpolymeren isolierstoffen. Kunstoffe, 60, 465-468.

APPENDIX A
APPARATUSES FROM OTHER WORKS FOUND IN LITERATURE

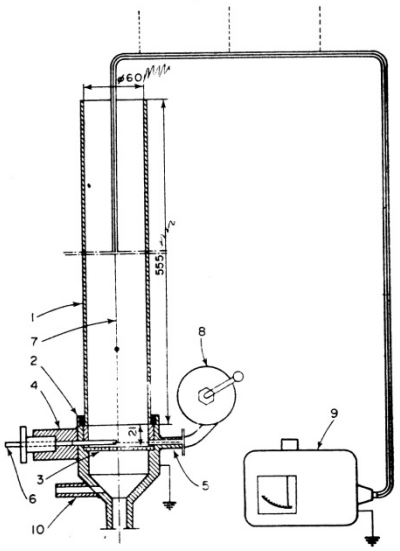


FIG. 1. Equipment

(1) Glass tube
(2) Metal base
(3) Sintered steel bottom
(4) Small rod support
(5) Opening (for thread)
(6) Small rod
(7) Electrode
(8) Small reel
(9) Electrometer
(10) Thermometer bore
—— Silk thread

Figure A.1: Vertical probe apparatus (adapted from Ciborowski and Wlodarski, 1962).
Column: 3D Rasotherm (0.049 m ID)
Particles: Vinyl polyacetate, polystyrol, sand (300-750 μm)

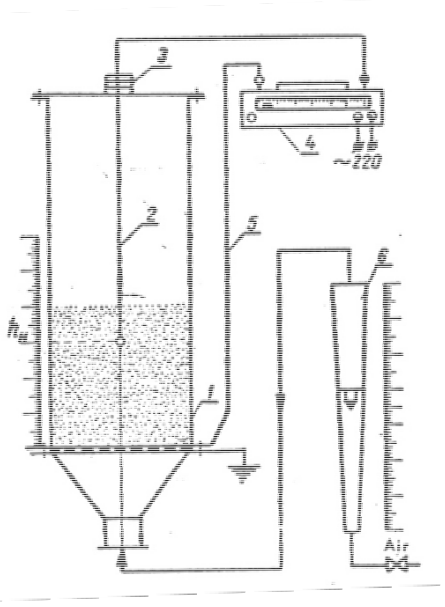


Figure A.2: Vertical probe apparatus (adapted from Kisel'nikov et al., 1967).
Column: Glass, Metal
Particles: BMX resin, ammonia sulphate, SG resin, polyacrylonitrile

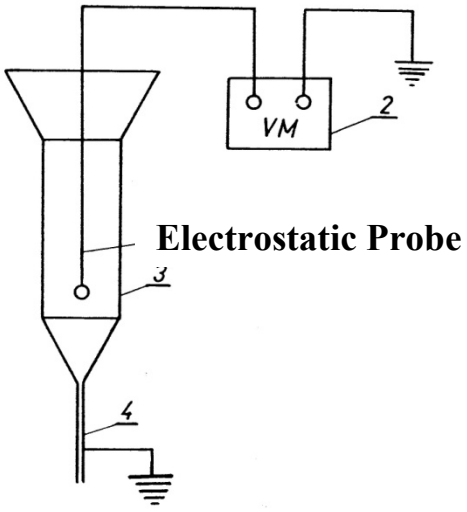


Figure A.3: Vertical probe apparatus (adapted from Bafrnec and Bena, 1972).
Column: 3D Metal (0.032 m ID, 0.26 tall)
Particles: Ballotini glass beads

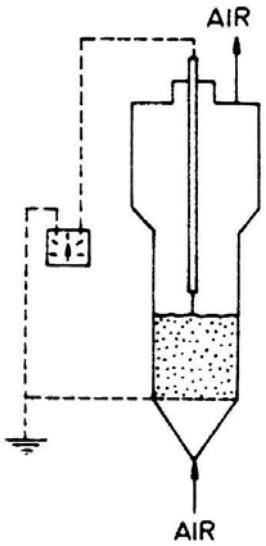


Figure A.4: Vertical probe apparatus used (adapted from Rojo et al., 1985).
Column: 3D Glass (0.035, 0.044, 0.049 m ID)
Particles: Ballotini glass beads

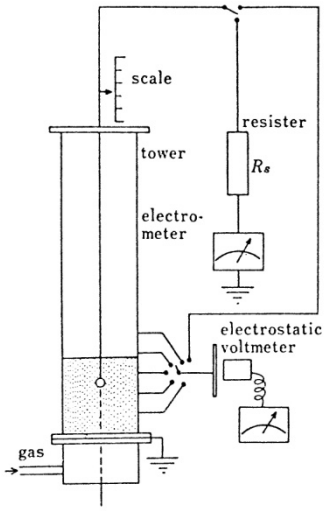


Figure A.5: Vertical probe apparatus (adapted from Fujino et al., 1985).
Column: 3D Steel and Acrylic (0.067 m ID)
Particles: Glass beads (200 and 250 μm, Neobeads (200 and 540 μm), PMMA (540 μm)

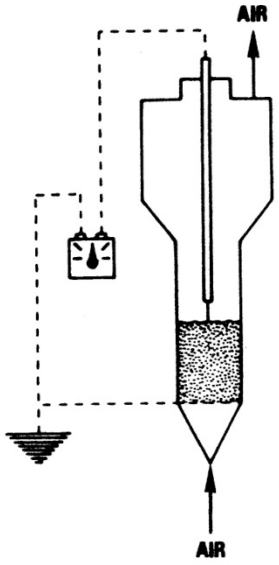


Figure A.6: Vertical probe apparatus (adapted from Guardiola et al., 1992).
Column: 3D Perspex (0.05 m ID)

Particles: Glass Beads (450 to 500 μm and 500-590 μm)

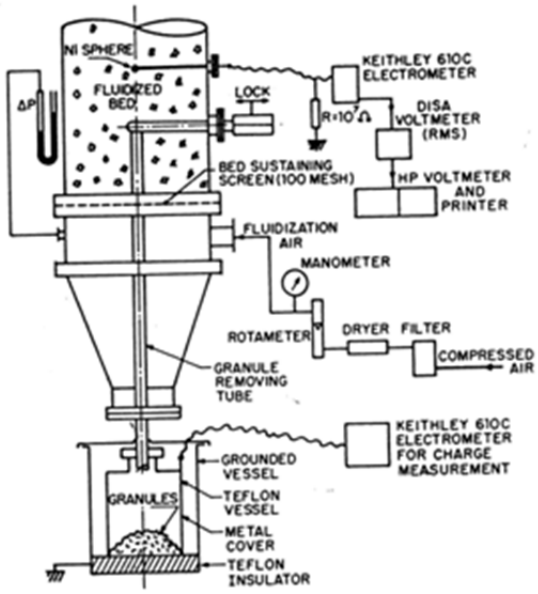


Figure A.7: The horizontal probe and Faraday cup apparatus (adapted from Tardos and Pfeffer, 1980).
Column: 3D Plastic (0.05 m ID)
Particles: Porcelain (2000 μm)

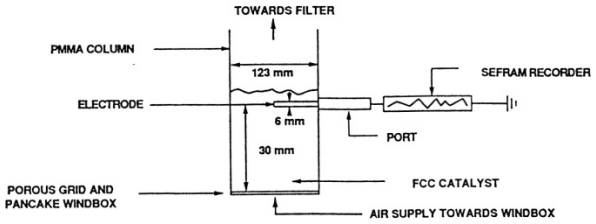


Figure A.8: The horizontal probe apparatus (adapted from Ham et al., 1992).

Column: 3D PMMA (0.123 m ID, 1.385 m tall)
Particles: FCC (82 μm)

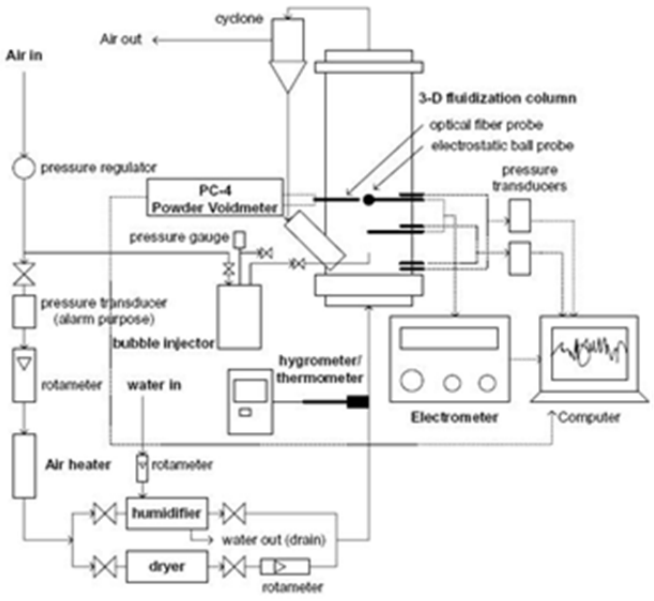


Figure A.9: The horizontal probe apparatus (adapted from Park et al., 2002).

Column: 2D Plexiglas (0.307 m wide, 0.022 m thick, and 1.24 m tall), 3D Plexiglas (0.0889 m ID, 1.21 m tall)

Particles: Polyethylene

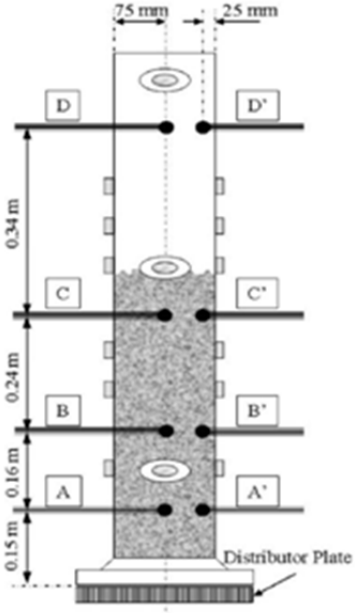


Figure A.10: The horizontal probe apparatus (adapted from Moughrabiah et al., 2009).

Column: 3D Stainless Steel (0.15 m ID, 2 m tall)

Particles: LLDPE (600 μm), HDPE (450 μm), Glass Beads (321 μm)

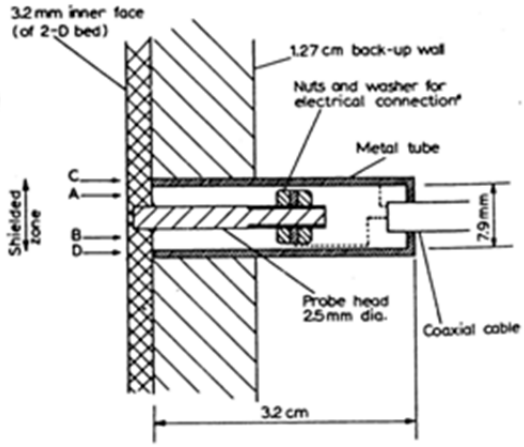


Figure A.11: The non-contacting horizontal probe apparatus (adapted from by Boland and Geldart, 1971/72).

Column: 2D Perspex (0.5 m by 0.13 m base), Perspex 0.05 m ID, 0.35 m tall)

Particles: Lead Glass Ballotini (200 to 300 μm)

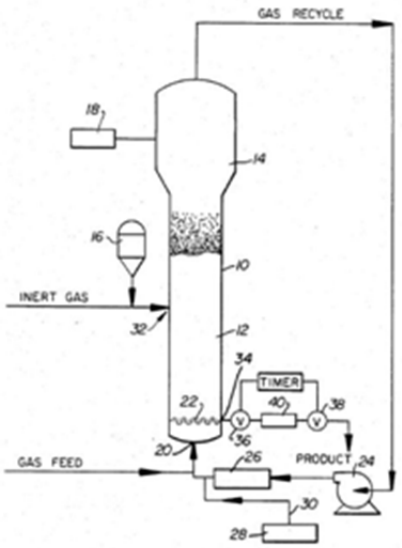


Figure A.12: The horizontal probe apparatus (adapted from Fulks et al., 1985).
Column: 3D Carbon Steel
Particles: Alpha-olefins

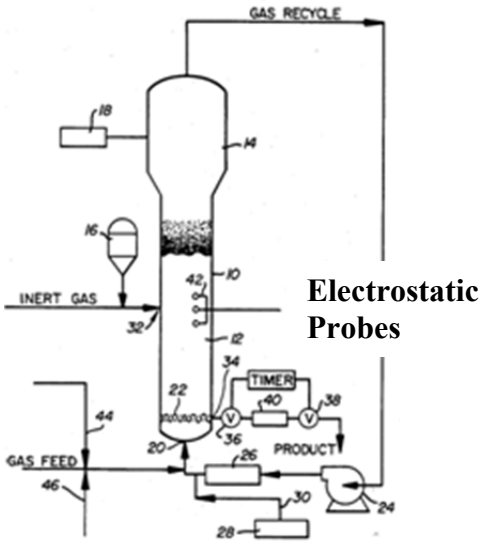


Figure A.13: The horizontal probe apparatus (adapted from Goode et al., 1989).
Column: 3D Carbon Steel
Particles: Olefins

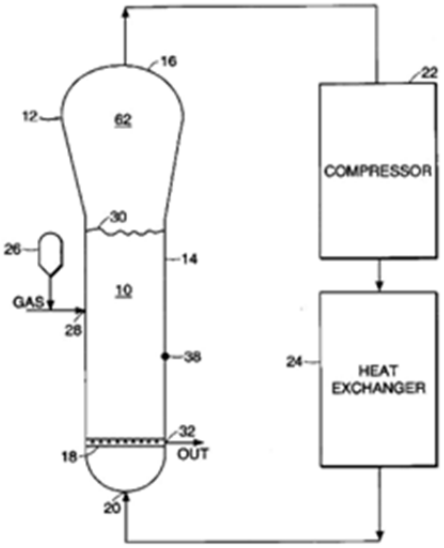


Figure A.14: The horizontal probe apparatus (adapted from Newton et al., 1999).
Column: 3D Carbon Steel
Particles: Polymers

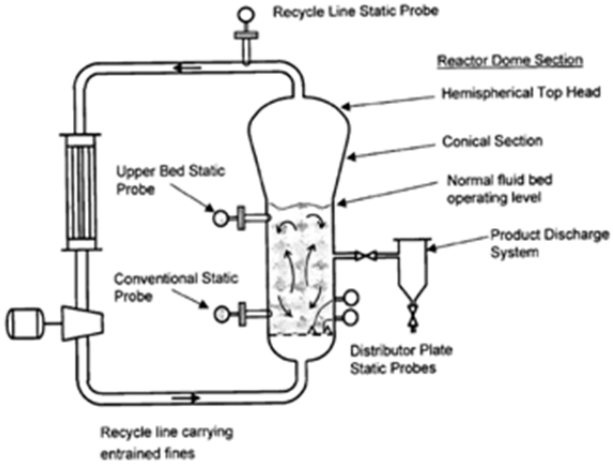


Figure A.15: The electrostatic probe apparatus (adapted from Hagerty et al., 2005).
Column: 3D (0.57 m ID, 4 m tall)
Particles: Polymers

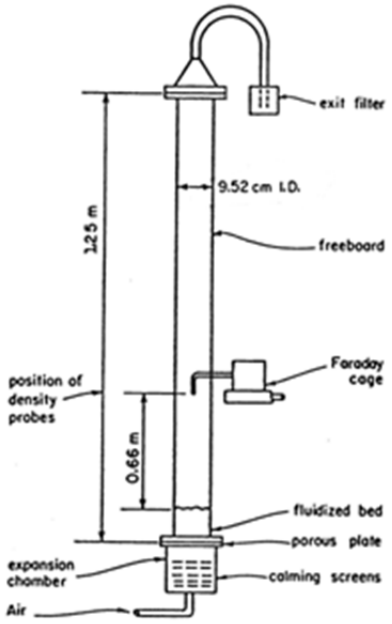


Figure A.16: The sampling Faraday cup apparatus (adapted from Fasso et al., 1982).

Column: 3D Plexglas (0.095 m ID, 1.25 m tall)
Particles: Glass Beads (30 to 55 μm)

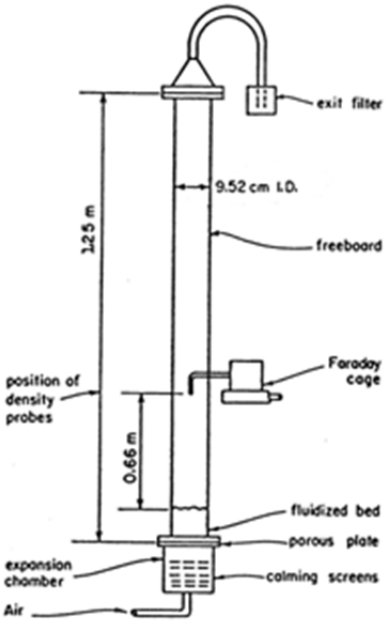
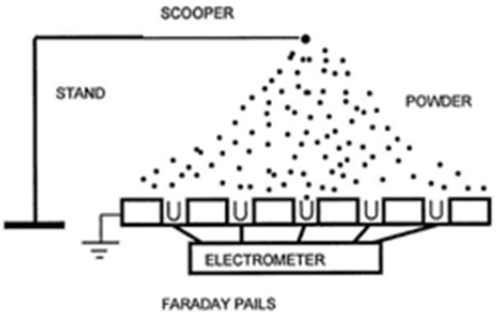
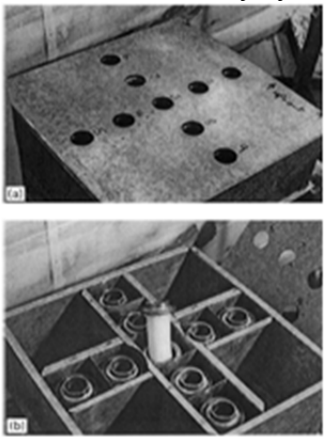


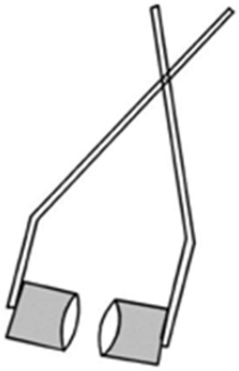
Figure A.17: The sampling Faraday cup apparatus (adapted from Wolny and Opalinski, 1983).

Column: 2D Perspex (0.4 m by 0.4 m base)

Particles: Polystyrene (1020 to 1200 μm)







a) **b)**

Figure A.18: a) The Faraday cup grid, and b) schematic of the scooper used to sample particles (adapted from Ali et al., 1998).
Column: 2D PVC (0.25 m wide, 0.25 m thick, 0.25 m tall)
Particles: Powder A (polyamide powder, 98 μm), Powder B (acrylic powder, 80 μm), Powder C (97% Powder A, 3 % metal powder, 88 μm)

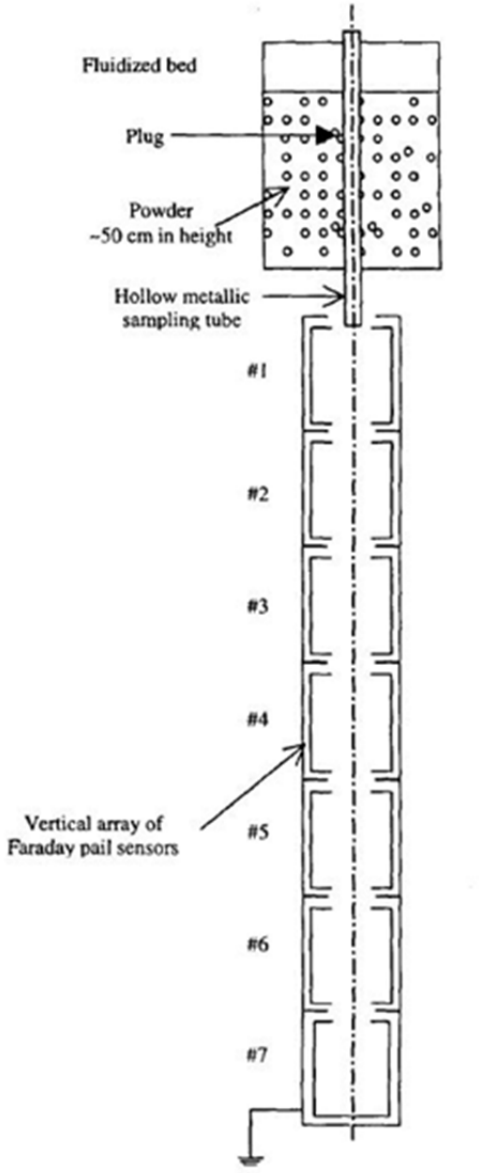


Figure A.19: The 7 vertical Faraday cup method (adapted from Zhao et al., 2000).
Column: 2D Steel (0.25 m wide, 0.25 m thick, and 0.6 m tall)

Particles: Three Powders (< 100 μm)

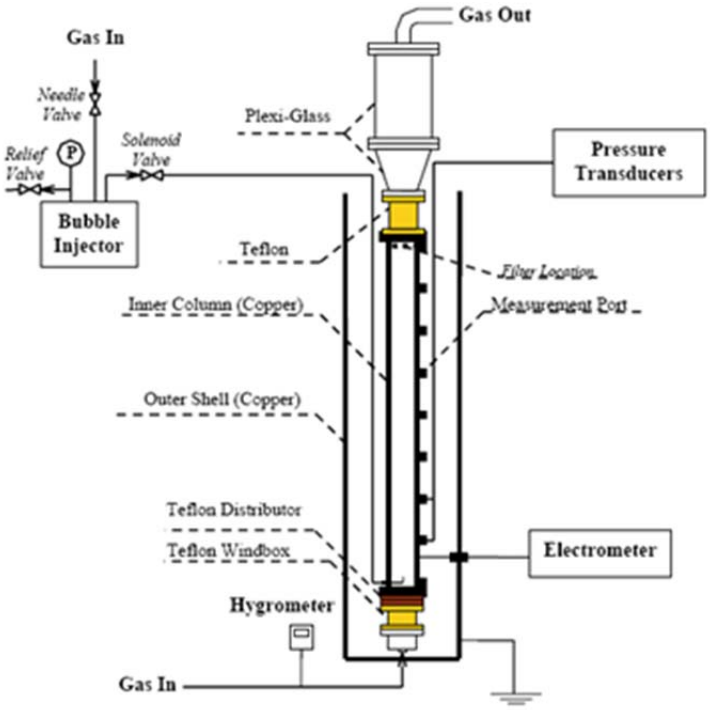


Figure A.20: The Faraday cup fluidization column (adapted from Mehrani et al., 2005).

Column: 3D Copper (0.1 m ID, 1.2 m tall)

Particles: Glass Beads (500 to 600 μm)

Glass Beads (420 to 752 μm), Polyethylene (38-876 μm, 500 to 600 μm)

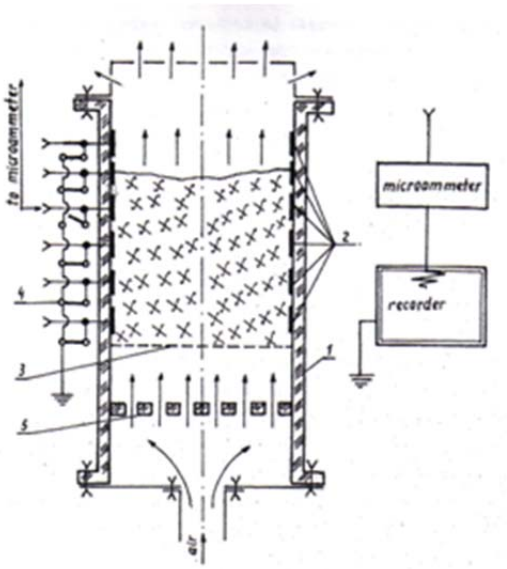


Figure A.21: Inner rings method (adapted from Gajewski, 1985).
Column: 3D Glass (0.25 m ID)
Particles: Polypropylene (500, 1000, 2000, 2500, 3000, 4500 μm)

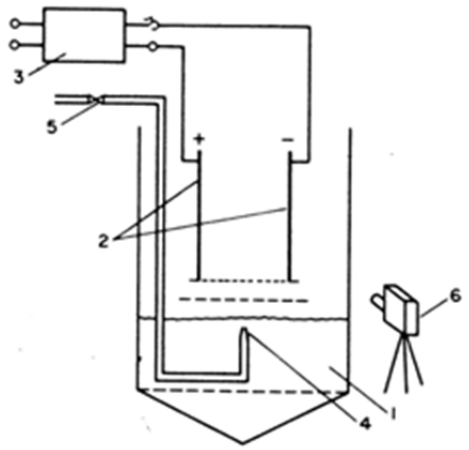


Figure A.22: Capacitance probe method (adapted from Wolny and Kazmierczak, 1989).
Column: 2D (0.2 m by 0.2 m base)

Particles: Polystyrene (474 μm)

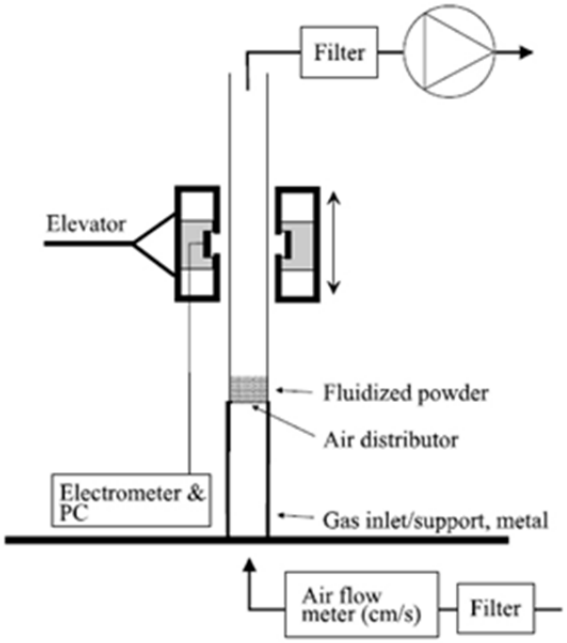


Figure A.23: The induction elevator ring method (adapted from Murtomaa et al., 2003).
Column: 3D Glass (0.02 m ID, 0.28 m tall), 3D Acrylic (0.02 m ID, 0.24 m tall)
Particles: Microcrystalline beads (180 μm), Lactose Monohydrate (180 μm), Glass Beads (1130 μm)

APPENDIX B
SEM PICTURES OF POLYETHYLENE PARTICLES AND ADDITIVES

This section focuses on the SEM pictures for all three polyethylene resins (PE_A, PE_B, and PE_C) as well as all of the additives (Additives A, B, C, and F). The Tescan Vega-II XMU VPSEM machine located at Carleton University (Ottawa, ON) was used to perform these tests.

B.1 Polyethylene Particles

Sieved polyethylene particles at three different size ranges were used (212-300, 500-600, and 710-1000 μm) for SEM analysis. The samples were not treated or coated prior to the image analysis. A magnification of 100x and the operating pressure in the chamber was at low vacuum (10 Pa) therefore the low vacuum secondary electron Tescan detector (LVSTD). Simultaneously, the backscatter electron detector (BSE) was used to measure the backscattered electrons. The results for PE_A, PE_B, and PE_C are shown in Figure B.1, Figure B.2, and Figure B.3, respectively.

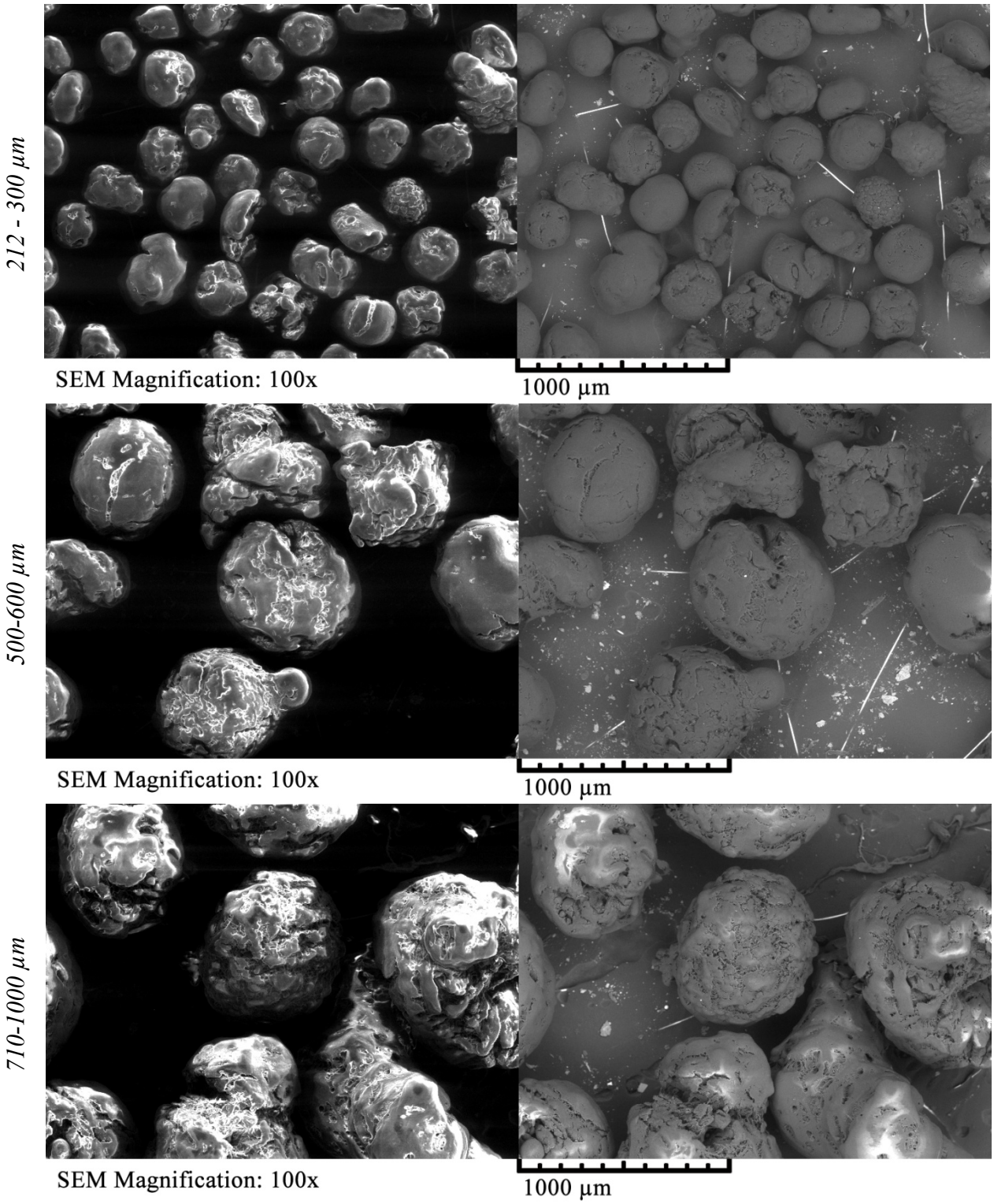


Figure B.1: The SEM pictures of the PE_A resin at three different sieved particle size ranges using the LVSTD (left) and BSE detectors (right) at 100x magnification.

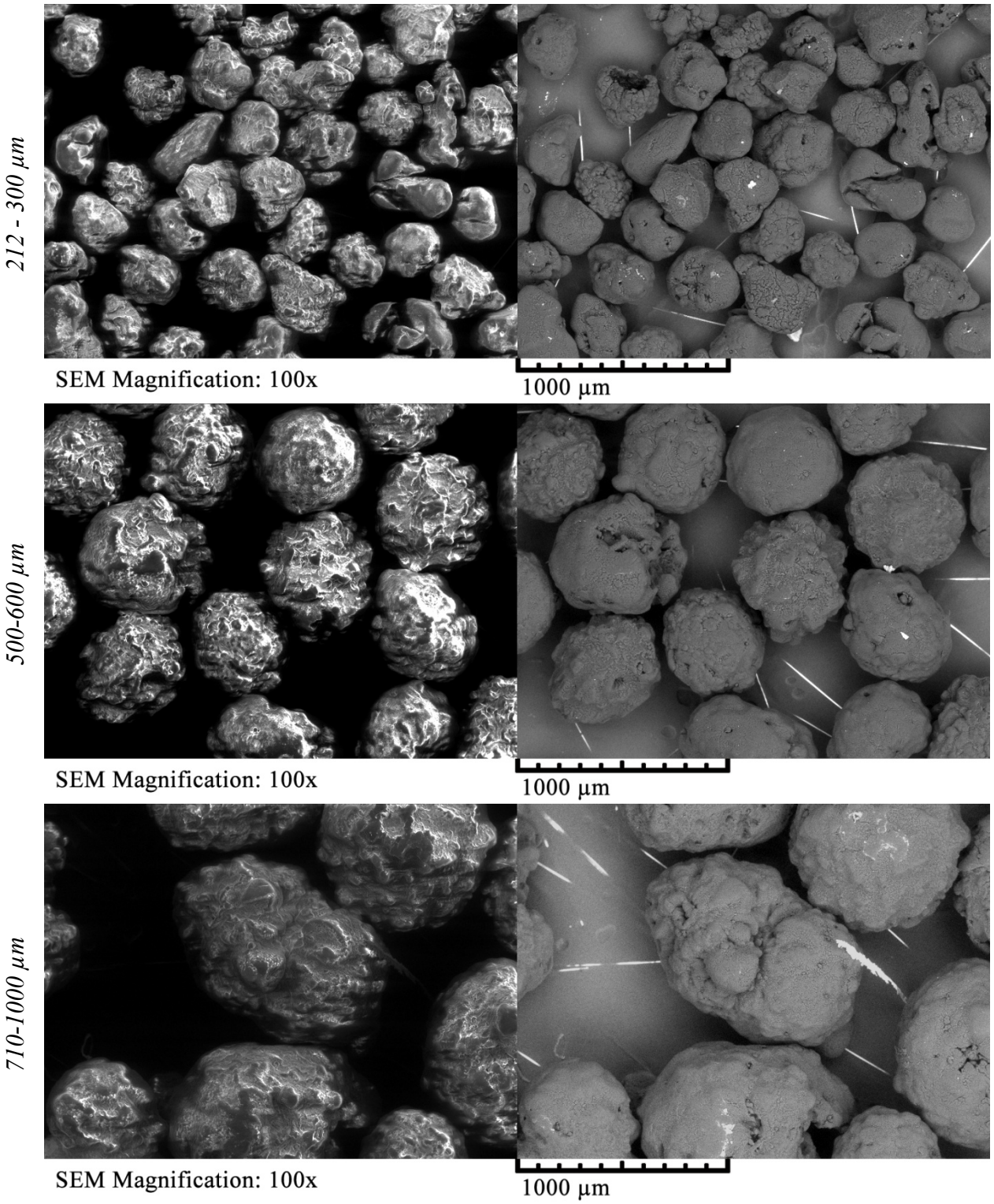


Figure B.2: The SEM pictures of the PE_B resin at three different sieved particle size ranges using the LVSTD (left) and BSE detectors (right) at 100x magnification.

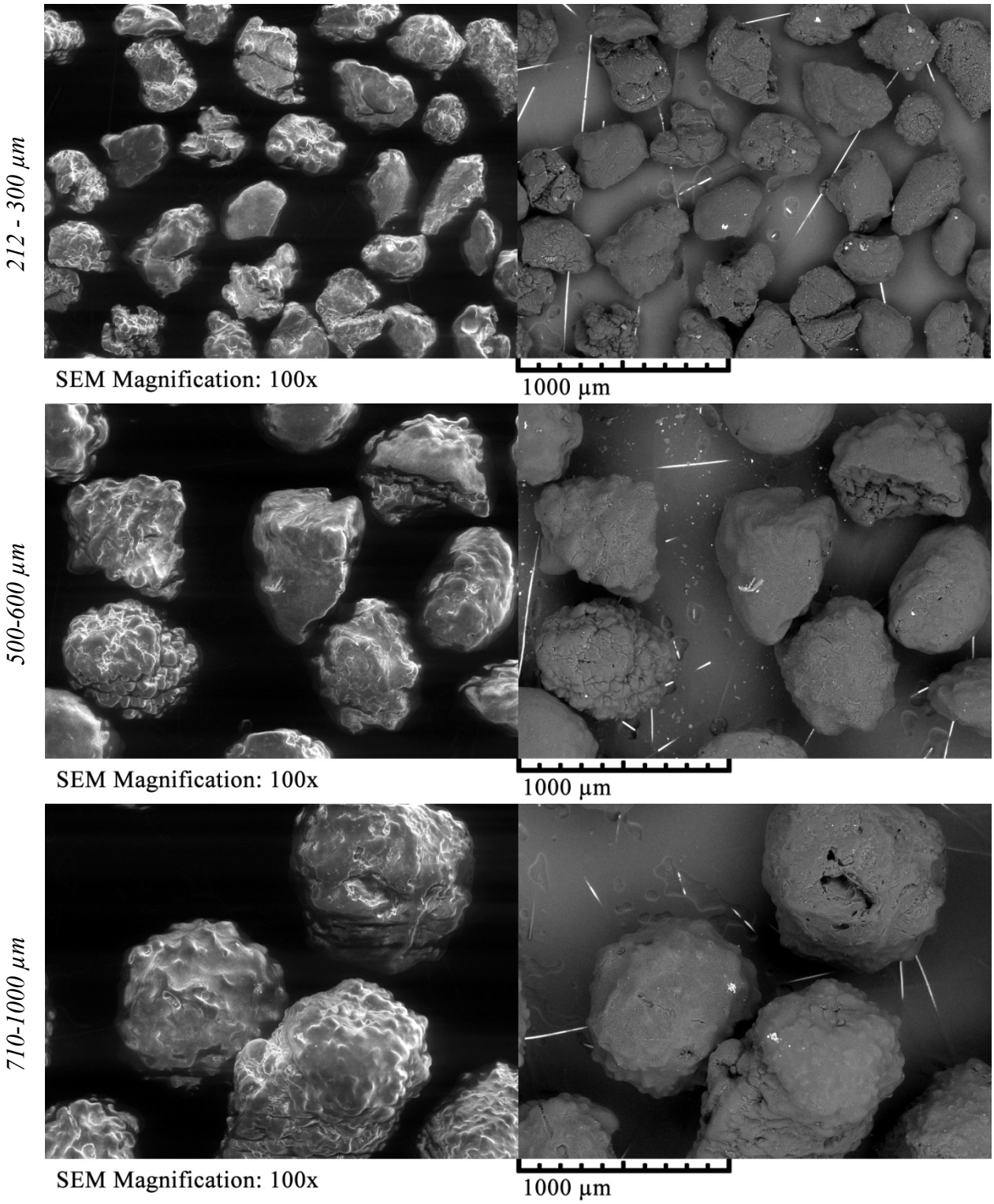
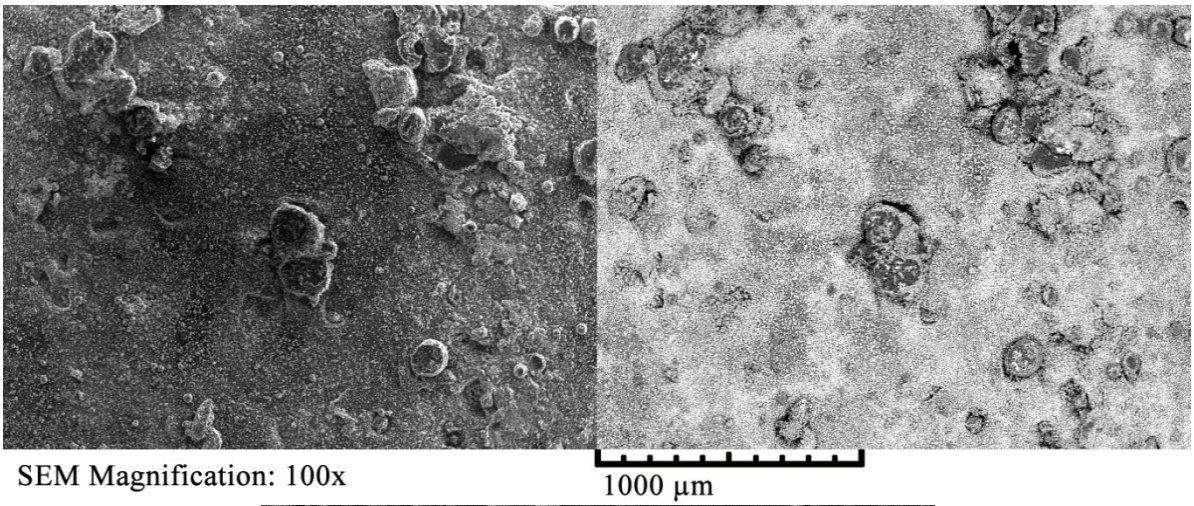
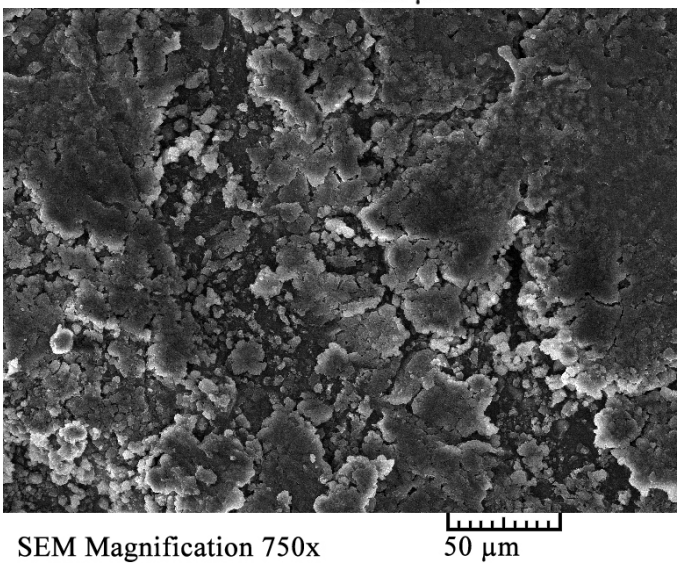


Figure B.3: The SEM pictures of the PE_C resin at three different sieved particle size ranges using the LVSTD (left) and BSE detectors (right) at 100x magnification.

B.2 Additives

Samples of the additives also underwent SEM image analysis. For each additive, three different magnifications were chosen; 100x, 750x, and 7000x. At 100x, the system operated under low vacuum mode (10 Pa) and used both LVSTD and BSE. In order to have a better quality picture at 750x and 7000x, the additives were first coated with gold and operated under high vacuum. The secondary electron detector (SE) was used in this case. The SEM pictures for Additives A, B, C, and F are shown in Figure B.4, Figure B.5, Figure B.6, and Figure B.7, respectively.





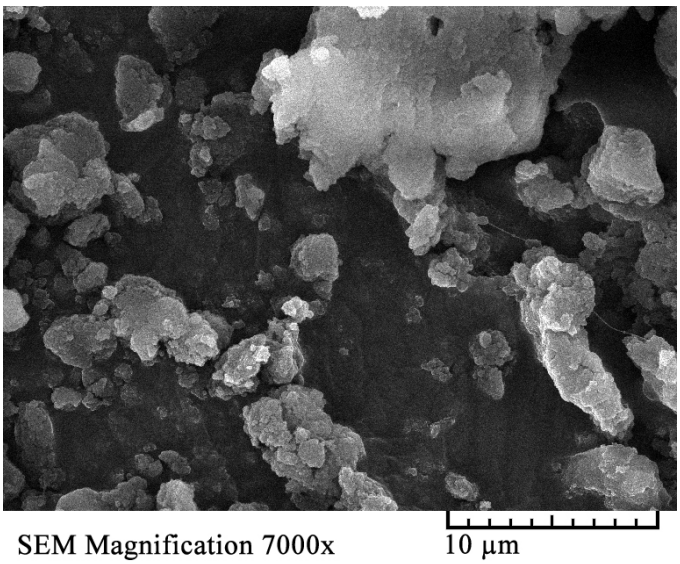
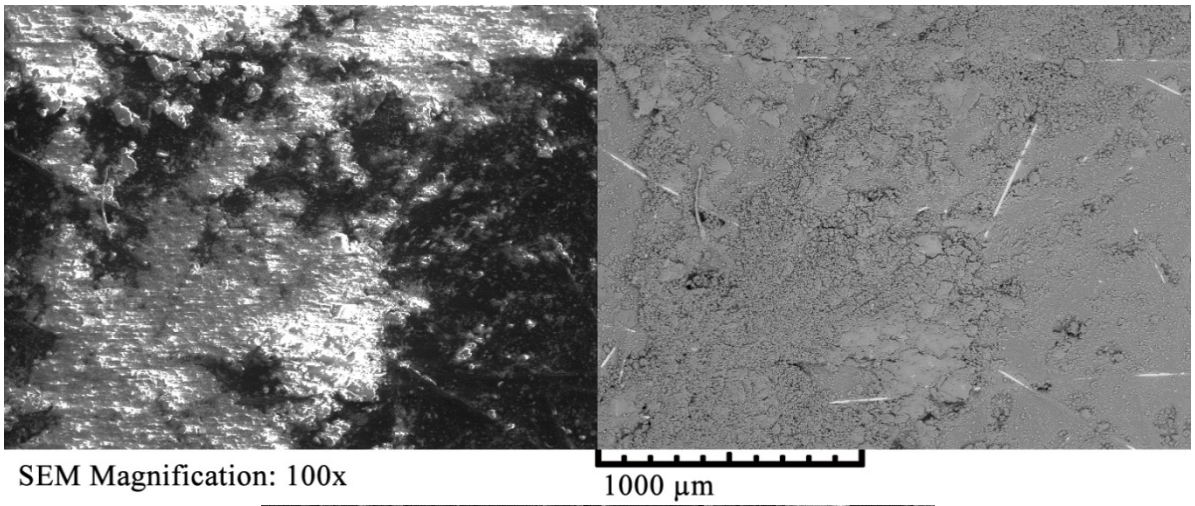
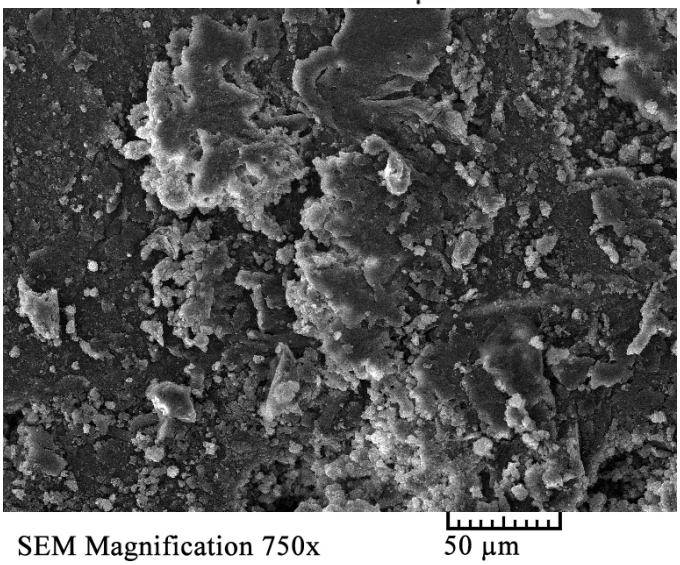


Figure B.4: The SEM pictures of Additive A at different magnifications. At 100x the LVSTD and BSE detectors were used. At 750x and 7000x the SE detector was used.





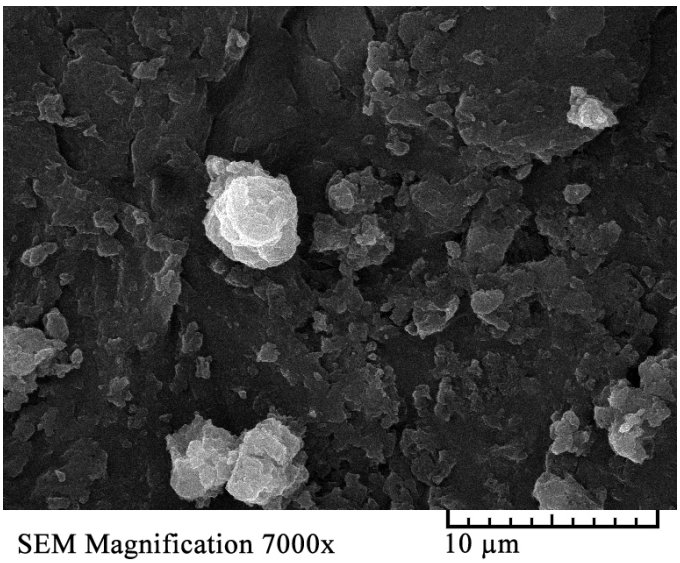


Figure B.5: The SEM pictures of Additive B at different magnifications. At 100x the LVSTD and BSE detectors were used. At 750x and 7000x the SE detector was used.

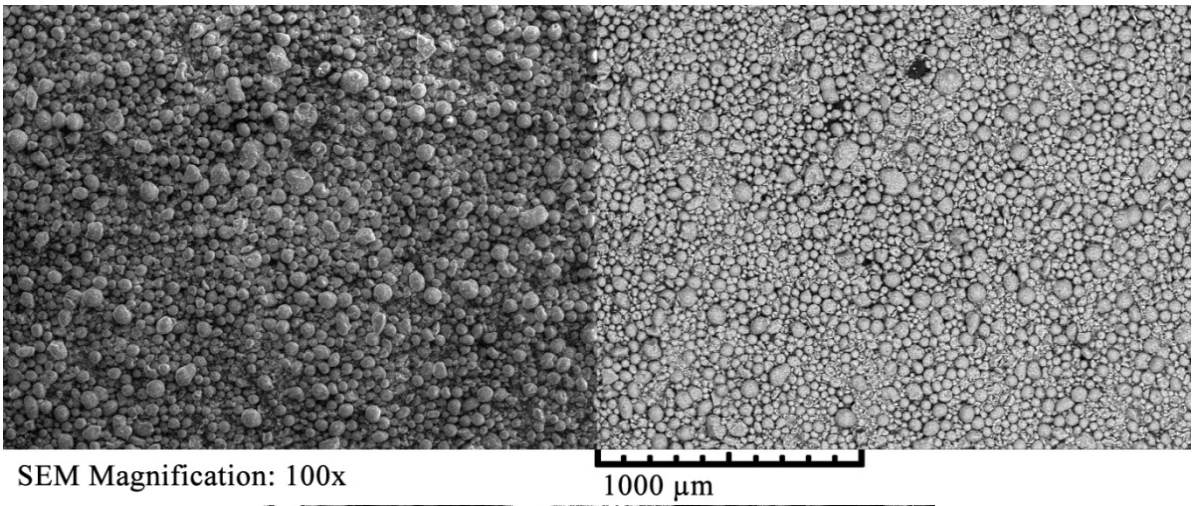


Figure B.6: The SEM pictures of Additive C at different magnifications. At 100x the LVSTD and BSE detectors were used. At 750x and 7000x the SE detector was used.

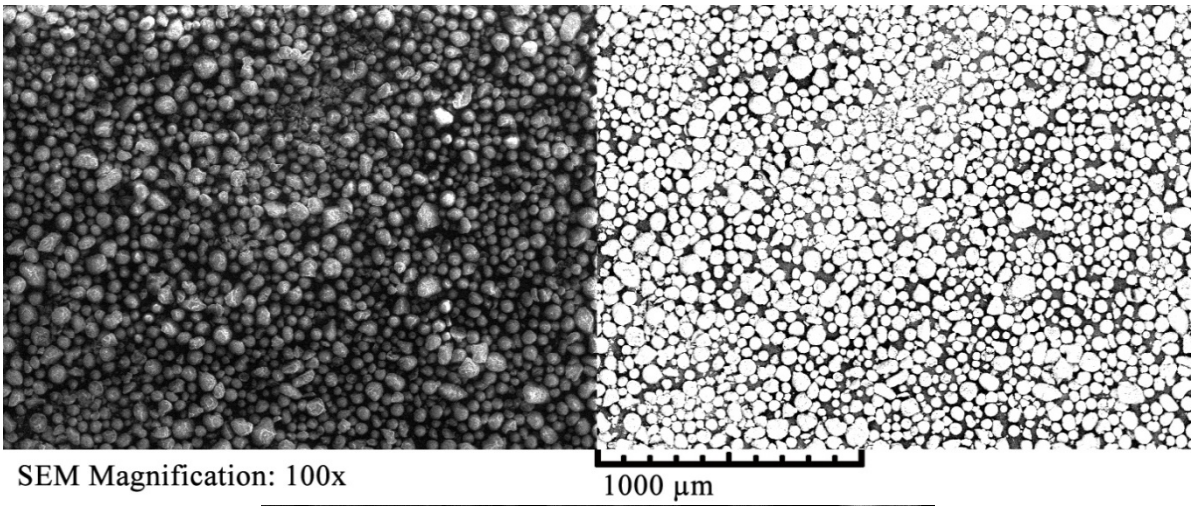


Figure B.7: The SEM pictures of Additive F at different magnifications. At 100x the LVSTD and BSE detectors were used. At 750x and 7250x the SE detector was used.

APPENDIX C
PRELIMINARY TESTING

C.1 Electrostatic Probe Background Measurement

Electrostatic probe background measurements were performed at the same time as the top Faraday cup measurements described in §2.3.2. The electrostatic was placed close to the distributor plate and would have been submerged in particles if any were present. The electrometer attached to the probe was set to measure the current on two trials and charge on another two trials.

Figure C.1 shows the background current and charge measurement by the electrostatic probe located at the bottom of the column for a period of one hour. The background measurement on current mode steadily fluctuated between -0.05 and -0.08 nA for both tests. This value was significantly lower than any of the measurements conducted with fluidization experiments and therefore deemed to be insignificant. On charge mode, the charge measured by the electrostatic probe had a maximum value of approximately -0.275 nC, which is also considered to be insignificant.

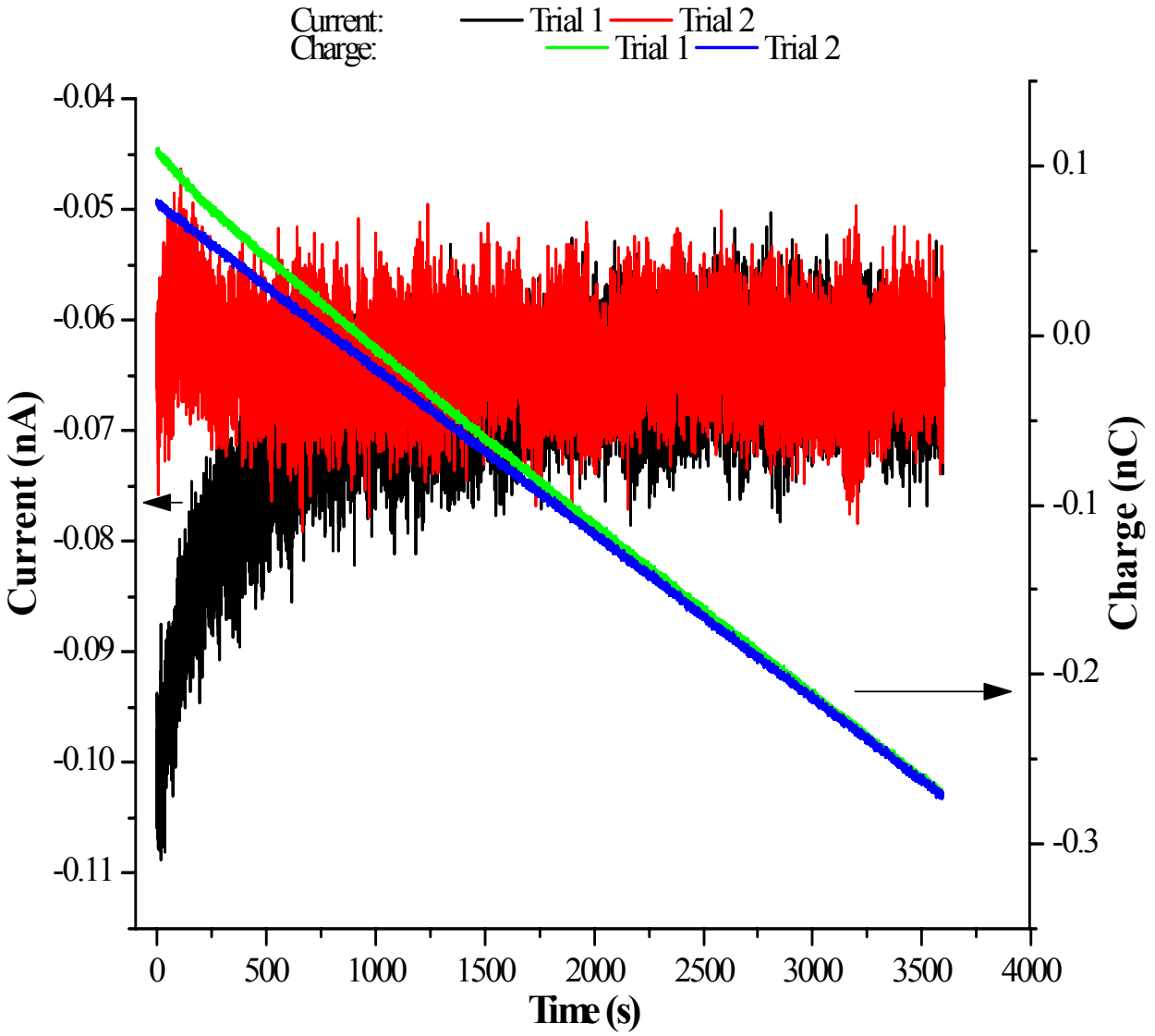


Figure C.1: The electrometer background charge and current measurement of the electrostatic probe placed at the bottom of the fluidization column for a period of one hour. No particles were present and no gas was sent through the fluidized bed.

Figure C.2 shows both the measured current and charge from the electrostatic probe located at the bottom of the column with increasing fluidizing gas volumetric flow rate. Both the current and the charge measured by the electrostatic probe were not affected by the increase in gas velocity.

All these preliminary experiments showed that the measurements from the electrostatic probe and the top Faraday cup were not affected by the fluidizing gas velocity.

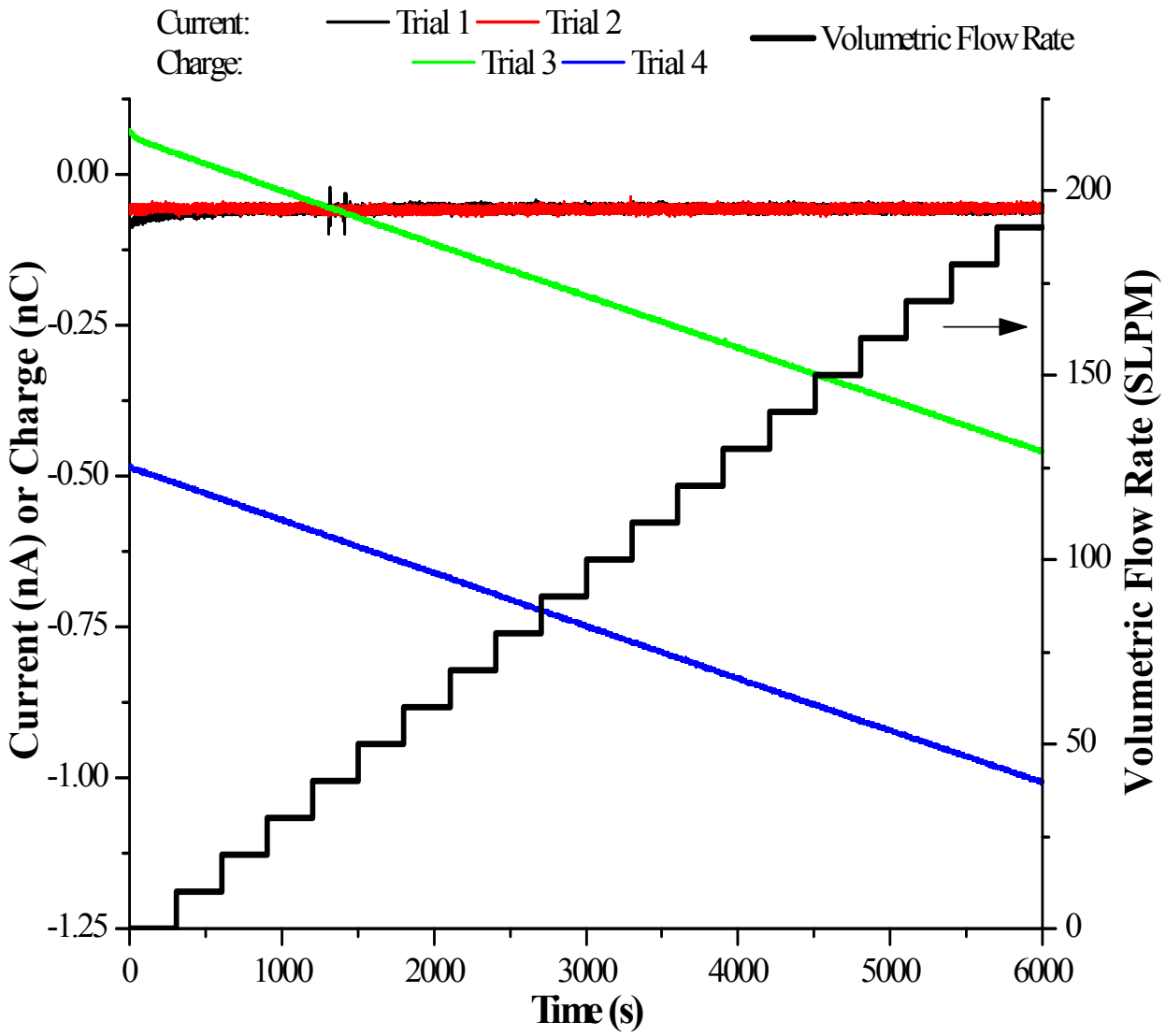


Figure C.2: The electrometer measurement of the electrostatic probe placed at the bottom of the fluidization column. Tests were performed on both current mode and charge mode. No particles were present with increasing gas volumetric flow rate.

C.2 Minimum Fluidization

As described in §3.3.1, the minimum fluidization velocity was experimentally calculated averaging the pressure fluctuations at a given gas velocity. The intersection between the sloped line of increasing pressure drop and the line through constant pressure drop was considered to be at the u_{mf} of the particles. The experiment was also repeated by decreasing the gas velocity an average of both of these values were used to determine the u_{mf} of the particles (Figure C.3).

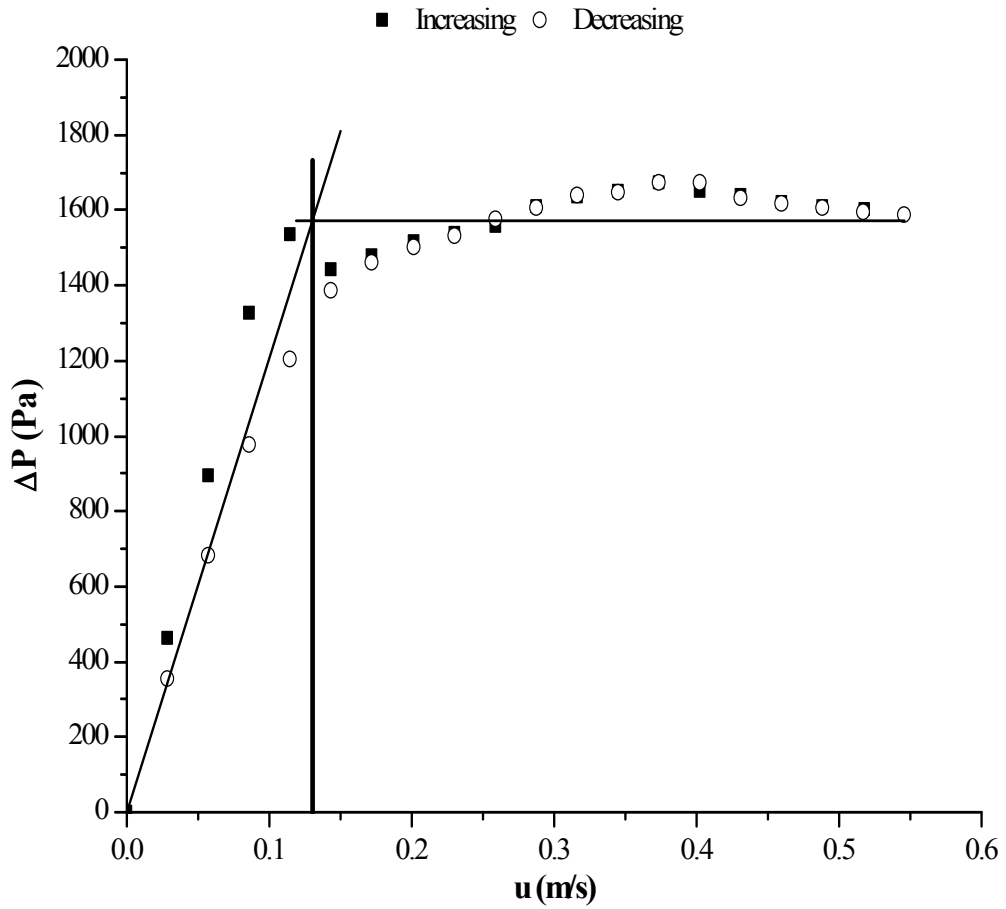


Figure C.3: Example of determining the minimum fluidization gas velocity through experimentation using PE_A particles.

C.2.1 Theoretical Calculations

There are numerous methods for theoretically estimating the minimum fluidization gas velocity. One method was reported by Grace (1982) as shown in Equation C.1 below.

$$Re_{mf} = \sqrt{C_1^2 + C_2 Ar} - C_1 \qquad [C.1]$$

Where Re_{mf} is the Reynolds Number at the minimum fluidization velocity, Ar is the Archimedes number, and $C_1 = 27.2$ and $C_2 = 0.408$ are constants according to Grace (1982). The Archimedes number is defined in Equation C.2.

$$Ar = \frac{d_P^3 \rho_f (\rho_P - \rho_f) g}{\mu^2} \quad [C.2]$$

where d_P is the diameter of the particle, ρ_P is the density of the particle, ρ_f is the density of the fluid, g is the gravitational acceleration, and μ is the fluid viscosity. The Reynolds number and minimum fluidization gas velocity can be described using Equation C.3.

$$Re_{mf} = \frac{d_P \rho_P u_{mf}}{\mu} \quad [C.3]$$

Equations C.2 and C.3 can be combined to yield Equation C.4.

$$u_{mf} = \frac{\mu \left(\sqrt{C_1^2 + C_2 Ar} - C_1 \right)}{d_P \rho_P} \quad [C.4]$$

Another method for estimating the minimum fluidization gas velocity was proposed by Kunii and Levenspiel (1991) and shown in Equation C.5.

$$u_{mf} = \frac{d_P^2 (\rho_P - \rho_f) g}{150 \mu} \cdot \frac{\varepsilon_{mf}^3 \phi^2}{1 - \varepsilon_{mf}} \quad [C.5]$$

where ε_{mf} is the void fraction at minimum fluidization and ϕ is the sphericity of the particles. As an example, using Equations C.4 and C.5, the theoretical minimum fluidization gas velocity was calculated and compared to the experimental value for one type of polyethylene resin as shown in Table 3.5; which showed relatively similar results. For all experiments performed in this work the experimental values of u_{mf} were used.

APPENDIX D

ADDITIVE EXPERIMENTS WITH PE_A AT 4 U_{MF}

Additional experiments with PE_A with Additives A, B, C, and F were performed at 0.1 m% at 4 u_{mf}. Figure D.1 shows the m% of from different givens in the fluidized bed. SEM Pictures taken from the Fines, Dropped, Loosely Bound, and Tightly Bound regions are shown in Figure D.2 to Figure D.5. The d_P50_N is shown in Figure D.6 while the cumulative charge of the Fines, the net q/m, and the $\hat{q}/\hat{A}$ of different regions in the fluidized bed are shown in Figure D.7, Figure D.8, and Figure D.9, respectively. The wall pictures for experiments with and without any additives are shown in Figure D.10. The electrostatic probes measurements for PE, PE-B, and PE-C are shown in Figure D.11, Figure D.12, and Figure D.13, respectively.

From the figures, it was clear that the additives had less of an effect on the electrostatic charge generation and particle wall fouling than at the lower gas velocity. This was likely due to a shorter residence time for the higher gas velocity which would reduce the amount of contact time between the additive and the particles and/or the column wall.

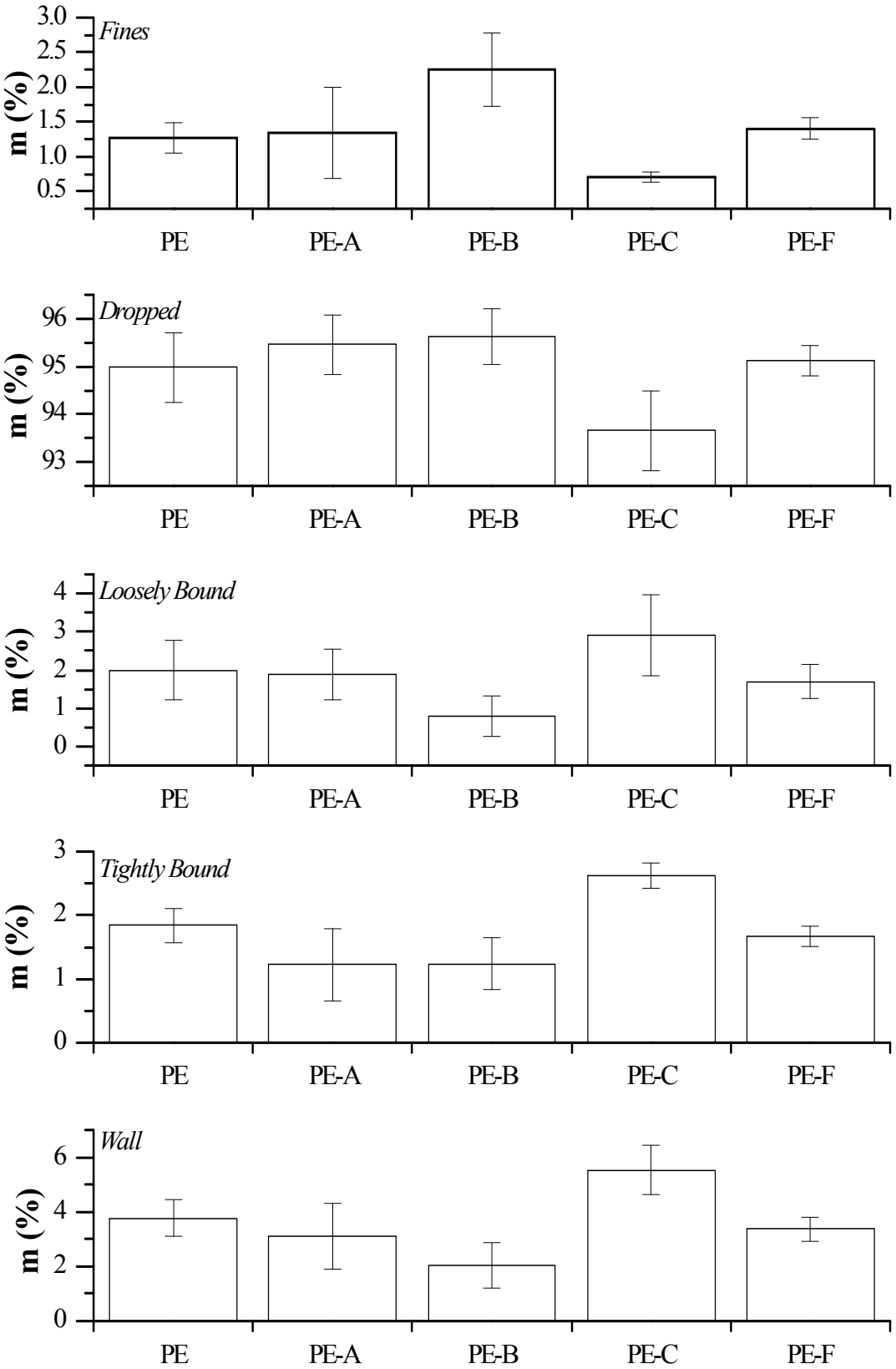


Figure D.1: The m% of the Fines, Dropped, Loosely Bound, Tightly Bound and Wall particles for experiments performed with and without additives with PE_A at 4 u_{mf}.

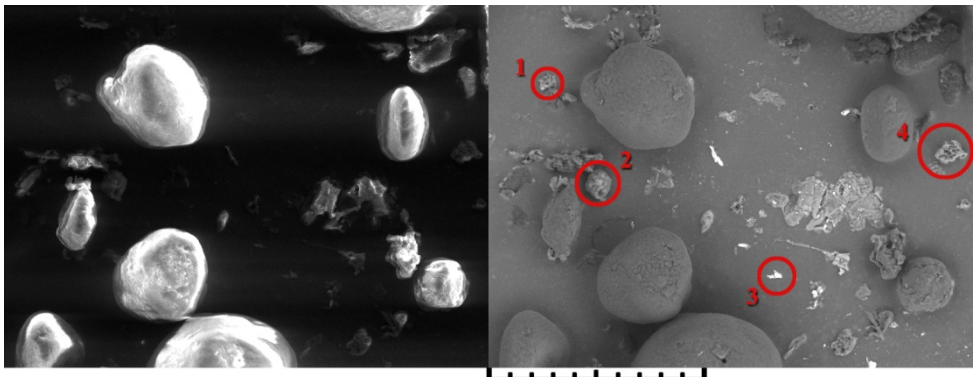
Fines

$d_{P,N1} = 0.012$

$d_{P,N2} = 0.020$

$d_{P,N3} = 0.006$

$d_{P,N4} = 0.0018$

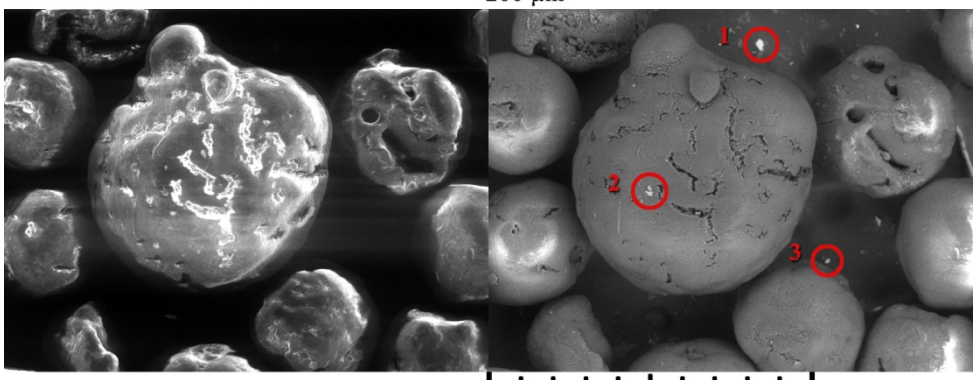


Dropped

$d_{P,N1} = 0.012$

$d_{P,N2} = 0.012$

$d_{P,N3} = 0.007$

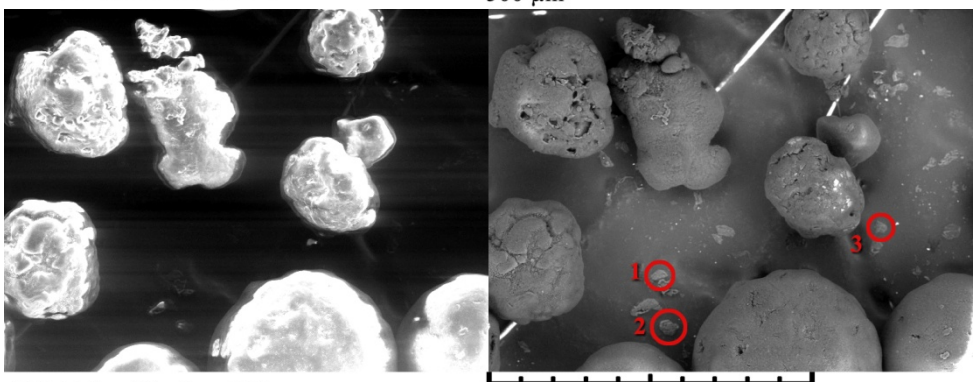


Loosely Bound

$d_{P,N1} = 0.015$

$d_{P,N2} = 0.020$

$d_{P,N3} = 0.072$



Tightly Bound

$d_{P,N1} = 0.014$

$d_{P,N2} = 0.029$

$d_{P,N3} = 0.013$

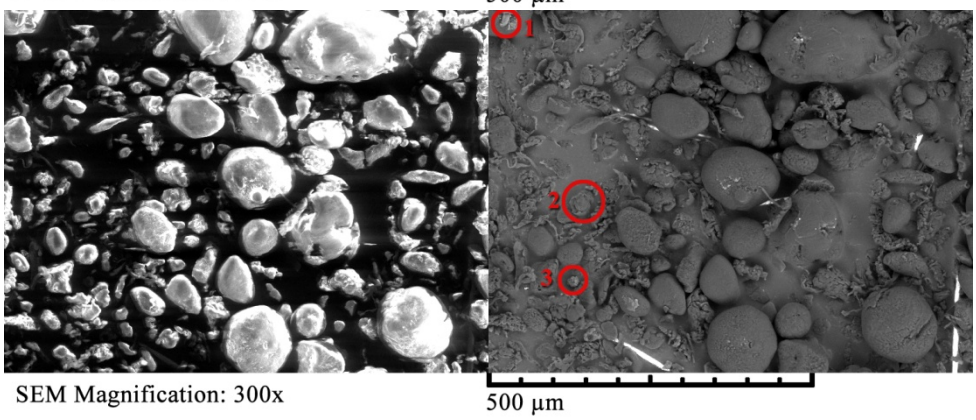


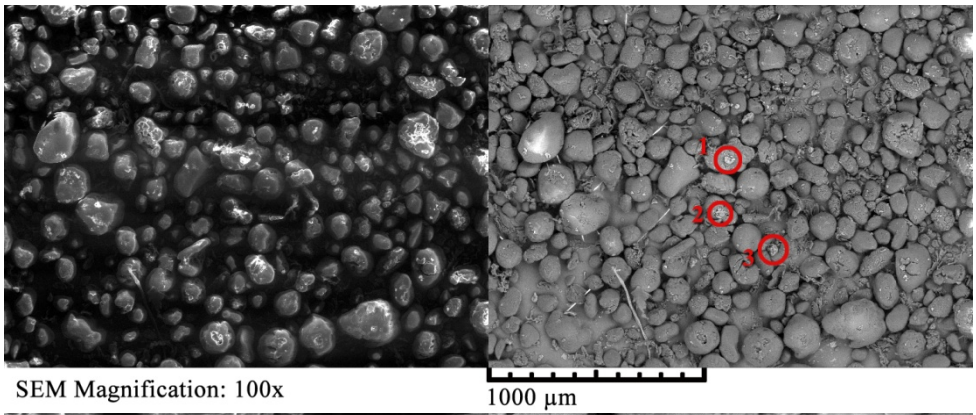
Figure D.2: SEM Pictures of the Fines, Dropped, Loosely Bound, and Tightly Bound particles when Additive A present at 4 u_{mf} with the PE_A resin.

Fines

$d_{P,N1} = 0.022$

$d_{P,N2} = 0.028$

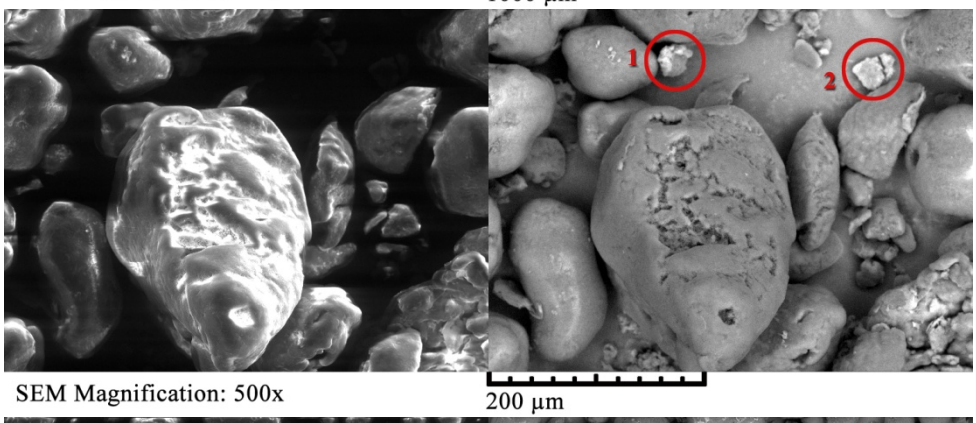
$d_{P,N3} = 0.030$



Dropped

$d_{P,N1} = 0.024$

$d_{P,N2} = 0.027$

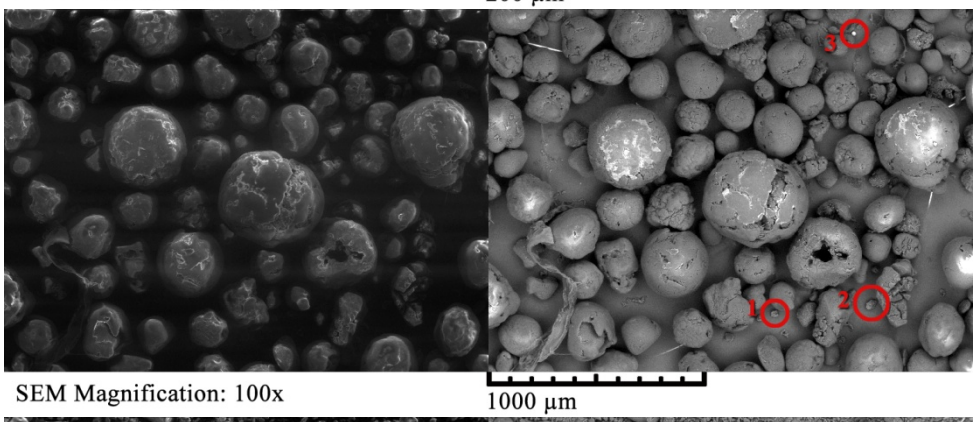


Loosely Bound

$d_{P,N1} = 0.031$

$d_{P,N2} = 0.038$

$d_{P,N3} = 0.019$



Tightly Bound

$d_{P,N1} = 0.025$

$d_{P,N2} = 0.022$

$d_{P,N3} = 0.023$

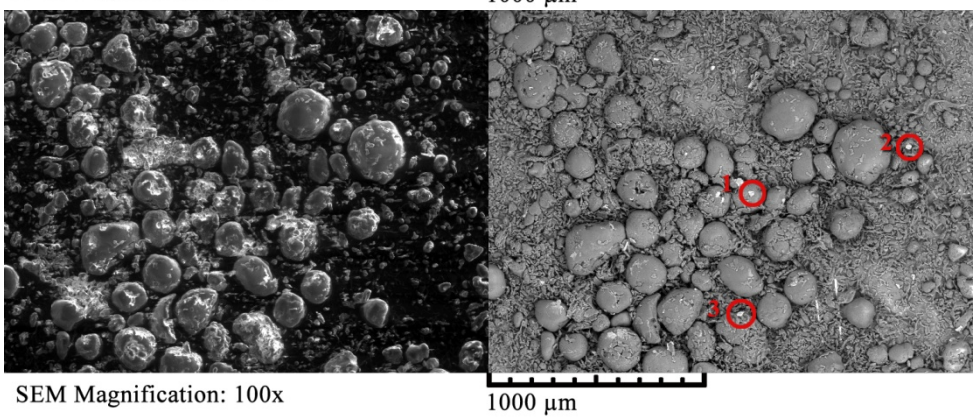


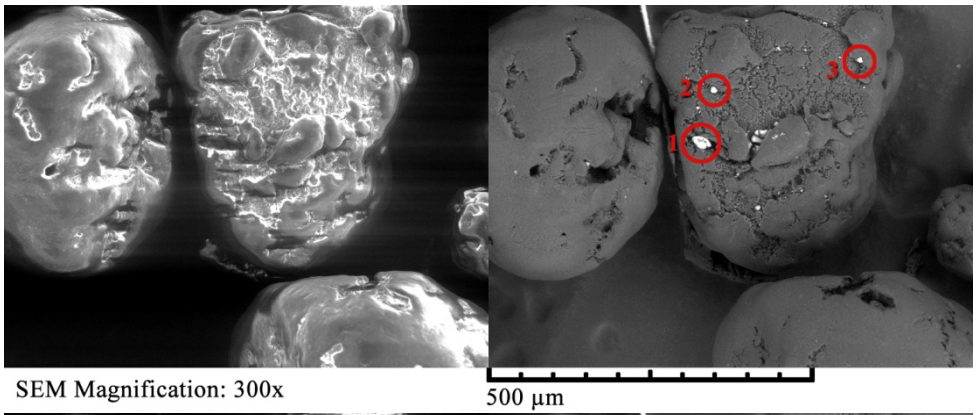
Figure D.3: SEM Pictures of the Fines, Dropped, Loosely Bound, and Tightly Bound particles when Additive B present at 4 u_{mf} with the PE_A resin.

Fines

$d_{P,N1} = 0.018$

$d_{P,N2} = 0.009$

$d_{P,N3} = 0.007$



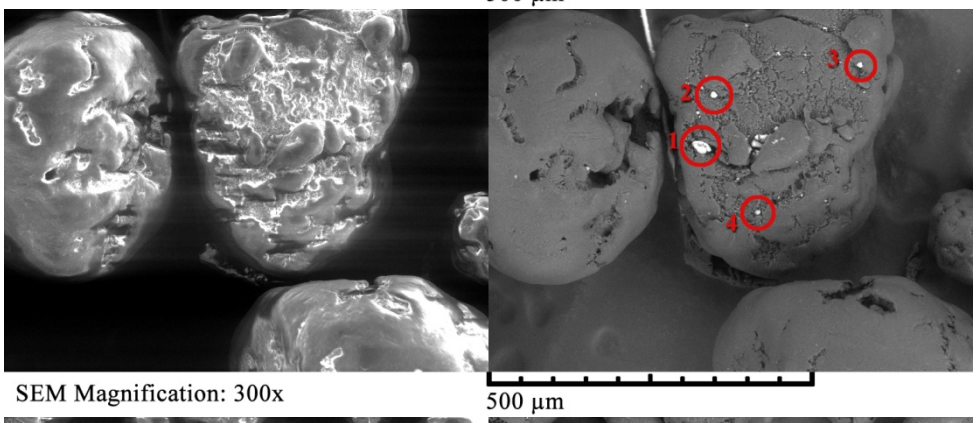
Dropped

$d_{P,N1} = 0.018$

$d_{P,N2} = 0.009$

$d_{P,N3} = 0.007$

$d_{P,N4} = 0.007$

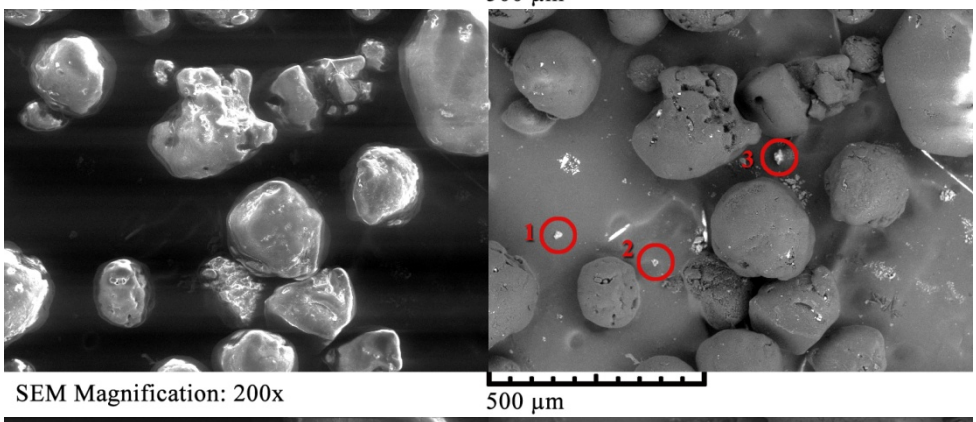


Loosely Bound

$d_{P,N1} = 0.015$

$d_{P,N2} = 0.013$

$d_{P,N3} = 0.022$



Tightly Bound

$d_{P,N1} = 0.036$

$d_{P,N2} = 0.008$

$d_{P,N3} = 0.010$

$d_{P,N4} = 0.007$

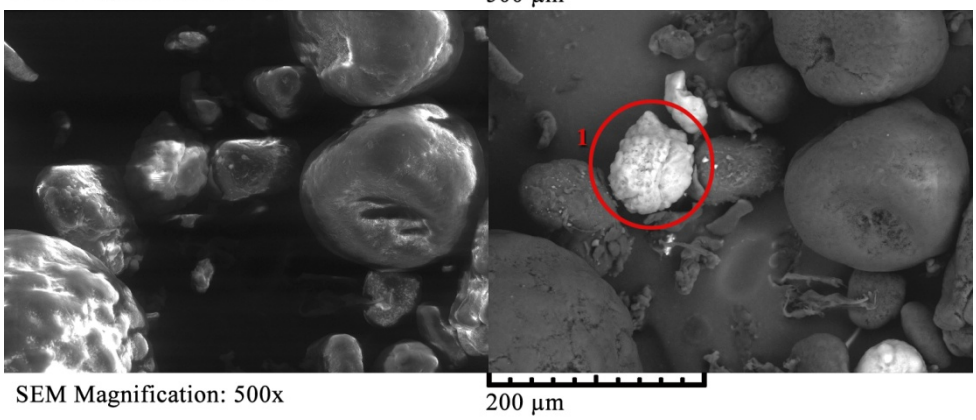


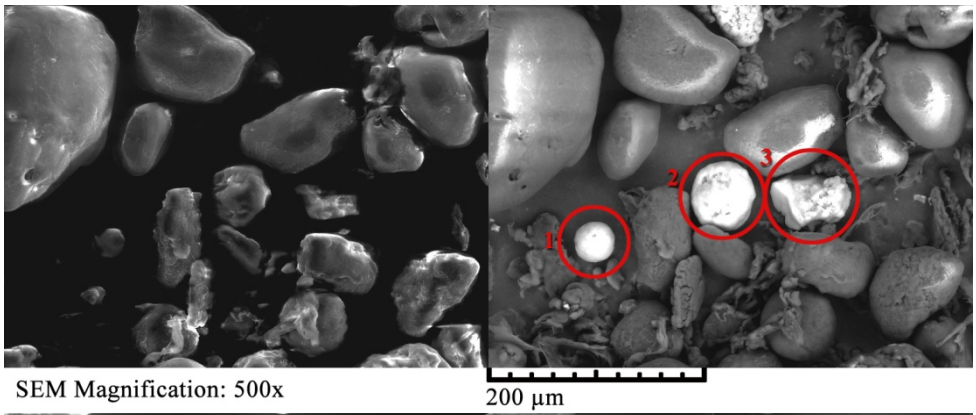
Figure D.4: SEM Pictures of the Fines, Dropped, Loosely Bound, and Tightly Bound particles when Additive C present at 4 u_{mf} with the PE_A resin.

Fines

$d_{P,N1}$ = 0.030

$d_{P,N2}$ = 0.049

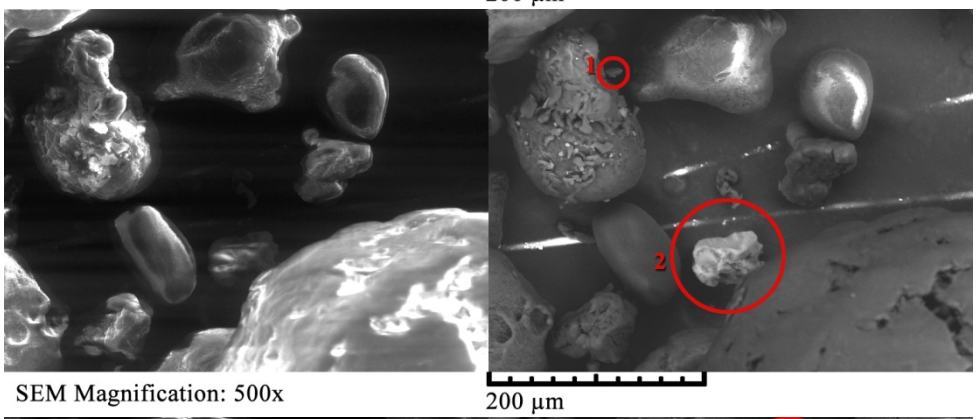
$d_{P,N3}$ = 0.049



Dropped

$d_{P,N1}$ = 0.009

$d_{P,N2}$ = 0.046

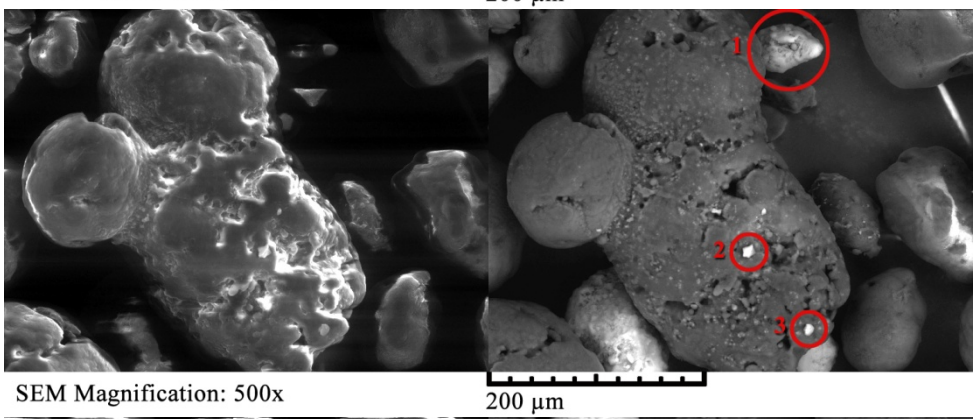


Loosely Bound

$d_{P,N1}$ = 0.041

$d_{P,N2}$ = 0.006

$d_{P,N3}$ = 0.005



Tightly Bound

$d_{P,N1}$ = 0.065

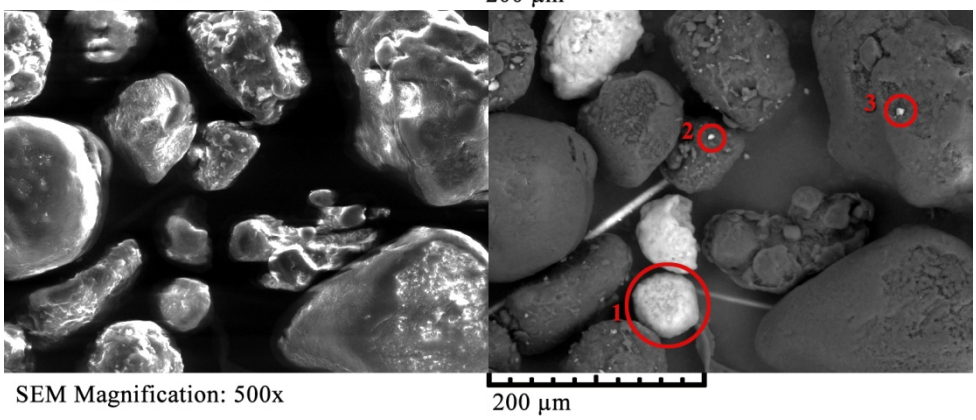


Figure D.5: SEM Pictures of the Fines, Dropped, Loosely Bound, and Tightly Bound particles when Additive F present at 4 u_{mf} with the PE_A resin.

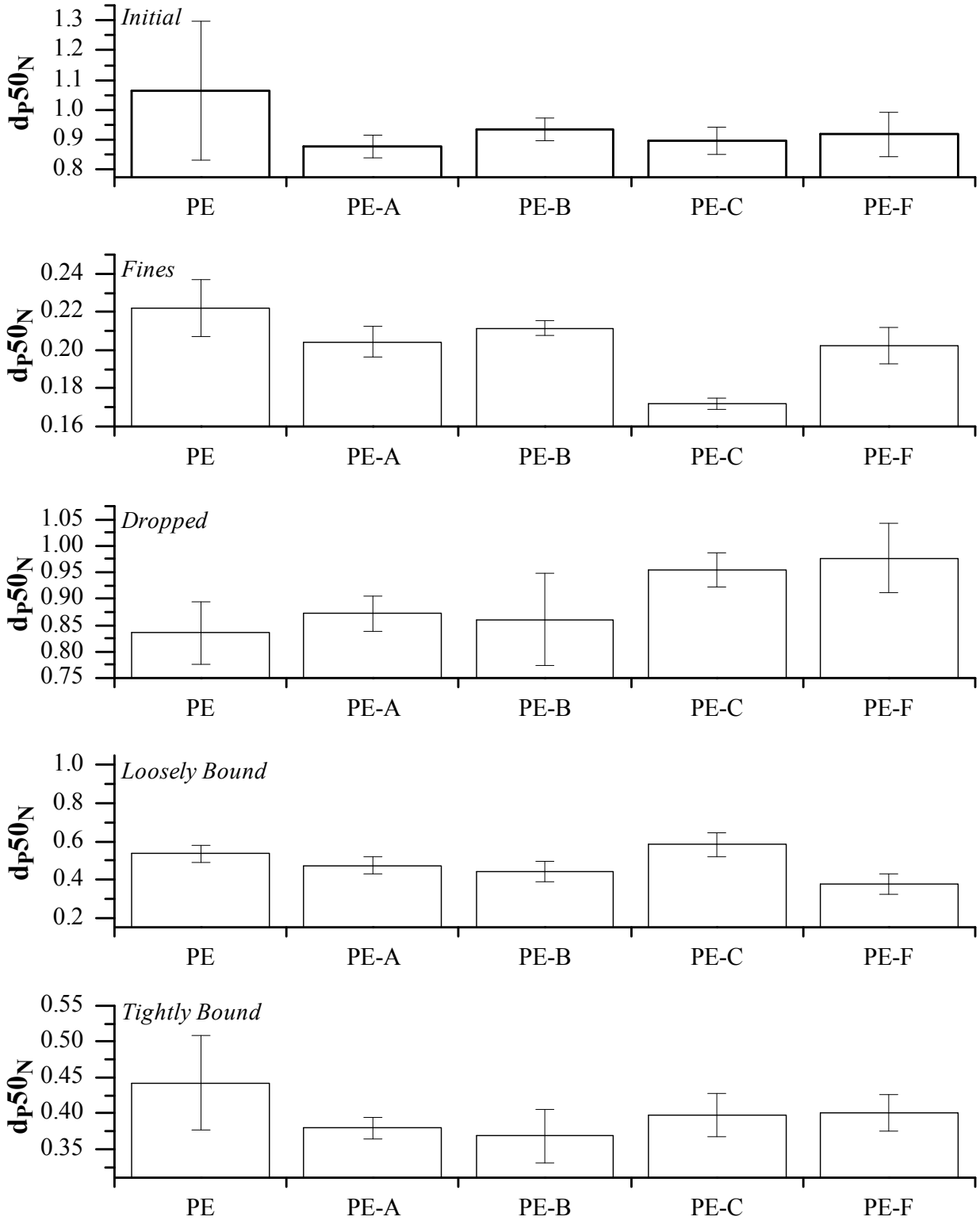


Figure D.6: The d_P50_N of the Initial, Fines, Dropped, Loosely Bound, and Tightly Bound particles for experiments performed with and without additives with PE_A resins at 4 u_{mf}.

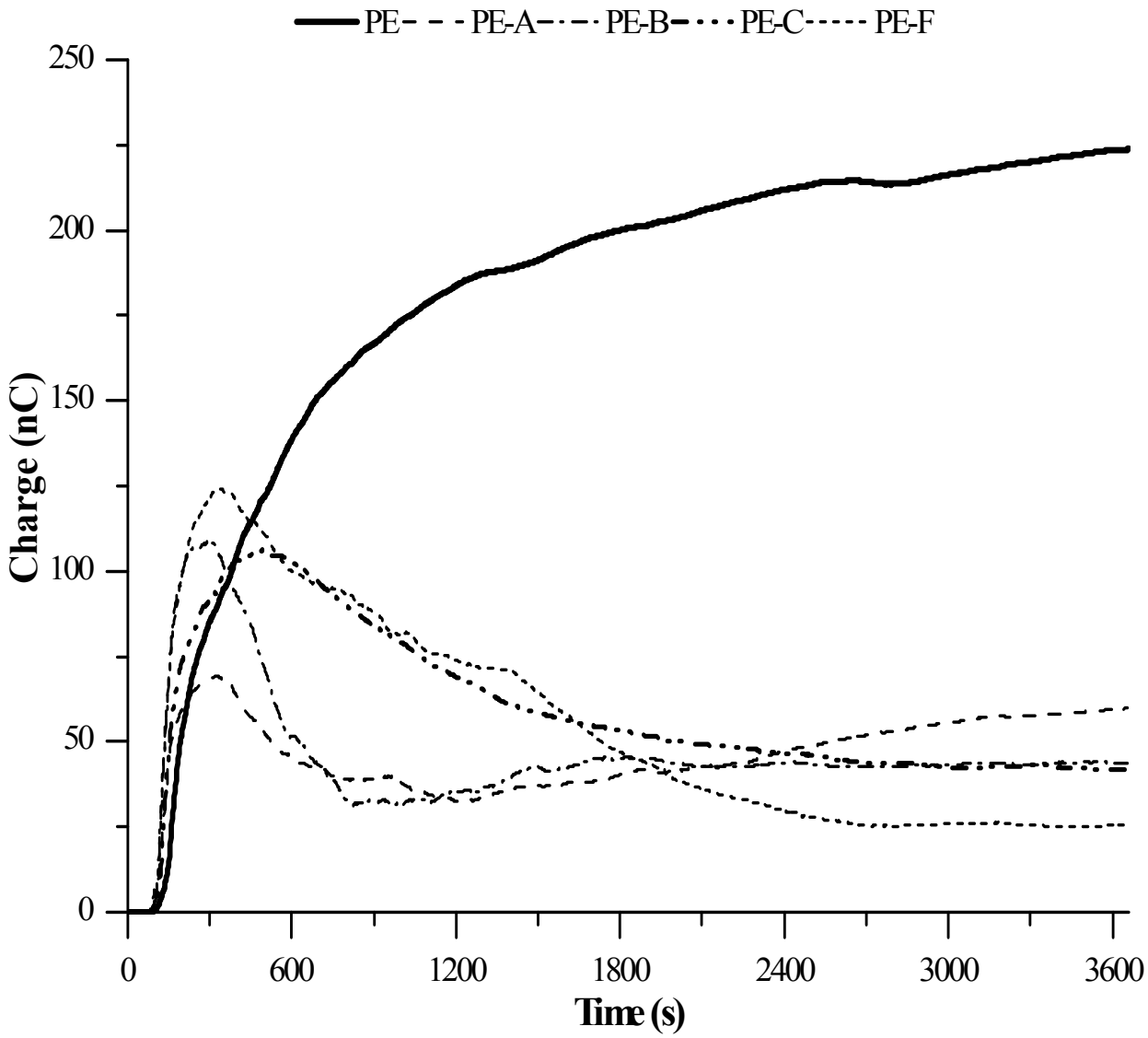


Figure D.7: Examples of the cumulative charge of the Fines measured during 60 min of fluidization with and without the additives with PE_A at 4 u_{mf}.

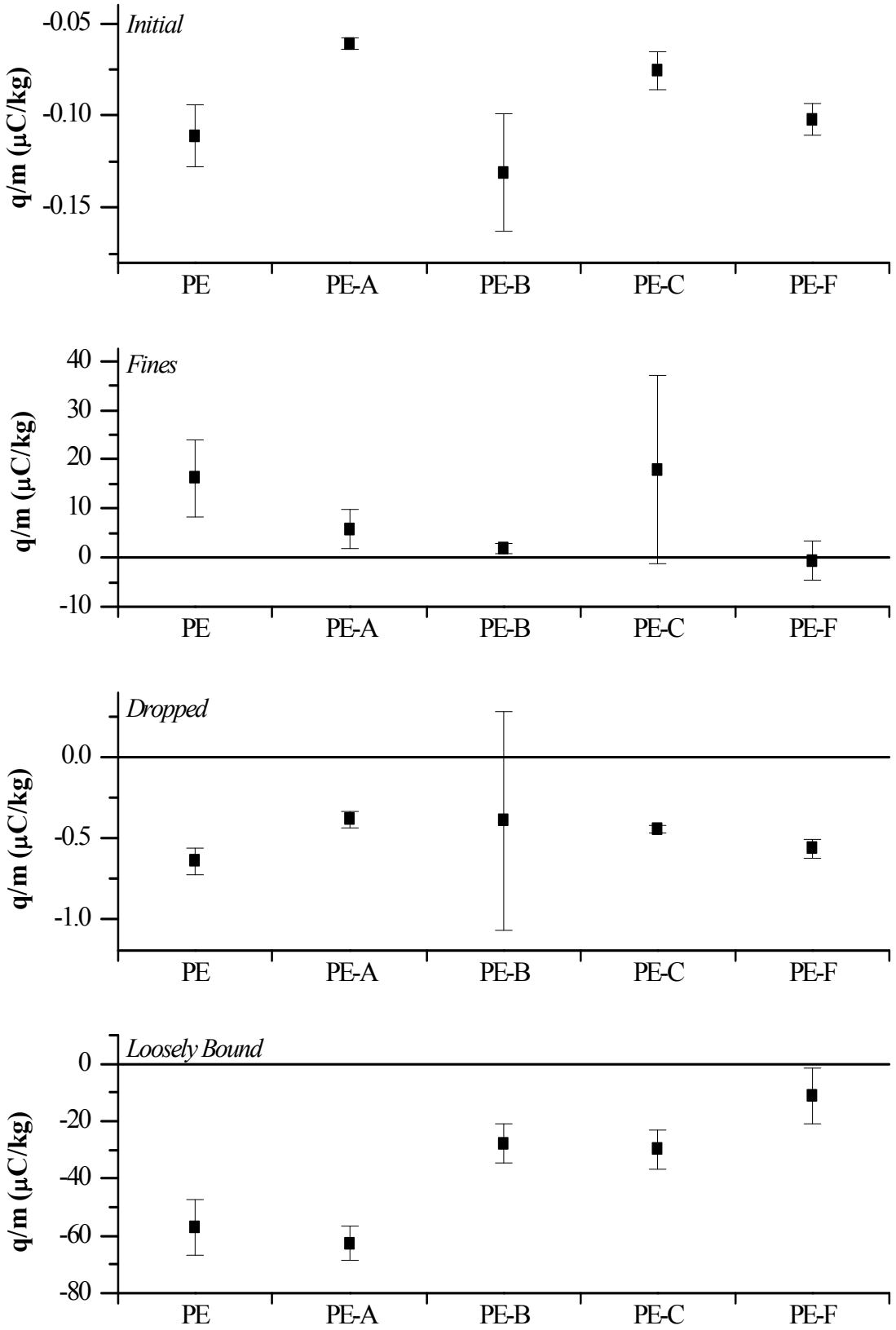


Figure D.8: The net q/m of the Initial, Fines, Dropped, and Loosely Bound particles for experiments performed with and without additives with PE_A at 4 u_{mf}.

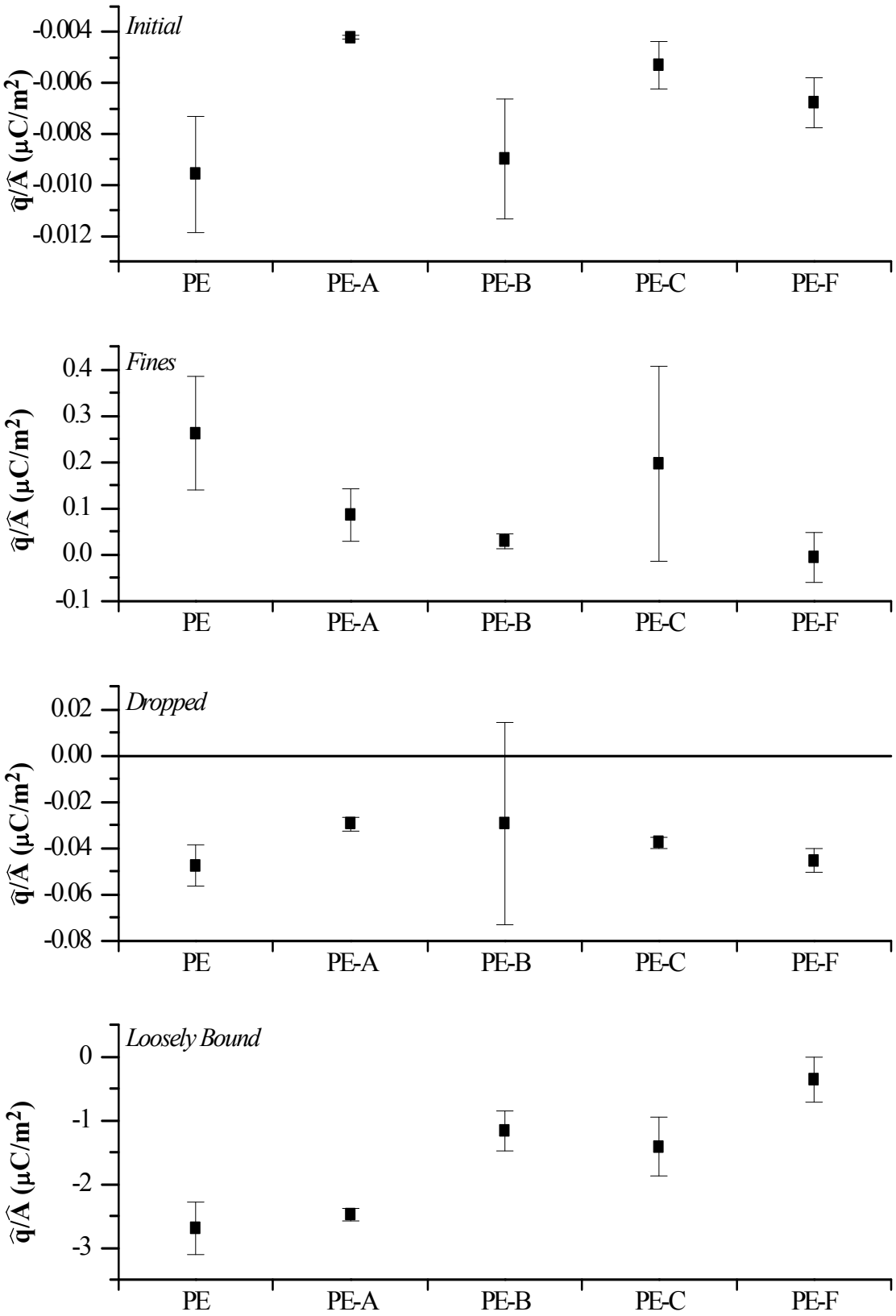


Figure D.9: The net $\hat{q}/\hat{A}$ of the Initial, Fines, Dropped, and Loosely Bound particles for experiments performed with and without additives with PE_A at 4 u_{mf}.



Figure D.10: Pictures of the wall particle layer with and without additives using the PE_A resin at 4 u_{mf}.

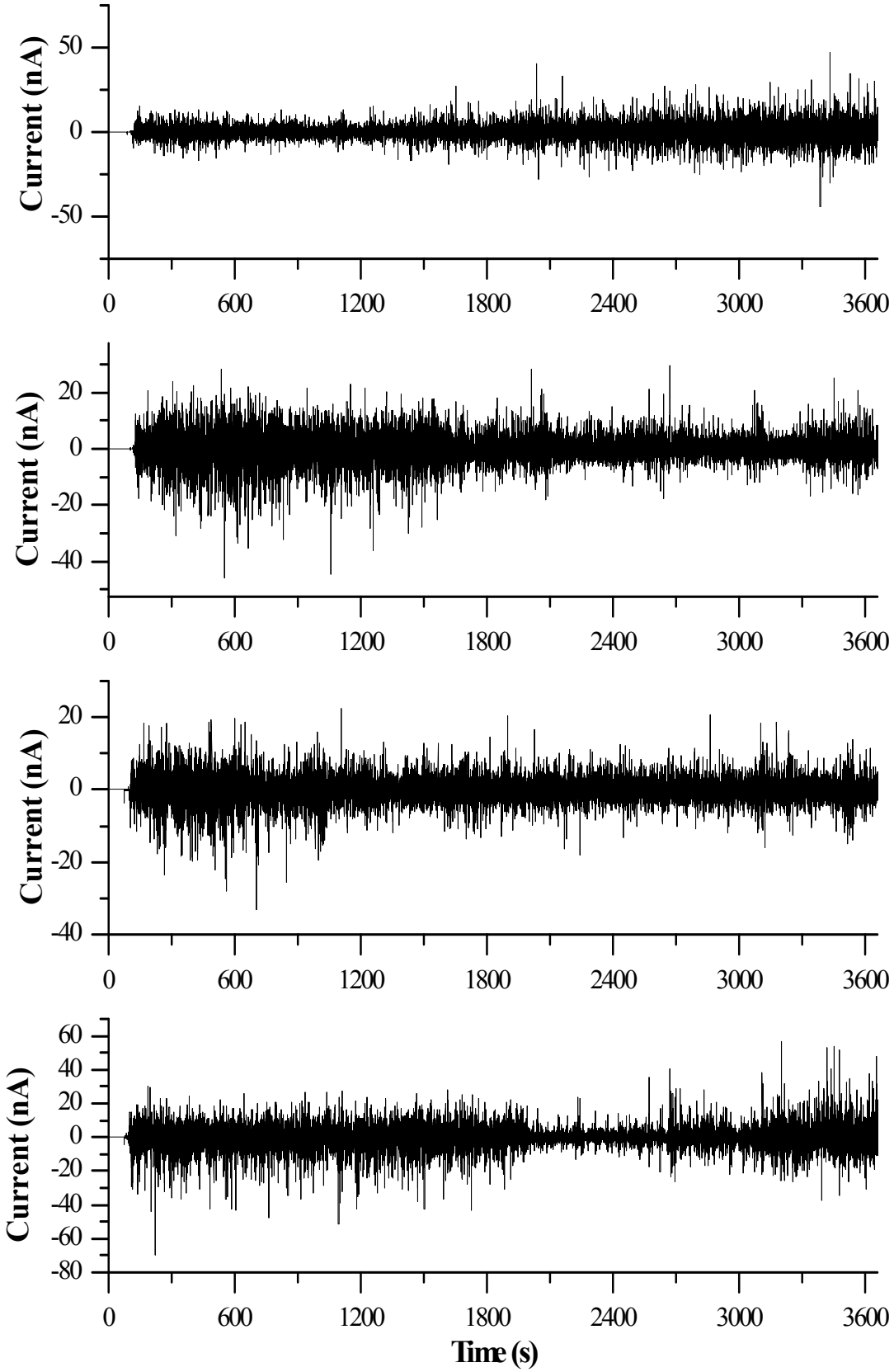


Figure D.11: The current measurements for trials with no additive for 60 min of fluidization with PE_A resin at 4 u_{mf}.

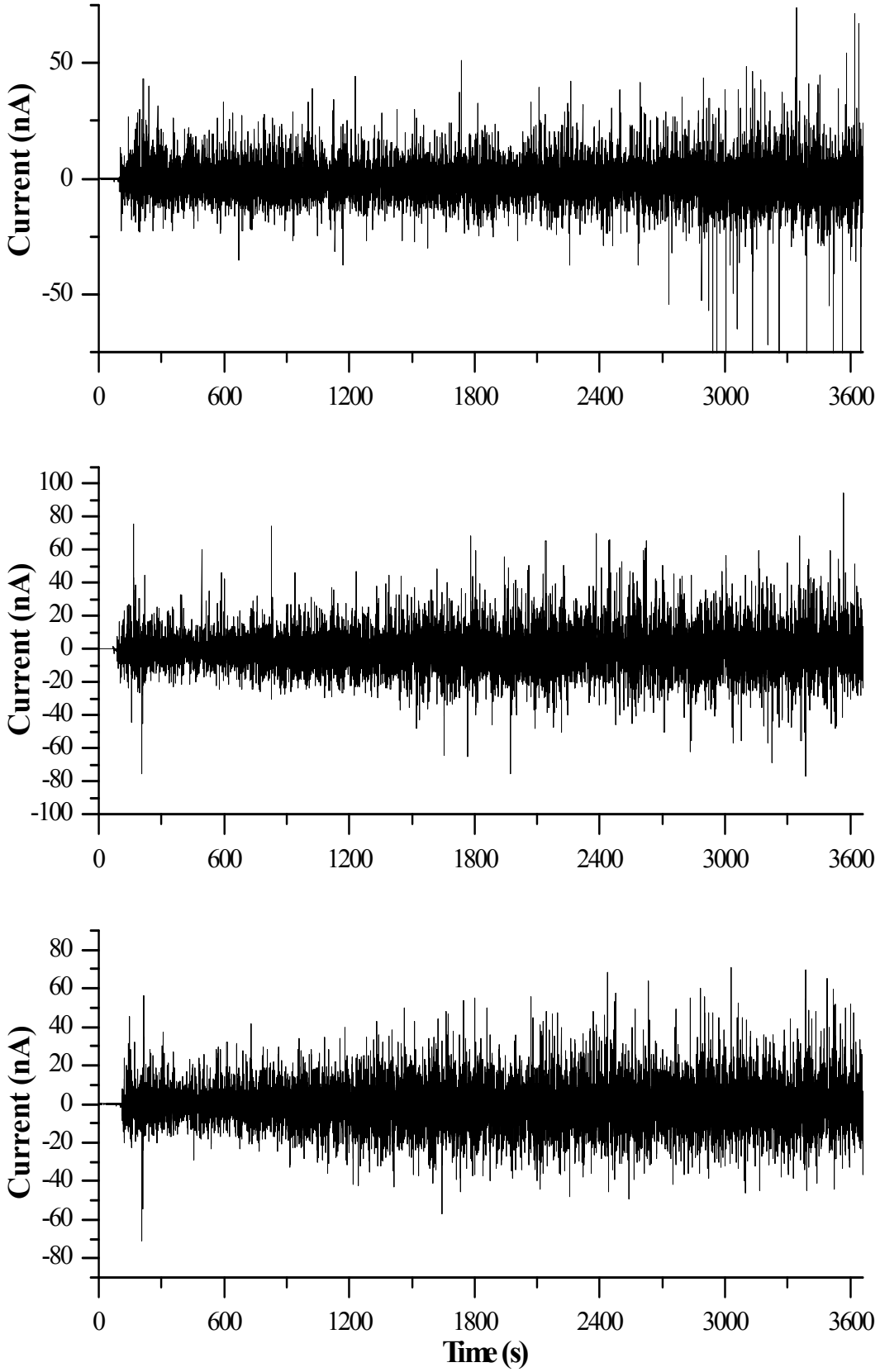


Figure D.12: The current measurements for trials with Additive B for 60 min of fluidization with PE_A resin at 4 u_{mf}.

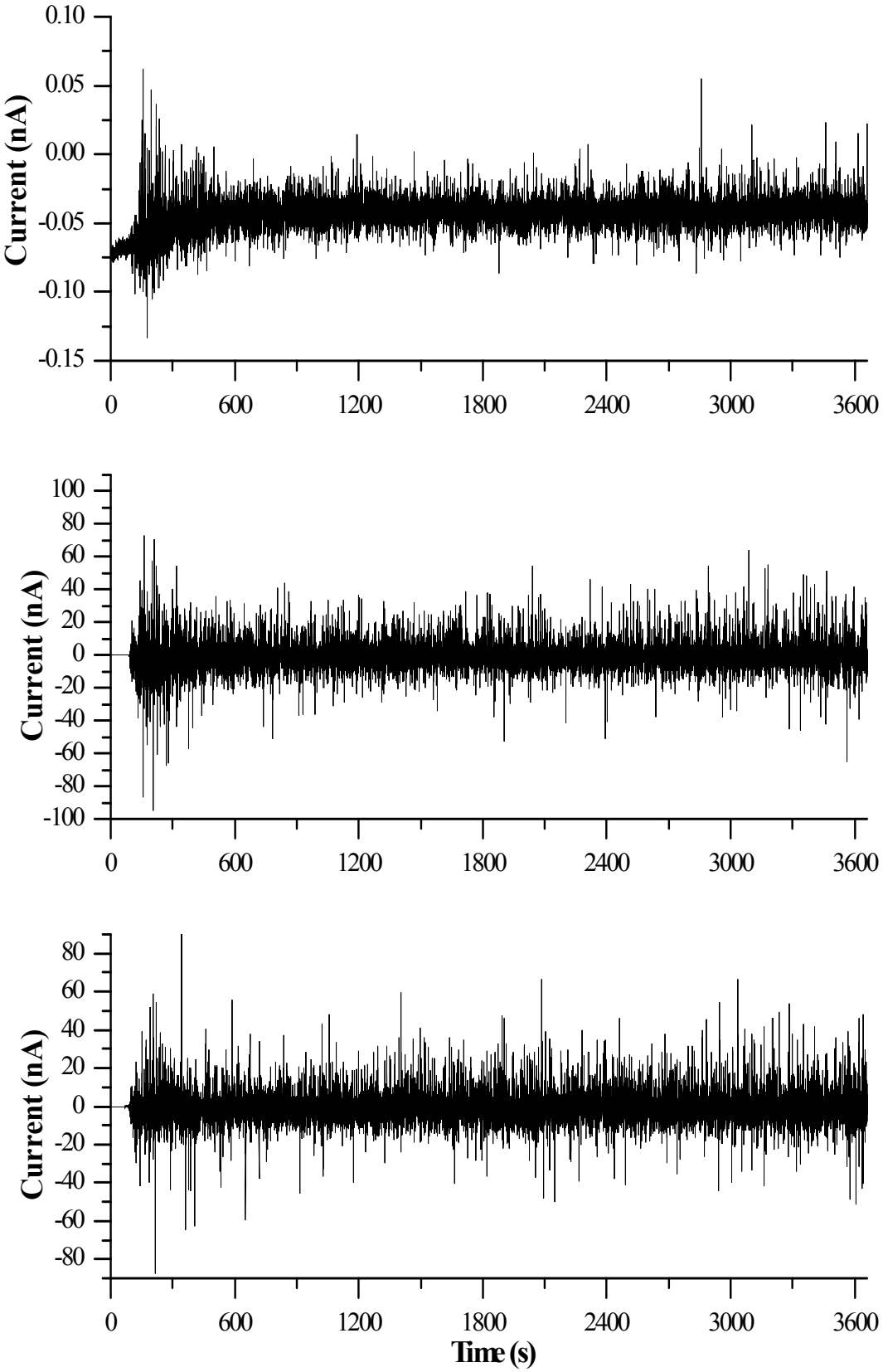


Figure D.13: The current measurements for trials with Additive F for 60 min of fluidization with PE_A resin at 4 u_{mf}.